PREFACE

This final report covers the work performed under Contract F33615-72-C-1757 during the period 1 June 1972 through 31 May 1975.

The research program discussed in this report was conducted by the Materials Engineering and Research Laboratory of the Pratt & Whitney Aircraft Division of United Technologies Corporation, East Hartford, Connecticut. Its purpose is to determine the reasons for the difference in the hot corrosion resistance of cobalt-base and nickel-base alloys.

The contract was accomplished under the technical direction of Dr. H. C. Graham of the Aerospace Research Laboratory, Air Force Systems Command, United States Air Force, Wright-Patterson Air Force Base, Ohio 45433. Dr. Graham is now with the Air Force Materials Laboratory, AFML/LGM.

Dr. F. S. Pettit, Program Manager, Materials Engineering and Research Laboratory, Pratt & Whitney Aircraft Division of United Technologies Corporation, directed this project. Mr. J. A. Goebel of the P&WA Materials Engineering and Research Laboratory was the principal investigator. The authors wish to acknowledge helpful discussions concerning the results provided by Dr. G. W. Goward, Dr. E. J. Felten and Mr. C. S. Giggins, as well as technical assistance from C. E. Londin, C. R. Shimoda, R. B. Burdon, M. F. Hornbecker, K. P. Gumz and A. R. Geary.

TABLE OF CONTENTS

TABLE OF CONTENTS (Cont'd)

LIST OF ILLUSTRATIONS

LIST OF ILLUSTRATIONS (Cont'd)

LIST OF ILLUSTRATIONS (Cont'd)

LIST OF ILLUSTRATIONS (Cont'd)

LIST OF ILLUSTRATIONS (Cont'd)

LIST OF ILLUSTRATIONS (Cont'd)

LIST OF ILLUSTRATIONS (Cont'd)

LIST OF ILLUSTRATIONS (Cont'd)

LIST OF TABLES

SECTION I

INTRODUCTION

1. BACKGROUND

The useful lives of nickel- and cobalt-base alloys in gas turbine engines are significantly reduced due to accelerated oxidation. This condition occurs when salts are ingested into the engine or when fuels are used which are contaminated with salts or other metallic impurities such as vanadium or lead. While in the past it was believed that such effects were confined to turbine engines used in marine environments or to those burning low grade fuels, it has now become apparent that this condition also prevails, but to a lesser degree, in military and commercial aircraft engines that burn high grade fuels. The factors which cause these problems in such aircraft engines appear to be related to the sporadic ingestion of salts from limited exposure to marine environments and to ingestion of particulate matter from runways or other contaminated environments. Accelerated oxidation, or hot corrosion as it is usually called, occurs because the alkali or alkali-earth sulfates as well as metal oxides which form in the combustor become deposited on the turbine alloys.

Sulfate ash deposition on turbine hardware results in serious problems in the effective utilization of gas turbines in aircraft service. Not only is the sulfur present in high-grade aircraft fuels a source of sulfate ash, but sulfates may also be present in the intake air (e.g., as sea salt). A number of mechanisms have been proposed to account for the sulfate-induced accelerated oxidation of alloys. All of these mechanisms usually consider Na_2SO_4 to be the component in the sulfate deposits which causes the increased oxidation. The use of Na_2SO_4 to model real sulfate ash deposits can be justified because it usually is a major constituent of real ash deposits, and the use of a single compound greatly simplifies the interpretation of experimental results.

At the present time, several mechanisms for the hot corrosion of many nickel-base alloys have been proposed; however, much less information is available on mechanisms of hot corrosion of cobalt-base alloys. Detailed studies on the hot corrosion of cobalt-base alloys should prove to be especially valuable since it has been qualitatively demonstrated that commercial cobalt-base superalloys generally are more resistant to hot corrosion than nickel-base superalloys.

2. HOT CORROSION MECHANISMS

The available literature concerning the hot corrosion of nickel- and cobalt-base alloys is voluminous. In general, however, the literature describes two types of work. The first type is that wherein numerous alloys with a variety of compositions have been tested, usually under dynamic conditions, by using burner rig tests (ref. 1 to 5). Results from this type of test are valuable for the selection of alloys for practical applications; however, in view of the variety and complexity of the alloys that are usually tested, as well as the lack of controlled conditions in these tests, the results can only be used to give qualitative descriptions concerning hot corrosion mechanisms. The other type of work is that performed in the laboratory usually under well defined conditions. While it is performed under conditions which may not be representative of those encountered in practice, it has provided the foundation from which the present hot-corrosion theory has evolved.

Simons, et al (ref. 6) were among the first to examine the hot corrosion problem in a fundamental manner. Since it was recognized that Na_2SO_4 was a necessary precursor for hot corrosion, these investigators examined the oxidation of alloys coated with Na_2SO_4. They concluded that Na_2SO_4 could induce accelerated oxidation of alloys providing a reducing agent was present to trigger the reaction. It was concluded that, as a result of the reduction of Na_2SO_4, low valent sulfur reacted with the alloy to form sulfides which in turn caused increased oxidation of the alloy. Seybolt (ref. 7 and 8) subsequently concluded that triggering of the reaction could be accomplished by conditions developed due to reaction between the alloy and Na_2SO_4. Seybolt proposed that accelerated oxidation of nickel-base alloys in the presence of Na_2SO_4 occurred because sulfur from the sulfate entered the alloy, causing the formation of sulfide phases and depletion in the alloy of elements necessary to develop a protective oxide scale. In addition, Seybolt proposed that the catastrophic nature of the attack was due to the rapid inward transport of liquid nickel sulfide and the simultaneous penetration of incompletely reacted liquid Na_2SO_4 which reacted with the residual alloy as penetration proceeded. Bornstein and DeCresente (ref. 9) also studied the Na_2SO_4-induced oxidation of nickel-base alloys and suggested that hot corrosion occurs because oxide ions are developed in the sulfate by sulfur entering the alloy. They proposed that these oxide ions prevent the formation of protective oxide scales.

Thermodynamic analyses were used by Quets and Dresher (ref. 10) and by Goebel and Pettit (ref. 11) to show that conditions are developed when Na_2SO_4 is on an alloy such that sulfur from the $NaSO_4$ will react with the alloy. Goebel and Pettit (ref. 11) also proposed that removal of sulfur from the Na_2SO_4 causes the oxide ion activity of the Na_2SO_4 to be increased to levels at which protective oxide layers are destroyed due to basic fluxing reactions of the following type:

$$MO \text{ (protective scale)} + 0^{2-} (Na_2SO_4) = MO_2^{2-} \text{ (nonprotective scale)} \quad (1)$$

Goebel et al (ref. 12 and 13) proposed that protective oxide scales can also be destroyed through acidic fluxing reactions with the Na_2SO_4 of the following type:

$$MO \text{ (protective scale)} = M^{2+} + 0^{2-} \text{ (nonprotective scale)} \quad (2)$$

In the case of acidic fluxing reactions, it was proposed (ref. 12 and 13) that the Na_2SO_4 becomes sufficiently acidic to flux protective oxide scales due to modification of the Na_2SO_4 by oxides of elements in the alloy (e.g., Mo, W, V) or by simultaneous deposition of such oxides along with the Na_2SO_4 as occurs upon using, for example, fuels containing vanadium.

Conde (ref. 14), Hurst et al (ref. 15), and Stringer (ref. 16) have proposed that sodium chloride can play an important role in the hot-corrosion process. Hurst et al (ref. 15) found that sodium chloride promoted mechanical failure of surface oxide scales even when the sodium chloride was in an entirely gaseous condition. Sodium chloride cannot be disregarded as a necessary or important factor in the hot corrosion of gas turbine hardware. Analyses of deposits on hardware taken from the turbine sections of service engines (aero, marine, or land based) show that Na_2SO_4 is always present. Depending on the particular engine application, lead and vanadium are also frequently detected. On the other hand, chloride is only

rarely detected, which is consistent with the higher vapor pressure of the chloride relative to that of Na_2SO_4. However, the amount of sodium chloride necessary to influence the hot corrosion process is not known; it may be quite small. In addition sodium chloride may play an important role in the hot corrosion process only at lower temperatures where it is more prevalent in ash deposits.

There are numerous other papers that could be discussed since they represent significant contributions to the hot corrosion literature. However, the papers that have been discussed are adequate to qualitatively introduce the mechanisms currently proposed to account for hot corrosion of materials. These mechanisms may be summarized as follows:

- Sulfide phases in the alloy, the formation of which occur due to the removal of sulfur from the Na_2SO_4 by the alloy, result in the development of nonprotective oxide scales.

- Excessive depletion from the alloy of elements necessary for the formation of a protective oxide scale occurs because of sulfide formation in the alloy or increased consumption of such elements due to oxide fluxing reactions.

- Fluxing of protective oxide scales by either oxide-ion enriched (basic) or oxide-ion deficient (acidic) Na_2SO_4 melts.

- Sodium chloride in Na_2SO_4 initiates hot-corrosion attack by promoting mechanical failure of surface oxide scales which allows ash deposits to have intimate contact with the alloy surface.

It is important to note that at the present time no single mechanism can be accepted as a general mechanism for hot corrosion attack. In fact, it is reasonable to suggest that since these mechanisms have been derived from the studies involving a wide range of exposure conditions and a variety of alloys, all the mechanisms are relevant and the remaining problems are ones of elaborating on current mechanisms and describing conditions and circumstances where one of these mechanisms is the dominant means by which hot corrosion attack occurs.

3. PROBLEM TO BE STUDIED

Even though a substantial amount of work has been performed on the hot corrosion of cobalt-base alloys (ref. 1 and 17 to 21), no work appears to have been done which rigorously examines the mechanisms. There is ample evidence from experiments using burner rig tests to show that the commercial cobalt-base alloys are more resistant at temperatures on the order of 900°C than the commercial nickel-base alloys (ref. 19). A number of qualitative explanations have been proposed to account for this increased resistance; these include the higher chromium contents of commercial cobalt-base alloys and the higher melting point of the cobalt sulfide-cobalt metal eutectic. Results obtained at Pratt & Whitney Aircraft (P&WA) from burner rig tests with Ni-25Cr-6Al* and Co-25Cr-6Al alloys indicate that certain cobalt-base alloys out-performed nickel-base alloys even when these alloys contain the same amount of chromium. In addition these tests were performed at 980°C which is substantially above the melting point of the cobalt sulfide-cobalt metal eutectic of 880°C.

*All alloy compositions are given in weight percent unless noted otherwise.

Some laboratory tests have been performed on the hot corrosion of cobalt-base alloys (ref. 21). These studies were not sufficiently extensive, however, to produce anything other than qualititive results which showed that the behavior of cobalt and cobalt-chromium alloys in Na_2SO_4 under an oxidizing environment is essentially the same as that of nickel and nickel alloys.

The hot corrosion theory for nickel-base alloys is now at a stage where a number of reasonable mechanisms have been developed. At present, however, it must be concluded that the hot corrosion of cobalt-base alloys has not been studied in sufficient detail to suggest meaningful conclusions concerning their hot corrosion mechanisms. It could logically be speculated that the hot corrosion mechanisms for cobalt-base alloys should be similar to those for nickel-base alloys, but such speculation cannot account for the results of burner rig tests which show that most cobalt-base alloys have superior hot corrosion resistance compared to nickel-base alloys. It is therefore apparent that additional experimental studies on the hot corrosion of cobalt-base alloys are necessary. It is also apparent that these studies should include an appropriate amount of both laboratory and burner rig testing in order to resolve the problem as it now exists.

The objective of this program is to determine the reasons for the difference in the hot corrosion performance of cobalt-base and nickel-base alloys. The general plan of the program is to examine critically the hot corrosion of cobalt-base alloys by means of laboratory tests and to compare these results to those for nickel-base alloys which are already available (ref. 12). The laboratory tests will be performed under a variety of conditions in order to produce hot corrosion under conditions that may prevail in some burner rigs. After hot corrosion mechanisms have been developed from results obtained in the laboratory, some alloys will be tested in a burner rig. The results from rig and laboratory tests will be critically compared in order to describe the hot corrosion process as it occurs in a burner rig. The program is thus designed to determine the basic similarities and differences in the hot corrosion mechanisms of nickel- and cobalt-base alloys and also to determine if these differences can be used to account for the relative resistances of these alloys under rig or engine conditions.

This program will be concerned only with Na_2SO_4 deposits. This is not to imply that the effects produced by NaCl are not important. It is believed, however, that degradation induced by Na_2SO_4 must be thoroughly understood before the effects produced by NaCl, as well as other contaminants in Na_2SO_4, can be logically incorporated into the overall theory.

The program plan designed to determine the reasons for the differences in the hot corrosion performance of cobalt-base and nickel-base alloys is divided into seven sequential tasks. Task I involves obtaining alloys with optimum homogenity and microstructural consistency as well as thoroughly characterizing all alloys. Tasks II, III, IV, V, and VI involve normal oxidation, oxidation using Na_2SO_4, presulfidation followed by oxidation, oxidation using SO_2, hot-stage microscope and crucible experiments; these laboratory experiments will be performed on different alloys. Task II is concerned with determining if Na_2SO_4 produces accelerated oxidation of cobalt, and, if so, the mechanism involved. Task III involves determining the hot corrosion mechanism for Co-35Cr and Co-25Al alloys as well as comparing the effects produced by chromium and aluminum in cobalt- and nickel-base alloys.

Task IV involves determining if acidic hot corrosion can be induced in cobalt alloys by tungsten and comparing the effects produced by tungsten in cobalt- and nickel-base alloys. Task V involves comparing the hot corrosion mechanisms of Co-25Cr-6Al and Ni-25Cr-6Al alloys and determining the effect of yttrium on the hot corrosion of these alloys. Task VI involves a comparison of the effects produced by molybdenum, tantalum, and titanium on the hot corrosion of cobalt- and nickel-base alloys as well as fully characterizing the hot corrosion mechanisms of cobalt alloys. Task VII involves comparing results from burner rig and laboratory tests and using the results from the previous tasks to characterize the hot corrosion process in a burner rig. Most of the experiments are to be performed at 1000°C in one atm of oxygen or air, but some experiments will be performed at temperatures as low as 700°C so that the temperature dependence of the hot corrosion mechanisms may be examined.

SECTION II

EXPERIMENTAL

1. INTRODUCTION

In this program the Na_2SO_4-induced hot corrosion of fourteen alloys was studied by using a variety of techniques. In this section the materials used in this program will be described and the reasons for selecting such materials will be presented. The experimental procedures and tests that were used throughout this program will then be discussed.

2. MATERIALS

The fabrication procedures used for the preparation of each of the pure metals and alloys studied in this program are given in Table I, and the chemical compositions are given in Table II.

TABLE I

FABRICATION PROCEDURE

Alloy Designation	Arc Melted	Hot Rolled	Vapor Deposit	Anneal 48 h. @ 1000°C	Anneal 48 h. @ 1200°C
Co	X	X		X	
Co-25Al	X				X
Co-35Cr	X	X		X	
Co-25Al-12W	X				X
Co-25Cr-12W	X	X		X	
NiCrAl			X	X	
NiCrAlY			X	X	
CoCrAl			X	X	
CoCrAlY			X	X	
Co-25Cr-6Mo	X	X		X	
Co-25Al-6Mo	X				X
Co-25Cr-12ta	X	X		X	
Co-25Al-12ta	X				X
Co-25Cr-3Al-5ti	X	X		X	
Ni-30Cr*	X				X
Co-35Cr*	X				X
NiCrAl Y*	X		X**		
CoCrAl Y*	X		X**		

* Rig test specimens
** .005" Vapor Deposits

TABLE II

CHEMICAL ANALYSES OF ALLOY MATERIALS

Alloy Designation	Al W/O	Cr W/O	W W/O	Mo W/O	Ta W/O	Ti W/O	Y W/O
Co-25Al	24.68						
Co-35Cr		34.45					
Co-25Al-12W	24.1		11.7				
Co-25Cr-12W		24.6	11.7				
NiCrAl	6.8	21.4					
NiCrAlY	7.2	22.4					.24
CoCrAl	6.0	23.0					
CoCrAlY	6.1	22.1					.54
Co-25Cr-6Mo		24.8		6.0			
Co-25Al-6Mo	24.9			5.6			
Co-25Cr-12Ta		24.7			11.6		
Co-25Al-12Ta	24.7				12.1		
Co-25Cr-3Al-5Ti	2.84	24.6				4.9	

In most cases the initial stage of preparation involved nonconsumable arc melting of high purity alloy ingredients followed by the casting of the liquid alloys into ½ in x ¾ in x 3 in bars. Materials with sufficient ductility were subsequently hot rolled and annealed at 1000°C in vacuum. In cases where the alloys could not be hot rolled, the cast alloys were annealed at 1200°C in a vacuum. The NiCrAl(Y) and CoCrAl(Y) alloys were prepared by using electron beam vapor deposition. This process was used since it was observed that the time required to initiate degradation of NiCrAl specimens was dependent on specimen microstructure and specimens with vapor-deposited microstructures were more resistant to the initiation of the attack. Furthermore, in practice, overlay coatings of NiCrAlY and CoCrAlY are usually deposited on alloys by using vapor deposition. In the following each of the materials that were studied will be described in more detail.

The material selected, with which to begin the studies, was pure cobalt, the base element of most of the alloys to be studied. Metallographic examination of the annealed cobalt sheet

showed a dense, defect-free structure composed of equiaxed grains. This material was determined by spectrographic analysis to be 99.8% free of impurities.

The Co-25Al and Co-35Cr alloys were selected for a study of the effect of aluminum and chromium on the hot corrosion of cobalt. The compositions of these alloys were selected such that continuous layers of Al_2O_3 and Cr_2O_3 should be formed on the Co-25Al and Co-35Cr alloys, respectively. Metallographic examination of the annealed Co-25Al alloy showed a dense, single phase (β-CoAl) structure. The rolled and annealed Co-35Cr alloy was composed of a dense, equiaxed, two-phase structure, in particular, γ-cobalt and σ-phase.

The Co-25Al-12W and Co-25Cr-12W alloys were selected for a study of the effects of tungsten on the hot corrosion of cobalt alloys. Alloys with aluminum and chromium were used to consider cases where external scales of Al_2O_3 or Cr_2O_3 were developed on the alloys. A tungsten concentration of 12 W/O was used because this is typical of tungsten concentrations in many cobalt-base superalloys (e.g. Haynes 188, WI 52). By using the light microscope, X-ray diffraction and the electron beam microprobe it was determined that the Co-25Al-12W alloy was composed of two phases. The major phase was β-CoAl which contained about 7% W. The minor phase was an α-W precipitate. The Co-25Cr-12W alloy was composed of two phases. The major phase was a cobalt solid solution which contained about 29% Cr and 4% W. The second phase was present as particles of Co_2 (W, Cr) (Laves phase) containing about 25% W and 20% Cr.

The Co-25Cr-6Mo, Co-25Al-6Mo, Co-25Cr-12Ta and Co-25Al-12Ta, alloys were selected to permit a comparison of the effects produced by molybdenum and tantalum to those observed for tungsten during the hot corrosion of cobalt-base alloys. The compositions of the molybdenum and tantalum-containing alloys were chosen such that the atomic fractions of molybdenum and tantalum were approximately equivalent to that of tungsten in the previously described Co-Cr-W and Co-Al-W alloys. A Co-25Cr-3Al-5Ti alloy was also included in this group of alloys so that the effect of titanium on the hot corrosion of cobalt alloys could be examined. The composition of this titanium alloy was chosen such that titanium and aluminum were on an approximately equal atom fraction basis and when taken together were equivalent to 6% aluminum to permit a comparison with a Co-25Cr-6Al alloy. The Co-25Cr-6Mo alloy contained primarily the cobalt solid solution but a small amount of an unidentified second phase was observed. The Co-25Al-6Mo alloy was composed of two phases, namely, a major phase of β-CoAl and minor second phase particles of α-molybdenum. All the phases in the Co-25Cr-12Ta alloy were not identified. The alloy contained two phases of which the major phase was γ-cobalt solid solution. The Co-25Al-12Ta alloy was also composed of two phases. The major phase was believed to be β-CoAl. A small amount of an unidentified second phase was observed at grain boundaries of the alloy. The major phase and minor phases in the Co-25Cr-3Al-5Ti alloy were believed to be γ-cobalt solid solution and β-CoAl, respectively.

NiCrAl, NiCrAlY, CoCrAl and CoCrAlY alloys were prepared using the electron beam vapor deposition process to form thick (70 mils) coatings of the alloys on 3 in x 2 in x 1/8 in Inconel sheets. This process depends upon a continuous feeding of ingot at a rate consistent with the evaporation rate of the liquid to control the composition of the deposit. For example, an alloy ingot of composition X is fed upward through a water-cooled crucible. As the ingot

emerges at the top of the crucible, a high-powered, focused electron beam is played on the emerging end, causing local melting and forming a liquid pool contained by the walls of crucible and solid ingot below. Elements of higher vapor pressures begin to evaporate immediately, while those with lower vapor pressures are accumulated in the liquid pool and become more concentrated with time, leading to increased amounts of these elements in the vapor phase. Under constant conditions, the liquid inventory of composition Y will approach equilbrium with a gaseous phase of composition X. Normally, with a finite supply of alloy for the molten pool, the compositions X and Y would exist only momentarily. In this case, more ingot material of composition X is fed into the molten pool and at precisely the same rate as vapors of composition X leave the pool. The result is a condition in which all three phases are in equilbrium with each other and the composition of the resulting coating can be kept constant, provided the process is maintained under constant conditions. Thus, control of composition is accomplished mainly in the casting process used to produce the ingot feed stock. The inconel sheets were removed from the vapor-deposited alloys by surface grinding and the alloys were then annealed 48 hours at 1000°C in argon. The chemical analyses of the vapor-deposited alloys are presented in Table II.

The microstructure of both the NiCrAl and NiCrAlY alloys were composed of fine γ' (Ni_3Al) particles in a matrix of the γ phase (nickel solid solution). In addition an yttride phase was present in the γ-phase of the NiCrAlY alloys. Both the CoCrAl and CoCrAlY alloys contained β-phase (CoAl) in a matrix of the α-cobalt solid solution, and yttrides were present in the CoCrAlY alloy at the interfaces formed between the β and solid solution phases.

3. SPECIMEN PREPARATION

The specimens used in experiments except the dynamic burner rig tests had dimensions of approximately 1 cm x 1 cm 0.1 cm and were polished to a No. 600 grit finish. All specimens were cleaned ultrasonically in trichlorethylene, rinsed in alcohol, and dried.

4. DESCRIPTION OF EXPERIMENTS

The experiments performed to obtain data from which hot corrosion mechanisms could be developed consisted of oxidation, oxidation of Na_2SO_4-coated specimens, oxidation of presulfidized specimens, and oxidation in SO_2. In addition, the hot corrosion of Na_2SO_4-coated specimens was observed visually by means of a hot-stage microscope; motion pictures of important features were also obtained. Finally, crucible experiments were used to examine reactions involving Na_2SO_4 and oxides. Details of each of these types of experiments are presented in the following.

a. Oxidation Experiments

Isothermal oxidation experiments were performed using all of the alloys to describe the oxidation of these materials in the absence of Na_2SO_4. The oxidation kinetics were determined by continuous weight change versus time measurements using an Ainsworth type FV-AU-2 vacuum microbalance. Specimens were inserted into the bottom of an enclosed apparatus which consisted of the microbalance and a high-temperature Marshall furnace. After introduction of the desired gas environment, the specimens were raised from the

cold zone to the hot zone. To terminate an experiment, the reverse procedure was used. Specimens were raised to the hot zone of lowered to the cold zone in less than 15 seconds. A more detailed description of this apparatus has been previously presented (ref. 22). The oxidation experiments were performed at 1000°C and in 1 atm of oxygen; however, some experiments were performed at lower temperatures and lower oxygen pressures to obtain additional data for comparison with Na_2SO_4-coated specimens. The oxygen used in all the experiments was passed through a magnesium perchlorate drying agent before being introduced into the oxidation apparatus.

b. Oxidation of Specimens Coated with Na_2SO_4

Oxidation of specimens coated with Na_2SO_4 was performed in order to obtain data from which the effects of Na_2SO_4 on the oxidation reaction could be determined. The Na_2SO_4 was applied to specimens by air spraying preheated (150°C) coupons with a saturated aqueous solution using reagent grade Na_2SO_4.

Isothermal oxidation experiments using Na_2SO_4-coated specimens were performed at 1000°C in one atm of oxygen. A few experiments were also performed at lower temperatures and lower oxygen pressures. Weight change versus time measurements were obtained in an apparatus similar to that described for the oxidation experiments, but the balance used in these measurements was an Ainsworth type 14-CS-AU-2 vacuum semi-microbalance. Two different thicknesses, 0.5 and 5 mg/cm^2, of Na_2SO_4 were used in the isothermal oxidation experiments. The experiments were performed for a period of 20 hours. Experiments were also performed in which specimens coated with 0.5 mg/cm^2 were oxidized isothermally for two hours, cooled to room temperature, recoated with 0.5 mg/cm^2 Na_2SO_4, and reoxidized for two hours. This procedure was repeated to obtain a total of 20 hours at temperature.

Another type of Na_2SO_4 experiment was also performed. In this experiment, the specimens coated with the 5 mg/cm^2 Na_2SO_4 were initially heated to 1000°C in an argon atmosphere (one atm) for one hour. After one hour the argon was replaced with one atm of oxygen and the oxidation was continued for 20 hours. This type of experiment was used to determine if pretreating a Na_2SO_4-coated alloy in a very low oxygen activity would change the Na_2SO_4-induced oxidation behavior of the alloy.

c. Presulfidation Experiments

The purpose of the presulfidation experiments was to determine the effect of sulfur on the oxidation of the alloys. These experiments were performed in two steps using a quartz spring balance, the features of which have been described previously (ref. 23 and 24). In the first step, alloy coupons were treated in an H_2S-H_2 gas mixture at 1000°C to form sulfidized surface layers on specimens. In the second step, the presulfidized specimens were oxidized at 1000°C in one atm of oxygen and the oxidation kinetics were obtained.

Two different H_2S-H_2 gas mixtures were used to sulfidize the specimens. These mixtures had H_2S-H_2 ratios of 2×10^{-1} ($P_{S_2} = 2 \times 10^{-4}$ atm) and 2×10^{-3} ($P_{S_2} = 2 \times 10^{-8}$ atm) which established sulfur activities above and below that for the cobalt-cobalt sulfide equilibrium (i.e., $P_{S_2} = 2 \times 10^{-6}$ atm), respectively. Two sulfur activities were used to presulfidize

the specimens in order to determine if the presence of certain sulfide phases were more detrimental than others to subsequent oxidation.

d. Oxidation in SO_2

The purpose of the experiments using SO_2 was to examine the oxidation of the materials in an environment which was both oxidizing and sulfidizing. These experiments were performed at 1000°C in flowing SO_2, ($P_{S_2} = 2.8 \times 10^{-8}$ atm, $P_{O_2} = 5.6 \times 10^{-8}$ atm) and continuous weight change versus time data were obtained by using the quartz spring balance.

e. Hot Stage Microscopy

Hot stage microscopy was used to visually observe the hot corrosion of Na_2SO_4-coated specimens. This technique was found to be helpful in obtaining data from which a mechanism for the hot corrosion of nickel was developed (ref. 11). The hot-stage microscope consisted of a 500 ampere, D.C. power supply and a resistance-heated platinum stage. The specimens were observed with a stereo microscope at magnifications up to 50X. The heating stage allowed specimens with dimensions of 1 cm X 1 cm to be used, and the observations were therefore made over relatively large surface areas. The experiments were performed at 1000°C in air; however, occasionally oxygen or argon atmospheres were used.

Important features of the hot-corrosion process were occasionally documented and recorded for further study by taking motion pictures.

f. Crucible Experiments

The purpose of the crucible experiments was to characterize reactions which could occur between Na_2SO_4 and oxides. In these experiments, Na_2SO_4 was added to Al_2O_3 or platinum crucibles along with tablets of different oxides (i.e. CoO, NiO, Al_2O_3, Cr_2O_3) and heated in air at 1000°C for two hours. To determine if reaction had occurred between an oxide tablet and the Na_2SO_4, the weight change of the tablet was determined and the Na_2SO_4 was analyzed after the test for the presence of metal constituents of the oxide. In addition, experiments were also performed in which the Na_2SO_4 was preconditioned with additions of oxides (e.g., Na_2O, WO_3) which could exert an influence on the reaction between Na_2SO_4 and the oxide tablets.

g. Dynamic Burner Rig Tests

A schematic diagram of the dynamic burner rig test apparatus is shown in Figure 1a. For these tests the burner was operated on JET-A fuel and compressed air. Automatic flame temperature control was achieved by a feedback-controller system which operated on the outputs of four Pt-Rh thermocouples positioned in the transition duct. Actual flame temperature control was maintained by automatic adjustment of the fuel-to-air ratio. At a gas temperature of 1040°C the gas velocity at the 3-inch nozzle is approximately 460 ft/sec at a mass flow of 22.7 lbs/min.

Hot corrosion tests were performed by maintaining solid (uncooled) test specimens at 1000°C (in a flame controlled at approximately 1030°C). In addition, an aqueous solution of Na_2SO_4 was injected into the burner near the fuel nozzle in order to provide continuous deposition of Na_2SO_4 on the specimens throughout the test. The injection of Na_2SO_4 into the burner was adjusted to attempt to achieve a deposition rate of approximately 0.25 mg/cm^2 hr (i.e., 5 mg/cm^2 in 20 hours). Periodic measurements indicated apparent deposition rates averaging 0.10 mg/cm^2 hr.

The alloys tested in the burner rig were Ni-30Cr, Co-35Cr, Ni-25Cr-6Al-0.5Y, Ni-25Cr-6Al, Co-25Cr-6Al-0.5Y, and Co-25Cr-6Al. Ducted rig test specimens were fabricated by first arc-melting each alloy on a copper hearth, and then casting the melt into a ½ in diameter mold. The cylindrical bars were machined into the desired shape and size as indicated in Figure 1b. In order to obtain NiCrAl(Y) and CoCrAl(Y) test specimens with microstructures similar to those used in the laboratory hot corrosion testing, 0.005 in thick vapor-deposited overlay coatings of the same composition were applied to the cylindrical bars after final machining. The coated specimens were then annealed two hours at 1035°C, peened (17N) and annealed two more hours at 1080°C. Test specimens were usually exposed continuously in the ducted burner rig for a 20-hour period, after which the specimens were removed, water-washed, weighed and examined.

h. Examination of Oxidized Specimens

The specimens from all tests were examined by standard analytical techniques. These techniques included use of the light microscope, electron beam microprobe, scanning electron microscope, and X-ray diffraction.

SECTION III

RESULTS AND DISCUSSION

1. INTRODUCTION

The sequence in which the experimental work was performed has been described in Section 1-3. In presenting the results which were obtained from these experiments it is convenient to alter this sequence since the results obtained in the dynamic burner rig tests are helpful in describing the hot corrosion degradation processes and because the effects produced by molybdenum are similar to those observed for tungsten.

In the following the Na_2SO_4-induced hot corrosion of cobalt will be initially examined and then the effects of aluminum and of chromium in cobalt alloys will be considered. The influence of tungsten on the hot corrosion of cobalt-aluminum and cobalt-chromium alloys will then be discussed and the effects of molybdenum, tantalum and titanium in such alloys will be described. Finally, the hot corrosion of NiCrAl and CoCrAl alloys will be examined and compared.

2. SODIUM SULFATE INDUCED HOT CORROSION OF COBALT

a. Introduction

The experiments designed to study the Na_2SO_4-induced accelerated oxidation of cobalt were performed primarily at 1000°C and in 1 atm of oxygen or in air. However, some experiments were performed at 1000°C using oxygen pressures as low as 0.1 atm and at 900°C, 850°C and 825°C using air.

b. Experimental

(1) Oxidation: Duplicate specimens of cobalt were oxidized at 1000°C in 1 atm of oxygen. Continuous weight change as a function of time measurements are presented in Figure 2. The reproducibility between experiments is satisfactory. A parabolic rate constant of 2.4×10^{-8} (gm^2/cm^4-sec) was obtained from these data in satisfactory agreement with literature values (ref. 25). The structure of a typical specimen after 20 hours of oxidation is presented in Figure 3a. The outer portion of the scale is dense whereas the inner portion adjacent to the metal is porous. Some of these pores appear to result from pull-out during metallographic preparation. However, the oxide immediately adjacent to the substrate contained a regular network of fine pores that apparently were developed during oxidation. On cooling, the oxide usually fractured in this network as shown in Figure 3a. The outer portion of the oxide contained a precipitate which is believed to be Co_3O_4 (ref. 26). This precipitate delineated grain boundaries, and the outer portion of the oxide scale appeared to be composed of large columnar grains.

(2) Oxidation of Specimens Coated with Na_2SO_4: The oxidation kinetics for specimens coated with different amounts of Na_2SO_4 and oxidized at 1000°C in 1 atm of oxygen are compared to those for oxidation of cobalt without Na_2SO_4 in Figure 2. These

results show that the oxidation of Na_2SO_4-coated cobalt in 1 atm of oxygen is less than that for uncoated specimens. Such results are in contrast to that for nickel where the initial oxidation kinetics of Na_2SO_4-coated specimens are substantially greater than those for uncoated specimens (ref. 11).

The weight change versus time data obtained from the oxidation of Na_2SO_4-coated cobalt did not conform to the parabolic rate law. It was observed, however, that these data could be divided into two regions where the kinetics could be approximated by the parabolic rate law. The first region extended from the beginning of weight change versus time measurements to about 6 hours. The second region was observed between oxidation times of about 10 to 20 hours. The parabolic rate constants obtained from these two regions are presented in Table III.

TABLE III

PARABOLIC RATE CONSTANTS FOR THE OXIDATION OF Na_2SO_4-COATED COBALT AT 1000°C IN 1 ATM OXYGEN

Amount Na_2SO_4 (mg/cm^2)	K_{p1} (gm^2/cm^4-sec)	K_{p2} (gm^2/cm^4-sec)
0.0	2.4×10^{-8}	- - - -
0.5	9.2×10^{-9}	1.8×10^{-8}
0.7	5.0×10^{-9}	1.6×10^{-8}
4.3	1.5×10^{-9}	7.7×10^{-9}
4.4	3.5×10^{-9}	5.8×10^{-9}*

*Poor conformance to parabolic rate law.

The observed parabolic rate constants indicate that Na_2SO_4-coated cobalt initially is oxidized at a rate significantly slower than that for normal oxidation of cobalt. However with time, the oxidation rate increases and appears to approach that for normal oxidation. The structure of a Na_2SO_4-coated specimen after 20 hours of oxidation is presented in Figure 3b. The oxide layer is thinner than that for normal oxidation which is consistent with the weight change versus time measurements. The oxide scale contains less porosity than that observed for normal oxidation and no porous zone of oxide is observed immediately adjacent to the substrate. This condition may result because the scale is separated from the substrate by a thin layer of sulfide which is liquid at temperature as indicated by the arrows in Figure 3b. Electron-beam microprobe analysis showed this sulfide zone contained approximately 67.5% Co and by difference 32.5% S. Sodium analyses performed on the CoO scales that were removed from oxidized specimens of Na_2SO_4-coated and Na_2SO_4-free cobalt showed that significant quantities of sodium were in the CoO formed on the Na_2SO_4-coated specimens. For example, one w/o of sodium was found in the oxide of Na_2SO_4-coated specimens compared to less than 0.02 w/o in the CoO formed by oxidation in the absence of Na_2SO_4.

Results obtained from visual observation of the oxidation of Na_2SO_4-coated cobalt specimens with a hot stage microscope, which will be discussed in detail subsequently, showed the oxidation of such specimens was dependent on oxygen pressure. In Figure 4, the surfaces of Na_2SO_4-coated specimens after oxidation in air and in 1 atm oxygen are compared to that for oxidation of cobalt without Na_2SO_4 in air. The surface of the Na_2SO_4-coated specimen that was oxidized in air is similar to that of nickel which has undergone Na_2SO_4-induced accelerated oxidation. A photograph showing the surface of such a nickel specimen is also included in Figure 4 for comparison. In view of these observations, the oxidation kinetics for Na_2SO_4-coated and Na_2SO_4-free cobalt were obtained at 1000°C in 0.1 atm of oxygen. The weight change versus time measurements from these experiments are presented in Figure 5, where it can be seen that the Na_2SO_4-coated specimens exhibited larger weight gains than the Na_2SO_4-free specimen. A surface photograph as well as a transverse section of a Na_2SO_4-coated specimen after oxidation in 0.1 atm of oxygen are shown in Figure 6. It is obvious that a nonprotective scale developed in numerous areas and accelerated oxidation has occurred.

The oxidation kinetics for cyclically (2-hour cycles) oxidized Na_2SO_4-coated (0.5 mg/cm^2 per cycle) specimens at 1000°C in 1 atm of oxygen were not significantly different from the isothermal data presented in Figure 2. In addition, the microstructures of specimens from the cyclic tests were essentially the same as those for isothermal tests in 1 atm of oxygen.

The Na_2SO_4-coated specimens that were annealed in argon at 1000°C prior to oxidation generally lost weight during the annealing treatment. For example after one hour at 1000°C a weight loss of 1.5 mg/cm^2 was observed which may be compared to a value of less than 0.1 mg/cm^2 for vaporization of Na_2SO_4 from platinum in argon. In addition, microprobe examination of the Na_2SO_4 remaining on the specimen surface after the preanneal showed that a substantial amount of cobalt had apparently dissolved or reacted with the Na_2SO_4 as shown in Figure 7. Oxidation of the argon preannealed specimens in 1 atm of oxygen produced oxidation kinetics and microstructures not significantly different from those obtained with Na_2SO_4-coated specimens that had not been annealed in argon.

(3) Oxidation of Presulfidized Specimens: Specimens of cobalt were presulfidized at 1000°C by heating in an $H_2S/H_2 = 0.2$ for 20 seconds. Typical specimens gained about 6 mg/cm^2 of sulfur as a result of this treatment. The kinetics obtained upon oxidizing such presulfidized specimens in flowing oxygen at 1000°C are compared to those for oxidation of cobalt in Figure 8. These results show that the presulfidized specimens have oxidation rates very similar to those for untreated cobalt. In addition, as shown in Figure 9, a relatively dense layer of CoO formed on such specimens above the sulfide zone.

(4) Oxidation in SO_2: Experiments performed with cobalt in flowing SO_2 at 1000°C also showed no evidence of accelerated oxidation of cobalt. The oxidation kinetics for specimens oxidized in SO_2 did not conform to any simple rate law but the weight gains of such specimens were only about 25% of those for oxidation of cobalt in 1 atm of oxygen at equivalent times. More importantly, a dense protective layer of CoO was observed on these specimens above a zone of cobalt sulfide as shown in Figure 10. These results show

rather conclusively that the formation of cobalt sulfide concomitantly with CoO need not result in the formation of a nonprotective CoO scale on cobalt.

(5) Hot Stage Microscopy: As mentioned previously, visual examination of Na_2SO_4-coated specimens during oxidation at 1000°C in air using a hot stage microscope showed that Na_2SO_4 induced accelerated oxidation of cobalt. Examination of the oxidation of numerous specimens in this manner as well as the study of motion pictures taken during oxidation of such specimens showed the following sequence of events during Na_2SO_4-induced accelerated oxidation of cobalt. Upon heating to 1000°C, an oxide scale formed beneath the Na_2SO_4. This scale was visible before and after the Na_2SO_4 melted. At times ranging from 2 to 5 minutes after the Na_2SO_4 melted, initiation of the attack occurred as the Na_2SO_4 penetrated the oxide scale in localized areas and spread laterally beneath the oxide scale. Subsequent to the initial penetration and stripping of the oxide layer, the detached oxide layer was observed to move upward, away from the metal surface in a manner suggesting the successive stripping of additional layers of newly-formed oxide. Evolution of a gas from the Na_2SO_4 beneath the detached oxide was also evident. For times beyond approximately 10 to 15 minutes, no further indications of surface activity were visible. Photographs are presented in Figure 11 which show the features that are developed on cobalt specimens as a result of the localized penetration and stripping of the protective oxide scales by the Na_2SO_4.

Photographs which show some of the morphological features developed during the initial stages of hot corrosion of cobalt are presented in Figures 12 and 13. The Na_2SO_4 was observed to form puddles on the oxide-covered specimen surface. An oxide slag was usually suspended in the puddles of Na_2SO_4, Figure 12a. At locations on the specimen surface where puddles of Na_2SO_4 were not evident, the oxide was covered with a thin layer of Na_2SO_4.

There was a definite difference between the morphology of the oxide beneath puddles and beneath the thin layers of Na_2SO_4 as shown in Figure 13b. Beneath the puddles the oxide grains were deeply dished whereas beneath the thin layer of Na_2SO_4 the oxide grains were only slightly dished and covered with needles. In addition these features were different from those observed for oxidation of specimens without Na_2SO_4, Figure 12c. Holes in the oxide were observed in both types of regions on the Na_2SO_4-coated specimens as shown in Figures 13a and 13b, and no cracks were evident near these eruptions. Moreover, where protrusions were not evident on the oxide, the oxide beneath the puddle of Na_2SO_4 contained deep depressions, Figure 13c, and the oxide beneath the thin layer of Na_2SO_4 had holes at grain boundaries Figure 13d. It is believed that all these data indicate that reaction between the CoO and the Na_2SO_4 does occur and that cracks are not required to have penetration of the oxide by the Na_2SO_4. Metallographic examination of transverse sections through specimens from the hot stage experiments showed that the oxide scale was frequently composed of layers of oxide as shown in Figure 14a.

Photographs to show that the Na_2SO_4 spreads laterally beneath the oxide from the localized sites of penetration are difficult to obtain. This difficulty arises because the oxide layer is thin and usually becomes detached from the metal during cooling even in those areas where the oxide was firmly attached to the metal during oxidation. In experiments

which were performed to determine whether or not presulfidized specimens would undergo more severe hot corrosion than cobalt specimens with no sulfur, however, photographs showing that Na_2SO_4 spreads beneath the oxide layer were obtained. A substantial difference between the hot corrosion of cobalt and presulfidized cobalt was not observed in these experiments. It was observed, however, that the oxide layer which formed on the top of the sulfide layer during heating to temperature wrinkled and cracked as the temperature of the specimens reached the melting point of the sulfide. To avoid this condition, a presulfidized specimen was heated to 1000°C in a hot stage microscope and allowed to oxidize 90 seconds in air, after which a crystal of Na_2SO_4 was placed on the surface of the specimen. Penetration of this oxide layer was observed and the specimen was rapidly cooled to room temperature. A photograph showing the microstructure of this specimen is presented in Figure 15a. This photograph and the X-ray images presented in Figures 15b and 15c are further confirmation that Na_2SO_4 strips or detaches the oxide layer after penetration of the oxide has occurred.

It is worth noting that visual observations of the oxidation at 1000°C in air of Na_2SO_4-coated nickel did not reveal localized penetration of an oxide scale by the Na_2SO_4 (ref. 11). In the case of nickel, the Na_2SO_4 was observed to melt and almost immediately an oxide film was observed to be floating on the Na_2SO_4. However, some of the microstructural features of the scale forming during the hot corrosion of nickel do suggest stripping of the scale as shown in Figure 14b. It therefore appears that Na_2SO_4 accelerates the oxidation of nickel by a mechanism similar to that of cobalt, in particular, by penetrating and stripping, successively, thin layers of protective oxide. However, in the case of nickel the oxide is more easily penetrated by the Na_2SO_4 perhaps because of the slower growth rate of NiO compared to CoO. To further examine this supposition, nickel specimens were preoxidized at 1000°C in air for periods of 10 minutes and 2 hours. The thickness of the NiO after 2 hours of oxidation was approximately the same as that of CoO developed on cobalt after 1 minute of oxidation in 1 atm of oxygen. Sodium sulfate quickly penetrated the NiO on the specimen that was preoxidized for ten minutes and accelerated oxidation occurred. The Na_2SO_4 did not penetrate the NiO on the specimen with the 2-hour preoxidation and no evidence of accelerated oxidation was observed.

(6) Crucible Experiments: To determine if the penetration of CoO scales by Na_2SO_4 could occur due to reaction between CoO and Na_2SO_4, flakes of CoO were immersed in Na_2SO_4 contained in a platinum crucible and heated in air at 1000°C. The CoO flakes were produced by oxidizing cobalt coupons at 1000°C in 1 atm of oxygen for 65 hours. The oxide scales were cleaved from these specimens and then subsequently annealed in air for 8 hours at 1000°C. The CoO was observed to lose weight during the first two hours of this crucible test after which no subsequent weight losses were observed. In addition, etching of the CoO surface was observed and chemical analysis of the Na_2SO_4 showed that cobalt was present in the Na_2SO_4. These results show that CoO reacts with Na_2SO_4. Similar experiments using NiO did not indicate any reaction between the NiO and the Na_2SO_4 had occurred. Results from similar experiments but with 1 w/o Na_2O added to the Na_2SO_4, indicated that both CoO and NiO reacted with the Na_2SO_4 melt.

The nature of the reaction between CoO and Na_2SO_4 is not clearly understood. It has been suggested previously (ref. 11) that excess oxide ions in Na_2SO_4 react with NiO to form

NiO_2^{2-}. It is proposed that CoO_2^{2-} is formed during reaction between CoO and the excess oxide ions in Na_2SO_4.

(7) Effects Produced by Temperature: In this program emphasis was placed on studies performed at 1000°C. In order to determine if the results obtained at 1000°C were generally valid at other temperatures, some experiments were also performed at 900°C and 825°C. Examination of the hot corrosion of Na_2SO_4-coated specimens at 900°C in air with the hot stage microscope showed the attack was identical to that observed at 1000°C.

Experiments performed with the hot stage microscope at 825°C in air using Na_2SO_4-coated cobalt showed that the Na_2SO_4 melted in localized areas even though the melting point of Na_2SO_4 is 883°C. No melting of the Na_2SO_4 was observed when Na_2SO_4-coated CoO tablets were heated to 825°C which shows that the localized melting must occur as a result of a reaction between the Na_2SO_4 and the cobalt substrate. Even though localized melting of the Na_2SO_4 on cobalt specimens was observed at 825°C, the liquid Na_2SO_4 was not observed to penetrate the scale which formed on the metal. These scales were not layered as observed at 1000°C but rather contained particles of cobalt sulfide in a matrix of cobalt oxide.

c. Interpretation of Results

The significant results obtained from the work with cobalt are summarized below:

- Sodium sulfate can cause accelerated oxidation of cobalt at 1000°C.
- At this temperature the accelerated oxidation occurs by localized penetration and stripping of the protective oxide scale.
- At this temperature the penetration of protective scales by liquid Na_2SO_4 is dependent on oxygen pressure; apparently penetration is favored by lower oxygen pressures.
- At 1000°C and at an oxygen pressure at which Na_2SO_4 does not induce accelerated oxidation of cobalt, thermal cycling of specimens does not induce accelerated oxidation.
- At 1000°C neither preformed sulfide zones on cobalt nor the introduction of sulfur into cobalt concomitantly with oxidation causes increased oxidation.
- Cobaltous oxide does react with Na_2SO_4 at 1000°C and this reaction is more extensive when Na_2O is added to the Na_2SO_4.
- Limited work at temperatures below 1000°C in air indicates that penetration of the scale along with detachment of the scales does occur at temperatures as low as 900°C.

- At temperatures below the melting point of Na_2SO_4 localized melting of the Na_2SO_4 had been observed at temperatures as low as 825°C, and reaction between the liquid Na_2SO_4 and the oxide layer does occur but not to the extent that the Na_2SO_4 penetrates the oxide layer.

The results can be used to develop a model for the hot corrosion of cobalt. Previous work (ref. 11) has shown that the construction of stability diagrams similar to the Pourbaix diagrams used in aqueous corrosion are useful in describing hot corrosion mechanisms. Such a diagram for cobalt is presented in Figure 16. The procedures as well as the assumptions used to construct such a diagram have been described (ref. 11). One feature of this diagram must be emphasized. The diagram defines phases that can coexist with Na_2SO_4. Sodium sulfate is therefore stable in all regions of the diagram and its composition is defined by the oxygen and SO_3 pressure scales on the diagram.

In order to use the diagram presented in Figure 16 to develop a model for the Na_2SO_4-induced accelerated oxidation of cobalt, it is necessary to select the pressures of oxygen and SO_3 which define the composition of the Na_2SO_4 prior to its reaction with cobalt. As discussed previously (ref. 11), oxygen and SO_3 pressures of 1 and 3×10^{-5}, respectively, are believed to be representative values to define the composition of the as-deposited Na_2SO_4. This composition is indicated in Figure 16 by the symbol X.

Upon heating a Na_2SO_4-coated specimen of cobalt to a temperature of 900°C or above, a continuous layer of CoO forms on the specimen before the Na_2SO_4 melts as indicated schematically in Figure 17a. When the Na_2SO_4 melts, an oxygen gradient is established across the Na_2SO_4 layer as a result of removal of oxygen from the Na_2SO_4 by the growing CoO scale. Removal of oxygen from the Na_2SO_4 causes the composition of the Na_2SO_4 at the CoO-Na_2SO_4 interface to be changed in the direction indicated by the arrows in Figure 16, and, as can be seen in this figure, conditions can be developed whereby the sulfur activity in the Na_2SO_4 is sufficient to form cobalt sulfide, especially in the metal beneath the CoO layer where the oxygen activity is relatively low. In Figure 16 it is also apparent that removal of oxygen from the Na_2SO_4 also causes the SO_2 pressure to be increased, and pressures close to 1 atm can be developed. The experimental results show that sulfur is removed from the Na_2SO_4 by the metal (see Figure 3b) and by SO_2 evolution. Removal of sulfur from the Na_2SO_4 will, in turn, cause the oxide ion (i.e.O^{2-}) concentration of the Na_2SO_4 to be increased. It is proposed that the resulting oxide ions react with the CoO to form CoO_2^{2-} ions which diffuse towards the Na_2SO_4/gas interface and decompose into CoO particles and oxide ions near this interface on account of the lower oxide ion concentration in this region of the Na_2SO_4. It is also proposed as indicated in Figure 17b that the reaction between oxide ions in the Na_2SO_4 and the CoO is more pronounced at certain sites along the CoO/Na_2SO_4 interface. Eventually the Na_2SO_4 penetrates the CoO layer in certain areas and then spreads laterally beneath it as indicated in Figure 17c. This lateral spreading of the Na_2SO_4 may occur by a fluxing reaction involving the formation of CoO_2^{2-} ions since conditions are ideal for the production of oxide ions when the Na_2SO_4 penetrates the scale and comes into contact with the metal.

After the initial CoO layer has been detached by the Na_2SO_4, the excess oxide ions produced by sulfur entering the metal are consumed by reaction with CoO and conditions become favorable for the formation of CoO on the metal. Consequently another layer of CoO is formed and eventually stripped by the same process as was the initial layer of CoO as shown in Figure 17d. This repetitive stripping action of the protective CoO by the Na_2SO_4 results in rapid oxidation of the metal. During this process the concentrations of oxide ions and CoO_2^{2-} ions in all of the Na_2SO_4 is gradually increasing. This condition causes the sulfur activity to decrease even when the oxygen activity of the Na_2SO_4 is low. Eventually sulfur no longer leaves the Na_2SO_4 to enter the metal, oxide ions are no longer produced, and the CoO is no longer stripped from the metal surface. Consequently the accelerated oxidation is no longer prevalent unless additional Na_2SO_4 is deposited on the specimen surface. The hot corrosion induced by Na_2SO_4 is therefore not self sustaining. Reising (ref. 27) proposed that as the thicknesses of nonprotective scales are increased, the Na_2SO_4 is largely in the porous scale rather than on the metal surface, and accelerated attack therefore stops. This condition is another reason for the absence of self-sustaining degradation.

It is necessary to note that the observed more severe hot corrosion at the edges of specimens is not inconsistent with the proposed model. It is now becoming apparent that during the oxidation of many metals and alloys even in the absence of Na_2SO_4, localized regions of separation are developed between oxide layers and the substrates (ref. 28). Moreover such conditions have been observed to be more extensive at the edges of specimens and at polishing marks on specimen surfaces. It therefore appears that the penetration of the oxide layer on cobalt does not have any preference for particular locations, but once penetration has been accomplished, stresses generated at specimen edges and polishing marks cause larger amounts of the oxide layer to become detached. The concept of rendering successive layers of CoO nonprotective as a result of the penetration and stripping action of Na_2SO_4 is also consistent with the observation that small amounts of Na_2SO_4 can cause much larger amounts of non-protective oxide to be formed. As pointed out by Reising et al (ref. 27), the molar ratio of nonprotective oxide (e.g. NiO, CoO) to Na_2SO_4 deposited on specimen surfaces is commonly between 10 and 100. It is obvious that all the nonprotective oxide cannot be formed due to fluxing of the oxide by oxide ions in the Na_2SO_4. In the localized penetration and stripping model, however, large amounts of oxide become nonprotective through the reaction of oxide ions with a small amount of oxide. For example, if it is assumed that a localized penetration of 5μ in diameter causes detachment of an oxide layer, with a thickness of 3μ, over an area of 10^4 square microns, Figures 11a and c, then the molar ratio of nonprotective oxide to the available Na_2SO_4 is about 3 for a specimen coated with 1 mg/cm^2 of Na_2SO_4. Moreover, the number of moles of oxide ions required to form the hole is at least 2 orders of magnitude less than the number of moles of oxide ions available in the Na_2SO_4 over 10^4 square microns. Consequently, the stripping process can occur numerous times and therefore produce large amounts of nonprotective oxide compared to the amounts of Na_2SO_4 deposited on the metal surface.

At temperatures below the melting point of Na_2SO_4 (883°C), accelerated attack of cobalt by a mechanism similar to that described for temperatures above the melting point

of Na_2SO_4 probably can occur. This is the case since it appears that the Na_2SO_4 composition can be modified due to reaction with cobalt whereby a lower melting phase is developed. At 825°C the modified Na_2SO_4 did not penetrate the CoO layer but the observed etch pits in the oxide indicated that localized, partial penetration of the CoO had occurred. It was also observed, however, that many more sulfides had been formed in the oxide layer at the lower temperatures. It has not been established that this condition causes accelerated oxidation but it must be considered an undesirable situation, which could result in increased oxidation along with or in place of the penetration and stripping mechanism.

The localized penetration and stripping of protective CoO by an oxide ion-enriched (basic) Na_2SO_4 melt is believed to be consistent with all the experimental data obtained in the present studies. The following remarks are offered to account for some of the results which may not appear to be consistent with the model.

- Sodium sulfate-induced accelerated oxidation was not observed at 1000°C in 1 atm of oxygen because the CoO layer formed prior to melting of the Na_2SO_4 was too thick to be penetrated by the Na_2SO_4. Transport of oxygen through the Na_2SO_4 deposit may be an important factor in achieving such a condition.

- The oxidation rate of Na_2SO_4-coated specimens which did not exhibit accelerated oxidation at 1000°C was less than that for oxidation of Na_2SO_4-free cobalt because sodium from the Na_2SO_4 was incorporated into the CoO scale which decreased the vacancy concentration of the CoO and thereby the growth rate of the scale.

- Cyclic oxidation of Na_2SO_4-coated specimens at 1000°C in 1 atm of oxygen did not result in accelerated oxidation because, even if the CoO cracks on cooling, a sufficiently thick layer of CoO forms on reheating to prevent penetration of the scale by the Na_2SO_4.

- Accelerated oxidation of the argon-preannealed specimens did not occur in 1 atm of oxygen at 1000°C because during the annealing treatment a sufficient amount of CoO was available to react with the oxide ions formed by sulfur entering the metal and by SO_2 evolution; conditions were therefore established whereby, upon subsequent oxidation, oxide ions were not produced in the Na_2SO_4.

- Neither presulfidized and subsequently oxidized specimens nor specimens oxidized in SO_2 exhibited accelerated oxidation because the introduction of sulfur into cobalt did not cause increased oxidation.

The mechanism that has been proposed for the hot corrosion of cobalt is very similar to that which has been proposed for nickel (ref. 11). The main difference between the models is that stripping of layers of oxide was not proposed for nickel, and all the accelerated attack was assumed to occur by the formation and decomposition of NiO_2^{2-} ions

at the NiO/Na_2SO_4 and Na_2SO_4/gas interfaces, respectively. In view of the results that have been obtained in the present studies with cobalt, it is now believed that stripping of NiO layers also occurs during the hot corrosion of nickel. It is therefore proposed that the mechanisms of Na_2SO_4-induced accelerated oxidation of cobalt and nickel are the same. The NiO scales on nickel are more susceptible to penetration by Na_2SO_4 than CoO on cobalt perhaps because the slower growth rate of NiO compared to CoO results in thinner NiO oxide barriers. A crucial feature of the Na_2SO_4-induced hot corrosion of both cobalt and nickel is the reduction of the oxygen pressure in the melt by these metals. Oxygen transport through the Na_2SO_4 from the gas is therefore of great importance. More rapid transport of oxygen through Na_2SO_4 contaminated with cobalt compared with melts contaminated with nickel could also result in a greater susceptibility of NiO to penetration by the liquid Na_2SO_4 (ref. 29).

3. SODIUM SULFATE INDUCED HOT CORROSION OF Co-25Al AND Co-35Cr ALLOYS

a. Introduction

The purpose of the studies using Co-25Al and Co-35Cr specimens was to examine the effect of aluminum and chromium on the Na_2SO_4-induced hot corrosion of cobalt. To achieve such an objective, it is desirable to use alloys with a range of aluminum and chromium compositions. In the interest of conservation, it was decided to first study the hot corrosion of Co-25Al and Co-35Cr alloys and then examine other alloy compositions as required to account for the effects produced by aluminum and chromium. In the following, results obtained from studies using Co-25Al and Co-35Cr will be presented and discussed. Results will then be presented from studies using other binary alloys and other tests to further describe the effects produced by aluminum and by chromium in cobalt- and nickel-base alloys. Finally, all the results will be used to attempt to describe the hot corrosion of binary cobalt and nickel base alloys containing either aluminum or chromium.

b. Co-25Al

The experiments designed to study the Na_2SO_4-induced accelerated oxidation of Co-25Al were performed at 1000°C using 1 atm of oxygen.

(1) Oxidation: Duplicate specimens of Co-25Al were oxidized at 1000°C in 1 atm of oxygen. Typical weight change data as a function of time are presented in Figure 18. The weight change versus time data as well as visual, metallographic and X-ray diffraction analyses of the oxidized specimens showed that an external, continuous layer of Al_2O_3 was formed on this alloy after a short transient period of oxidation during which some localized CoO and spinel phases were formed. The surfaces of the oxidized specimens from which the Al_2O_3 scale spalled during cooling were found to be extremely uneven. Studies concerned with the adhesion of Al_2O_3 to nickel- and cobalt-base alloys have shown that surfaces with such a topology are developed due to separation between the Al_2O_3 scale and the substrate at localized sites during oxidation (ref. 28).

(2) Oxidation of Specimens Coated with Na_2SO_4: Results from weight change versus time measurements for the isothermal oxidation of Na_2SO_4-coated Co-25Al specimens at 1000°C in 1 atm of oxygen are compared to those obtained with Na_2SO_4-free specimens in Figure 18. These results show that the thicker Na_2SO_4 coatings (i.e., 5 mg/cm^2 Na_2SO_4) induced accelerated oxidation of the Co-25Al alloy. Prior to the onset of this increased oxidation, however, an incubation period is evident during which the oxidation rate appears to be slower than that for oxidation of the Na_2SO_4-free specimens. The oxidation kinetics for the specimen coated with the thinner layer of Na_2SO_4 (i.e., 0.6 mg/cm^2 Na_2SO_4) indicate that accelerated oxidation has not occurred.

Metallographic examination of the oxidized specimens that had been coated with about 5 mg/cm^2 of Na_2SO_4 was consistent with the weight change versus time measurements. A photograph of a transverse section through the specimen which had undergone accelerated oxidation is presented in Figure 19. The oxide scale formed on this specimen contained CoO and $CoAl_2O_4$ in addition to Al_2O_3. Sulfide particles were also present in the alloy beneath the oxide layer. The microstructures of the specimens with the thinner coatings of Na_2SO_4, for which the weight change data indicated that accelerated oxidation had not occurred, were not similar to those obtained upon oxidizing Na_2SO_4-free specimens. The microstructures of these former specimens had much larger aluminum-depleted zones than those of the Na_2SO_4-free specimens. In addition, sulfide particles were present in the alloy in localized areas.

To determine if sulfur had entered the alloy prior to the onset of accelerated oxidation, specimens of Co-25Al were coated with Na_2SO_4, oxidized in 1 atm of oxygen at 1000°C for different times, and the sulfur concentration in the alloys after water washing was determined. The aluminum content of the Na_2SO_4 was also determined by analyzing the wash water. In addition, the oxidation kinetics of all of these specimens were determined to insure that accelerated oxidation had not occurred. The results from these analyses are presented in Table IV. These results show that sulfur from the Na_2SO_4 does enter the alloy prior to the onset of accelerated oxidation. A significant amount of aluminum was not detected in the Na_2SO_4.

Cyclic oxidation of Na_2SO_4-coated specimens at 1000°C, where the specimens were cycled to room temperature every 2 hours and a fresh deposit of Na_2SO_4 was applied (0.5 mg/cm^2), always caused more severe degradation than isothermal oxidation of Na_2SO_4-coated specimens or cyclic oxidation of Na_2SO_4-free specimens. Metallographic examination of the Na_2SO_4-coated specimens after the cyclic tests showed that a thick oxide scale containing Al_2O_3, CoO and spinel had been formed. Sulfide particles were evident in the alloy.

Weight change versus time measurements obtained for the oxidation of Na_2SO_4-coated specimens that had been annealed 1 hour in argon prior to oxidation showed that accelerated oxidation had occurred. However, this accelerated oxidation was evident from the beginning of the weight change measurements. No incubation period prior to the onset of accelerated oxidation was evident. The microstructural features of the argon-annealed and subsequently oxidized Na_2SO_4-coated specimens were the same as those previously described for the accelerated oxidation of Na_2SO_4-coated specimens which had not been annealed.

TABLE IV

SULFATE, SULFUR, AND ALUMINUM ANALYSES OF Na_2SO_4-COATED Co-25Al AFTER OXIDATION AT 1000°C IN 1 ATM OXYGEN*

Oxidation Time (min)	Amount Na_2SO_4 mg/cm^2 Initial	Final	Sulfur in Alloy (μg/cm^2)	Aluminum in Leach Water mg/cm^2
0	4.9	4.5	16	0.004
5	5.1	1.8	77	0.004
60	6.0	1.3	73	0.004
240	4.7	1.1	149	0.004

*Accelerated oxidation was not observed for any of the specimens used in these analyses.

(3) Oxidation of Presulfidized Specimens: The weight change versus time measurements that were obtained from the oxidation (1000°C, 1 atm oxygen) of presulfidized specimens were not meaningful since sulfur was removed from these specimens during oxidation via the formation of SO_2. Consequently, the weight changes of the specimens were influnced not only by oxide formation but also by sulfur loss. Sulfur dioxide was detected in the effluent gas in the experiments using specimens that had been presulfidized in either the low ($H_2S/H_2 = 2 \times 10^{-3}$) or the high ($H_2S/H_2 = 0.2$) ratio H_2S-H_2 gas mixture. The fact that sulfur was oxidized during oxidation of the presulfidized specimens indicates that protective oxide scales were not formed on these alloys, thus allowing access of oxygen to the sulfur-enriched substrate. Metallographic examination of the presulfidized and oxidized specimens confirmed that protective Al_2O_3 scales had not been formed on these specimens as shown in Figure 20. In addition, X-ray diffraction analyses of the scales from these specimens showed that the scales contained Al_2O_3, CoO and spinel.

The results obtained from the oxidation of presulfidized Co-25Al show that the introduction of sulfur into this alloy can result in conditions whereby subsequent oxidation takes place at increased rates compared to those for oxidation of sulfur-free specimens.

(4) Oxidation in SO_2: The oxidation kinetics for Co-25Al in flowing SO_2 at 1000°C did not conform to any simple rate law. During the first 6 hours the weight gains of specimens were about the same as that for oxidation of this alloy in 1 atm of oxygen and metallographic examination of oxidized specimens as well as X-ray diffraction analyses of spalled scales showed that external scales of Al_2O_3 had formed during oxidation in SO_2. For times beyond 6 hours, the weight gains of specimens oxidized in SO_2 were about 2 to 3 times greater than that for specimens oxidized in 1 atm of oxygen. A typical microstructure of Co-25 Al oxidized 16 hours in flowing SO_2 is shown in Figure 21. A relatively thick oxide

has been formed on this specimen and sulfide particles are evident in the alloy substrate. X-ray diffraction analysis identified Al_2O_3 and CoO in the scale removed from the specimen that was oxidized 16 hours, and Al_2O_3, CoO and spinel in the scale removed from the specimen that was oxidized 22 hours.

The results obtained from the experiments in SO_2 are not sufficient to describe the oxidation of Co-25 Al in SO_2. These results do show, however, that after about 16 hours continuous layers of Al_2O_3 are not found on this alloy during oxidation in an environment containing both oxygen and sulfur.

(5) Hot Stage Microscopy: The oxidation of Na_2SO_4-coated specimens of Co-25 Al was studied at 1000°C in both 1 atm of oxygen and air by using the hot stage microscope. No significant difference was observed between experiments performed in 1 atm of oxygen or air. Evidence of Na_2SO_4-induced accelerated oxidation of Co-25Al was consistently observed with the hot stage microscope. When a Na_2SO_4-coated specimen was heated the Na_2SO_4 was observed to melt and an oxide scale, identified by X-ray diffraction analysis as Al_2O_3, was observed to develop on the alloy beneath the Na_2SO_4. In about 2 to 5 minutes after the Na_2SO_4 had melted, although occasionally longer times were required, it was observed that the Na_2SO_4 penetrated the Al_2O_3 in localized areas and then spread laterally beneath this layer of oxide as had been observed for the Na_2SO_4-induced accelerated oxidation of cobalt. After stripping of the initial layer of Al_2O_3 by the Na_2SO_4, numerous areas of the alloy surface were observed to contain a black oxide which was identified as CoO. A photograph showing a transverse section through a specimen from the hot stage experiments is shown in Figure 22.

The results from studies with the hot stage microscope and the oxidation kinetics for isothermal oxidation both show that an incubation period occurs prior to the onset of Na_2SO_4-induced accelerated oxidation of Co-25Al. In general, the length of the incubation period as determined from the oxidation kinetics was on the order of hours whereas it was on the order of minutes based on the observation with the hot stage microscope. Comparison of specimens from both tests showed that accelerated oxidation did occur more quickly in the apparatus used for the hot stage microscope than in the apparatus used to obtain weight-change versus time data. It is believed that specimens are heated to 1000°C in a shorter time in the former apparatus and therefore thinner oxide layers are developed on such specimens prior to melting of the Na_2SO_4 which in turn may result in shorter incubation times.

(6) Crucible Experiments: To determine if a reaction occurred between Al_2O_3 and Na_2SO_4, a single crystal tablet of Al_2O_3 was placed in a platinum crucible containing Na_2SO_4 and the crucible was heated for 2 hours at 1000°C in air. No detectable weight change was observed in the Al_2O_3 after the Na_2SO_4 had been removed by washing with hot water. When this experiment was repeated with Na_2SO_4 that contained 1% Na_2O, the Al_2O_3 tablet lost weight and aluminum was detected in the Na_2SO_4. These results show that as the activity of Na_2O in Na_2SO_4 is increased, reaction between the Na_2SO_4 and the Al_2O_3 can occur.

(7) Summary of Important Results: The studies involving the oxidation of Na_2SO_4-coated Co-25Al at 1000°C have produced the following significant results:

- Sodium sulfate induces accelerated oxidation of Co-25Al.
- Sodium sulfate-induced accelerated oxidation of Co-25Al occurs by localized penetration of the Al_2O_3 scale formed on this alloy followed by lateral spreading of the Na_2SO_4 beneath the oxide scale.
- There is an induction or incubation period prior to the onset of Na_2SO_4-induced accelerated oxidation of Co-25Al.
- The duration of the incubation period is controlled by the time required for the Na_2SO_4 to penetrate the Al_2O_3 scale.
- The incubation period is not present during oxidation of argon-preannealed specimens.
- The oxidation rate of the alloy during the incubation period appears to be slower than that for the oxidation of Na_2SO_4-free Co-25Al.
- The accelerated oxidation of Co-25Al becomes more severe as the amount of the Na_2SO_4 deposit is increased.
- Cyclic oxidation of Co-25Al causes the Na_2SO_4-induced attack to become more severe.
- The introduction of sulfur into Co-25Al prior to or concomitant with oxidation causes increased oxidation of this alloy.
- During the incubation period sulfur from the Na_2SO_4 does enter the alloy.
- As the Na_2O component of the Na_2SO_4 is increased, reaction between Na_2SO_4 and Al_2O_3 does occur.

(8) Mechanism for the Na_2SO_4-Induced Hot Corrosion of Co-25Al: The results that have been obtained show that the mechanism of Na_2SO_4-induced accelerated oxidation for Co-25Al is similar in some respects to that for cobalt and nickel. In particular, in all three cases the Na_2SO_4 eventually penetrates the oxide scales and strips them from the substrate surfaces. In the case of the Co-25Al alloy, after penetration of the Al_2O_3 scale by the Na_2SO_4 sulfides are formed in this alloy which subsequently result in more severe oxidation. No apparent deleterious effects from sulfide formation have been observed for the hot corrosion of cobalt or nickel.

In the mechanism that has been proposed for cobalt, it appears that initial

penetration must be caused by reaction of CoO with oxide ions in the Na_2SO_4. A stability diagram similar to the one for cobalt can be used to show the phases of aluminum which are stable in Na_2SO_4. Such a diagram is presented in Figure 23. The features of this diagram that are of importance to the present discussion are that Al_2O_3 is stable in the as-deposited Na_2SO_4 but as oxygen is removed from the Na_2SO_4 by the alloy, conditions will be developed which are favorable for sulfur to enter the alloy with the attendant formation of oxide ions in the Na_2SO_4. It therefore appears that penetration of the Al_2O_3 scale by the Na_2SO_4 must be caused by sulfur entering the alloy or by the production of oxide ions in the Na_2SO_4 which react with the Al_2O_3 scale. This supposition is supported by the results which show penetration of the Al_2O_3 by the Na_2SO_4 is favored by an argon preanneal or by thicker Na_2SO_4 deposits since both of these conditions can be expected to establish higher sulfur activities in the Na_2SO_4 as well as higher oxide ion concentrations when the sulfur enters the alloy. For example, the oxygen activity at the alloy/Na_2SO_4 interface should be less than that in the gas because oxygen must diffuse through the layer of Na_2SO_4. It is believed that the oxidation rate of the alloy during the incubation period is less than that for oxidation of the Na_2SO_4-free alloy because the lower oxygen pressure established at this interface shortens the transient period of oxidation that Co-25Al undergoes prior to the formation of a continuous Al_2O_3 scale. The argon preanneal or thicker layers of Na_2SO_4 should cause the oxygen activity at the alloy/Na_2SO_4 interface, or the oxide/Na_2SO_4 interface when the oxide layer develops, to be decreased with an attendant increase in the sulfur activity.

The mechanism by which oxide ions in the Na_2SO_4 could cause penetration of the scale is similar to that which has already been proposed for cobalt. The oxide ions would react with the Al_2O_3 to form aluminate ions in the Na_2SO_4. The observed lack of aluminum in the Na_2SO_4 during the incubation period, as determined by the chemical analyses presented in Table IV, does not mean that aluminate ions or some complex ion of aluminum had not been formed. The sensitivity of the analysis may have been too low.

The introduction of sulfur into the substrate could also result in penetration of the oxide layer by the Na_2SO_4. Kear (ref. 30) has observed the segregation of sulfur to grain boundaries of alloys with attendant deterioration of the creep strength of such materials and he has suggested the accumulation of sulfur at the Al_2O_3/substrate interface may decrease the adhesion of Al_2O_3 to the alloy. It therefore is possible that the introduction of sulfur into the alloy by the Na_2SO_4 causes substantially more separation between the oxide and the alloy to be developed than would normally occur in the absence of Na_2SO_4. Such a condition could eventually result in the development of cracks in the Al_2O_3 scale and thereby allow the Na_2SO_4 to penetrate the scale. Of course it is also possible that cracks are present in the Al_2O_3 scale even without any effects produced by sulfur.

In an attempt to determine whether sulfur, oxide ions or preexisting cracks had caused penetration of the Al_2O_3, experiments using the hot stage microscope were performed at 1000°C in air using Na_2SO_4-coated Co-25Al where Cr_2O_3 particles were added to the Na_2SO_4. The addition of Cr_2O_3 to Na_2SO_4 should cause the oxide ion concentration of the Na_2SO_4 to be decreased and the sulfur activity of the Na_2SO_4 to be

increased. Such a condition would therefore be expected to inhibit penetration of the scale via reaction of oxide ions, promote penetration due to effects caused by sulfur, and to have no effect if penetration occurs via preexisting cracks. Upon heating several of these specimens to 1000°C, the Na_2SO_4 was observed to melt and become yellow due to the formation of chromate ions in the Na_2SO_4. Penetration of the scale was not observed after ten minutes of oxidation. The results of these experiments indicate that penetration of the Al_2O_3 scale is caused by a reaction involving oxide ions.

The results that have been obtained for the Na_2SO_4-induced accelerated oxidation of Co-25Al are applicable to a temperature of 1000°C. Hot corrosion of this alloy at lower temperatures can be expected to be initiated by localized penetration of the oxide scale by the Na_2SO_4 as long as a liquid Na_2SO_4 phase is developed on the alloy surface. Finally, it should be emphasized, that while penetration of the Al_2O_3 barrier is proposed to occur as a result of reaction between the barrier and oxide ions in the Na_2SO_4, the formation of sulfides in the alloy also results in increased oxidation after the protective barrier has been destroyed. It has been observed that protective barriers of Al_2O_3 are not formed on aluminum sulfide during oxidation (ref. 24). It appears that the Al_2O_3 scales which develop on aluminum sulfide during oxidation may be in tension in view of the molar volumes of the oxide and sulfide. Such a condition may cause the Al_2O_3 to be nonprotective.

c. Co-35Cr

Oxidation experiments with Co-35Cr at 1000°C in one atm of oxygen produced results which showed that a continuous layer of Cr_2O_3 was not formed on this alloy under such experimental conditions. It was found, however, that continuous external Cr_2O_3 scales were developed on this alloy during oxidation at 1000°C in 0.1 atm of oxygen. One of the objectives of this program is to compare the influence of Na_2SO_4 on the oxidation of cobalt-base alloys upon which Al_2O_3 and Cr_2O_3 scales are stable; therefore, the Co-35Cr alloy was tested in all experiments at 1000°C in 0.1 atm of oxygen unless noted otherwise.

(1) Oxidation: Typical weight change versus time measurements obtained from the oxidation of Co-35Cr at 1000°C in 0.1 atm of oxygen are presented in Figure 24. These data conformed to a parabolic rate law after approximately two hours of oxidation. A parabolic rate constant of 2.5×10^{-11} gm^2/cm^4-sec was obtained from these data which is similar to that for the growth of Cr_2O_3 on a Ni-30Cr alloy under similar conditions (ref. 31). Metallographic examination of oxidized Co-35Cr specimens showed that a continuous external layer of Cr_2O_3 had been formed on this alloy.

(2) Oxidation of Specimens Coated with Na_2SO_4: The oxidation kinetics in 0.1 atm of oxygen for Na_2SO_4-coated (5 mg/cm^2) and Na_2SO_4-free Co-35Cr specimens are compared in Figure 24. The initial weight gains for the Na_2SO_4-coated specimens are slightly greater than those for the specimen without Na_2SO_4. The subsequent weight losses of the Na_2SO_4-coated specimens show that vaporization of Na_2SO_4, as well as reactions between Cr_2O_3 and Na_2SO_4 to form volatile products are also occurring along with oxidation of the alloy. The oxidation kinetics for specimens coated with 0.5 mg/cm^2

of Na_2SO_4 were similar to those for 5 mg/cm^2. However, the initial weight gains were not significantly different from those of the Na_2SO_4-free specimen, and the subsequent weight losses were smaller than those for specimens coated with 5 mg/cm^2 of Na_2SO_4.

Comparison of the microstructures of oxidized specimens showed that thicker oxide scales had been formed on the Na_2SO_4-coated specimens than on Na_2SO_4-free specimens. This condition was especially obvious on specimens coated with 5 mg/cm^2 of Na_2SO_4, as shown in Figure 25. Electron beam microprobe analysis of the oxide scale formed on the Na_2SO_4-coated specimen showed that the inner portion of the scale was Cr_2O_3 whereas the outer portion contained a substantial amount of cobalt in addition to chromium. In comparison, a significant amount of cobalt in the scale formed on the Na_2SO_4-free specimen was not obvious. These results show that Na_2SO_4 accelerated the oxidation of Co-35Cr by prolonging the transient period of oxidation during which a continuous layer of Cr_2O_3 is being developed.

The results obtained from cyclic oxidation of Na_2SO_4-coated specimens in 0.1 atm of oxygen did not differ significantly from those obtained in the isothermal experiments. The weight changes as a function of time were similar to those presented in Figure 24 for Na_2SO_4-coated specimens. In addition, the microstructures were similar to that presented in Figure 25b.

In Figure 26, weight change versus time data obtained from the oxidation of Na_2SO_4-coated specimens that had been annealed in argon for one hour prior to oxidation are compared to data for a specimen that had not been annealed as well as to data for oxidation of a Na_2SO_4-free specimen. This comparison shows that the initial weight gains of the preannealed specimens are greater than those for both the unannealed and Na_2SO_4-free specimens. Metallographic examination of the Na_2SO_4-coated specimens after the argon anneal showed that more severe oxidation had occurred at some areas over the specimen surfaces than others, as shown by the surface photograph in Figure 27a. A photograph which shows the oxide and alloy microstructure in an area of severe attack is presented in Figure 27b. A relatively thick and apparently porous oxide scale has been formed on the alloy above a zone of chromium sulfide. In the areas of less severe attack, numerous sulfides were visible in the substrate but the oxide layer was substantially thinner than that on the specimen shown in Figure 27. Subsequent oxidation of the preannealed specimens did not produce microstructures significantly different from that shown in Figure 27. It was apparent, however, that a continuous Cr_2O_3 layer was not developed on this alloy. The significance of the results obtained from the oxidation of preannealed specimens is that by establishing a low oxygen activity over the surface of the Na_2SO_4-coated alloy more severe degradation of the alloy by the Na_2SO_4 has occurred.

(3) Oxidation of Presulfidized Specimens: In order to analyze the effluent gas for SO_2, the oxidation of presulfidized Co-35Cr specimens was performed in flowing oxygen at 1000°C. Specimens of Co-35Cr that had been presulfidized in the low ratio H_2S-H_2 gas mixture (i.e., $H_2S/H_2 = 2 \times 10^{-3}$), gained about 3 mg/cm^2 over about a three-hour period. Metallographic examination of these presulfidized specimens showed that a continuous sulfide layer had been formed on the surfaces of the specimens. Sulfide

particles were also observed in the alloy beneath the external sulfide layer. Weight change versus time data obtained for oxidation of presulfidized Co-35Cr in flowing oxygen are compared to that for oxidation of this alloy with no pretreatment in Figure 28. The weight gains as a function of time for the presulfidized alloy were less than that for the specimen with no pretreatment. These results show that during the annealing treatment chromium in the alloy diffused to the surface to form a chromium-rich sulfide layer and that during subsequent oxidation a protective layer of Cr_2O_3 formed on the sulfide layer. This condition was substantiated by metallographic examination as well as by the observation that no SO_2 was detected in the exiting gas after about four minutes of oxidation. The presulfidized alloy specimen oxidized at a slower rate than the specimen without a treatment since a continuous layer of Cr_2O_3 is not developed on the latter specimen during oxidation in one atm of oxygen.

Problems were encountered when attempts were made to oxidize specimens that had been presulfidized in the high H_2S/H_2 ratio (i.e., $H_2S/H_2 = 0.2$). A large amount of sulfides was formed (e.g., $\Delta M/A = 7$ mg/cm^2 after one minute of pretreatment), and these sulfide layers partially spalled from the specimen upon being transferred from the apparatus used to sulfidize specimens to the one used for oxidation. Therefore, it was not possible to obtain oxidation kinetics for such presulfidized specimens. However, during the oxidation of specimens for which some of the sulfide layer still remained on the specimen surface, SO_2 was detected in the exiting gas for oxidation times as long as 20 hours. These results indicate that protective oxide scales are not formed during oxidation of the specimens presulfidized in the H_2S-H_2 mixture with the high H_2S/H_2 ratio.

(4) Oxidation in SO_2: The weight change versus time data obtained from the oxidation of Co-35Cr in SO_2 were difficult to interpret since it was found that both sulfide and oxide phases were being formed simultaneously. Even though much of the scales spalled from the specimens on cooling, it was determined that these scales were at least an order of magnitude thicker than those formed on Co-35Cr during oxidation for equivalent times in 0.1 atm of oxygen. In addition, X-ray diffraction analyses of the spalled scale showed that a substantial amount of CoO had been formed. The mechanism by which Co-35Cr is oxidized in SO_2 is not understood, but the important point is that this alloy has been oxidized much more severely than if oxidation had been performed in oxygen at a pressure equivalent to that established by the dissociation of SO_2 (i.e., $\sim 10^{-7}$ atm); therefore, sulfur must have influenced the oxidation of this alloy.

(5) Hot Stage Microscopy: Visual examination of the oxidation of Na_2SO_4-coated specimens in air at 1000°C with the hot stage showed that this alloy was not severely attacked. The Na_2SO_4 was observed to melt and turn yellow due to the formation of chromate ions as a result of the reaction between the Na_2SO_4 and the oxide scale which had formed on the alloy beneath the Na_2SO_4. No penetration of the oxide scale by the Na_2SO_4 was observed. Metallographic examination of specimens from these experiments showed microstructures similar to those for Na_2SO_4-coated specimens which had been oxidized in 0.1 atm of oxygen.

(6) Crucible Experiments: Tablets of Cr_2O_3 were heated in air for two hours at 1000°C in a platinum crucible containing Na_2SO_4. The tablet was found to have lost

0.1 mg/cm^2 of weight after this treatment. Visual examination of the Cr_2O_3 tablet after this test also showed that reaction had occurred with the Na_2SO_4 since the surface of the tablet was etched. When a similar experiment was performed using Na_2SO_4 containing one percent Na_2O, a weight loss of 5.1 mg/cm^2 was observed. These results show that Na_2SO_4 reacts with Cr_2O_3 and the reaction is increased as the Na_2O component of Na_2SO_4 is increased.

To examine the amount of reaction between Na_2SO_4 and the Cr_2O_3 formed on Co-35Cr during oxidation at 1000°C in 0.1 atm of oxygen, Na_2SO_4-coated specimens were oxidized for various time intervals and the chromium content of the Na_2SO_4 remaining on the surface was determined. Analyses also were performed to determine the amount of sulfur that had entered the alloy from the Na_2SO_4. These results are presented in Table V.

The results presented in Table V show that Na_2SO_4 remains on the specimen surface for up to eight hours, sulfur from the Na_2SO_4 enters the alloy, and chromium is present in the Na_2SO_4 melt. It is worth noting that the amount of chromium in the Na_2SO_4 on the Co-35Cr specimen after one hour (i.e., 0.3 mg/cm^2) is greater than the weight loss of the Cr_2O_3 tablet in the crucible test using Na_2SO_4 (i.e., 0.1 mg/cm^2) even though this latter weight loss also includes oxygen. This indicates that more reaction has occurred in the former case due to the production of oxide ions in the Na_2SO_4 as a result of sulfur from the Na_2SO_4 entering the alloy or being evolved as SO_2.

TABLE V

SULFATE, SULFUR, AND CHROMIUM ANALYSES OF Na_2SO_4-COATED Co-35Cr AFTER OXIDATION AT 1000°C IN 0.1 ATM OXYGEN

Oxidation Time (min)	Amount Na_2SO_4 mg/cm^2		Sulfur in Alloy μg/cm^2	Chromium in Leach Water mg/cm^2
	Initial	Final		
0	5.4	5.3	5	0.0005
5	4.2	2.7	6	0.03
30	4.5	2.6	14	0.04
60	4.5	3.7	56	0.32
480	4.1	2.4	91	0.41

(7) Summary of Important Results: The studies involving the oxidation of Na_2SO_4-coated Co-35Cr at 1000°C have produced the following significant results:

- Sodium sulfate causes the oxidation of Co-35Cr to be increased but this condition exists only during the initial stages of oxidation during which a Cr_2O_3 barrier is being developed.

- The introduction of sulfur into Co-35Cr can cause accelerated oxidation; such effects, however, appear to be confined to situations where sulfur activities sufficient to form cobalt sulfide on pure cobalt are developed over this alloy.

- During the oxidation of Na_2SO_4-coated Co-35Cr specimens a continuous barrier of Cr_2O_3 is developed on this alloy, but prior to and after the formation of this barrier, sulfur is being added to the alloy and chromium is dissolving into the Na_2SO_4.

(8) Mechanism for the Na_2SO_4-Induced Hot Corrosion of Co-35Cr: The accelerated oxidation of Na_2SO_4-coated Co-35Cr occurs because the Na_2SO_4 deposit increases the transient period of oxidation during which a continuous layer of Cr_2O_3 is being developed on this alloy. It has been observed that some of the chromium from the alloy does react with the Na_2SO_4. It has also been observed that sulfur from the Na_2SO_4 does enter the alloy. Both of these conditions can be expected to have adverse effects on the development of a continuous barrier of Cr_2O_3 on the alloy. The accelerated oxidation that occurred on the Co-35Cr alloy is not severe because, even with a Na_2SO_4 deposit, the alloy eventually becomes covered with a continuous layer of Cr_2O_3. For alloys with chromium concentrations lower than 35%, an even longer transient oxidation time is to be expected before a continuous layer of Cr_2O_3 is formed when a deposit of Na_2SO_4 is present. When chromium concentrations in the starting alloy are sufficiently low, a Na_2SO_4 deposit can cause a dramatic increase in the oxidation rate because the oxidation rate would be controlled by transport through CoO when Na_2SO_4 is present as opposed to transport through Cr_2O_3 on the Na_2SO_4-free specimens.

There are important differences between the mechanisms by which Na_2SO_4 causes increased oxidation of Co-25Al and Co-35Cr. In the case of Co-25Al, a protective barrier of Al_2O_3 is developed, but this barrier is eventually rendered nonprotective through the localized penetration and stripping action of the Na_2SO_4. In the case of Co-35Cr, the Na_2SO_4 inhibits the initial development of the Cr_2O_3 barrier, but once this barrier is developed it is essentially unaffected by the Na_2SO_4. This difference between Al_2O_3 and Cr_2O_3 scales will be discussed in more detail subsequently. At this point it is sufficient to note that the reaction of Cr_2O_3 with Na_2SO_4 is dependent on oxygen pressure whereas the Al_2O_3 reaction is not. Chromium reacts with Na_2SO_4 initially but the amount of this reaction can become less as the oxygen activity gradient is established across the Na_2SO_4. In the case of Al_2O_3, the amount of the reaction can only increase as the oxygen gradient is developed across the Na_2SO_4.

d. Comparison of Nickel and Cobalt Base Systems Containing Aluminum or Chromium

In using laboratory tests to compare the hot corrosion of alloys, it is desirable to use a test which gives comparative results similar to those that may be obtained in practice. On the other hand, to examine certain features of the hot corrosion process it may be appropriate to use a test which establishes conditions that are widely different from those believed to be present in practice.

The conditions (i.e., gas composition, temperature) which exist in gas turbines during operation are just beginning to be defined. Recent studies (ref. 32) concerned with dynamic gas - temperature measurements in a gas turbine transition duct exit have shown surface temperature fluctuations exceeding 15°C take place about once every second. Techniques to determine the fluctuations in gas composition are not currently available. Gas composition measurements are extremely difficult to perform because of the low residence times associated with gas turbine combustion chambers (e.g. 5-10 millisec.) (ref. 33) and calculations which assume equilibrium conditions must be used to obtain approximate descriptions of the gas environment (ref. 34). While a substantial effort should be made to describe the conditions which exist in a gas turbine, it is obvious that at present any experiments which begin to simulate the conditions in gas turbines, such as those using a dynamic combustion burner rig, will suffer from poorly defined experimental conditions. It was therefore decided to develop a laboratory test that at least contained some of the features which may prevail in a gas turbine while still retaining definition of experimental conditions.

Tschinkel (ref. 34) has shown the equilibrium flame gas in a turbine operating at temperatures up to 1200°C contains primarily nitrogen and oxygen in a ratio not substantially different from that for air. Service experience with gas turbines has shown that hot corrosion is usually observed when salts or ash are deposited on hardware. The compositions of these deposits are dependent upon the operating conditions of the particular gas turbine. In most instances, however, such deposits contain Na,Ca and sulfate. In turbines which operate in marine environments, chloride has been detected but at concentrations substantially less than that of sulfate. It is reasonable to suppose therefore that a laboratory test should include periodic applications of Na_2SO_4 and the gas may be air. This test should also include thermal cycling of specimens. The frequency of these cycles cannot be as high as those observed experimentally (ref. 32) but cycles with larger amplitudes and lower frequencies should afford a means to include the effects produced by cracking and spalling of oxides in the test.

The hot corrosion test that was developed consisted of cyclic oxidation in air. Specimens were automatically cycled between the test temperature and room temperature once every hour (50 minutes in furnace hot zone, 10 minutes air cool). The specimens were suspended on platinum wire and were moved to and from the vertical furnace by using a pneumatic cylinder and an electronic timer. The hot zone of the furnace was three inches in length which allowed twelve specimens to be tested simultaneously. The hot zone temperature was controlled to better than ±2 C. Controlled amounts of reagent grade Na_2SO_4 were applied to the specimens periodically. Prior to applying fresh Na_2SO_4, the specimens

were washed with distilled water, weighed and examined visually. Fresh Na_2SO_4 was usually applied every 20 cycles. More frequent applications of Na_2SO_4 were used when weight change data or visual examinations were considered to be necessary at less than 20 cycles. Weight change versus time data obtained from cyclic hot corrosion testing of Co-25Al and Ni-25Al alloys at 1000°C are presented in Figure 29. These data illustrate what may be considered a limitation of the test, in particular, some specimens lose weight as a result of spalling of the oxidation products whereas the oxidation products do not spall from others. This condition could be eliminated by removing all of the oxidation products prior to weighing the specimens. Such a procedure is not always appropriate, however since it is often desirable to retain as much of the oxidation products as possible for metallographic examination. In this test either large weight gains or losses indicate severe degradation but metallographic examination is always necessary to substantiate such a condition.

The data presented in Figure 29 as well as the microstructures presented in Figure 30 show that severe hot corrosion of both Co-25Al and Ni-25Al has occurred. This hot corrosion degradation occurs sooner for specimens coated with 5 mg/cm^2 Na_2SO_4 than 0.5 mg/cm^2. It is worth noting that 0.5 mg/cm^2 of Na_2SO_4 did not produce a significant amount of accelerated oxidation of these two alloys under isothermal conditions. The results obtained from this cyclic hot corrosion test and results presented previously indicate the Na_2SO_4-induced hot corrosion of these alloys at 1000°C occurs as follows. Deposits of Na_2SO_4 penetrate* the Al_2O_3 scales which are formed on these two alloys. This penetration occurs due to reaction between oxide ions in the Na_2SO_4 and the Al_2O_3 (basic fluxing) . Once penetration of the Al_2O_3 by the Na_2SO_4 has been achieved, either due to basic fluxing or cracking of the Al_2O_3 under the influence of thermally induced stresses, the Na_2SO_4 spreads laterally beneath the Al_2O_3 scale and particles of aluminum sulfide are developed within the alloy. Subsequent oxidation proceeds at an increased rate since the aluminum which is combined with sulfur in the alloy is not used effectively to form a protective layer of Al_2O_3. This situation continues indefinitely under conditions where the alloys are exposed continuously to thermal cycles and fresh deposits of Na_2SO_4. Severe oxidation of these two alloys therefore ensues. It must be emphasized that basic fluxing of the Al_2O_3 by oxide ions in the Na_2SO_4 does cause accelerated oxidation. Nevertheless, when these alloys are exposed continuously to thermally induced stresses and fresh deposits of Na_2SO_4, the hot corrosion degradation occurs because of the formation of a deleterious sulfide in the alloys. Finally, it should also be noted that no significant difference has been observed between the rates or mechanisms for Na_2SO_4-induced hot corrosion of Co-25Al and Ni-25Al.

Weight change versus time data obtained for the laboratory cyclic hot corrosion testing of Ni-30Cr and Co-35Cr are compared in Figure 31. Data are also included in this Figure for the cyclic oxidation of these alloys without Na_2SO_4 as well as for oxidation in the dynamic burner rig. There is not a significant difference between the weight losses of these two alloys in the cyclic hot corrosion test. Moreover, cyclic oxidation without Na_2SO_4 has caused about the same weight losses as cyclic oxidation with Na_2SO_4. In the cyclic test, with or without Na_2SO_4, a continuous barrier of Cr_2O_3 was formed on both the Ni-30Cr and Co-35Cr alloys, Figure 32. The weight losses observed for these two alloys in the burner rig were substantially greater than those of the laboratory test, Figure 31.

*Deposits of Na_2SO_4 exceeding 0.5 mg/cm^2 are required for penetration of the Al_2O_3 under isothermal conditions.

The leading edges of the specimens from the burner rig were always more severely attacked than the trailing edges as shown in Figure 33. The microstructure of these alloys at the trailing edge, Figure 33b, was not unlike that observed after testing these alloys in the laboratory cyclic hot corrosion test, Figure 32. The microstructures of the leading edges of specimens from the burner rig were significantly different from those for the laboratory test, Figure 33a. For example, leading edge microstructures contained virtually continuous zones of sulfides beneath the oxide scale, and it was apparent that preferential oxidation of these sulfides was responsible for the severe degradation.

The results obtained from the cyclic hot corrosion tests show that hot corrosion behavior of Ni-30Cr and Co-35Cr are very much the same. Both alloys repeatedly form continuous barriers of Cr_2O_3, even in the presence of Na_2SO_4 deposits and thermally induced stress. The more severe degradation of the leading edges of specimens of these alloys in the burner rig is believed to have been caused by the high gas velocity in this test. Previous studies (ref. 35) have shown that alloys with Cr_2O_3 scales are more severely degraded in high velocity dynamic oxidation tests than in laboratory furnace tests, whereas alloys with Al_2O_3 scales exhibited about the same amount of degradation in both tests. This acceleration in the oxidation rate has been attributed to an enhanced loss of chromium from the alloy owing to more rapid volatization of CrO_3 from the scale in the dynamic environment than is experienced in static atmospheres. If the more severe degradation is caused by loss of chromium it would be expected that similar microstructures could be developed in the laboratory tests by testing specimens of Ni-30Cr and Co-35Cr for sufficiently long periods of time. Another procedure would be to test an alloy with a lower chromium concentration in the cyclic tests. A photograph showing the microstructure developed in a Ni-10Cr alloy after cyclic hot corrosion testing is presented in Figure 34. Very severe attack has occurred. Liquid nickel sulfide is evident and discontinuous Cr_2O_3 is associated with the nickel sulfide. These results show that after Cr_2O_3 scales are no longer formed on Ni-Cr and Co-Cr alloys, very severe hot corrosion takes place supposedly because of the formation and oxidation of liquid sulfide phases.

The hot corrosion tests which have been performed on the nickel and cobalt base alloys were such that relatively thin layers of Na_2SO_4 were present on the surface of the specimens. Such conditions do not permit an examination of the reactions that may be taking place between the alloy and the melt because the amount of Na_2SO_4 is so small. To attempt to examine the alloy-Na_2SO_4 reactions, alloys were placed in platinum crucibles that contained about 1 gram of Na_2SO_4. The specimen geometry was such that the specimen extended from the melt but that portion which extended from the melt was covered with a thin layer of Na_2SO_4 due to the wetting action of the melt as indicated in Figure 35. The weight changes observed after 2 hours in this test for a number of Ni-Cr, Ni-Al, Co-Cr and Co-Al alloys are presented in Table VI. Since the specimens were water-washed and dried prior to weighing, weight changes differing by less than a few milligrams are not considered significant because the oxidation products spalled in varying degrees.

Table VI

WEIGHT CHANGE AFTER 2 HOURS IN CRUCIBLE TEST AT 900°C IN AIR

Alloy	$\Delta m/A$ (mg/cm^2)
Ni	1.4
Ni-6Al	38
Ni-14Al	261
Ni-31Al	0.1
Ni-5Cr	0.5
Ni-10Cr	0.09
Ni-30Cr	0.0
Co-10Al	-0.10
Co-25Al	-0.13
Co-20Cr	-0.24
Co-30Cr	-0.06

The only alloys which have apparently undergone severe attack are Ni-6Al and Ni-14Al. These results were confirmed by metallographic examination. Protective barriers of either NiO, Al_2O_3, CoO or Cr_2O_3 were evident on the alloys that had undergone small weight changes whereas extremely thick scales such as those shown in Figure 36 were observed in specimens exhibiting large weight increases. Examination of these thick reaction products with the electron probe showed that the part of the scale immediately adjacent to the Na_2SO_4 contained globules of liquid nickel sulfide, Figure 37, whereas the scale immediately adjacent to the alloy contained metallic nickel particles in a matrix containing Na, S, O and Al, Figure 38. These results indicate that some nickel-aluminum alloys can react extensively with large quantities of Na_2SO_4. Such reactions may also occur with smaller amounts of Na_2SO_4, but evidence for these reactions may be difficult to detect.

The results obtained with the crucible partial immersion tests can be more logically discussed by using stability diagrams. The stability diagram presented in Figure 39 shows the phases of nickel and aluminum that can be stable in Na_2SO_4. It is to be noted that NiO was apparently not stable in the reaction product that was formed on the Ni-14Al specimen. This indicates that the oxygen pressure in the Na_2SO_4 has been reduced such that nickel sulfide and Al_2O_3 are the stable phases in the reaction product as indicated in Figure 39. Such a condition is especially favorable for the production of oxide ions since sulfur and oxygen are rapidly removed from the Na_2SO_4 by the nickel and aluminum respectively. The oxide ions along with oxygen from the Na_2SO_4 can therefore react with aluminum in the alloy to form aluminate ions which are soluble in the Na_2SO_4, Figure 39. A situation is therefore developed whereby the Na_2SO_4 enriched in oxide ions literally selectively dissolves the aluminum from the alloys. The aluminum content of the alloy is critical to this process. When the aluminum concentration is high, the surface of the alloy becomes covered with Al_2O_3 which prevents further reaction of the alloy with the melt. When the aluminum content is low, the oxygen activity may not be reduced to the level at which NiO is not stable and therefore a liquid sulfide is not formed whereby sulfur is rapidly removed from the melt.

Stability diagrams can also be used to account for the results obtained with the Ni-Cr alloys in the modified crucible tests. As can be seen in Figure 40, much larger oxide ion activities are required to react with Cr_2O_3 than Al_2O_3 at low oxygen pressure. Even though NiO may not be stable, the Cr_2O_3 will not as readily react with the Na_2SO_4.

In the case of the cobalt base alloys, Figure 41, it is to be noted that lower oxygen activities are required to prevent the formation of CoO, and solid rather than liquid sulfides may be formed when the oxygen pressure is reduced to levels where CoO is not stable. Both of these conditions will inhibit reaction between cobalt base alloys and the Na_2SO_4. Finally it should be emphasized that depletion of the melt of oxygen is a critical requirement for the severe degradation. Any elements which increase transport of oxygen through the Na_2SO_4 will therefore inhibit the onset of the catastrophic degradation or prevent it from ever occurring. Chromium, and as mentioned previously cobalt (ref. 29) may increase the transport of oxygen through the Na_2SO_4.

In summary the addition of aluminum or chromium to nickel or cobalt improves the isothermal hot corrosion resistance provided the concentrations of these elements are sufficient to form continuous barriers of either Al_2O_3 or Cr_2O_3. Nickel-base alloys which contain insufficient aluminum can become severely degraded via a basic fluxing process since the formation of discontinuous Al_2O_3 causes the oxygen activity to be reduced below that required to form NiO and aluminum is selectively leached from alloys by the Na_2SO_4. Such conditions are evidently not established in cobalt-aluminum nor nickel-chromium alloys. It appears as though cobalt-base systems are not susceptible to this type of degradation because lower oxygen activities are necessary to prevent the formation of CoO. Even if such oxygen activities could be developed for cobalt-base systems, solid sulfides are formed rather than liquid sulfides, and this inhibits the production of the oxide ions required to leach the aluminum. Chromium does not cause this type of Na_2SO_4-induced degradation in nickel-base alloys because much larger oxide ion activities are required to leach chromium from alloys than aluminum. It is also possible that both cobalt and chromium inhibit depletion of oxygen in the Na_2SO_4 by enhancing the transport of oxygen from the gas through the Na_2SO_4.

In the absence of effects produced by oxide ions in the Na_2SO_4, the introduction of sulfur from the Na_2SO_4 into cobalt or nickel alloys containing either aluminum or chromium causes increased degradation. Cobalt and nickel alloys containing sufficient aluminum to stabilize the β-aluminide phase are severely degraded because the formation of aluminum sulfide prevents the development of protective barriers of Al_2O_3. Cobalt- and nickel-base alloys containing chromium are more resistant to the effects caused by sulfur than these alloys with aluminum. The chromium must be depleted from these alloys before severe degradation can occur via the preferential oxidation of sulfides. High velocity gas streams are more effective in depleting these alloys of chromium than static environments.

4. THE EFFECT OF TUNGSTEN ON THE HOT CORROSION OF COBALT BASE ALLOYS

a. Introduction

The experiments designed to study the influence of tungsten on the Na_2SO_4-induced hot corrosion of Co-Al and Co-Cr alloys were performed at 1000°C using oxygen or air. The alloys used in this portion of the program were Co-25Al-12W and Co-25Cr-12W. The compositions and microstructures of these alloys have been described in Section II of this report. These particular alloy compositions were chosen since it appeared that external oxide scales of Al_2O_3 and Cr_2O_3 should be formed on the surfaces of Co-25Al-12W and Co-25Cr-12W, respectively, during oxidation in the absence of Na_2SO_4. The results could therefore be compared to those obtained with Co-25Al and Co-35Cr alloys upon which Al_2O_3 and Cr_2O_3 scales, respectively, are also developed during oxidation in the absence of Na_2SO_4.

b. Experimental Results

(1) Oxidation: After a transient period of oxidation the weight change versus time data obtained from the oxidation of Co-25Al-12W in 1 atm of oxygen conformed to the parabolic rate law with a rate constant of about 0.8×10^{-13} (gm^2/cm^4 sec). This rate constant is similar to that obtained for the oxidation of Co-25Al and is typical of rate constants obtained for alloys where the oxidation rate is controlled by transport through an Al_2O_3 scale (ref. 36). Metallographic examination of oxidized specimens as well as X-ray diffraction analysis showed that a thin continuous layer of Al_2O_3 was developed on this alloy during oxidation.

The Co-25Cr-12W alloy was oxidized at 1000°C in both 0.1 and 1 atm of oxygen. The weight change versus time data obtained for oxidation in 0.1 atm of oxygen conformed to the parabolic rate law after an initial period of transient oxidation and yielded a parabolic rate constant of 1.1×10^{-11} (gm^2/cm^4-sec) which is similar to that for the growth of Cr_2O_3 on nickel-chromium alloys (ref. 31). Metallographic examination of oxidized specimens as well as X-ray diffraction analyses of spalled oxides showed that the principal oxide formed on the specimens during oxidation in 0.1 atm of oxygen was Cr_2O_3. The oxidation kinetics for Co-25Cr-12W specimens that were oxidized in 1 atm of oxygen also approximated the parabolic rate law with a rate constant of 7.2×10^{-11} (gm^2/cm^4-sec). The oxide scale which formed on this alloy during oxidation in 1 atm of oxygen was thicker than that formed during oxidation in 0.1 atm of oxygen and contained CoO, $CoCr_2O_4$ as well as Cr_2O_3. Metallographic and electron beam microprobe examinations showed that the inner part of this oxide scale adjacent to the alloy was Cr_2O_3. These results show that during the oxidation of the Co-25Cr-12W alloy continuous layers of Cr_2O_3 are developed on this alloy for both oxidation in 0.1 atm and 1 atm of oxygen. However, the transient period during which the continuity of the Cr_2O_3 is being developed is longer for oxidation in 1 atm of oxygen.

(2) Oxidation of Specimens Coated with Na_2SO_4: As is obvious from examination of Section II of this report, a number of different experiments were performed so that the effect of Na_2SO_4 on the oxidation of Co-25Al-12W and Co-25Cr-12W alloys could be examined. In the following the results obtained from each type of experiment with both alloys are presented.

(a) Isothermal Oxidation at 1000°C: Specimens of Co-25Al-12W were coated with various amounts of Na_2SO_4 and then oxidized in 1 atm of oxygen at 1000°C. Figure 42 shows the kinetic data obtained for Co-25Al-12W coated with 5 mg/cm^2 Na_2SO_4 compared to the data obtained for Co-25Al under the same conditions. Although weight losses were occasionally observed during the initial stages of oxidation for Na_2SO_4-coated specimens of Co-25Al-12W, after long periods the oxidation rate for most of the specimens eventually increased. In these cases the weight gains were significantly greater and of longer duration than for Na_2SO_4-coated Co-25Al (Figure 42), or for Co-25Al-12W oxidized without Na_2SO_4.

Visual and metallographic examination of the oxidized Co-25Al-12W specimens showed that during the period of small weight gains or weight losses, the surfaces of specimens were covered principally with Al_2O_3 scales. When the kinetics of the specimens were observed to accelerate, localized areas over the specimen surface were found to contain additional oxide phases (i.e., CoO, $CoAl_2O_4$). The structure of the oxide layer in an area where these other oxides in addition to Al_2O_3 had been formed is presented in Figure 43 which also contains a photograph of this alloy after oxidation without Na_2SO_4 for comparison. It appeared that structures of the oxide scale such as those shown in Figure 43b, once developed, apparently became larger by lateral growth as oxidation was continued. The amount of Na_2SO_4 deposited on the surface of specimens did not have any obvious effects on the performance of the Co-25Al-12W alloy. Localized areas of nonprotective oxide were observed to be developed on specimens containing as little as 0.5 mg/cm^2 of Na_2SO_4.

To determine if and when the tungsten from the alloy enters the Na_2SO_4, specimens of Co-25Al-12W were oxidized for various times and the Na_2SO_4 was analyzed for sodium, sulfate, tungsten, and aluminum. The amount of sulfur in the substrate was also determined. The results from these analyses are presented in Table VII. It can be seen that the amount of sodium and sulfate on the specimen surface does decrease as a function of time at temperature with the sulfate decreasing at the faster rate. Sulfur was also observed to enter the alloy. However, significant amounts of tungsten or aluminum were not detected in the Na_2SO_4.

Weight change versus time curves for the oxidation of Na_2SO_4-coated and Na_2SO_4-free Co-25Cr-12W specimens are compared in Figure 44. The specimens with the coatings of Na_2SO_4 initially gained weight more rapidly than specimens without Na_2SO_4. However, this condition is evident only during the first hour of oxidation after which weight losses were observed. The weight losses must be caused by the evolution of gaseous products. The fact that weight losses are observable indicates the pickup of oxygen is not substantially greater than that for the oxidation of Na_2SO_4-free specimens. The scales which formed on Na_2SO_4-coated specimens during oxidation were determined by X-ray diffraction analyses

to contain CoO, $CoCr_2O_4$ and Cr_2O_3. Examination of such specimens with the electron beam microprobe showed the Cr_2O_3 in the scale developed as a continuous layer over the alloy, Figure 45. Within the alloy voids and particles of chromium sulfide were also evident. The thickness of the Cr_2O_3 layer developed on the Co-25Cr-12W alloy was greater than that formed on Co-35Cr after oxidation in Na_2SO_4. In addition, the weight gains of Na_2SO_4-coated Co-25Cr-12W specimens during the initial stages of oxidation were greater than those for Co-35Cr, Figure 44. Results obtained from chemical analyses of Na_2SO_4 removed from Co-25Cr-12W specimens after different oxidation times are presented in Table VIII. The amounts of sodium, sulfate and sulfur detected follow the same patterns as those observed with the Co-25Al-12W alloy, Table VII. In the case of the Co-25Cr-12W alloy, significant amounts of tungsten as well as chromium were also detected. The chromium content of the Na_2SO_4 was less than that observed in Na_2SO_4 removed from the Co-35Cr alloy. For example after 60 and 480 minutes of oxidation, the Na_2SO_4 from Co-25Cr-12W contained 0.003 and 0.026 mg/cm^2 of chromium, respectively, whereas values of 0.32 and 0.41 were obtained for the Co-35Cr alloy.

(b) Argon-Preanneal Experiments: Weight change versus time data obtained for a specimen of Co-25Al-12W which had been coated with Na_2SO_4, annealed for 1 hr. in argon at 1000°C, and subsequently oxidized at 1000°C in 1 atm of oxygen are presented in Figure 46. These data indicate that the argon pretreatment has caused catastrophic oxidation of this alloy to occur virtually from the beginning of the weight change measurements during oxidation in oxygen. A typical microstructure of a specimen oxidized under these conditions is presented in Figure 47a. The oxide scale is extremely thick. A more detailed view of the microstructure developed at the scale-alloy interface is presented in Figure 47b. It can be seen that because of the rapid oxidation rate of this alloy, the depleted zone is very thin, and also contains particles of aluminum sulfide. The oxide scale adjacent to the alloy is enriched in tungsten, Figures 47c and 47d. Tungsten is also evident throughout the scale but appears as a discrete network except near the scale/alloy interface. Cobalt, aluminum and sodium were also evident in the oxide scale and had relatively uniform distributions across the scale which included the tungsten-rich zone. Since Na_2SO_4-induced catastrophic oxidation was observed for the Co-25Al-12W alloy but not Co-25Al, and tungsten was observed to be concentrated in the scale at the scale/alloy interface, it appears that tungsten must participate in the catastrophic oxidation process. Sodium sulfate-induced catastrophic oxidation of a Ni-27.7al-12.3W alloy also has been observed (ref. 12).

TABLE VII

SODIUM, SULFATE, SULFUR, TUNGSTEN AND ALUMINUM ANALYSES OF Na_2SO_4-COATED Co-25Al-12W AFTER OXIDATION AT 1000°C IN 1 ATM OF OXYGEN

Oxidation Time (min)	Amount Na_2SO_4 Initial (millimoles/cm^2)	Percent Sodium Remaining	Percent Sulfate Remaining	Sulfur in Alloy ($\mu g/cm^2$)	Tungsten in Na_2SO_4 mg/cm^2	Aluminum in Na_2SO_4 mg/cm^2
0	0.035	100	100	<10	<0.1	<0.005
5	0.040	100	94	13	<0.1	<0.005
30	0.037	89	92	47	<0.1	<0.005
60	0.039	96	87	54	<0.1	<0.005
300	0.036	68	67	92	<0.1	<0.005
1200	0.040	75	43	76	<0.1	<0.005
60*	–	–	42	–	<0.1	<0.005

*Argon annealed specimen

TABLE VIII

SODIUM, SULFATE, SULFUR, TUNGSTEN AND CHROMIUM ANALYSES OF Na_2SO_4-COATED Co-25Cr-12W AFTER OXIDATION AT 1000°C IN 0.1 ATM OF OXYGEN

Oxidation Time (min)	Amount Na_2SO_4 Initial (millimoles/cm^2)	Percent Sodium Remaining	Percent Sulfate Remaining	Sulfur in Alloy ($\mu g/cm^2$)	Tungsten in Na_2SO_4 mg/cm^2	Chromium in Na_2SO_4 mg/cm^2
0	0.035	96	97	16	<0.05	<0.003
5	0.037	89	83	98	0.93	0.014
30	0.038	93	87	136	0.66	<0.003
60	0.038	70	66	93	0.61	<0.003
300	0.040	85	60	76	1.09	0.014
480	0.035	70	37	136	1.01	0.026

Neither tungsten nor aluminum were detected in the Na_2SO_4 from Co-25Al-12W specimens after the argon anneal. This absence of tungsten indicates the pretreatment does not necessarily permit tungsten to enter the Na_2SO_4 during subsequent oxidation. The microstructure of a Na_2SO_4-coated, Co-25Al-12W specimen after a one hour anneal in argon at 1000°C is presented in Figure 48a. The zone depleted of aluminum indicates that upon subsequent oxidation a substantial amount of tungsten may be oxidized and become available to react with the Na_2SO_4. Since it appeared that tungsten must enter the Na_2SO_4 during the subsequent oxidation of the argon annealed specimens, an argon preannealed specimen was oxidized for one hour and water washed. The analysis of this wash water showed that 0.7 mg of tungsten (0.24 mg/cm^2) was present. The oxidation kinetics before and after the water wash are presented in Figure 49. It can be seen that catastrophic oxidation occurred during the first hour of oxidation. However, the oxidation rate decreased significantly after the water wash. The microstructure of this oxidized specimen is presented in Figure 48b. In some areas the beginning of what appears to be the development of a more dense and perhaps protective scale beneath the outer porous scale is evident. These results show that the formation of tungsten oxides is not a sufficient condition for catastrophic oxidation of this alloy, in particular, the tungsten oxides must be formed when a salt such as Na_2SO_4 is present on the alloy surface.

Weight change versus time data obtained for a specimen of Co-25Cr-12W which had been coated with Na_2SO_4, annealed in argon at 1000°C, and subsequently oxidized at 1000°C in 0.1 atm of oxygen are presented in Figure 44. It can be seen that the initial weight gains of Na_2SO_4-coated specimens with and without the argon preanneal are both greater than those for the oxidation of a Na_2SO_4-free specimen. The subsequent weight changes are difficult to compare since the Na_2SO_4-coated specimen without the argon anneal shows weight losses due to evolution of gaseous species. The specimen with the argon preanneal does not show such weight losses perhaps because most of the volatile species are evolved during the argon preanneal. A typical microstructure of a specimen, coated with Na_2SO_4, annealed in argon and then oxidized is presented in Figure 50. The outer portion of the scale on this specimen appears to be porous whereas the inner portion is dense, continuous Cr_2O_3. The important point to be noted in the results obtained with the Na_2SO_4-coated, argon preannealed specimens of Co-25Cr-12W is that the annealing pretreatment has not induced sustained catastrophic oxidation as was the case for Co-25Al-12W specimens.

(c) Cyclic Oxidation at 1000°C: Results obtained from the cyclic oxidation of Na_2SO_4-coated specimens of Co-25Al-12W in 1 atm of oxygen at 1000°C are presented in Figure 51. These weight change versus time measurements show that catastrophic oxidation of this alloy has occurred after about three cycles. Visual examination of such oxidized specimens showed that the attack was uniform over the alloy surface and that the oxide scale was extremely thick. Metallographic examination showed microstructures similar to the argon preannealed and oxidized Na_2SO_4-coated specimens, Figure 47. It is important to notice that the cyclic oxidation of Na_2SO_4-coated Co-25Al specimens (2 hr cycles) did not cause as severe oxidation as has been observed for Co-25Al-12W specimens, Figure 51. These results are consistent with the proposal that tungsten is causing catastrophic oxidation of the Co-25Al-12W alloy. It appears that during the first two cycles the alloy is depleted of aluminum and upon the third cycle sufficient tungsten is introduced into the Na_2SO_4 to cause catastrophic oxidation.

The results obtained from weight change versus time measurements of cyclically oxidized, Na_2SO_4-coated, Co-25Cr-12W specimens are presented in Figure 52. Even though cracking and some spalling of the oxide was observed during the cyclic test, these weight change versus time data are not substantially greater than those for this alloy in isothermal oxidation without a Na_2SO_4 coating. Results obtained from metallographic examination of Na_2SO_4-coated specimens of Co-25Cr-12W that had been cyclically oxidized showed microstructures similar to those obtained for specimens which had been tested under similar conditions but had been oxidized isothermally rather than cyclically, Figure 50. Such results show, that even with thermal cycling (2 hr cycles), protective layers of Cr_2O_3 are developed on Na_2SO_4-coated specimens of Co-25Cr-12W.

(3) Experiments Concerned with the Effects Produced by Sulfur: The experiments concerned with the effects produced by sulfur on the oxidation of Co-25Al-12W and Co-25Cr-12W consisted of the oxidation of presulfidized specimens and oxidation of specimens in SO_2.

(a) Oxidation of Presulfidized Specimens: To examine the effect of sulfur on the oxidation of the Co-25Al-12W alloy, specimens were sulfidized and then oxidized. Specimens sulfidized at 1000°C for about two minutes in an H_2S-H_2 mixture with $H_2S/H_2 = 0.2$ gained about 3 mg/cm^2 in weight due to sulfur pickup. The sulfidized specimens were oxidized by changing the gas environment without cooling specimens. Weight change versus time measurements obtained from the oxidation of such a specimen in 1 atm of oxygen at 1000°C are presented in Figure 53. These results show that the sulfidizing pretreatment has caused the alloy to oxidize more rapidly than what was observed without the pretreatment. The weight gain is actually larger than that indicated in Figure 53 since SO_2 was detected in the effluent gas during the experiment (e.g., equivalent to about 0.5 mg/cm^2 of sulfur over the first three hours of the experiment). The microstructure of presulfidized and oxidized specimens were similar to those observed with Co-25Al specimens, Figure 20. The oxide scale contained other oxides in addition to Al_2O_3 and particles of aluminum sulfide were evident in the substrate. Oxidation of specimens presulfidized in a lower H_2S/H_2 ratio (i.e., 0.002), but having about the same amount of sulfur pickup as those presulfidized in the high ratio, produced similar results as those obtained for the higher ratio. The results obtained from the oxidation of presulfidized specimens of Co-25Al-12W show sulfur does cause the oxidation rate of this alloy to be increased. It appears such a condition occurs since Al_2O_3 scales are not developed effectively on this alloy when particles of aluminum sulfide are on or near the surface of the alloy. Similar effects of sulfur have been observed for Co-25Al. While sulfur does cause increased oxidation of Co-25Al-12W, the magnitude of the increase is extremely small compared to the catastrophic oxidation of this alloy which was observed with Na_2SO_4 deposits under certain conditions (e.g., argon preanneal or cyclic conditions).

Specimens of Co-25Cr-12W were sulfidized in the two different H_2S-H_2 gas mixtures and oxidized. In each gas mixture the time of presulfidization was adjusted such that the specimens gained about 7 mg/cm^2 of sulfur. Weight change versus time data obtained for the oxidation of such specimens in a flowing argon-oxygen gas mixture ($p_{Ar} = 0.9$, $p_{O2} = 0.1$) are presented in Figure 54. Both presulfidized specimens showed larger weight gains than the specimen with no sulfidizing pretreatment. In addition slightly more oxidation

actually occurred than indicated by the weight change data since SO_2 was detected in the effluent gas (e.g., 1 and 0.3 mg/cm^2 of sulfur during 20 hours of oxidation for specimens presulfidized in the high and low ratio, respectively). The microstructures of presulfidized specimens after oxidation are shown in Figure 55. A thick oxide scale has been developed on the specimen which was presulfidized in the high ratio prior to oxidation. Numerous sulfides are evident in the substrate of this specimen and it appears that these sulfides are being preferentially oxidized, Figure 55a. A thin, dense layer of Cr_2O_3 developed on the specimen which was sulfidized in the low ratio prior to oxidation, Figure 55b.

The results which have been obtained with the presulfidized and oxidized specimens of Co-25Cr-12W show that the introduction of sulfur into this alloy can cause accelerated oxidation. It appears that the increased oxidation occurs due to the preferential oxidation of sulfides in the alloy. Since the preferential oxidation of sulfides was only observed with specimens presulfidized in the high ratio, it appears that the formation of such sulfides is dependent on the sulfur activity established at the surface of the alloy. The sulfides which were formed after presulfidizing Co-25Cr-12W in the high ratio were found to contain cobalt and chromium. In view of results obtained from the oxidation of presulfidized Ni-Cr alloys (ref. 24), it is believed that the observed preferential oxidation of sulfides in the Co-25Cr-12W alloy may have resulted from the formation of a Co-Cr-S phase which was liquid at the temperature of oxidation.

(b) Oxidation in SO_2: The weight change versus time measurements for the oxidation of Co-25Al-12W in SO_2 at 1000°C were about twice as large as those for oxidation of this alloy in oxygen. Examination of specimens after oxidation in SO_2 by using an optical microscope showed sulfide particles had been formed in the alloy beneath an oxide scale. The fact that the alloy simultaneously reacted with oxygen and sulfur in the SO_2 makes an interpretation of the kinetics difficult. Comparison of the oxide scales developed on this alloy after oxidation in oxygen and after oxidation in SO_2 showed that a thicker scale had been developed after oxidation in SO_2. Such a condition shows that sulfur has caused more rapid oxidation of this alloy.

The weight change versus time data obtained for the oxidation of the Co-25Cr-12W alloy in SO_2 at 1000°C were a factor of two greater than those for oxidation in oxygen. Results obtained from the examination of the microstructure of this specimen with the electron beam microprobe indicated that the external scale was Cr_2O_3 and that internal sulfide particles were present which contained chromium. Oxide stringers associated with the sulfides appeared to form due to the preferential oxidation of a sulfide phase beneath the external Cr_2O_3 layer.

(4) Hot Stage Microscopy: The oxidation in air at 1000°C of Na_2SO_4-coated specimens of Co-25Al-12W and Co-25Cr-12W has been observed by using the hot stage microscope. These experiments were performed for times of about 30 minutes. In the case of the Co-25Al-12W alloy, an oxide scale was observed to form beneath the Na_2SO_4. No penetration of this scale by the Na_2SO_4 was observed. This condition was markedly different from that observed for the Co-25Al alloy where the Na_2SO_4 was observed to penetrate and spread laterally beneath the oxide scale. An oxide scale was also observed

to form beneath the Na_2SO_4 on a Co-25Cr-12W specimen. In some regions on the surface of this specimen, oxide protrusions were observed to develop. Such protrusions were not observed on specimens of Co-35Cr.

(5) Crucible Experiments: To determine if WO_3, when added to Na_2SO_4, could influence the reaction between Na_2SO_4 and CoO, Al_2O_3, Cr_2O_3 and NiO, crucible experiments were performed whereby the weight changes of oxide tablets were determined after exposure to various melts. The effects produced by melts of Na_2SO_4, Na_2SO_4 + 7 mole percent Na_2WO_4 and Na_2WO_4 + 7 mole percent WO_3 were examined. The melt containing Na_2SO_4 + 7 mole percent Na_2WO_4 was prepared by adding WO_3 to Na_2SO_4 in an amount, which in view of the following reaction

$$WO_3 + Na_2SO_4 = Na_2WO_4 + SO_3$$

would produce 7 mole percent of Na_2WO_4 in Na_2SO_4. This mixture was heated one-half hour at 1000°C in air in a platinum crucible and the liquid melt was examined at temperature with a microscope at 25X. No solid particles were visible, which showed all the WO_3 had reacted with the Na_2SO_4. In addition, the melt decreased in weight by an amount about equal to that for the SO_3 evolution required for complete reaction between WO_3 and Na_2SO_4. The melt containing Na_2WO_4 + 7 mole percent WO_3 was prepared by adding an appropriate amount of WO_3 to Na_2WO_4 and heating for 30 minutes at 1000°C. As in the case of the previous melt no solid particles were evident in the Na_2WO_4 + 7 mole percent WO_3 melt after this treatment. Tablets of oxide were added to separate portions of these melts and heated 2 hours at 1000°C in air. The weight change of the tablets was then determined after washing the tablets with distilled water.

The results obtained from these experiments are presented in Table IX. It can be seen that as the activity of WO_3 in the melts is increased, the amount of reaction between the melts and CoO or Al_2O_3 increases. The results obtained with Cr_2O_3 and NiO do not follow the same pattern. Chromia has a great affinity for oxide ions and so the reaction may decrease for a low WO_3 activity since the addition of WO_3 decreases the oxide ion activity. At high WO_3 activities the Cr_2O_3 may then donate oxide ions to the melt. In the case of NiO the amount of reaction at high WO_3 activities may be less than at low values due to the formation of solid $NiWO_4$. Regardless of the patterns of the weight changes, the important points to be established are that reactions between the tablets and the melts did occur, the products of these reactions usually were not formed on the surfaces of the tablets but rather in the melts, and larger amounts of reactions usually occurred as the amount of WO_3 in the melts was increased. Such conditions indicate that WO_3, when present in $NaSO_4$ melts, can destroy protective scales of CoO, NiO, Al_2O_3 and even Cr_2O_3 via an acidic fluxing reaction whereby oxide ions are donated to the melt by these oxide scales.

TABLE IX

WEIGHT CHANGES OF OXIDE TABLETS AFTER IMMERSION IN VARIOUS MELTS FOR 2 HOURS AT 1000°C IN AIR

Oxide	Na_2SO_4 (mg/cm^2)	Na_2SO_4-7 mole percent Na_2WO_4 (mg/cm^2)	Na_2WO_4 + 7 m/o WO_3 (mg/cm^2)
CoO	-0.4	- 8.3	-74.1
Al_2O_3	0	- 0.5	- 4.8
Cr_2O_3	-0.3	- 0.1	- 4.7
NiO	0	-77.5	-49.3

(6) Experiments Using Tungsten Oxide Vapor: Since the crucible experiments indicated that WO_3 in Na_2SO_4 may destroy protective oxide scales on alloys, experiments were performed in oxygen containing tungsten oxide vapor. Specimens of Co-25Al-12W and Co-25Al were coated with Na_2SO_4 and heated in a tube furnace at 1000°C. Flowing oxygen was passed through the furnace tube and a reservoir of WO_3 was placed upstream from the specimens at 975°C. The activity of WO_3 in the gas may be defined as

$$a_{WO_3} = \left[\frac{p_{(WO_3)_3}}{p^{\circ}_{(WO_3)_3}} \right]^{1/3}$$

where $p_{(WO_3)_3}$ is the pressure of $(WO_3)_3$ in the flowing oxygen and $p^{\circ}_{(WO_3)_3}$ is the pressure of $(WO_3)_3$ over solid WO_3 at the temperature of interest. In view of the vapor pressure of WO_3 (ref. 37), the activity of WO_3 over the specimens should be 0.7 providing equilibrium conditions are established. After 24 hours under such conditions catastrophic oxidation of neither the Co-25Al-12W nor the Co-25Al alloy was evident. Since the pressure of $(WO_3)_3$ over solid WO_3 at 975°C is about 2.4×10^{-8} atm, it is possible that the oxygen was not saturated with $(WO_3)_3$ vapor. In addition, some of the Na_2SO_4 must be converted to Na_2WO_4 before catastrophic effects can be expected.
more severe conditions, the experiment was repeated, however, the specimens were coated with Na_2WO_4 rather than Na_2SO_4, since by not requiring conversion of Na_2SO_4 to Na_2WO_4 a higher WO_3 activity could possibly be established in the liquid on the specimen surfaces. Catastrophic oxidation of both the Co-25Al-12W and Co-25Al specimens was evident after 24 hours.

Results obtained from microprobe examination of the Co-25Al-12W specimen which was coated with Na_2WO_4 and heated in oxygen containing tungsten oxide vapor are presented in Figure 56. These results are similar to those presented previously for a specimen that had been coated with Na_2SO_4, annealed in argon and oxidized, Figure 47, however, sulfur was not present in the substrate of the specimen with the Na_2WO_4 coating. As shown in Figures 56a and 56b, the oxide scale contains a tungsten enriched zone immediately above the alloy which appears to be composed of two phases. The probe traces, Figure 56c show that one of the phases contains cobalt and tungsten whereas the

other phase is enriched in aluminum. Immediately above this tungsten-rich zone in the scale, a zone containing a network of tungsten-rich oxide interdispersed with oxides of cobalt and aluminum is evident, Figure 56b. The catastrophic attack of the Co-25Al alloy was not uniform. Some areas were attacked only moderately whereas other areas had undergone severe attack and had structures typical of those for catastrophic oxidation of Co-25Al-21W.

Experiments were also performed in which Na_2WO_4-coated specimens of Co-25Al-12W and Co-25Al were oxidized in oxygen. Weight change versus time data are presented in Figure 57. Severe oxidation of the Co-25Al-12W had occurred and microstructures similar to those shown in Figure 56a were observed with the optical microscope. The Co-25Al alloy exhibited much less severe attack when oxidized in oxygen as opposed to oxygen containing tungsten oxide vapor. For example weight gains of 4 and 13 mg/cm^2 were obtained for Na_2WO_4-coated specimens of Co-25Al oxidized 20 hours in oxygen and oxygen with tungsten oxide vapor, respectively. The microstructures of these specimens showed that although the oxidation was nonuniform on both, the oxide scale is much thicker on the specimen oxidized in the environment containing tungsten oxide vapor.

Results obtained from the oxidation of Na_2WO_4-coated specimens of Co-25Cr-12W and Co-35Cr in oxygen at 1000°C are presented in Figure 58. The weight increase of the Co-25Cr-12W is substantially greater than that for Co-35Cr. Examination of the microstructures of these specimens showed that a protective layer of Cr_2O_3 had developed on the Co-35Cr alloy but not on the Co-25Cr-12W. In fact the structure, Figure 59a, and composition, Figure 59b, of this latter specimen contains features similar to that observed for the catastrophic oxidation of the Co-25Al-12W alloy, Figures 47 and 56.

A specimen of Co-35Cr was also coated with Na_2WO_4 and oxidized at 1000°C in oxygen containing tungsten oxide vapor. The conditions were the same as those described previously for the Co-25Al-12W alloy. Examination of this specimen after the experiment showed that oxidation had occurred nonuniformly. About three-quarters of the specimen surface was covered with a thin oxide of what appeared to be Cr_2O_3. The remainder of the specimen surface was covered with a porous scale about six times thicker than the thin oxide layer. The results obtained with the Co-35Cr alloy indicate that the $(WO_3)_3$ vapor in the oxygen may have caused the formation of the thick porous scale since the oxidation of this alloy with a Na_2WO_4 coating in oxygen not containing $(WO_3)_3$ vapor did not result in the development of a thick porous scale.

(7) Additional Experiments: Results have been obtained which show that tungsten can cause catastrophic oxidation of Co-25Al-12W when Na_2SO_4 is present on the surfaces of specimens. Results have also been obtained which indicate a similar condition may also occur for Co-25Cr-12W. In an attempt to develop conditions which may favor the initiation of Na_2SO_4-induced catastrophic oxidation, an alloy of Co-20Cr-12W was coated with Na_2SO_4 and oxidized in oxygen at 1000°C. Weight change versus time data obtained for the oxidation of this alloy with and without Na_2SO_4 are compared in Figure 60 and photomicrographs of the oxidized specimens are presented in Figure 61. These data show that catastrophic oxidation of Co-20Cr-12W has occurred in the presence of a Na_2SO_4 deposit.

Specimens of Co-25Cr-12W and Ni-25Cr-12W were also subjected to the laboratory cyclic hot corrosion test (i.e., 1 hour cycles, periodic deposition of Na_2SO_4). Weight change versus time measurements are presented in Figure 62. Both specimens have been severely degraded. The degradation of the Co-25Cr-12W alloy was much greater than that for Co-35Cr in this same test as can be seen by comparing data presented in Figures 31 and 62. The microstructure of the scale on the Co-25Cr-12W specimen is similar to that observed for the Na_2SO_4-induced catastrophic oxidation of Co-25Al-12W. A continuous layer of Cr_2O_3 was not formed on the alloy. It is believed that such results show tungsten can cause catastrophic oxidation of Co-25Cr-12W in the presence of Na_2SO_4, providing the test conditions are severe enough to deplete the alloy sufficiently of chromium.

c. Summary and Discussion of Results

In discussing the results obtained from experiments to determine the effect of tungsten on the Na_2SO_4-induced hot corrosion of Co-25Al-12W and Co-25Cr-12W alloys, it is convenient to first consider the former alloy and then the latter.

(1) Co-25Al-12W: Before utilizing the results for the Na_2SO_4-induced hot corrosion of Co-25Al-12W to account for the effects of tungsten, it is worthwhile to summarize the meaningful results which have been obtained. It is believed that the following results are relevant to the effects produced by tungsten during Na_2SO_4-induced hot corrosion of alloys.

- Continuous layers of Al_2O_3 are developed on Co-25Al-12W and Co-25Al alloys during oxidation in oxygen or air.
- Isothermal oxidation of Na_2SO_4-coated Co-25Al-12W and Co-25Al resulted in accelerated oxidation; the initiation of accelerated oxidation of Co-25Al-12W alloy occurred after longer periods of oxidation than that observed for Co-25Al.
- The Na_2SO_4-induced accelerated oxidation of Co-25Al-12W under isothermal conditions, once initiated, appeared to continue indefinitely whereas that for Co-25Al existed only for a relatively short period of time.
- Sustained catastrophic oxidation of Na_2SO_4-coated Co-25Al-12W was observed after an argon pretreatment or as a result of cyclic oxidation; such conditions also caused more extensive oxidation of Co-25Al but the oxidation was not self-sustaining nor therefore catastrophic.
- Catastrophic oxidation was also observed for Na_2WO_4-coated Co-25Al-12W under isothermal conditions; Na_2WO_4 did not induce catastrophic oxidation of Co-25Al unless tungsten oxide vapor was present in the gas environment.

- The catastrophic oxidation of Co-25Al-12W ceased when the Na_2SO_4 was removed from the surfaces of specimens.

- The oxide scale which formed during catastrophic oxidation of Co-25Al-12W contained all the elements in this alloy and the tungsten was concentrated in a zone adjacent to the alloy.

- Liquid solutions of Na_2SO_4 and tungsten oxide reacted with Al_2O_3, CoO and NiO tablets, and the amount of these reactions increased as the mole fraction of tungsten oxide in the liquid was increased; the products of these reactions were not formed on the surfaces of the oxide tablets.

- The introduction of sulfur into Co-25Al and Co-25 Al-12W caused increased oxidation of both alloys due to the formation of aluminum sulfides which possessed poor oxidation resistance; W did not influence the degradation of these alloys by sulfur.

- All the results obtained with the Co-25 Al-12W alloy appeared to be similar to those for an equivalent nickel-base system; the nickel-base systems did appear to require less severe conditions to initiate catastrophic oxidation.

In view of the results which have been obtained, the following description of the Na_2SO_4-induced hot corrosion of Co-25Al-12W under isothermal conditions can be developed. When Na_2SO_4 is deposited on the surface of this alloy, the Na_2SO_4 melts upon heating to 1000°C and a continuous layer of Al_2O_3 is developed between the Na_2SO_4 and the alloy. The Al_2O_3 on this alloy is not penetrated by the Na_2SO_4 during the initial stages of isothermal oxidation, as occurs in the case of Co-25Al, since the small amounts of tungsten oxide formed during the transient period of oxidation maintain the oxide ion activity of the Na_2SO_4 at levels too low to allow localized penetration of the Al_2O_3 via a basic fluxing reaction. Continued oxidation of the Co-25Al-12W alloy eventually results in the development of localized regions of degradation of the protective Al_2O_3 scale which become larger with time. This localized destruction of the oxide barrier may occur as a result of the development of cracks in the barrier or of localized acidic fluxing. The process by which degradation of the alloy spreads from these sites of localized Na_2SO_4 penetration involves effects produced by tungsten oxides which are formed as the Na_2SO_4 reacts with the aluminum-depleted alloy at the base of the penetration sites. Such effects will be discussed in the following paragraph where cyclic oxidation of Co-25Al-12W is considered.

In the case of Cyclic oxidation of Na_2SO_4-coated Co-25Al-12W during the initial cycle, conditions are the same as those described in the previous paragraph on isothermal oxidation. Subsequent oxidation cycles afford easy access of the Na_2SO_4 to the alloy surface due to spalling and cracking of the Al_2O_3 under the influence of thermally induced stresses. As the cyclic oxidation process continues, more tungsten oxides are formed because of depletion of the alloy of aluminum. The tungsten oxides react with the Na_2SO_4 to

form an acidic melt (i.e. melt deficient in oxide ions) which is an effective flux for CoO and Al_2O_3. This fluxing reaction can be described as follows where CoO is taken as an example. Cobalt in the alloy is oxidized and reacts with WO_3, dissolved in the melt, according to the following reaction

$$CoO + WO_3 = Co^{2+} + WO_4^{2-}.$$

The cobalt and tungstate ions diffuse through the melt away from the alloy surface to the outer part of the melt where the above reaction takes place in the reverse direction due to the lower WO_3 activity. In view of this condition the melt is continually enriched in WO_3, and CoO is precipitated in the outer region of the melt as a nonprotective zone. As the activity of WO_3 in the melt is increased to even higher values, the following reactions may occur:

$$CoO + 2WO_3 = Co^{2+} + W_2O_7^{2-}$$

$$CoO + 3WO_3 = Co^{2+} + W_3O_{10}^{2-}$$

where again these reactions proceed to the right at the alloy/melt interface and the left at the outer portions of the melt away from the alloy. Similar reactions to those described for CoO may be expected for Al_2O_3. The network of Al_2O_3 stringers within the tungsten rich zone, however, indicates some sort of stripping action of the melt rather than dissolution followed by precipitation. As a result of these fluxing reactions very little protection is afforded to the alloy by the oxide scales and catastrophic oxidation ensues.

In the proposed degradation process, it is to be noted that Na_2WO_4 will be more effective in inducing catastrophic oxidation of Co-25Al-12W than Na_2SO_4, since less tungsten oxides are necessary to develop a melt with acidic fluxing properties. It should also be obvious that sulfur does not play an important role in the catastrophic oxidation. In the case of the cyclic, Na_2SO_4-induced hot corrosion of Co-25Al, the oxidation of aluminum sulfides causes hot corrosion degradation. In the case of Co-25Al-12W, however, the conditions which would allow the oxidation of sulfides also introduce tungsten into the Na_2SO_4 and catastrophic oxidation occurs.

Previous hot corrosion studies (ref. 12) with Ni-27Al-12W have shown that 0.5 mg/cm^2 Na_2SO_4 will induce self-sustaining catastrophic hot corrosion of that alloy under isothermal conditions at 1000°C. Moreover, the microstructure and composition of the corrosion scale have been determined to be virtually identical to that found on catastrophically attacked Co-25Al-12W. It is therefore believed that the mechanism of hot corrosion attack of this type of nickel base alloy is the same as that which has been described for Co-25Al-12W. On the other hand, the resistance to the initiation of Na_2SO_4-induced catastrophic hot corrosion appears to be greater for the cobalt-base alloy, since thermal cycling, an argon preanneal, or WO_3 vapor are required to initiate the attack of Co-25Al-12W. In contrast to this, the nickel base alloy suffers this kind of attack under isothermal conditions. The reasons for this observed difference in behavior are not available.

(2) Co-25Cr-12W: As in the case of the Co-25Al-12W alloy, before discussing the Na_2SO_4-induced hot corrosion of Co-25Cr-12W it is helpful to itemize the following relevant results.

- Continuous layers of Cr_2O_3 are formed on Co-25Cr-12W and Co-35Cr during oxidation in oxygen or air.

- Isothermal oxidation of Na_2SO_4-coated Co-25Cr-12W resulted in accelerated oxidation during the initial stages of oxidation, but a protective layer of Cr_2O_3 was eventually developed on this alloy; the amount of oxidation of Co-25Cr-12W during this initial period was greater than that for Co-35Cr.

- Catastrophic oxidation of Co-25Cr-12W but not Co-35Cr was observed after testing of this alloy in the cyclic hot corrosion test (1 hr cycles); Na_2SO_4-induced catastrophic oxidation of a Co-20Cr-12W alloy under isothermal conditions was observed.

- Oxidation of Na_2WO_4-coated Co-25Cr-12W resulted in more severe degradation than that for Na_2SO_4-coated Co-25Cr-12W; the features of the scale which was formed on the Na_2WO_4-coated specimen were similar to those associated with catastrophic oxidation.

- Liquid solutions containing Na_2SO_4, Na_2WO_4 and WO_3 reacted with Cr_2O_3; it appears such reactions are most effective for melts containing either high (basic) or low (acidic) oxide ion concentrations.

- Tungsten oxide vapor in oxygen caused severe, localized areas of oxidation to be developed on a Na_2SO_4-coated Co-35Cr specimen.

- The introduction of sulfur into Co-25Cr-12W caused a substantial increase in the oxidation rate of this alloy due to preferential oxidation of a sulfide phase that may have been liquid at the temperature of oxidation.

- The results obtained for the oxidation of Co-25Cr-12W in the presence of Na_2SO_4 were not significantly different from those for equivalent nickel-base systems.

The results which have been obtained show that in the presence of Na_2SO_4 and thermally induced stresses, catastrophic oxidation of Co-25Cr-12W occurs. The process by which the catastrophic oxidation occurs appears to be the same as that for the Co-25Al-12W alloy. More severe conditions, are required, however, to initiate catastrophic oxidation of Co-25Cr-12W than Co-25Al-12W. It is possible that such an effect occurs because more acidic melts (i.e. higher tungsten oxide activities) are required to flux Cr_2O_3 than Al_2O_3.

Under less severe conditions (e.g. isothermal oxidation, infrequent thermal cycling) sufficient tungsten oxides are not introduced into the Na_2SO_4 and catastrophic oxidation does not occur. Under such conditions an oxide scale is developed between the Na_2SO_4 and the alloy. It appears that during this transient period of oxidation two processes are occurring. Sulfur from the Na_2SO_4 is entering the alloy and a continuous layer of Cr_2O_3 is developing on the alloy. In areas where the Cr_2O_3 is not continuous, sulfides are formed in the alloy which are subsequently preferentially oxidized. This condition results in increased oxidation of the alloy during the initial stages of oxidation until the Cr_2O_3 layer becomes completely continuous. Once the Cr_2O_3 scale has become continous, the increased oxidation ceases since the barrier of Cr_2O_3 not only inhibits the diffusion of sulfur into the alloy but also isolates the sulfides from oxygen. A description of the sulfides which are necessary for preferential oxidation is not available. Preferential oxidation of sulfides was observed only for the Co-35Cr rig test specimen. It is believed that this type of attack occurs when sufficiently large quantities of sulfur are introduced into the alloy that liquid sulfide phases can form. Since Na_2SO_4-coated laboratory test specimens of Co-25Cr-12W appeared to suffer sulfidation attack, such sulfide phases may be more easily formed in this alloy than in Co-35Cr, either because of the lower chromium content or because tungsten favors their formation.

Data obtained from the cyclic hot corrosion testing of Co-25Cr-12W and Ni-25Cr-12W alloys are compared in Figure 62. It should be noted that catastrophic degradation of both of these alloys has occurred. Severe degradation of the Co-25Cr-12W alloy was not observed in the cyclic hot corrosion test using 2-hour cycles, Figure 52, because this milder test did not deplete the alloy sufficiently of chromium to permit the oxidation of the tungsten in this alloy. Sufficient work has not been done to allow a thorough comparison of the behavior of the Co-25Cr-12W and Ni-25Cr-12W alloys. The weight change data from the cyclic test, as well as results obtained from metallographic examination of the specimens from this test, indicate that catastrophic hot corrosion of Ni-25Cr-12W occurs by the same process as has been proposed for Co-25Cr-12W. The major difference between the hot corrosion of these two alloys appears to be in the time required to initiate the hot corrosion degradation.

5. EFFECTS PRODUCED BY Mo, Ta, and Ti ON THE HOT CORROSION OF COBALT BASE ALLOYS

a. Introduction

The overall objective of this task was to study the effect of molybdenum, tantalum, and titanium, present as alloying elements, on the hot corrosion behavior of cobalt alloys. In particular, one specific objective was to determine if molybdenum or tantalum is detrimental or beneficial to the hot corrosion behavior of alumina and chromia forming cobalt base alloys. To accomplish this, alloys with the following nominal composition were fabricated: Co-25Cr-6Mo, Co-25Al-6Mo, Co-25Cr-12Ta, Co-25Al-12Ta.

Co-25Cr-3Al was selected as the base alloy to study the effect of titanium because it is a close analogue to the type of nickel base alloy (i.e. NiCrAl) for which titanium is believed to have beneficial effects when substituted for aluminum. The alloy selected for this study was Co-25Cr-3Al-5Ti.

The fabrication procedures used in the preparation of these materials, as well as the actual composition are presented in Section III.

It was recognized that the limited number of alloys which were to be studied for this part of the program would not permit the development of extensive and detailed explanations for the effects of molybdenum, tantalum, and titanium in cobalt base alloys.

b. Experimental Results

(1) Oxidation Studies: Before the hot corrosion experiments were conducted, isothermal oxidation experiments were performed at 1000°C. The results of these experiments are discussed in the following paragraphs according to alloy composition.

The weight change versus time data obtained from the oxidation of the Co-25Al-6Mo alloy in 1 atm of oxygen conformed to the parabolic rate law. A parabolic rate constant of 2×10^{-12} gm^2/cm^4-sec was obtained which is close to that for growth of Al_2O_3 on Co-25Al. Visual examination of the spalled oxide after the test indicated that a continuous layer of Al_2O_3 had been developed on this alloy beneath transient oxides composed predominantly of CoO.

The oxidation kinetics obtained for the Co-25Al-12Ta alloy in 1 atm of oxygen did not conform to the parabolic rate law. The measured weight changes of the specimen were very small (e.g. 0.3 mg/cm^2 after 20 hrs). X-ray diffraction analysis showed that the spalled oxide was α-Al_2O_3. Visual examination of the spalled Al_2O_3 with the light microscope indicated that very little transient oxidation had occurred prior to the development of a continuous layer of Al_2O_3.

Results obtained from the oxidation of the Co-25Cr-6Mo alloy showed that a continuous layer of Cr_2O_3 was not developed on this alloy during oxidation in 1 atm of oxygen. The parabolic rate constant for oxidation in 1 atm of oxygen was about 10^{-9} gm^2/cm^4-sec and a substantial amount of CoO was observed on the surface of this alloy. Since it was desired to examine the hot corrosion of this alloy under conditions where a Cr_2O_3 scale was formed on the alloy, oxidation experiments were performed in 0.1 atm of oxygen. A parabolic rate constant of 5×10^{-12} gm^2/cm^4-sec was obtained for oxidation in 0.1 atm of oxygen which is smaller than the rate constant for the growth of Cr_2O_3 on Co-35Cr under similar conditions (i.e., 2×10^{-11} gm^2/cm^4-sec). X-ray diffraction analyses as well as visual examination of the oxides formed on the alloy during oxidation in 0.1 atm of oxygen indicated that a continuous layer of Cr_2O_3 was formed on this alloy beneath transient oxides of CoO.

In view of the results obtained with the Co-25Cr-6Mo alloy, the Co-25Cr-12Ta alloy was oxidized in oxygen at pressures of 0.1 and 1 atmospheres. The parabolic rate constants obtained from these experiments were 1.7×10^{-11} and 1.3×10^{-11} gm^2/cm^4-sec for oxidation in 0.1 and 1 atm oxygen, respectively. Visual examination as well as X-ray diffraction analyses indicated that a continuous layer of Cr_2O_3 was formed on the Co-25Cr-12Ta alloy during oxidation in oxygen at pressures of either 0.1 or 1 atmospheres.

A parabolic rate constant of 3.9 X 10^{-11} gm^2/cm^4 was obtained for the oxidation of the Co-25Cr-3Al-5Ti in 1 atm of oxygen. X-ray diffraction analyses showed that the oxide scale which was formed on this alloy contained TiO_2, $CoCr_2O_4$ and Cr_2O_3. The value of the parabolic rate constant is characteristic of the growth of a continuous layer of Cr_2O_3 on this alloy.

Metallographic examination of the specimens from the oxidation experiments supported the identification of the oxidation products as determined by visual and X-ray diffraction results, and confirmed the presence of the rate-controlling oxide film (e.g. Cr_2O_3 or Al_2O_3) as implied by the oxidation kinetics.

The results of the oxidation studies can be summarized as follows. Continuous external scales of Al_2O_3 were formed on the Co-25Al-6Mo and on the Co-25Al-12Ta alloys during oxidation in 1 atm oxygen at 1000°C. Continuous films of Cr_2O_3 were developed on the Co-25Cr-6Mo and Co-25Cr-12Ta alloys in 0.1 atm oxygen. Oxidation of the Co-25Cr-12Ta in 1 atm oxygen also resulted in external Cr_2O_3 formation, whereas at this higher oxygen pressure the Co-25Cr-6Mo formed only CoO as a continuous barrier. The oxidation of the Co-25Cr-3Al-5Ti alloy is more complex. Although substantial quantities of TiO_2 are formed externally, the oxidation rate is controlled by the growth of a Cr_2O_3 layer below the TiO_2. Beneath the Cr_2O_3, however, stringers of Al_2O_3 were present, and it appeared as though these formed a nearly continuous layer of Al_2O_3.

c. Oxidation Experiments Using Na_2SO_4 Deposits

Both isothermal and cyclic oxidation experiments using Na_2SO_4 were performed. The results will be presented by considering the Al_2O_3 formers first, then the Cr_2O_3 formers and the alloy with titanium last.

(1) Co-25Al-6Mo, Co-25Al-12Ta: Weight change versus time data obtained from the isothermal oxidation of Co-25Al-6Mo alloy with different amounts of Na_2SO_4 are presented in Figure 63. These data show that specimens with Na_2SO_4 deposits have undergone more oxidation than was observed for oxidation without a Na_2SO_4 deposit. These increases in the amount of oxidation, however, are not as large as those observed for Na_2SO_4 deposits on Co-25Al, Figure 63. On the other hand, it is apparent that the oxidation rates of the Na_2SO_4-coated Co-25Al-6Mo specimens, while initially slow, began to increase significantly after about 10 hours oxidation. In order to determine if continued oxidation beyond 20 hours would lead to eventual severe or catastrophic oxidation, a specimen coated with 5 mg/cm^2 was oxidized for 65 hours. It was observed that although the accelerated oxidation rate persisted up to 65 hours, severe or catastrophic attack was not initiated.

The results of experiments with Co-25Al-12Ta, Figure 64, were similar to those for Co-25Al. After a period during which no accelerated oxidation occurs, the rate suddenly increases and then eventually decreases again.

Based upon metallographic examination, it was determined that continuous layers of Al_2O_3 were not present on the Co-25Al-6Mo and Co-25Al-12Ta specimens after oxidation with Na_2SO_4. The oxide scales were thick and zones of what appeared to be aluminum sulfide particles were evident in the alloys beneath the oxide scales. The structures of these two alloys were very similar to that observed with oxidized specimens of Na_2SO_4-coated Co-25Al.

Weight change data obtained from cyclic hot corrosion testing (0.5 mg/cm Na_2SO_4) of Co-25Al-6Mo and Co-25Al-12Ta are compared to that obtained previously for Co-25Al and Co-25Al-12W alloys in Figure 65. These data as well as visual observations of specimens from this test indicate that the amounts of degradation of the Co-25Al-6Mo and Co-25Al-12W alloys are about the same, and both of these alloys are degraded more severely than the Co-25Al alloy. It appears that cyclic conditions can induce catastrophic hot corrosion of the Co-25Al-6Mo alloy. The results obtained with the Co-25Al-12Ta alloy, Figure 65, indicate that the degradation of this alloy is less severe than that observed for Co-25Al. It appears that tantalum may not induce catastrophic oxidation as do molybdenum and tungsten.

In the cyclic hot corrosion test, thick oxide scales were developed on the Co-25Al-6Mo and Co-25Al-12Ta alloys, Figure 66a and 66c. The structure of the scale which was formed on the Co-25Al-6Mo alloy was similar to that observed with the Co-25Al-12W alloy; in particular, a thick, stratified scale was evident, Figure 66a, above a thin diffusion zone in the alloy, Figure 66b. This diffusion zone contained virtually no sulfides whereas sulfides were evident in the diffusion zone on the Co-25Al-12W specimen. The microstructure of the Co-25Al-12Ta was similar to that of the Co-25Al in the cyclic hot corrosion tests. Beneath the oxide scale on the Co-25Al-12Ta alloy, a thick zone of sulfide particles was clearly evident, Figure 66d.

The results obtained from the oxidation of specimens of each alloy that were coated with Na_2SO_4 and annealed for 1 hour in argon at 1000°C prior to oxidation were substantially the same as those without the argon treatment (Figures 63 and 64) except that no incubation period was observed.

(2) Co-25Cr-6Mo, Co-25Cr-12Ta: Weight change versus time data obtained from the isothermal oxidation of Co-25Cr-6Mo and Co-25Cr-12Ta alloys with Na_2SO_4 deposits are presented in Figure 67. Oxidation of the Co-25Cr-6Mo alloy with Na_2SO_4 in 1 atm of oxygen was much greater than that observed for this alloy without Na_2SO_4, Figure 67a. When similar experiments were performed on 0.1 atm of oxygen, Figure 67b, weight losses rather than weight gains of the Na_2SO_4-coated specimens were observed. Weight losses were also observed for Co-25Cr-12Ta specimens with Na_2SO_4 deposits in 1 atm of oxygen, Figure 67c. Weight loss curves under isothermal conditions have been obtained for the oxidation of a number of alloys with Na_2SO_4 deposits in this program. It has been found that such results usually occur when a protective layer of oxide is developed on alloys beneath the Na_2SO_4. The weight losses are believed to occur because the mass changes produced by the evolution of gases exceed those produced due to oxide formulation. The very severe oxidation of the Co-25Cr-6Mo alloy in 1 atm of oxygen when coated with Na_2SO_4, Figure 67a, shows that the oxide layer which is developed on this alloy under such conditions is less protective than that which is developed on the alloy in the absence of

a Na_2SO_4 deposit. As discussed previously, a protective layer of Cr_2O_3 is not formed on this alloy during oxidation in 1 atm of oxygen and the oxide scale would therefore be expected to contain a substantial amount of molybdenum oxides.

Examination of transverse microsections of these specimens showed that continuous, external layers of Cr_2O_3 appeared to have been formed on the Na_2SO_4-coated Co-25Cr-6Mo and Co-25Cr-12Ta alloys during isothermal oxidation in 0.1 atm of oxygen. Sulfide particles were evident in these alloys beneath the C_2O_3 scales. Similar microstructures were observed with Na_2SO_4-coated speciments of Co-25Cr-12Ta after oxidation in 1 atm of oxygen. Extremely thick scales were observed on the Co-25Cr-6Mo alloy, however, after oxidation of Na_2SO_4-coated specimens in 1 atm of oxygen. These thick scales had features similar to those of catastrophic oxidation induced by acidic fluxing.

Cyclic hot corrosion tests (0.5 mg/cm^2 Na_2SO_4) with Co-25Cr-6Mo and Co-25Cr-12Ta specimens were performed in both 1 and 0.1 atm of oxygen. Some of these results are presented in Figure 68 where data for Co-25Cr-12W and Co-35Cr have been included for comparison. Cyclic oxidation of Co-25Cr-6Mo with Na_2SO_4 in 1 atm of oxygen resulted in very severe hot corrosion degradation. Such a result is not surprising because this alloy is severely degraded even under isothermal conditions, Figure 67a. Results obtained for cyclic hot corrosion testing of Co-25Cr-6Mo in 0.1 atm of oxygen are also presented in Figure 68. Large weight losses typical of those for Na_2SO_4-induced oxidation were not observed but visual examination of this specimen indicated severe hot corrosion had occurred. One of the shortcomings of the cyclic test is that occasionally only portions of the oxide scale may spall and severe oxidation can take place with relatively small weight changes of specimens. It is therefore necessary to use the weight change data, visual observations and metallographic examination in combination to describe the severity of the degradation. Metallographic examination of the Co-25Cr-6Mo specimens after the cyclic hot corrosion test in 0.1 atm of oxygen showed that severe degradation of the Co-25-6Mo alloy had occurred. The structure of this alloy was very similar to that observed with the other alloys that contained molybdenum or tungsten. The oxide scale was thick and stratified, Figure 69a, and only a very thin diffusion zone was evident in the alloy beneath this oxide scale, Figure 69b.

The weight change data obtained for the Co-25Cr-12Ta alloy in the cyclic hot corrosion test were not influenced by oxygen pressure and weight losses less than those for Co-35Cr were observed, Figure 68. Visual observations of these specimens were consistent with the weight change data. The microstructure of the Co-25Cr-12Ta alloy after testing in the cyclic hot corrosion test was similar to that observed previously with the Co-35Cr alloy. A continuous layer of Cr_2O_3 appeared to have been developed on this alloy and sulfide particles, some of which were preferentially oxidized, were evident in the alloy, Figure 69.

The kinetic data obtained from the oxidation of Co-25Cr-12Ta which was coated with Na_2SO_4 and annealed in argon prior to oxidation was similar to that for specimens without an argon anneal. In contrast to this, Co-25Cr-6Mo treated in the same manner suffered severe oxidation as shown in Figure 70a. The microstructure of this specimen had features typical of those associated with catastrophic oxidation induced by acidic Na_2SO_4, Figures 70b and 70c.

(3) Co-25Cr-3Al-5Ti: A comparison of the kinetics obtained for specimens of Co-25Cr-3Al-5Ti with and without Na_2SO_4 have shown that the weight gains observed for the specimens with Na_2SO_4 deposits were slightly less than those observed for oxidation without Na_2SO_4. For example after 20 hours of oxidation weight gains of 1 and 2 mg/cm^2 were observed for specimens with and without Na_2SO_4, respectively. Such results indicate the oxide layer developed on this alloy beneath the Na_2SO_4 is the same as that which is formed when Na_2SO_4 is not present. The smaller weight gains probably result from evolution of gases from the specimens covered with Na_2SO_4 deposits. An examination of the microstructure of the Na_2SO_4-coated specimen showed that a continuous Cr_2O_3 layer had been developed during oxidation in 1 atm of oxygen. Sulfide particles, which were evident in the alloy beneath the Cr_2O_3 scale, may consist of chromium and titanium sulfides.

Results obtained from the cyclic hot corrosion testing of the Co-25Cr-3Al-5Ti alloy are presented in Figure 71. Data obtained for Co-35Cr and Ni-13Cr-3Al-5.3Ti specimens in this test are also included for comparison. The weight losses for the Co-25Cr-3Al-5Ti alloy are less than those for Co-35Cr. The oxide scale did not spall from the Ni-13Cr-3Al-5.3Ti alloy, Figure 71, but the large weight gains observed indicate severe hot corrosion had occurred. Visual observation of the surfaces of the specimens from this test indicated that the Co-25Cr-3Al-5Ti alloy had undergone less attack than the Co-35Cr or Ni-13Cr-3Al-5.3Ti alloys. The external oxide formed on the Co-25Cr-3Al-5Ti after 300 cycles appeared to be mainly Cr_2O_3, however, a significant amount of internal oxide protrusions and sulfide particles were evident, Figure 72. This evidence supports the conclusion that the alloy was not severely attacked in this test.

Results obtained from the oxidation of Co-25Cr-3Al-5Ti which had been coated with Na_2SO_4 and annealed in argon for 1 hour prior to oxidation were similar to those obtained without an argon anneal. Kinetic and metallographic evidence indicates that the behavior of this specimen is essentially like that for other Na_2SO_4-coated specimens of this alloy which already has been described.

d. Oxidation of Presulfidized Specimens

Specimens of Co-25Al-6Mo, Co-25Al-12Ta, Co-25Cr-6Mo, Co-25Cr-12Ta and Co-25Cr-3Al-5Ti were presulfidized in a H_2S-H_2 gas mixture at 1000°C with H_2S/H_2 = 0.2 and subsequently oxidized in oxygen. These specimens were not cooled to room temperature during the period over which the gas was changed from the H_2S-H_2 mixture to oxygen. The sulfidizing pretreatment was performed for about 2 minutes during which the specimens gained about 3 mg/cm^2.

The weight change versus time curves obtained by oxidizing presulfidized specimens of Co-25Al-12Ta and Co-25Al-6Mo alloys showed that this pretreatment caused increased oxidation. For example, after 20 hours of oxidation the presulfidized specimens gained four to five times as much weight as specimens which had not been presulfidized. The microstructures of the presulfidized specimens after oxidation were similar to those observed after oxidation of Na_2SO_4-coated specimens of these alloys. A continuous layer of Al_2O_3 was not developed on these alloys and particles of aluminum sulfide were evident in the alloys beneath the oxide scale.

The weight change versus time data obtained for the oxidation of presulfidized specimens of Co-25Cr-12Ta and Co-25Cr-3Al-5Ti showed that the pretreatment had caused increased oxidation of these two alloys. This increased oxidation occurred during the initial stages of oxidation. Metallographic examination of presulfidized specimens after 20 hours of oxidation showed that continuous layers of Cr_2O_3 were eventually developed on both alloys. It therefore appears that the sulfidizing pretreatment prolongs the transient period of oxidation during which continuous layers of Cr_2O_3 are being developed on these two alloys.

The sulfidizing pretreatment caused severe oxidation of the Co-25Cr-6Mo alloy to occur, Figure 73a. After the pretreatment a layer of sulfide was evident on this alloy, Figure 73b. After oxidation of such a specimen, a thick nonprotective oxide scale was evident, Figure 73c. The structure of this thick oxide scale was similar to that observed after catastrophic oxidation induced by Na_2SO_4, Figures 69a and 69b, but a sulfide zone was also evident beneath the oxide scale on the presulfidized and oxidized specimen, Figure 73c. It is necessary to emphasize that very severe oxidation of the Co-25Cr-6Mo alloy was observed in 1 atm of oxygen even without a Na_2SO_4 deposit or a sulfidizing pretreatment. A protective layer of Cr_2O_3 was developed on this alloy only after the oxygen pressure was reduced to 0.1 atm. It therefore appears that the sulfidizing pretreatment may have prevented the development of a protective Cr_2O_3 scale on this alloy during oxidation in 0.1 atm of oxygen.

e. Hot Stage Experiments

Specimens of Co-25Al-6Mo, Co-25Al-12Ta, Co-25Cr-6Mo, Co-25Cr-12Ta and Co-25Cr-3Al-5Ti were coated with Na_2SO_4 and oxidized in air at 1000°C in the hot stage microscope. The features which were observed were consistent with the results that were obtained from previous experiments with these alloys.

In the case of the Co-25Al-12Ta and Co-25Al-6Mo alloys, a thin layer of oxide was observed to form beneath the Na_2SO_4. After about two to three minutes the Na_2SO_4 was observed to penetrate the oxide layer formed on Co-25Al-12Ta alloy and spread laterally beneath this oxide layer. The Na_2SO_4 did not penetrate the oxide which formed on the Co-25Al-6Mo alloy after five minutes of oxidation. Upon thermally cycling the Co-25Al-6Mo specimen, the Na_2SO_4 was observed to spread laterally beneath the oxide scale. Such results indicate that molybdenum does inhibit the penetration of Al_2O_3 scales by Na_2SO_4. It is believed that such a condition occurs because of the introduction of molybdenum oxides, which are formed during the transient period of oxidation, into the Na_2SO_4 and the oxide ion concentration of the Na_2SO_4 is consequently decreased.

Protective oxide layers were observed to be formed beneath the Na_2SO_4 on specimens of Co-25Cr-12Ta, Co-25Cr-6Mo and Co-25Cr-3Al-5Ti alloys. The Na_2SO_4 did not penetrate these oxide scales after five minutes of oxidation. The Na_2SO_4 became dark yellow in color which indicates chromium entered the Na_2SO_4. A few particles of oxide were observed floating upon the Na_2SO_4 but no indications of rapid oxidation were evident.

f. Crucible Experiments

To permit examination of the reaction between TiO_2 and Na_2SO_4, tablets of monocrystalline TiO_2 (Rutile) were immersed in Na_2SO_4 and heated in air at 1000°C. After 42 hours, a weight gain of the TiO_2 specimen of about 0.1 mg/cm^2 was observed. A deposit which was identified by X-ray diffraction as $Na_2O \cdot 6TiO_2$ was evident on the surface of the specimen. A similar experiment was performed using Na_2SO_4 containing 1 w/o Na_2O. A weight gain of the TiO_2 specimen of about 3.5 mg/cm^2 was observed after 2 hours. A relatively thick deposit was observed on the surface of this specimen which was identified as $Na_2Ti_3O_7$ ($Na_2O \cdot 3TiO_2$). A third experiment was also performed using Na_2SO_4 containing 10 w/o WO_3. This mixture was heated for 2 hours before the TiO_2 tablet was added. After 2 hours a weight loss of the TiO_2 tablet of about 0.5 mg/cm^2 was observed. In addition etch pits were evident on the surface of this specimen. The results which have been obtained from the crucible experiments show TiO_2 can react with basic and acidic melts of Na_2SO_4. In the case of basic melts, it appears that reaction between the TiO_2 and oxide ions results in the formation of a reaction product which is solid at 1000°C. For acidic melts the TiO_2 apparently dissolves into the melt by donating oxide ions.

Sodium sulfate melts containing 10 w/o of either TiO_2 or Ta_2O_5 powders were also heated 2 hours at 1000°C in air. Weight losses of 4.4 and 47.3 mg were observed for the melts containing TiO_2 and Ta_2O_5, respectively. A weight loss of 0.9 mg was observed for pure Na_2SO_4, These results indicate SO_2 is evolved during the reaction of TiO_2 and Ta_2O_5 with reagent grade Na_2SO_4. More importantly, it appears that more reaction occurs in the case of Ta_2O_5 than TiO_2.

To determine if MoO_3, when added to Na_2SO_4, would cause catastrophic oxidation of Co-25Cr-12Ta and Co-25Cr-3Al-5Ti alloys, specimens of these alloys were coated with Na_2SO_4 (1 mg/cm^2) and oxidized at 1000°C for 8 hours in flowing oxygen containing molybdenum oxide vapor. The molybdenum oxide vapor was added to the gas by flowing the oxygen over a platinum crucible containing MoO_3 at 800°C. The Na_2SO_4-coated specimens were placed in the hot zone of a horizontal furnace and the platinum crucible was placed upstream from the specimens where the temperature of the furnace was 800°C. Based upon the vapor pressure of MoO_3 (ref. 37), the activity of MoO_3 in the gas at 1000°C was approximately 0.1. Extremely thick oxide scales were developed on these two alloys during oxidation under such conditions. These scales spalled extensively upon cooling to room temperature. Weight losses of 243 and 198 mg/cm^2 were determined for the Co-25Cr-12Ta and Co-25Cr-3Al-5Ti alloys, respectively. These result show that the addition of MoO_3 to Na_2SO_4 can cause catastrophic oxidation to occur for alloys which do not contain molybdenum or tungsten.

g. Summary of Relevant Results

The significant experimental results can be summarized as follows:

(1) Co-25Al-6Mo: Oxidation of the Co-25Al-6Mo alloy in oxygen results in the formation of a continuous external Al_2O_3 film. Isothermal oxidation of Na_2SO_4-coated specimens of this alloy leads to accerated, but not catastrophic degradation. Under

these conditions, the degradation is similar to that for Na_2SO_4-coated Co-25Al. Pre-sulfidation of this alloy followed by oxidation resulted in attack which was similar to that for the isothermal oxidation of Na_2SO_4-coated specimens. On the other hand, Na_2SO_4-coated specimens were catastrophically degraded in cyclic oxidation, after only a few hours of exposure. The structures of the oxide scales formed during catastrophic oxidation of this alloy were similar to those formed on Co-25Al-12W and on Ni-27.7Al-12W alloys during Na_2SO_4-induced attack.

(2) Co-25Cr-6Mo: Specimens of this alloy formed external Cr_2O_3 layers in experiments at 0.1 atm oxygen pressure, but not at 1.0 atm oxygen pressure. When specimens which had been coated with Na_2SO_4 were isothermally oxidized in 0.1 atm oxygen, accelerated attack was not observed, whereas in 1.0 atm oxidation,catastrophic oxidation occurred. On the other hand, cyclic oxidation of Na_2SO_4-coated specimens in 0.1 atm oxygen did result in catastrophic attack of the alloy. In addition, catastrophic isothermal oxidation of Na_2SO_4-coated specimens occurred in 0.1 atm oxygen when annealed in argon prior to oxidation. Severe degradation was also observed after presulfidation. The oxide scales formed on specimens which had undergone catastrophic attack induced by Na_2SO_4 were thick and porous, and similar in structure to those formed on Co-25Cr-12W under similar conditions.

(3) Co-25Al-12Ta, Co-25Cr-12Ta: These alloys readily formed Al_2O_3 and Cr_2O_3, respectively, during oxidation at 1000°C. The results of experiments with Na_2SO_4 and with presulfidation treatments indicated that these alloys were degraded no more severely than the corresponding base alloys without tantalum (i.e. Co-25Al and Co-35Cr). In fact, weight change data obtained from the cyclic hot corrosion tests indicated that these alloys may be somewhat more hot corrosion resistant than the corresponding base alloys, although microstructural characteristics of the tantalum-containing alloys were similar to those formed in base alloy hot corrosion specimens.

(4) Co-25Cr-3Al-5Ti: Oxidation of this alloy in the absence of Na_2SO_4 results in the formation of a noncontinuous TiO_2 external layer, a continuous Cr_2O_3 internal layer, and an internal zone of Al_2O_3 protrusions. The oxidation rate is similar to that for Cr_2O_3-forming alloys. Specimens which had been coated with Na_2SO_4 or presulfidized prior to oxidation were not severely attacked. Examination of the microstructures indicated that in all cases continuous Cr_2O_3 barriers were eventually formed on this alloy.

(5) Crucible Experiments: Titania and Ta_2O_5 react with oxide ions in Na_2SO_4 which causes SO_2 evolution. These oxides do not apparently make the Na_2SO_4 as acidic, however, as WO_3 or MoO_3. In the case of TiO_2 such a condition may be due to the formation of a solid reaction product that inhibits the reaction.

Molybdenum oxide vapor can induce catastrophic oxidation of Na_2SO_4-coated alloys which do not contain molybdenum.

h. Interpretation of Results

(1) Effects Produced by Molybdenum: The results obtained with the Co-25Al-6Mo and Co-25Cr-6Mo alloys show that molybdenum produces effects during the hot corrosion of alloys similar to those observed previously with tungsten. In particular, molybdenum prevents the onset of accelerated oxidation induced by basic Na_2SO_4 since molybdenum oxides in the Na_2SO_4 cause the oxide ion activity of the Na_2SO_4 to be reduced to levels below that required for reaction with the oxide scales. Molybdenum can, however, cause catastrophic oxidation of Na_2SO_4-coated alloys. Such a condition occurs after a sufficient amount of molybdenum has been introduced into the Na_2SO_4 whereby protective oxide scales are not stable in the acidic Na_2SO_4 melt. The mechanism by which molybdenum causes acidic attack of these alloys is believed to be essentially the same as that described previously for tungsten. Exposure conditions which tend to damage the normally protective oxide scale formed on this alloy will favor the onset of catastrophic hot corrosion. In particular thermal cycling, which may crack the oxide scales would be expected to favor the initiation of acidic attack.

The important points to be derived from this study are as follows:

- The presence of molybdenum in nickel-and cobalt-base alloys may be beneficial or may be detrimental to the hot corrosion degradation of the alloy.

- The effect of molybdenum on the hot corrosion processes is determined by the amount of molybdenum (as MoO_3) which can react with the Na_2SO_4. For low activities of MoO_3, the effect of molybdenum is similar to that of chromium in reducing the oxide ion activity of the melt and thereby prolonging the life of the protective oxide films. At higher activities of MoO_3 (e.g. 0.1) the Na_2SO_4-MoO_3 melt prevents the formation of protective scales. Protective oxide scales are not stable because they react with the melt by donating oxide ions to the melt. It is important to emphasize that, while oxides of molybdenum, tungsten and vanadium decrease the oxide ion activity of the Na_2SO_4 melt, protective oxide barriers (e.g. Al_2O_3, CoO, NiO) donate oxide ions to the modified melts at oxide ion activities higher than would be required for pure Na_2SO_4. In other words, the presence of MoO_3, WO_3 or V_2O_5 in the Na_2SO_4 increases the solubility product of Al_2O_3, CoO and NiO in the Na_2SO_4.

- There appear to be no fundamental differences in the effect of molybdenum on nickel-or cobalt-base alloys.

(2) Effects Produced by Ta: The results obtained from the Co-25Al-12Ta and Co-25Cr-12Ta alloys indicate that tantalum does not detrimentally affect the oxidation of Na_2SO_4-coated specimens. Although the results of crucible experiments indicate that Ta_2O_5 reacts with Na_2SO_4 to increase the activity of SO_3 in the melt, it appears that oxide scales such as Al_2O_3 and Cr_2O_3 are stable in this melt. Previous studies have shown that Cr_2O_3 reacts with Na_2SO_4 in the same manner as Ta_2O_5, and it has been proposed that this reaction accounts for the ability of chromium in nickel and cobalt base alloys to inhibit the basic fluxing of Al_2O_3 films. For this reason tantalum in Co-25Al would be expected to inhibit the onset of accelerated oxidation caused by Na_2SO_4. It is not understood why such an effect was not observed.

The significant point to be emphasized here is that tantalum has potential application in cobalt-base alloys as a replacement for such hardening elements as tungsten and molybdenum, and the results of the present studies have shown that tantalum apparently does not have a deleterious effect on the hot corrosion behavior of these alloys. On the other hand, insufficient work was performed to identify the exact role of tantalum in the hot corrosion processes.

(3) Effects Produced by Ti: The data which are available from studies with the Co-25Cr-3Al-5Ti alloy are not sufficient to permit a meaningful discussion of the effects produced by titanium on the hot corrosion of alloys. Since the results obtained with this alloy were similar to those obtained with Co-25Cr-6Al, it appears that titanium does not produce any deleterious effects. Titanium alloy additions might be expected to have beneficial effects from two standpoints. In the first place, it appears that in basic Na_2SO_4 melts, TiO_2 reacts with Na_2O to form a solid reaction product on the surface of the TiO_2. For alloys which are susceptible to basic fluxing, an external layer of TiO_2 might be expected to inhibit the basic fluxing process. In the present work, the alloy studied was a chromia-former and therefore not susceptible to attack by a basic melt. In the second place, the affinity of titanium for sulfur might be used to inhibit the degradation of alloys which occurs as a result of preferential oxidation of liquid sulfides. More experimental work is required in order to evaluate these possible effects of titanium. It should be noted, however, in cases where titanium is attempted to be used, the concentration of titanium cannot be so large that the alloy oxidation rate is controlled by transport through a titanium oxide scale, because such a scale affords much less oxidation resistance than either Al_2O_3 or Cr_2O_3.

6. COMPARISON OF THE HOT CORROSION NiCrAl(Y) AND CoCrAl(Y) ALLOYS

a. Introduction

In the previous sections of this report, the hot corrosion of cobalt was compared to that of nickel, and then the hot corrosion of binary alloys of these two metals containing chromium or aluminum was compared. The effect of adding tungsten, molybdenum or tantalum to these binary alloys was then examined. In the present section, the effects produced by chromium, aluminum and yttrium in nickel and cobalt alloys will be compared. The compositions and structures of the NiCrAl, NiCrAlY, CoCrAl and CoCrAlY alloys which were used in this portion of the program have been described in Section II of the present report. It was desired to have these alloys contain about 25% Cr and 6% Al. Such concentrations of chromium and aluminum were selected, since it was desired to compare the hot corrosion of cobalt and nickel-base alloys under conditions where the alloys contained a substantial amount of chromium but still contained enough aluminum for the formation of continuous Al_2O_3 scales during isothermal oxidation. Some of these alloys also contained about 0.1% yttrium, in order to determine if elements used to improve oxide adhesion (e.g. Y, Sc, La, etc.) may also influence the hot corrosion of alloys.

b. Experimental Results

(1) Oxidation: Alloys of NiCrAl, NiCrAlY, CoCrAl and CoCrAlY were oxidized in 1 atm of oxygen at 1000°C. Continuous external layers of Al_2O_3 were observed to have formed on all of these alloys after a transient period of oxidation during which other oxides (i.e. Cr_2O_3, NiO, CoO, $NiCr_2O_4$, $CoCr_2O_4$) were evident. The parabolic rate constants obtained from the weight change versus time data were consistent with those obtained in other studies (ref. 28) involving alloys upon which external Al_2O_3 scales are developed during oxidation.

(2) Oxidation of Specimens Coated with Na_2SO_4: In the following, results obtained from the oxidation of Na_2SO_4-coated specimens of NiCrAl, NiCrAlY, CoCrAl and CoCrAlY are presented.

(a) Isothermal Oxidation at 1000°C: Isothermal oxidation experiments in 1 atm of oxygen using two different amounts of Na_2SO_4 (i.e. 0.5 and 5.0 mg/cm^2) were performed. Examination of weight change versus time data as well as the microstructures of oxidized specimens showed that a significant amount of hot corrosion degradation had not occurred for any of the alloys coated with 0.5 mg/cm^2 of Na_2SO_4.

Weight change versus time data obtained from the oxidation of specimens coated with 5.0 mg/cm^2 of Na_2SO_4 are presented in Figure 74. Those data obtained for the CoCrAl (Y) (CoCrAl and CoCrAlY) alloys were essentially similar to those obtained with 0.5 mg/cm^2 Na_2SO_4. The microstructure of a typical specimen after oxidation with a Na_2SO_4 deposit is presented in Figure 75a. It can be seen that a continuous layer of Al_2O_3 is present on the specimen surface. Beneath the Al_2O_3 layer some oxidation products are evident. Such products were only observed on the alloys which contained yttrium. It is believed that these products are oxides and sulfides of yttrium.

The weight change versus time data obtained for the oxidation of NiCrAl (Y) alloys with 5 mg/cm^2 of Na_2SO_4 are also presented in Figure 74. It can be seen that the weight changes of such specimens are usually substantially greater than those for the CoCrAl(Y) specimens. In some experiments, increased oxidation of NiCrAl or NiCrAlY was not observed even with 5 mg/cm^2 of Na_2SO_4. A microstructure typical of either NiCrAl or NiCrAlY, for the case where increased oxidation was observed, is shown in Figure 75b. A thick oxide scale, composed of NiO, Cr_2O_3 and Al_2O_3, is evident. In addition, it is obvious that preferential oxidation of these alloys has occurred whereby portions of the alloys have become completely enveloped with oxide, Figure 75b. Numerous sulfides are also evident within these alloys. The sulfides in the alloy near the external oxide scales had shapes which indicated some of these sulfides may have been liquid at the temperature of oxidation, Figure 76. Examination of these sulfide particles with the electron-beam microprobe showed that there were two types of sulfides in those regions of the alloy where preferential oxidation was evident, Figure 76. One type of sulfide contained predominantly chromium with a small amount of nickel. The other type of sulfide contained predominantly nickel with a small amount of chromium. Aluminum was not detected in either of the two sulfide phases. It was determined that preferential oxidation occurred where these sulfides were present in

the alloy, Figure 76a. Examination of these sites of preferential oxidation with the electron-beam microprobe indicated oxides of chromium and aluminum were present, Figure 77. More importantly, however, these probe data showed that the protrusions of oxide which extended into the alloy contained sodium and sulfur, Figure 77. Such results are similar to those obtained with Ni-14Al in the crucible test and indicate that Na_2SO_4 may play an important role in the development of the oxide protrusion.

In the experiments where increased oxidation of NiCrAl or NiCrAlY was not observed, even with 5 mg/cm^2 of Na_2SO_4, sulfides having morphologies suggesting that they had been liquid during oxidation and sites of preferential oxidation of these sulfides at which Na_2SO_4 was present were not observed. It therefore appears as though these features are an important part of the hot corrosion process for these alloys. Data available for the Ni-Cr-S phase diagram (ref. 38) indicates liquid phases can be formed at sulfur activities below that for the Ni-liquid nickel sulfide equilibrium. In addition, it has been determined that the formation of a liquid sulfide phase in Ni-Cr alloys (ref. 4) causes accelerated oxidation. It therefore seems reasonable that the formation of the liquid sulfide has caused the accelerated oxidation. On the other hand, the presence of aluminum in the oxide product at the site of the preferential attack but not in the sulfides is confusing. Such a condition indicates the aluminum is oxidized prior to or along with the formation of the sulfide.

(b) Oxidation of Argon-Annealed Na_2SO_4 Coated Specimens: The results obtained from the oxidation of Na_2SO_4-coated specimens of NiCrAl, NiCrAlY, CoCrAl and CoCrAlY that were annealed for 1 hour in argon prior to oxidation were similar to those obtained with Na_2SO_4-coated specimens that were not annealed. In particular, the NiCrAl and NiCrAlY specimens gained substantially more weight than either CoCrAl or CoCrAlY specimens. In addition, protective layers of Al_2O_3 had formed on the CoCrAl and CoCrAlY alloys, whereas thicker scales containing NiO and Cr_2O_3 had formed on the NiCrAl and NiCrAlY alloys above a zone of sulfides having a liquid-like morphology.

(c) Cyclic Oxidation of Na_2SO_4-Coated Specimens: Cyclic oxidation (1 hour cycles) testing of all four alloys was performed using both 0.5 and 5 mg/cm^2 of Na_2SO_4, deposited at regular intervals. Cyclic oxidation testing of these alloys without applying Na_2SO_4 as well as dynamic burner rig hot corrosion tests were also performed.

The weight change data obtained with these alloys in the cyclic laboratory test are compared in Figure 78 and photographs showing some microstructures of specimens from these tests are presented in Figures 79 and 80. Cyclic oxidation without Na_2SO_4 of the NiCrAl and CoCrAl alloys resulted in depletion of aluminum from these alloys with the formation of external Cr_2O_3 scales, Figures 79c and 80c. Less depletion of aluminum occurred in the cyclic test when these alloys contained yttrium because the Al_2O_3 scales were more adherent and consequently the oxide scales usually were composed of predominantly Al_2O_3 after 350 cycles, Figures 79d and 80d. Cyclic hot corrosion testing using 0.5 mg/cm^2 Na_2SO_4 did not cause very severe degradation of any of the alloys after 300 hours of testing compared to cyclic oxidation without Na_2SO_4 as can be seen by comparing Figures 78a and 78c. The microstructures of the specimens from the cyclic test using 0.5 mg Na_2SO_4, Figures 79a and 80a, were different from those obtained without

any deposit but the amount of degradation was not severe in either case. Electron beam microprobe examination of specimens from the cyclic test using 0.5 mg/cm^2 Na_2SO_4 showed that the alloys had been depleted of aluminum but still contained substantial amounts of chromium, Figure 81.

Cyclic hot corrosion testing using 5 mg/cm^2 Na_2SO_4 resulted in severe degradation of the NiCrA1 and NiCrA1Y alloys, Figure 78b, after as little as 30 cycles. The microstructures of the specimens that had been severely attacked, Figure 79b, were similar to those described previously for the isothermal tests using 5 mg/cm^2 Na_2SO_4 deposits, Figures 75b and 76. Examination of such microstructures with the electron beam microprobe showed that the alloys had been severely depleted of both aluminum and chromium, Figure 82a. Even though the NiCrAl and NiCrAlY alloys were severely depleted of chromium and aluminum, it was determined that continual deposition of Na_2SO_4 was required in order to sustain the rapid degradation of these alloys. For example, it was observed in the cyclic hot corrosion test that severe hot corrosion attack of NiCrA1 subsided if Na_2SO_4 was removed from the specimen, Figure 82b. In addition, continuous weight change versus time data obtained in the cyclic hot corrosion test underwent an abrupt change when the Na_2SO_4 was removed from the specimen, Figure 82c. These data show that hot corrosion degradation occurred after about 10 cycles. The square of the weight changes obtained between cycles 10 and 14 are plotted versus time in Figure 82d. These data do not conform to the parabolic rate law but a straight line can be drawn through the data points to obtain a rate constant. This rate constant has no theoretical significance but can be used to compare the hot corrosion rate of the alloy with rate constants for other systems. The rate constant is 1.4×10^{-8} gm^2/Cm^4-sec, whereas at 1000°C the parabolic rate constants for the growth of NiO on nickel, Cr_2O_3 on a Ni-30Cr alloy and Al_2O_3 on NiCrA1 are about 10^{-10}, 3×10^{-11} and 3×10^{-13} gm^2/cm^4-sec, respectively.

The CoCrA1 and CoCrA1 (Y) alloys were much more resistant to initiation of hot corrosion than the NiCrA1(Y) alloys. Severe degradation of CoCrA1 or CoCrA1Y was not observed after 300 cycles using 5 mg/cm^2 Na_2SO_4 deposits, Figure 78b. After such periods of testing, the microstructures of the CoCrA1 or CoCrA1Y alloys were not significantly different from those obtained by using 0.5 mg/cm^2 Na_2SO_4, Figures 80a and b. As the cyclic testing of the CoCrA1 alloy using 5mg/cm^2 Na_2SO_4 was extended beyond 300 cycles, evidence of more severe degradation began to become apparent. Surface and microstructural features observed after 400 cycles are presented in Figure 83. It is obvious that rather severe degradation of this alloy has begun to take place and the features of the degradation are similar to those observed for the severe hot corrosion of the NiCrA1(Y) alloys.

The data obtained with the NiCrA1(Y) and CoCrA1(Y) alloys in the cyclic hot corrosion test show that the severe degradation with microstructures such as that shown in Figure 75b, are preceded by a milder type of hot corrosion with microstructures such as that shown in Figure 79a. Such a sequence was verified by cyclic hot corrosion tests using a Ni-15Cr-6A1 alloy. This alloy was tested to determine if a 0.5 mg/cm^2 Na_2SO_4 deposit could cause severe hot corrosion at 1000°C. After 300 cycles of testing, severe degradation of this alloy was not observed and the microstructure was typical of the mild

form of hot corrosion, Figure 84a. After 520 cycles, however, it became evident that more severe attack was beginning to occur and a microstructure typical of the more severe form of hot corrosion was evident, Figure 84b.

Surface photographs of NiCrA1(Y) and CoCrA1(Y) alloys obtained after different amounts of burner rig testing at 1000°C with a Na_2SO_4 deposition rate of 0.1 mg/cm^2-hr are presented in Figure 85. The superior hot corrosion resistance of the CoCrA1(Y) alloys compared to the NiCrA1(Y) alloys is obvious. Weight change data and microstructural features obtained with NiCrA1(Y) specimens in the laboratory cyclic hot corrosion test and the burner rig test are compared in Figure 86. The microstructural features are very similar but there is no agreement between the weight change data. It was observed that the oxide scales spalled extensively from the coupons used in the laboratory test whereas much less spalling took place from the cylindrical rods used in the burner rig and this condition may account for the observed difference in the weight change data. Data obtained from testing CoCrA1(Y) alloys in the laboratory and in the burner rig are compared in Figure 87. The specimens tested in the burner rig exhibited a large initial weight loss, but then the weight changes of the specimens in both tests are quite similar. The burner rig specimens had threaded ends by which they were supported, Figure 1b. It is believed these initial losses in weight may have been caused by the loss of metal as the specimens were screwed into the specimen holders. The microstructures of the CoCrA1(Y) specimens from the laboratory test and the rig test were very similar as can be seen by comparing Figures 87b and 87c.

(3) Experiments Designed to Examine the Influence of Sulfur: To determine the influence of sulfur on the oxidation of NiCrA1(Y) and CoCrA1(Y) alloys, experiments were performed in which presulfidized specimens were oxidized and specimens were also oxidized in SO_2. The results obtained from such experiments are presented in the following.

(a) Oxidation of Presulfidized Specimens: Three different types of experiments were performed by using presulfidized specimens. One type involved the isothermal oxidation of specimens which had been previously subjected to a sulfidizing environment for about 20 seconds. Another involved the oxidation of specimens which had been completely sulfidized (i.e., the specimens were equilibrated with the sulfidizing environment prior to oxidation). The third type of experiment involved cyclic oxidation of sulfidized specimens where the sulfidizing treatment was repeated at the same time intervals as those at which Na_2SO_4 was deposited on specimens in the cyclic hot corrosion test.

The results obtained from the isothermal oxidation of specimens that had been previously suflidized (i.e. 20 seconds in gas with H_2S/H_2 = 0.2 at 1000°C, 3-7 mg/cm^2 of sulfur picked up by specimens) are presented in Figure 88. The weight gains of the CoCrA1 and CoCrA1Y alloys are virtually the same as those obtained for the oxidation of these two alloys without the sulfidizing pretreatment. In contrast, the sulfidizing pretreatment has caused both the NiCrA1 and NiCrA1Y alloys to be oxidized at accelerated rates.

Typical microstructures for some of these alloys are shown in Figure 89. Very little oxidation of the CoCrAl or CoCrAlY, Figure 89a, alloys was evident. It appeared as though a continuous layer of Al_2O_3 had formed upon the sulfide layer which developed during the sulfidizing pretreatment. Both the NiCrAl, Figure 89b, and NiCrAlY specimens had microstructures similar to those observed with Na_2SO_4-coated specimens of these alloys which had undergone accelerated oxidation. In particular, preferential oxidation of sulfides had occurred, and the morphology of these sulfides was such that it appeared as though the sulfides had been liquid at the temperature of oxidation. The microstructures of the CoCrAl and NiCrAl specimens after the sulfidizing treatment but prior to oxidation are presented in Figure 90. It is important to note that only solid sulfides appear to have formed on the CoCrAl alloy, whereas liquid nickel sulfide was formed on the NiCrAl specimen.

When specimens of NiCrAl and CoCrAl were equilibrated with the sulfidizing gas environment (i.e. $H_2S/H_2 = 0.2$), subsequent oxidation in oxygen at 1000°C resulted in the formation of protective barriers of Al_2O_3 on the NiCrAl alloy but a nonprotective oxide scale was formed on the CoCrAl alloy and SO_2 was detected to be evolved from the specimen. The more severe oxidation of the equilibrated CoCrAl specimens is not surprising. It appears as though the sulfur activity in these specimens is such that SO_2 evolution prevents the formation of a protective oxide barrier. The development of protective oxide barriers on the equilibrated NiCrAl specimens is confusing. Oxidation of the metallic components in the equilibrated NiCrAl specimen should cause the sulfur activity to increase to a level at which SO_2 is involved. It appears that the sulfur activity in this system does not increase as rapidly during subsequent oxidation as it must in the CoCrAl system.

Specimens of NiCrAl were also presulfidized in a gas mixture with H_2S/H_2 ratio of 0.04. This ratio was used, rather than one that established a sulfur activity at which the liquid nickel sulfide melt was not stable, because previous work (ref. 24) had shown presulfidization in such a gas mixture did not affect the oxidation of NiCrAl. The NiCrAl specimens were presulfidized for 200 seconds and had weight gains between 2-5 mg/cm^2. Oxidation of these specimens did not result in accelerated oxidation. It appeared as though protective layers of Al_2O_3 had been formed on the specimens. It was also observed that, while the liquid sulfide phase had been formed during the sulfidizing treatment, it was rapidly converted to chromium sulfide and the oxide barrier appeared to have developed on this latter sulfide. It therefore appears as though the formation of liquid nickel sulfide in NiCrAl alloys can cause rapid oxidation only when this sulfide exists as a zone near the surface of the alloy, as opposed to being uniformly distributed throughout the alloy. This situation indicates that the cause for the rapid oxidation must be related to some condition which develops or exists as the liquid sulfide reacts with the alloy. A reasonable supposition is that the liquid provides a rapid transport medium for oxygen into the alloy.

The results obtained from the experiments using presulfidized specimens show that appropriate amounts of sulfur in NiCrAl(Y) alloys can decrease the oxidation resistance of these materials. Deposition of Na_2SO_4 on alloys will provide the source for the sulfur. However, removal of sulfur from the Na_2SO_4 will produce oxide ions which also can affect the oxidation of the alloys in a deleterious manner. In order to attempt to differentiate

between the effects produced by sulfur and oxide ions in the Na_2SO_4, presulfidized specimens and specimens coated with Na_2CO_3 were cylically ozidized and the results were compared to those obtained with Na_2SO_4 deposits. In the experiments where presulfidized specimens were used the sulfidizing pretreatment was performed at a frequency equal to that at which Na_2SO_4 was applied to specimens in the cyclic hot corrosion test and the amount of sulfur added to the alloy per unit area during each sulfiding pretreatment was equal to the sulfur in a 5 mg/cm^2 deposit of Na_2SO_4.

The results obtained from these tests when NiCrAl specimens were used are presented in Figure 91a. The weight losses of the specimens with deposits of Na_2CO_3 are much less than those of specimens with Na_2SO_4 deposits, whereas the data obtained with the presulfidized specimen are similar to that observed with Na_2SO_4 deposits. The results obtained when CoCrAl(Y) specimens were used in these tests are presented in Figure 91b. The Na_2CO_3-coated specimens have undergone much more severe degradation than the Na_2SO_4-coated specimens whereas the data obtained with the presulfidized specimens is similar to that obtained with Na_2SO_4-coated specimens. The results that have been obtained from these experiments rather conclusively show that sulfur from the Na_2SO_4 must play a significant role in the hot corrosion of NiCrAl. The reasoning for such a statement is as follows. It is apparent that the oxide ion content of Na_2CO_3 is sufficient to cause a substantial amount of oxidation of both NiCrAl and CoCrAl alloys. The attack of CoCrAl is more severe than NiCrAl, perhaps because cobaltous oxide can dissolve in Na_2CO_3 at lower oxide ion activities than NiO. The lack of attack of CoCrAl with Na_2SO_4 deposits can be rationalized by supposing that very little sulfur is removed from the Na_2SO_4 and therefore the oxide ion activity is low. In the case of the NiCrAl alloy, it can be argued that more attack is observed by Na_2SO_4 than Na_2CO_3 because the Na_2SO_4 deposit establishes a larger activity of oxide ions than Na_2CO_3. Such a condition can be achieved, however, only when the alloy removes the sulfur from the Na_2SO_4, and it has been determined that such quantities of sulfur in this alloy will result in accelerated oxidation.

(b) Oxidation in SO_2 at 1000°C: Specimens of NiCrAl, NiCrAlY, CoCrAl and CoCrAlY were oxidized in flowing SO_2 at 1000°C for about 20 hours. External scales of Al_2O_3 were developed on all of the alloys. The oxidation of these alloys did not appear to be significantly different from that observed for these alloys in oxygen. A few sulfide particles were evident in these alloys beneath the oxide scales. The sulfides appeared to be chromium sulfide or yttrium sulfide in the case of the alloys that contained yttrium.

(4) Oxidation of Na_2SO_4 – Coated Alloys using the Hot Stage Microscope: Specimens of the four alloys were coated with Na_2SO_4 and oxidized in air at 1000°C in a hot stage microscope. After melting, the Na_2SO_4 always became yellow in color, which showed that some Cr_2O_3 on the alloy surface had reacted with the Na_2SO_4. A layer of Al_2O_3 was observed to have formed beneath the molten Na_2SO_4 on both the CoCrAl and CoCrAlY specimens. Usually similar results were obtained with the NiCrAl and NiCrAlY alloys. In some experiments, however, oxides other than Al_2O_3 formed in localized regions on the surfaces of the NiCrAl and NiCrAlY specimens. In those areas

where Al_2O_3 scales were not observed to have formed, more severe oxidation was evident and it is believed such conditions may mark the initiation of localized hot corrosion degradation of the NiCrAl and NiCrAlY alloys.

(5) Oxidation of Na_2SO_4 – Coated Specimens in Oxygen Containing Oxide Vapors: To determine if MoO_3, when added to Na_2SO_4, would cause catastrophic oxidation of NiCrAl, NiCrAlY, CoCrAl, CoCrAlY, Ni-30Cr, Co-35Cr and Ni-25Al alloys, specimens of these alloys were coated with Na_2SO_4 and oxidized at 1000°C for 8 hours in flowing oxygen containing molybdenum oxide vapor at an activity of about 0.1. An experiment of this type was also performed by using specimens with no Na_2SO_4 coatings. The results obtained from these experiments are presented in Table X. It can be seen that all of the alloys which were coated with Na_2SO_4 have undergone severe oxidation. This was confirmed by metallographic examination of the oxidized specimens. The specimens which were not coated with Na_2SO_4 were oxidized more than that observed for pure oxygen. Metallographic examination of these latter specimens confirmed, however, that the oxidation was substantially less than that for specimens coated with Na_2SO_4. These results show that MoO_3, at an activity of less than unity, does react with oxide scales such as Al_2O_3, Cr_2O_3, NiO and CoO. In addition, the products of these reactions afford less protection to the alloys than do the unmodified oxide scales. More importantly, Na_2SO_4 permits the reactions between MoO_3 and these oxides to occur more effectively. It is proposed that this effective destruction of the protective oxide scales occurs because solutions of Na_2SO_4 and MoO_3 react with such oxides via an acidic fluxing process (ref. 12).

An experiment was also performed in which Na_2WO_4-coated specimens of NiCrAl, NiCrAlY, CoCrAl and CoCrAlY were oxidized in flowing oxygen having an activity of WO_3 equal to 0.7. The weight changes of the specimens after 24 hours of oxidation are presented in Table X.

TABLE X

WEIGHT CHANGES OF SPECIMENS OXIDIZED IN OXYGEN CONTAINING OXIDE VAPOR

	$\Delta M/A$ (mg/cm^2) p_{O_2} = 1 atm, a_{MoO_3} = 0.1		$\Delta M/A$ (mg/cm^2) p_{O_2} = 1 atm, a_{WO_3} = 0.7
	8 hrs, 1000°C		24 hrs, 1000°C
Alloy	Na_2SO_4 Coating	No Coating	Na_2WO_4 Coating
NiCrAl	- 85.6	+ 0.2	-0.4
NiCrAlY	- 63.1	+ 1.3	+1.8
CoCrAl	- 35.6	-10.8	-6.7
CoCrAlY	+ 85.2*	-41.3	+2.5
Ni-30Cr	- 81.3	0	
Co-35Cr	- 91.2	- 7.5	
Ni-25Al	-167.2	+ 1.90	

*Very severe oxidation of this alloy had occurred, but much of the oxide remained attached to the alloy.

These weight changes as well as visual examination indicate that a substantial amount of oxidation has not occurred. In view of the results obtained with the Co-25Al-12W and Co-25Cr-12W alloys in this program, one would expect WO_3 to produce conditions similar to those produced by MoO_3. It is believed the observed lack of severe oxidation on the alloys oxidized in oxygen containing WO_3 may have occurred due to insufficient WO_3 in the oxygen. The vapor pressure of WO_3 is orders of magnitude less than that for MoO_3 and equilibrium between the gas and the WO_3 in the platinum crucible probably was not achieved.

(6) Additional Experiments: During the time period that the hot corrosion of NiCrAl (Y) and CoCrAl (Y) alloys was being examined in this program, it became apparent that certain other additional experiments would be helpful to describe the degradation process of these materials. In the following, such experiments are described and the relevant results are also presented.

Comparison of data obtained in the cyclic oxidation test (1 hour cycles) for Ni-30Cr, Figure 31, and the NiCrAl (Y) alloys, Figure 78b, shows that the NiCrAl (Y) alloys were degraded more severely than the Ni-30Cr alloy. This condition may occur because of the higher chromium content of the Ni-30Cr alloy or because of aluminum in the NiCrAl (Y) alloys. In Figure 92, weight change versus time data for the cyclic hot corrosion of Ni-30Cr, Ni-30Cr-6Al and Ni-15Cr-6Al are compared. Upon comparing the data obtained for Ni-30Cr and Ni-30Cr-6Al, it is apparent that for more than 50 hours less degradation of the Ni-30Cr-6Al alloy has occurred than that observed for the Ni-30Cr alloy. For cyclic oxidation times greater than about 50 hours, however, the degradation of the Ni-30Cr-6Al is much more severe than that for Ni-30Cr. Metallographic examination of the specimens from this test showed that the Ni-30Cr specimen was still in the initiation stage of hot corrosion. The chromium in this specimen had not been depleted to the extent that the liquid nickel sulfide could be developed with the attendant severe oxidation. The addition of aluminum to Ni-30Cr decreases the amount of degradation which takes place during the initiation stage but it also decreases the length of the initiation stage and so eventually much more degradation is observed with the alloy that contains aluminum. Comparison in Figure 92 of the data for Ni-30Cr-6Al and Ni-15Cr-6Al shows that as the chromium content of the alloy is increased, the initiation time required for the onset of severe hot corrosion attack is also increased.

Since the addition of 6 percent aluminum to Ni-30Cr decreases the hot corrosion resistance of this alloy, it becomes important to determine if aluminum concentrations in excess of 6 percent also produce undesirable effects. Weight change versus time data obtained for the cyclic hot corrosion of NiCrAlY and CoCrAlY alloys with different aluminum concentrations are presented in Figure 93. Severe hot corrosion of the Ni-17Cr-11Al-0.5Y alloy was not observed until after about 1000 cycles, Figure 93, whereas the Ni-15Cr-6Al-0.1Y began to degrade after less than 50 cycles. Prior to the onset of hot corrosion degradation of the Ni-17Cr-11Al-0.5Y alloy, it appeared that a continuous Al_2O_3 scale was developing on this alloy beneath oxides of NiO and Cr_2O_3. Examination of this alloy using optical metallography after hot corrosion degradation had been initiated, however, showed features similar to those described previously for the hot corrosion of Ni-25Cr-6Al specimens. These results indicate aluminum in NiCrAl alloys improves the

hot corrosion resistance since continuous scales of Al_2O_3 are developed for longer periods of time. When the alloy becomes depleted in aluminum to levels where continuous Al_2O_3 scales are not developed, however, the remaining aluminum then appears to cause more severe subsequent degradation. The weight changes for the CoCrAlY alloys, Figure 93, indicate hot corrosion degradation does not occur until beyond 1400 cycles. It also appears that the degradation of the alloy with the lower aluminum content occurs before that of the alloy with the higher aluminum content.

The modified crucible experiments, described previously, Figure 35, were also used to examine the effect of aluminum on hot corrosion of NiCrAl alloys. As discussed previously, a Ni-5Cr specimen was not severely attacked in the crucible test, Table VI. Specimens of Ni-8Cr-6Al and Ni-10.5Cr-13.4Al were subjected to the crucible test. Very severe degradation of the Ni-8Cr-6Al alloy was observed, Figure 94, and the resulting microstructure was very similar to that observed for a Ni-6Al alloy in this test, Figure 36. The Ni-10.5Cr-13.4Al alloy was not severely attacked in this test. It appeared as though a protective layer of Al_2O_3 had been developed on this alloy. The effects produced by aluminum on the hot corrosion of NiCrAl alloys in the crucible test can be seen to be similar to those obtained from the laboratory cyclic hot corrosion test.

In view of the observed difference between the hot corrosion resistance of NiCrAl (Y) and CoCrAl (Y) alloys, it was necessary to determine if the Na_2SO_4 on the surface of these two types of alloys contained different amounts of impurities due to reaction with oxides formed during the transient period of oxidation. Chemical analyses of Na_2SO_4 deposits removed from a Ni-30Cr-6Al alloy after oxidation showed chromium was the only impurity which was present. Aluminum was not detected. For example, after 1, 2 and 4 hours of oxidation at 1000°C in 1 atm of oxygen, approximately 0.14 to 0.21 mg/cm^2 of chromium was detected in the Na_2SO_4. Examination of the Na_2SO_4 removed from Co-25Cr-6Al-0.5Y specimens after oxidation for 20 and 67 hours of oxidation showed 0.06 and 0.13 mg/cm^2 of chromium was present in the Na_2SO_4, respectively. In these analyses, the Na_2SO_4 deposits were not analyzed for either nickel or cobalt. Previous analyses performed on the Na_2SO_4 removed from nickel and cobalt specimens did not detect any of these two elements in the Na_2SO_4. It appears that the Na_2SO_4 on the surfaces of NiCrAl (Y) and CoCrAl (Y) contains the same impurities. The chromium level of the Na_2SO_4 from NiCrAl, however, appears to be greater than that from CoCrAl. Such a condition shows that more oxide ions are produced in the Na_2SO_4 on NiCrAl.

The onset of severe hot corrosion degradation of NiCrAl (Y) and CoCrAl (Y) alloys occurred at localized areas on the surfaces of specimens and the degradation then spread laterally until the whole surface was covered. The edges of specimens, where spalling of the Al_2O_3 was most extensive, were common sites for initiation of this severe degradation. Since spalling of the Al_2O_3 scales is a precursor to severe hot corrosion attack, yttrium produces a beneficial effect by improving the adhesion of the Al_2O_3 scales. Such an effect was not evident on the Ni-25Cr-6Al and Ni-25Cr-6Al-0.2Y alloys because of their low aluminum content. The beneficial effect of yttrium is evident upon comparing the CoCrAl and CoCrAlY alloys tested either in the cyclic laboratory test, Figure 80, or the dynamic burner rig, Figure 85. In discussing the effects produced by yttrium on the hot corrosion of NiCrAlY and CoCrAlY alloys, it is worth mentioning that yttrium-rich particles were

observed on Al_2O_3 scales after hot corrosion tests with Na_2SO_4. These particles had the shapes of lily pads and appeared to extend completely through the Al_2O_3 scales. Similar structures were not observed during oxidation of these alloys without Na_2SO_4. It was not apparent that the development of these yttrium-rich particles had a significant influence on the hot corrosion behavior of the alloys.

The localized nature with which hot corrosion is initiated on NiCrAl (Y) and CoCrAl (Y) alloys is related in part to the spalling of the Al_2O_3 scales from these alloys. It was observed, however, that the initiation of hot corrosion degradation of Ni-17Cr-12Al-0.5Y occurred much sooner on alloys in the as-cast condition than on alloys in the vapor-deposited condition. It has been found that more adherent scales are developed on NiCrAlY alloys in the vapor-deposited condition (Ref. 28) and this may account for the superior hot corrosion resistance of the alloy in the vapor-deposited condition. The greater homogeneity of the vapor-deposited alloy may also be a factor, since the localized nature of initiation of the attack indicates that compositional inhomogeneities may play a significant role in the initiation process.

c. Summary and Discussion of Results

The important results obtained from the hot corrosion studies with NiCrAl, NiCrAlY, CoCrAl and CoCrAlY alloys are summarized in the following.

- External, continuous layers of Al_2O_3 were formed on the NiCrAl, NiCrAlY, CoCrAl and CoCrAlY alloys used in this program during oxidation.

- The Na_2SO_4-induced hot corrosion of NiCrAl (Y) and CoCrAl (Y) alloys can be divided into two stages, namely, an initiation stage during which the corrosion rate is not substantially greater than that for oxidation in the absence of Na_2SO_4 and a propagation stage for which the corrosion rate is at least a factor of 10 greater, and commonly a factor of 100 greater than that for oxidation in the absence of Na_2SO_4.

- The time required to initiate severe attack of NiCrAl (Y) alloys is much less than that for CoCrAl (Y) alloys with the same chromium and aluminum concentrations.

- As the amount of the Na_2SO_4 deposit is increased, the time required to initiate the severe attack is decreased.

- As the chromium concentration of the alloys is increased, the time required to initiate severe attack is increased; increasing the aluminum concentration beyond about 6 percent also prolongs the initiation stage, but at concentrations below 6 percent, aluminum decreases the time required for initiation of severe corrosion.

- The initiation stage consists of the progressive depletion of first the aluminum and then the chromium from the alloys.

- Yttrium prolongs the initiation stage by improving the adhesion of Al_2O_3 and thereby inhibiting the depletion of aluminum from the alloy.

- The propagation stage evidently becomes dominant as the chromium and aluminum concentrations approach some critical levels at which sulfur and oxygen are rapidly removed from the Na_2SO_4 by the alloy and the oxide ion activity of the Na_2SO_4 is consequently increased; the rapid corrosion appears to occur for two reasons, namely, reaction of elements in the alloy with oxide ions in the sulfate and preferential oxidation of liquid sulfides that are formed in the alloy.

- The oxidation of CoCrAl alloys is not influenced by sulfur as much as NiCrAl alloys apparently because liquid sulfide can be formed in NiCrAl alloys at a lower sulfur activity than in CoCrAl alloys.

Since the hot corrosion mechanisms of NiCrAl and CoCrAl alloys are believed to be essentially the same, it is convenient to use the results first to develop a model for the Na_2SO_4-induced hot corrosion of NiCrAl and then consider what modifications are needed for the CoCrAl alloys. In the case of NiCrAl alloys with large aluminum concentrations (e.g., 10-12%), a continuous barrier of Al_2O_3 is developed between the Na_2SO_4 and the alloy, Figure 95a. Sulfur can diffuse from the Na_2SO_4 through the Al_2O_3 to form chromium sulfide particles in the alloy but the effects produced by this condition on the corrosion are small. Continued oxidation under cyclic conditions leads to aluminum depletion and eventually the alloy surface, exposed as a result of the previous thermal cycle, is not covered by a continuous barrier of Al_2O_3. Other alloys with lower aluminum concentrations may arrive at this state after fewer thermal cycles or even under isothermal conditions, since some sulfur is removed from the Na_2SO_4 by the alloy, and the oxide ions produced by such a condition can dissolve some of the Al_2O_3.

Before describing the hot corrosion mechanism any further, it is necessary to note that the results which have been obtained indicate that transport of oxygen from the gas through the Na_2SO_4 appears to be a very important part of the hot corrosion process. In the initiation stage, the oxygen flux through the layer of Na_2SO_4 is sufficient to satisfy the demands of the alloy, and the composition of the Na_2SO_4 is such that only oxide phases are stable. The onset of the development of the conditions which eventually lead to severe hot corrosion is marked by the condition that the flux of oxygen through the sulfate layer can no longer satisfy the increased demands of the alloy. The increased demands arise because less protective oxides are being developed and the composition of the Na_2SO_4 is therefore changed such that SO_2 is evolved, sulfides are stable as well as oxides, and as shown in Figure 39, compositions can be achieved where some of the oxides begin to dissolve in the Na_2SO_4.

In the case of NiCrAl or NiCrAlY alloys the continuous Al_2O_3 barrier, Figure 95a, begins to break down in localized areas, and in such areas large amounts of aluminum and

chromium are leached from the alloys by the oxygen-deficient Na_2SO_4, Figure 95b. The reason that both chromium and aluminum are leached from the alloy by the modified Na_2SO_4 is not fully understood. The experimental results show that Na_2SO_4 is more effective in leaching chromium when aluminum is also present in the alloy. It appears as though rapid dissolution takes place when the oxygen activity is reduced below that required for NiO to be stable. As a result of the leaching process the alloys become severely depleted of aluminum and chromium, and liquid nickel sulfide is formed at the base of the Na_2SO_4-oxide protrusions, Figure 95c. The leaching of aluminum and chromium from the alloy by the Na_2SO_4 results in more severe degradation than would be observed if the alloys were insulated from the Na_2SO_4 by a continuous barrier of either Al_2O_3 or Cr_2O_3. This increased degradation can be considered to occur because of the production of oxide ions in the Na_2SO_4, which in turn gives rise to the leaching action of the melt. The formation of liquid nickel sulfide also affects the corrosion of the alloy as will be discussed in the following paragraph.

The selective removal of aluminum and chromium from the alloys is the first part of the degradation process. Accompanying the dissolution of aluminum and chromium from the alloy is the formation of liquid nickel sulfide. In practice, the amount of Na_2SO_4 deposited at any one time is usually small, in the range 0.05 to 5 mg/cm^2, and only a limited amount of aluminum and chromium can dissolve in the Na_2SO_4. After the Na_2SO_4 is saturated with these elements, the liquid nickel sulfide begins to react with the alloy. Thermodynamic conditions favor the formation of chromium sulfide. It appears, however, that the liquid sulfide provides a means for oxygen to rapidly enter the alloy, and Al_2O_3 and Cr_2O_3 particles are formed at the interface between the alloy and the melt, Figure 96a rather than chromium sulfide which is only stable deeper in the alloy or the liquid sulfide where the oxygen activity is lower. The rapid inward movement of oxygen through the liquid sulfide does not allow any diffusion of chromium or aluminum from the alloy, and the volume fractions of Al_2O_3 or Cr_2O_3 are not sufficient to permit the development of continuous barriers of these oxides on the alloy surfaces. The absence of the development of Al_2O_3 or Cr_2O_3 barriers on, in, or beneath the liquid nickel sulfide is another cause for rapid oxidation of the alloys. This process, however, does not continue indefinitely because the liquid sulfide phase can be removed from the surface of the alloy by reaction of the sulfur with chromium deeper in the alloy. The hot corrosion process is therefore not self-sustaining but requires deposition of Na_2SO_4 for additional degradation of the alloy.

The hot corrosion of CoCrAl alloys takes place by the same mechanism as that for NiCrAl alloys. The conditions which result in very rapid oxidation are developed slower in CoCrAl than in NiCrAl alloys. The production of oxide ions in the Na_2SO_4, and consequently the dissolution of chromium and aluminum in the Na_2SO_4, takes place at a slower rate on CoCrAl alloys compared to NiCrAl alloys because the oxygen pressure in the Na_2SO_4 must be reduced to lower levels to prevent CoO formation in the cobalt-base system, rather than to prevent NiO formation in the nickel-base system, Figure 41. In addition, even when cobalt oxide is not stable, the production of oxide ions in the cobalt-base system is not as efficient as the equivalent nickel-base system because solid sulfides are frequently developed in the CoCrAl alloys, Figure 95d, compared to liquid sulfides in

the NiCrAl alloys. The solid sulfides in the CoCrAl alloys not only inhibit the production of oxide ions but these sulfides do not lead to preferential oxidation of aluminum and chromium from the alloy as do the liquid sulfides, Figure 96b.

Increasing the chromium concentrations of NiCrAl and CoCrAl alloys improves the hot corrosion resistance of these alloys because the development of liquid sulfide phases and the unrestricted production of oxide ions in the Na_2SO_4 can occur only after the chromium content of these alloys is below some critical value. Increasing the aluminum content beyond that at which continuous barriers of Al_2O_3 are developed also improves the hot corrosion behavior of these alloys because continuous Al_2O_3 barriers do not permit a large oxygen gradient to be established across the Na_2SO_4 deposit. Under conditions where continuous Al_2O_3 barriers are not developed, however, aluminum produces very deleterious effects on the hot corrosion of NiCrAl alloys because a very steep oxygen activity gradient is established across the Na_2SO_4 which results in the removal of sulfur from the Na_2SO_4, the formation of sulfides in the alloy, and the production of oxide ions in the Na_2SO_4. Small amounts of aluminum in cobalt-base alloys do not appear to produce the same deleterious effects as those observed in nickel-base alloys. It appears as though in the cobalt-base systems the oxygen activity in the Na_2SO_4 over the alloy is not reduced below that required for the formation of cobaltous oxide.

SECTION IV

CONCLUDING REMARKS

The results which have been obtained in this program show that the Na_2SO_4-induced hot corrosion of alloys can be divided into two stages, in particular, an initiation stage and a propagation stage, Figure 97. The initiation stage involves those processes which determine the nature of the propagation stage. The propagation stage consists of those processes by which alloy components are converted to oxides.

The processes which take place during the initiation stage result in a transition of reaction product barriers from that formed on alloys during oxidation in the absence of Na_2SO_4 to much less protective barriers typical of the Na_2SO_4-induced propagation mode. The initiation stage of hot corrosion is affected by the following:

- Composition of the alloy
- Fabrication condition of the alloy
- Specimen geometry
- Temperature
- Time
- Composition of deposit
- Amount of deposit
- Composition of environment
- Environmental features
  (thermal cycling, mechanical wear)

There are at least two modes by which the Na_2SO_4-induced hot corrosion of alloys can be propagated. One mode involves successive steps of basic fluxing followed by the preferential oxidation of sulfides. The other mode results in the catastrophic oxidation of alloys due to what can be called acidic fluxing reactions.

The basic fluxing-sulfidation mode involves the production of oxide ions in the Na_2SO_4 as a result of the removal of sulfur from the Na_2SO_4 by the alloy. Both the formation of oxide ions in the Na_2SO_4 and the formation of sulfide phases in the alloys can contribute to the increased oxidation. Of the materials studied in this program, nickel, cobalt, Ni-25Al, Co-25Al, Ni-30Cr, Co-35Cr, NiCrAl, NiCrAlY, CoCrAl and CoCrAlY alloys undergo Na_2SO_4-induced hot corrosion via the basic fluxing-sulfidation propagation mode. In the case of nickel and cobalt, the attack is due to a basic fluxing process, whereas Co-25Al and Ni-25Al involve a substantial amount of preferential sulfide oxidation. In the case of NiCrAl and NiCrAlY alloys, both basic fluxing and preferential sulfide oxidation play significant roles in the hot corrosion process.

The basic fluxing-sulfidation propagation mode is not self-sustaining. Sodium sulfate deposition is required in order to have this propagation mode continue. Chromium and aluminum can be used to inhibit the onset of the basic fluxing-sulfidation propagation mode but in the case of aluminum continuous scales of Al_2O_3 must be developed on the alloys otherwise aluminum will produce deleterious effects in nickel-base systems. This latter condition is a major difference between nickel and cobalt alloys, namely, cobalt-base alloys are much more resistant to the initiation of the basic fluxing-sulfidation propagation mode than nickel-base alloys. This is especially the case for CoCrAl and NiCrAl alloys with the same chromium and aluminum concentrations. Such cobalt-base alloys are more resistant than nickel-base alloys because fewer oxide ions are produced in Na_2SO_4 on the cobalt base alloys, and the resulting sulfides are more resistant to oxidation.

The acidic fluxing propagation mode results in nonprotective oxide scale formation since oxide scales dissolve in the Na_2SO_4-melt by donating oxide ions to the melt. Oxide scales which normally would be stable in Na_2SO_4 become unstable when the Na_2SO_4 contains a sufficient amount of MoO_3 or WO_3. Alloys studied in the present program which exhibit hot corrosion attack via acidic fluxing were Ni-25Al-12W, Co-25Al-12W, Ni-25Cr-12W, Co-25Cr-12W and these same systems containing 6Mo in place of 12W. Since Mo or W play an important role in the degradation process, the attack is self-sustaining because Mo or W can be continually added to Na_2SO_4 from the alloy. The only reliable technique to prevent hot corrosion via acidic fluxing is to remove or at least decrease the concentration of Mo and/or W in the alloy. It appears, however, that increasing the chromium content of the alloy permits using higher concentrations of the elements that cause acid attack. There is not a significant difference between the resistance of nickel and cobalt-base alloys to the acidic fluxing propagation mode.

The results obtained in this program are not adequate to permit an extensive description of the effects produced by tantalum or titanium on the hot corrosion of cobalt- or nickel-base alloys. No obvious deleterious effects of these two elements on the hot corrosion resistance of alloys was observed.

The conclusions arrived at in this program are based primarily upon laboratory testing as opposed to dynamic burner rig testing. Nevertheless, the results obtained from the limited amount of burner rig testing that was performed in this program indicate the conclusions also apply to burner rig tests. The materials that were studied in this program were not as complex as those of the nickel- and cobalt-base superalloys which are used in practice. The materials that were studied, however, did contain the major alloying elements of the superalloys. It therefore is believed that the results obtained from this program are essentially applicable to more complex systems. For example, the hot corrosion of B-1900, IN-100, MAR-M200, Hastelloy-X, Haynes 188 and WI-52 is proposed to occur via the acidic fluxing propagation mode, whereas the attack of IN-738 and X-40 usually involves the basic fluxing-sulfidation propagation mode.

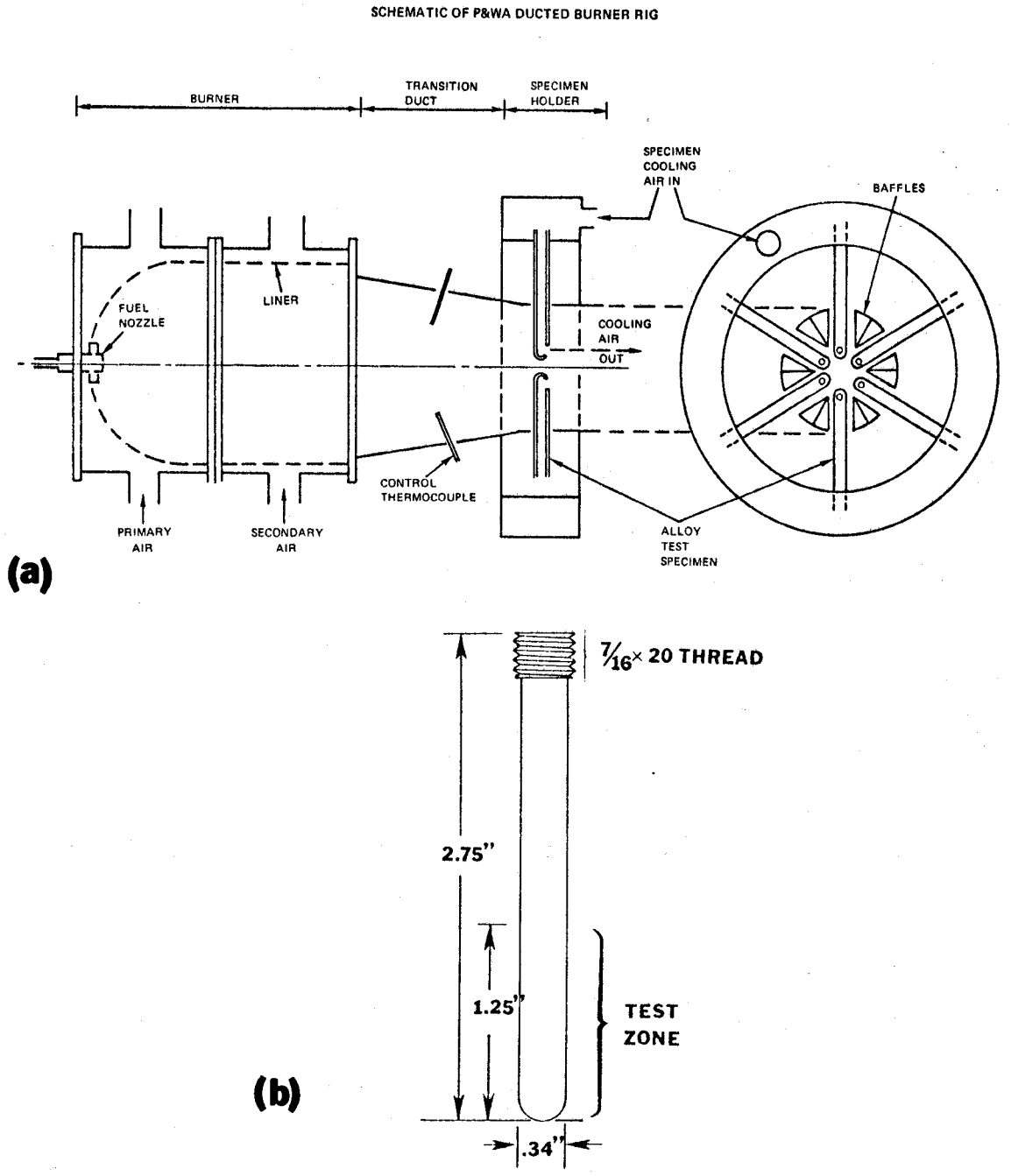

Figure 1 a) Schematic diagram of ducted burner rig used for hot corrosion testing. Although hollow, air-cooled specimens can be used (as shown), solid, uncooled specimens (not shown) were used in the present program. In order to insure uniformity of flame exposure to each specimen, the entire array (six specimens) is oscillated in the holder about the burner axis. The maximum metal temperature range under these conditions is 25°C (e.g. 987-1012°C). b) Diagram showing a solid test specimen for the ducted burner rig.

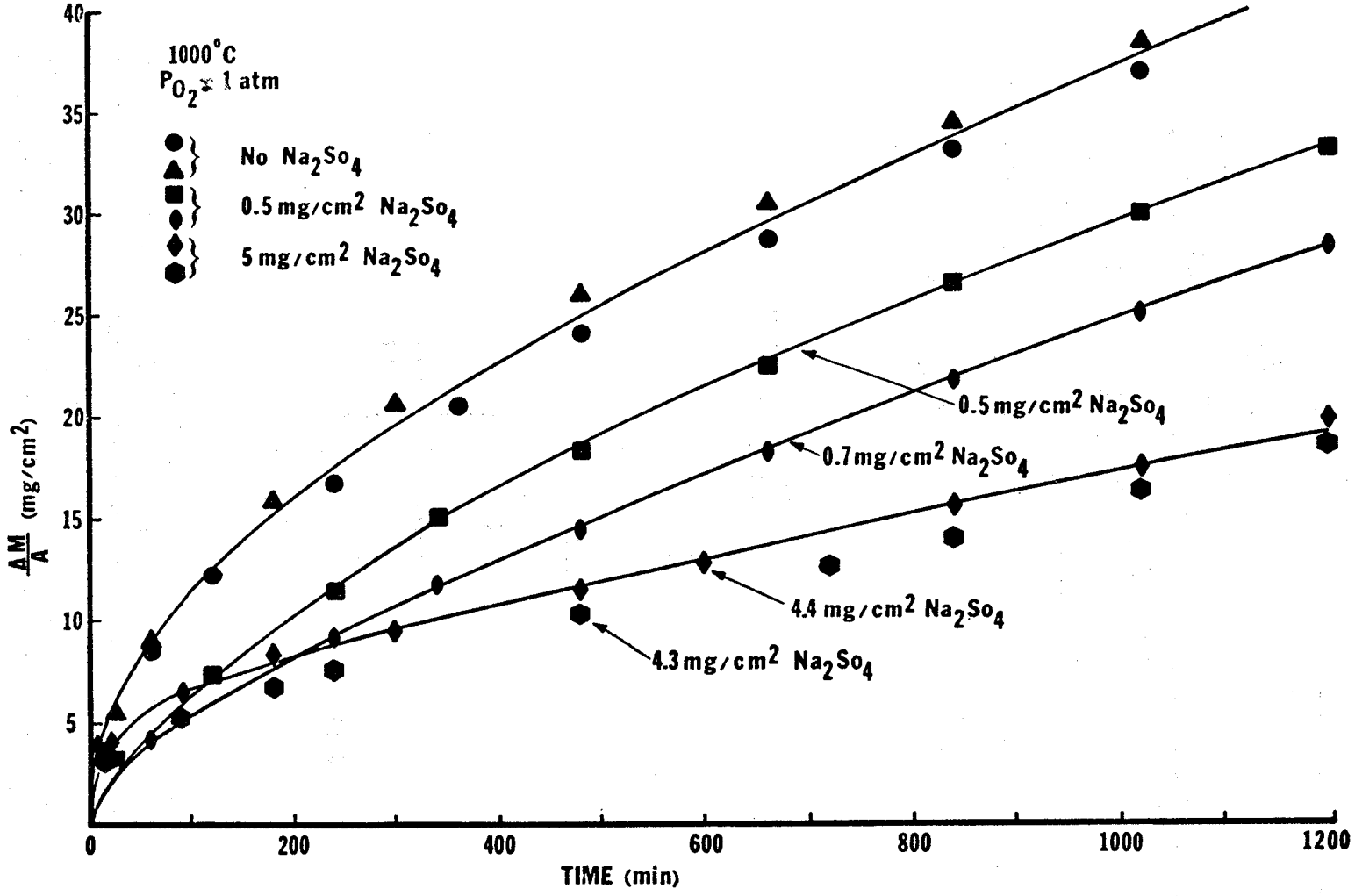

Figure 2 Oxidation kinetics for cobalt with and without Na_2SO_4 at 1000°C in 1 atm of oxygen.

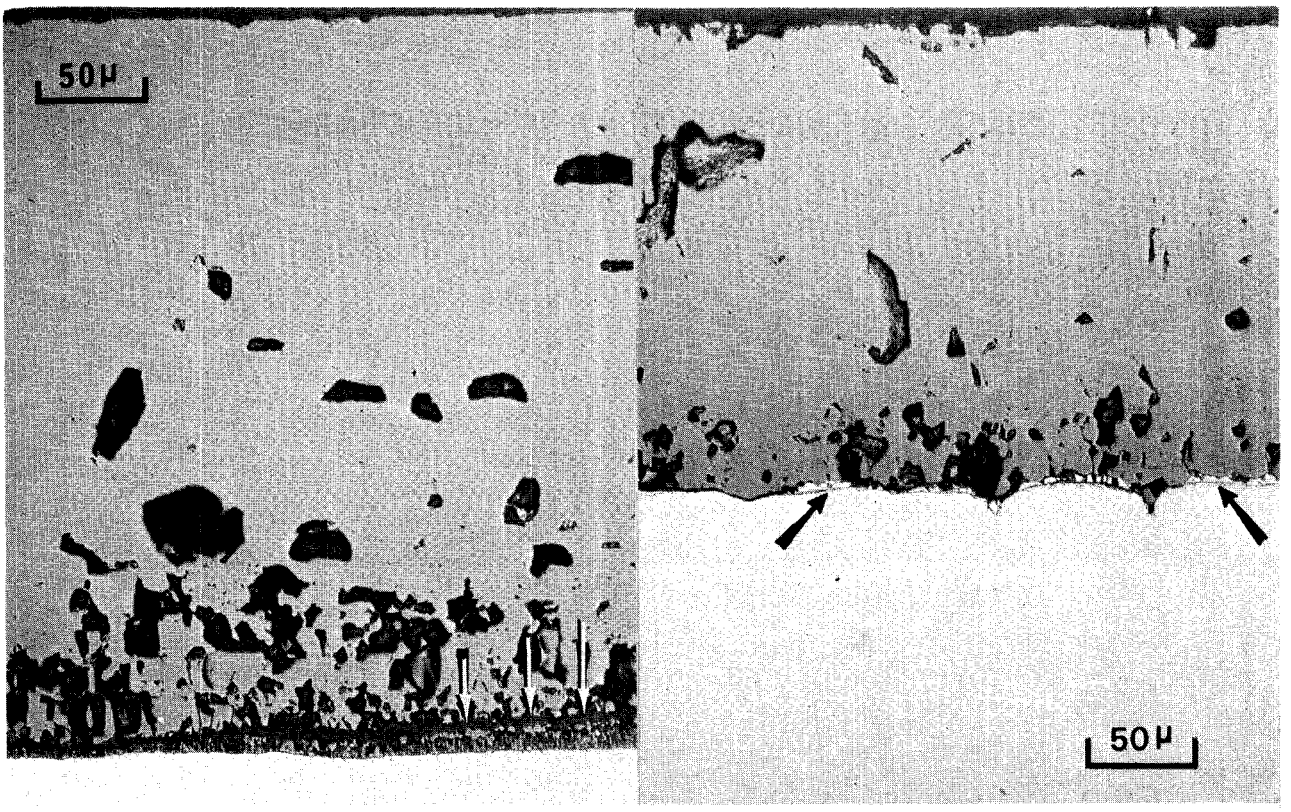

Figure 3 Oxide scales developed on cobalt specimens after 20 hrs oxidation at 1000°C in 1 atm oxygen. a) Microstructure developed after oxidation without Na_2SO_4. The oxide layer has fractured upon cooling in the porous zone (arrows) immediately adjacent to the metal. b) Oxide scale developed on cobalt coated with 0.5 mg/cm^2 Na_2SO_4. A thin layer of cobalt sulfide, which was probably liquid at 1000°C is indicated by arrows. The inner zone of oxide is less porous than that developed during oxidation of cobalt without Na_2SO_4.

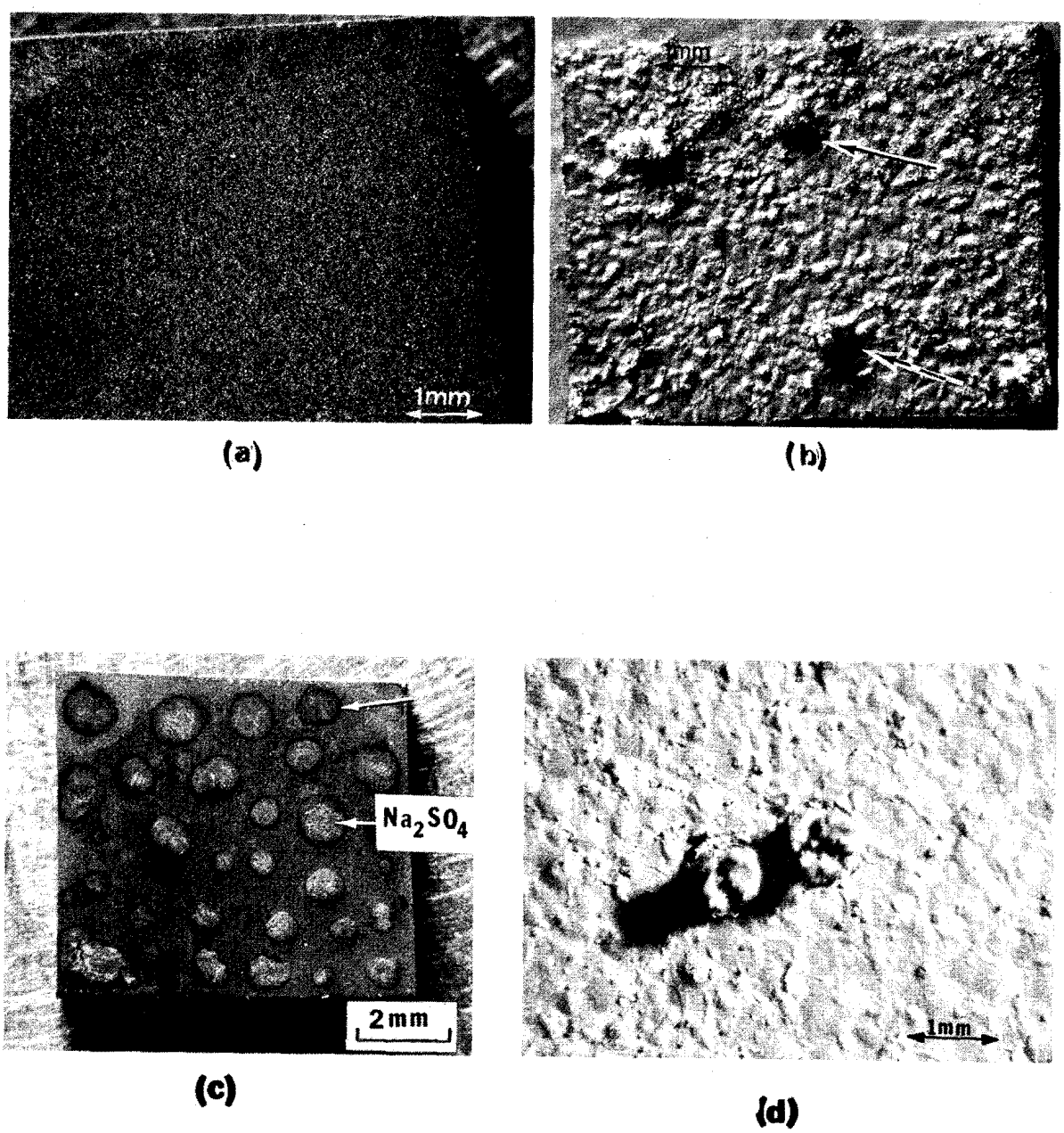

Figure 4 Surface photograph and microphotographs of cobalt that was coated with 3.5 mg/cm^2 of oxidation at 1000°C on cobalt after oxidation in air (a), on Na_2SO_4-coated cobalt after oxidation in air (b), on Na_2SO_4-coated cobalt after oxidation in 1 atm or oxygen (c), and on Na_2SO_4-coated nickel after oxidation in air (d).

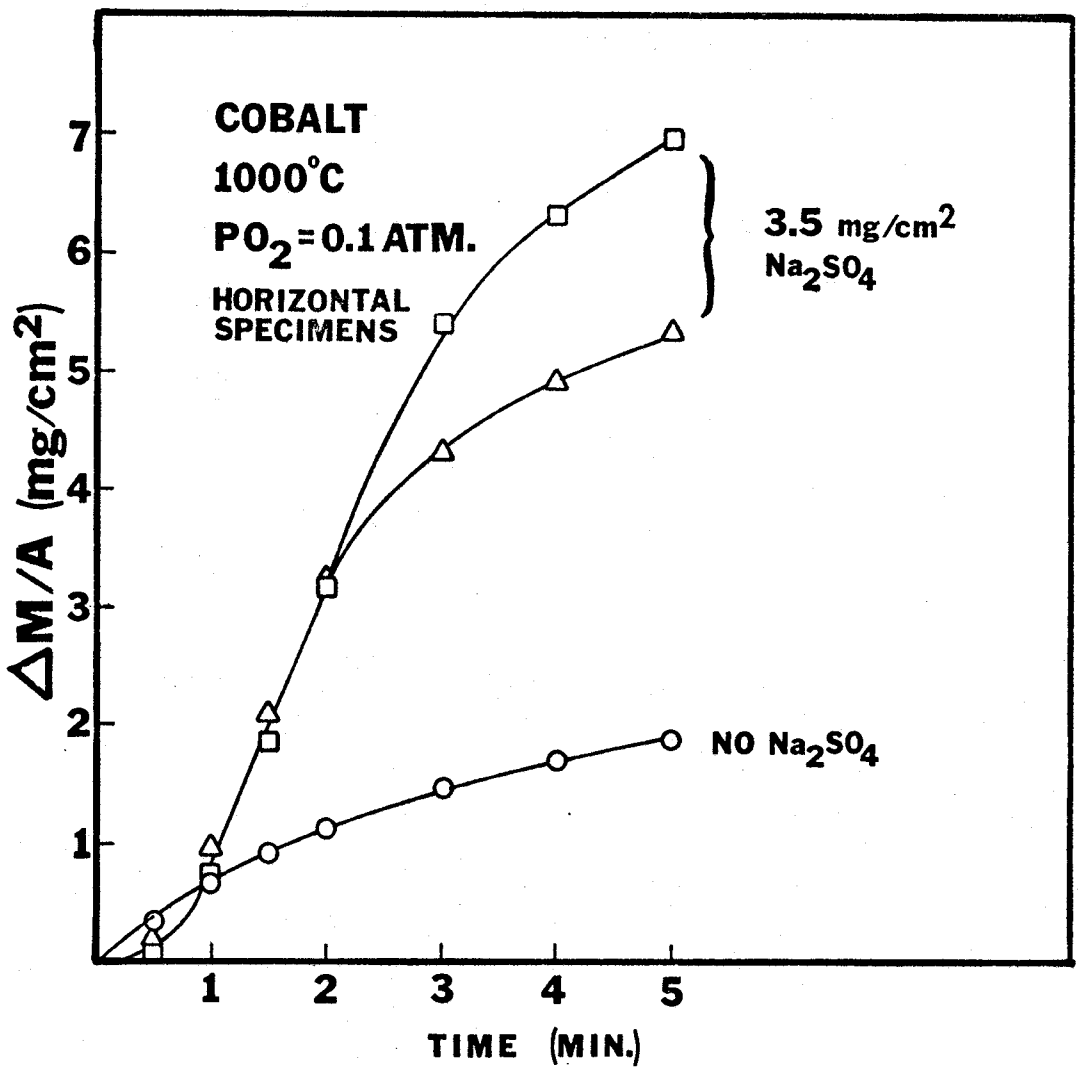

Figure 5 Comparison of the oxidation kinetics for cobalt with and without Na_2SO_4. The larger weight gains of the specimens with Na_2SO_4 indicate that Na_2SO_4 can induce accelerated oxidation of cobalt.

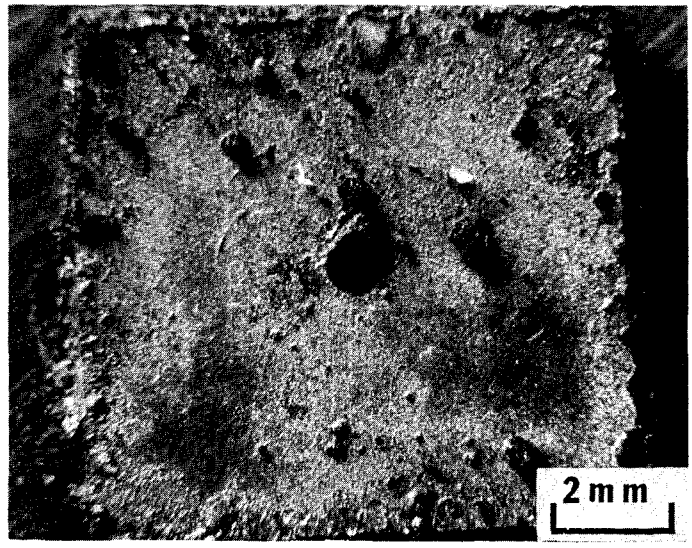

(a)

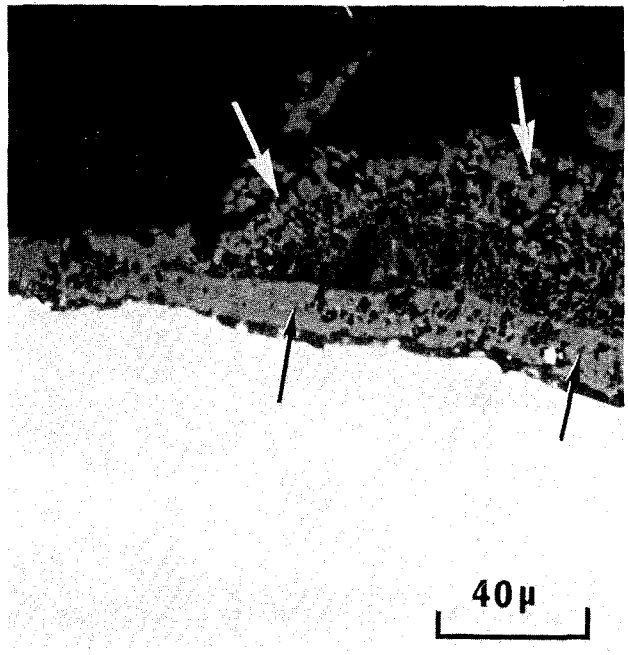

(b)

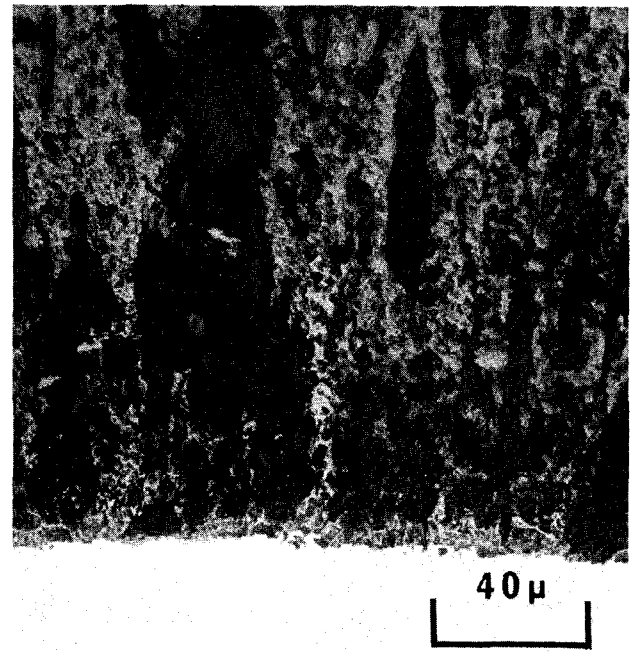

(c)

Figure 6 Surface photograph and microphotographs of cobalt that was coated with 3.5 mg/cm^2 Na_2SO_4 and oxidized 5 minutes in 0.1 atm of oxygen at 1000°C. a) The surface morphology is typical of that observed for specimens which have undergone Na_2SO_4-induced accelerated oxidation. b) Transverse section through specimen showing protective oxide (black arrows) and nonprotective oxide (white arrows) layer. c) Totally nonprotective oxide layer found in some areas of specimen.

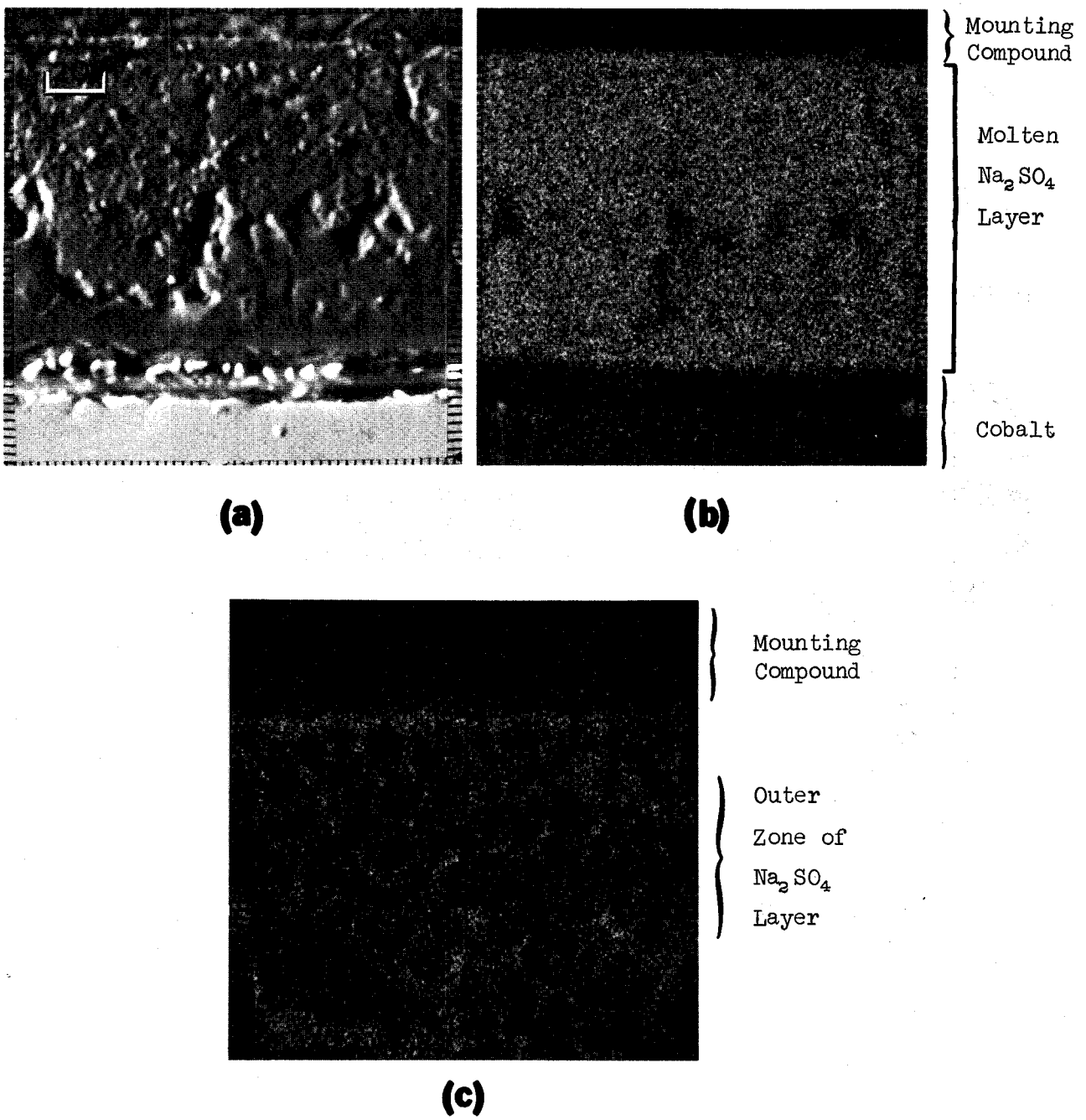

Figure 7 Electron microprobe analysis of molten Na_2SO_4 layer on cobalt after one hour treatment in argon at 1000°C. a) Electron back scatter image showing Na_2SO_4 layer covering cobalt. b) Sulfur X-ray image. c) Cobalt X-ray image of outer zone of Na_2SO_4 layer showing presence of cobalt within the Na_2SO_4.

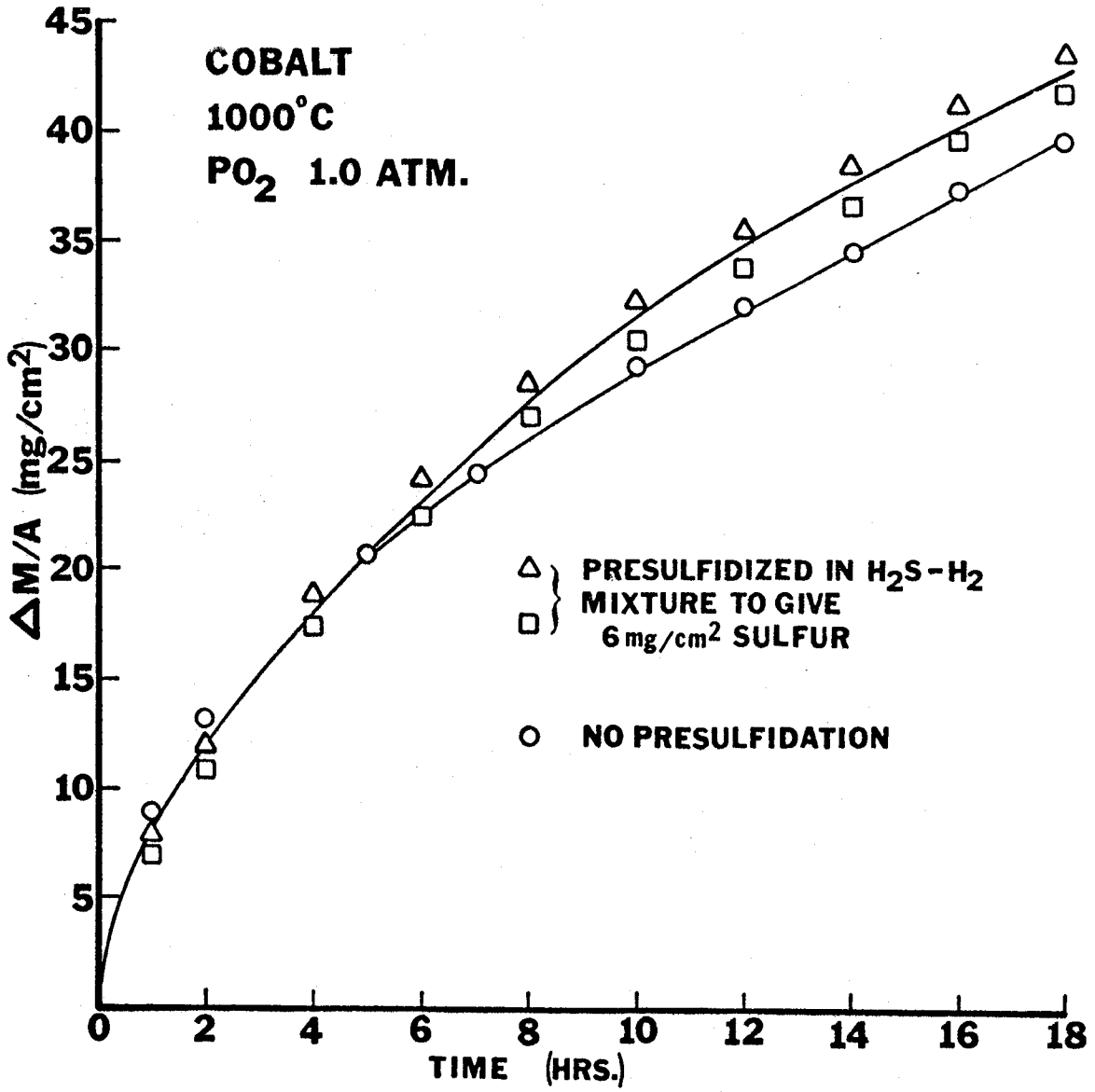

Figure 8 Comparison of the oxidation kinetics of presulfidized cobalt ($H_2S/H_2 = 0.2$) to those for cobalt with no pretreatment.

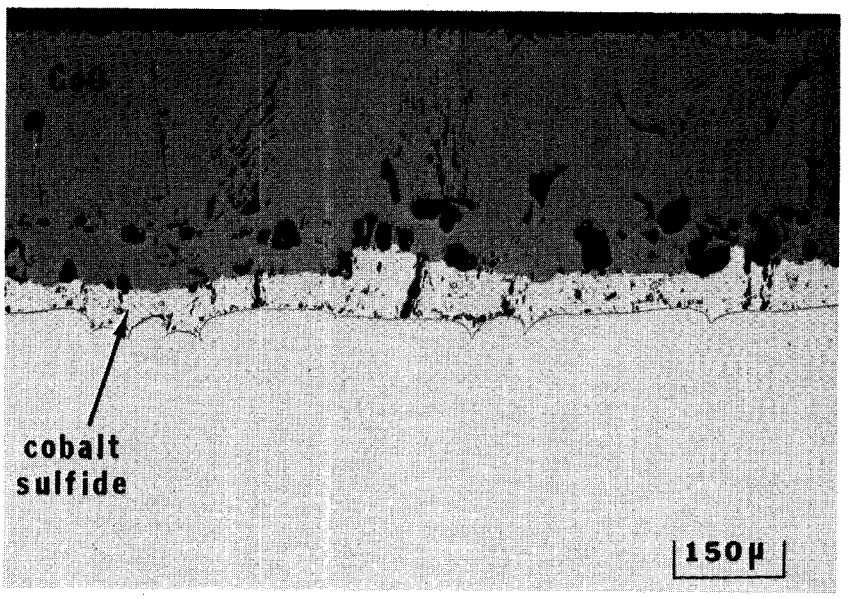

Figure 9 Microstructure of presulfidized cobalt (H_2S/H_2 = 0.2) after 20 hrs. of oxidation at 1000°C in 1 atm of oxygen. A dense layer of CoO has been formed upon the sulfide layer.

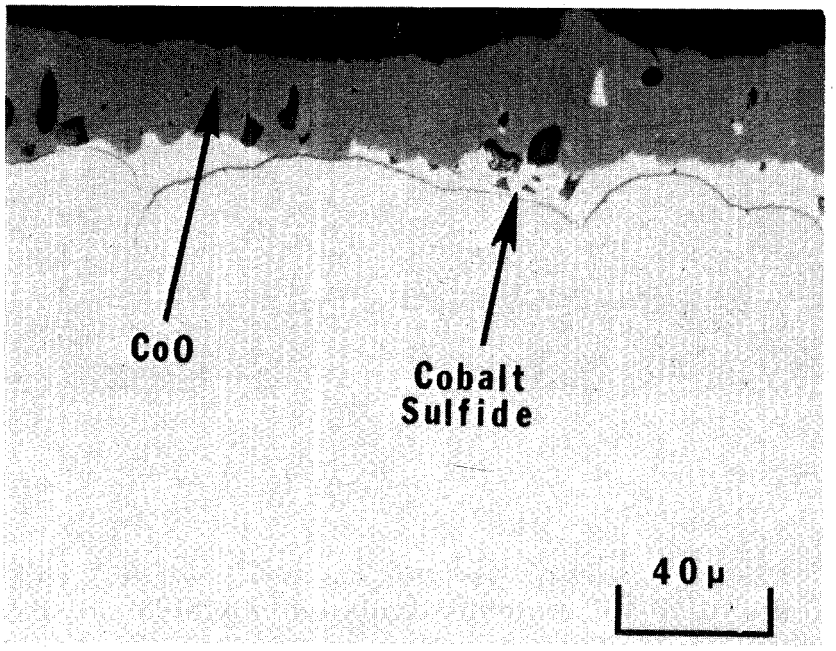

Figure 10 Microstructure of cobalt specimen after 7.8 hrs. of oxidation in flowing SO_2 at 1000°C. The CoO is dense and has formed above a zone of cobalt sulfide.

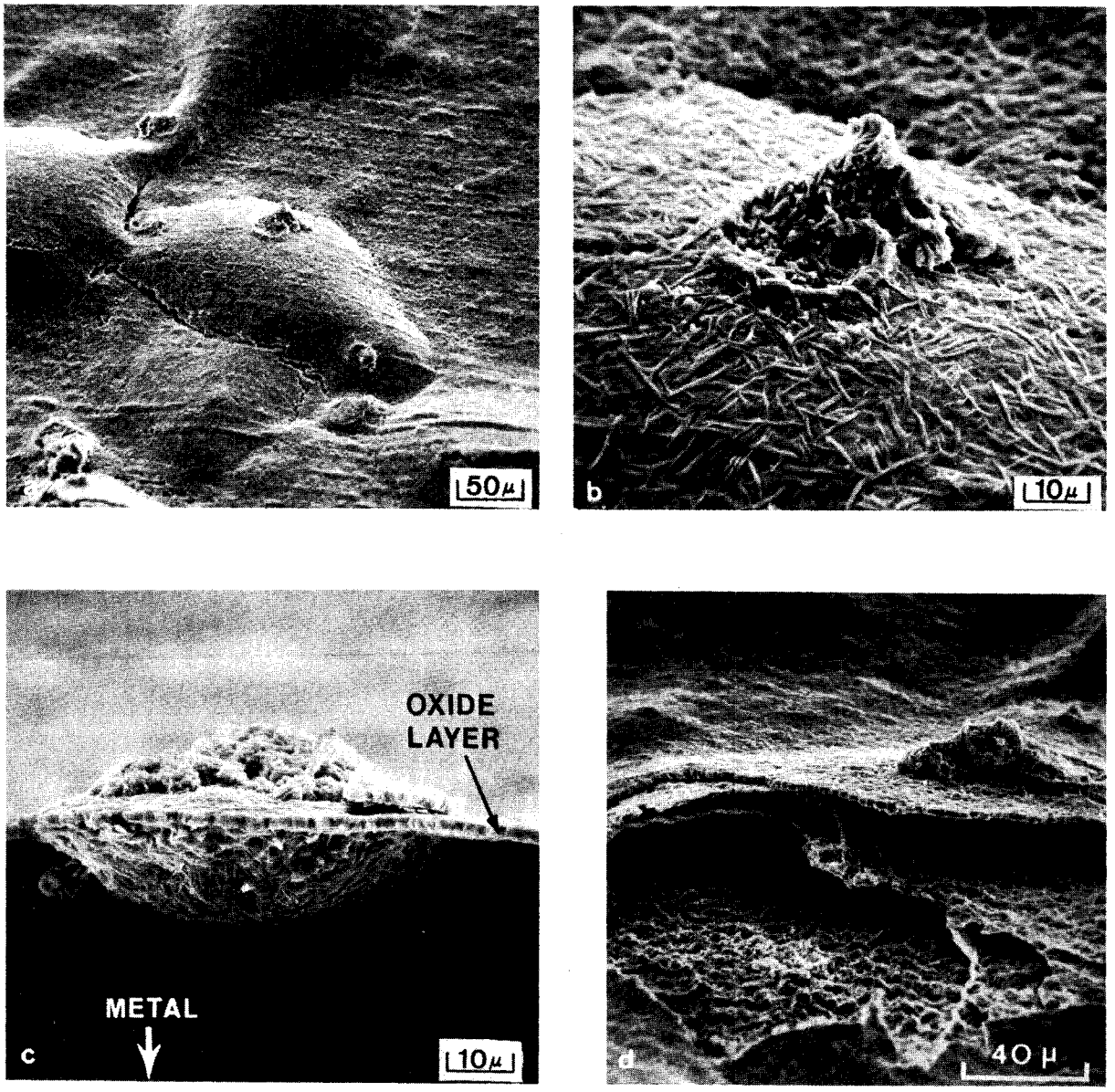

Figure 11 Features of the oxide scale formed on Na_2SO_4 – coated cobalt after oxidation in air at 1000°C. After 30 sec., the oxide layer has become detached from the metal (a), and holes are visible on the surface of the oxide (a & b); beneath the holes, oxidation products were evident (c). After 3 min. oxidation, layers of CoO formed by successive localized penetrations (at holes) and lateral spreading of Na_2SO_4 beneath the CoO layers, (d).

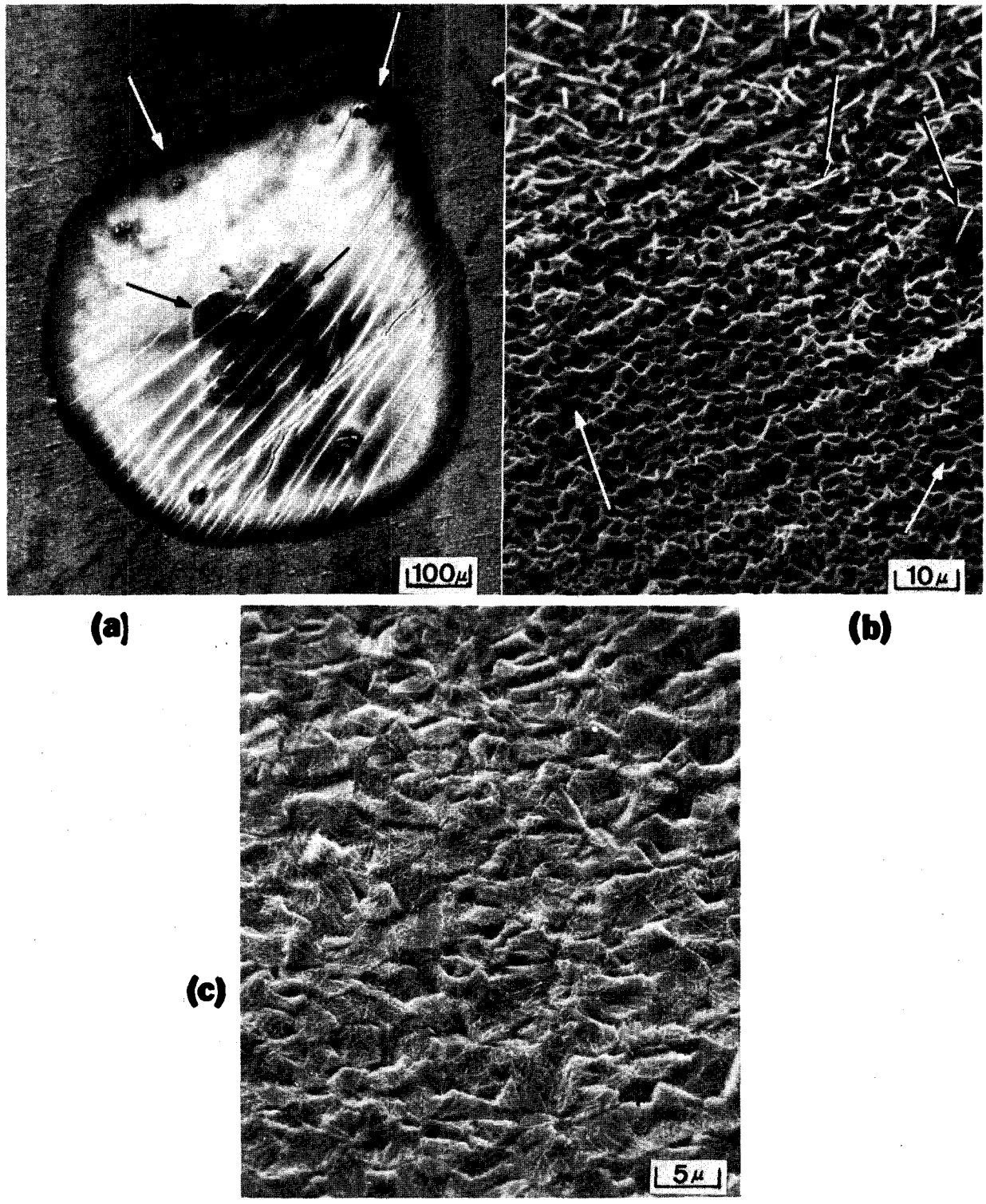

Figure 12 a) During oxidation of cobalt the Na_2SO_4 formed puddles (white arrows) in which particles of slag (black arrows) were suspended (30 secs at 1000°C in air). b) After washing the Na_2SO_4 from the specimen, the exposed oxide surface was highly irregular (white arrows) whereas in other areas (black arrows) the oxide was covered with needles and was less irregular. c) Photograph showing features of oxide surface after the oxidation of cobalt with no Na_2SO_4 (30 secs at 1000°C in air).

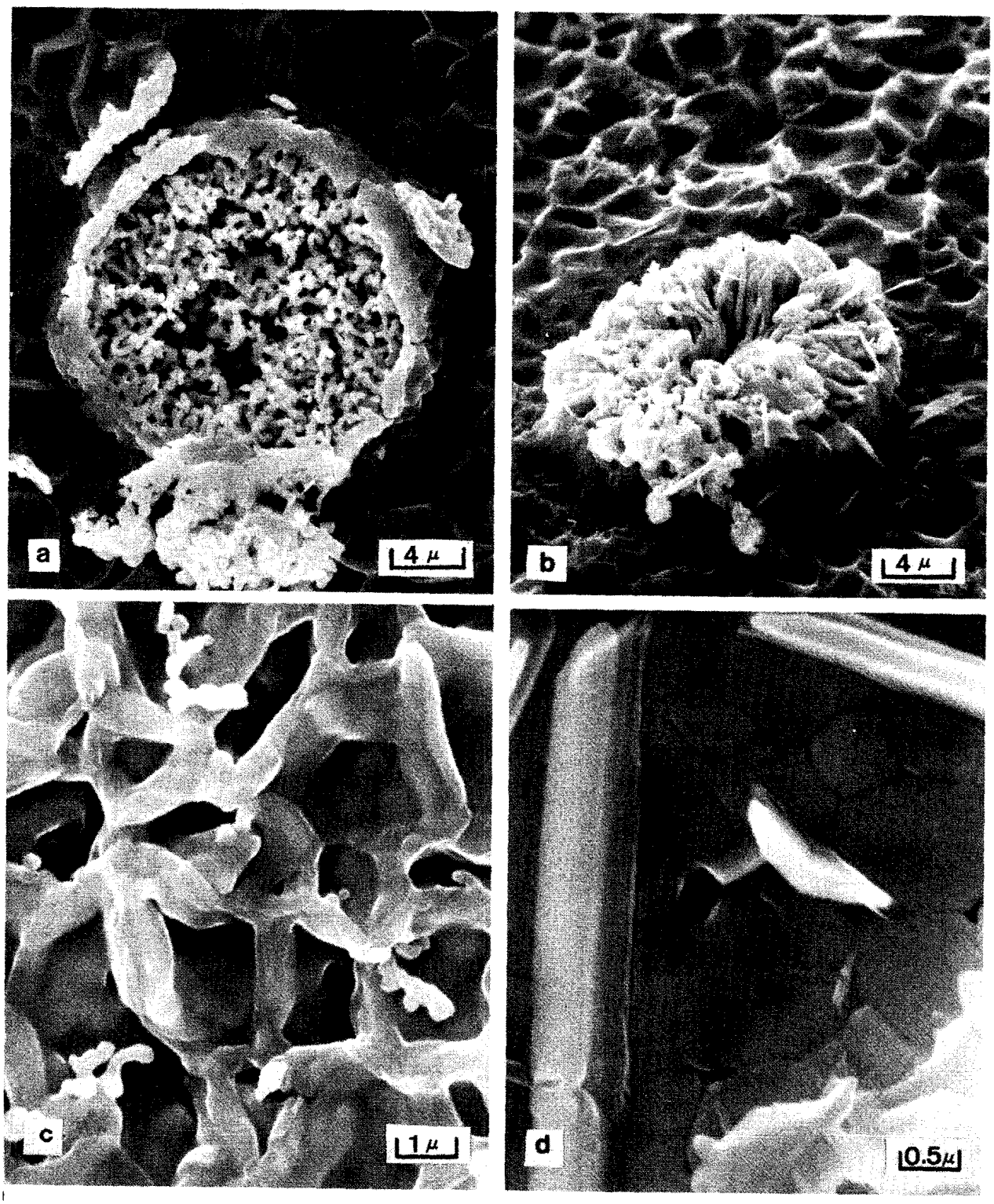

Figure 13 Features which indicated the Na_2SO_4 had penetrated the CoO layer were evident on the oxide surface at areas where Na_2SO_4 puddles had been present (a) as well as in those areas where the Na_2SO_4 had been present as a thin layer (b). In addition the oxide formed beneath the Na_2SO_4 puddles contained deep depressions (c) and small holes at oxide grain boundaries were evident (d) in areas where the Na_2SO_4 had been present as a thin layer. (conditions: 30 seconds of oxidation at 1000°C in air).

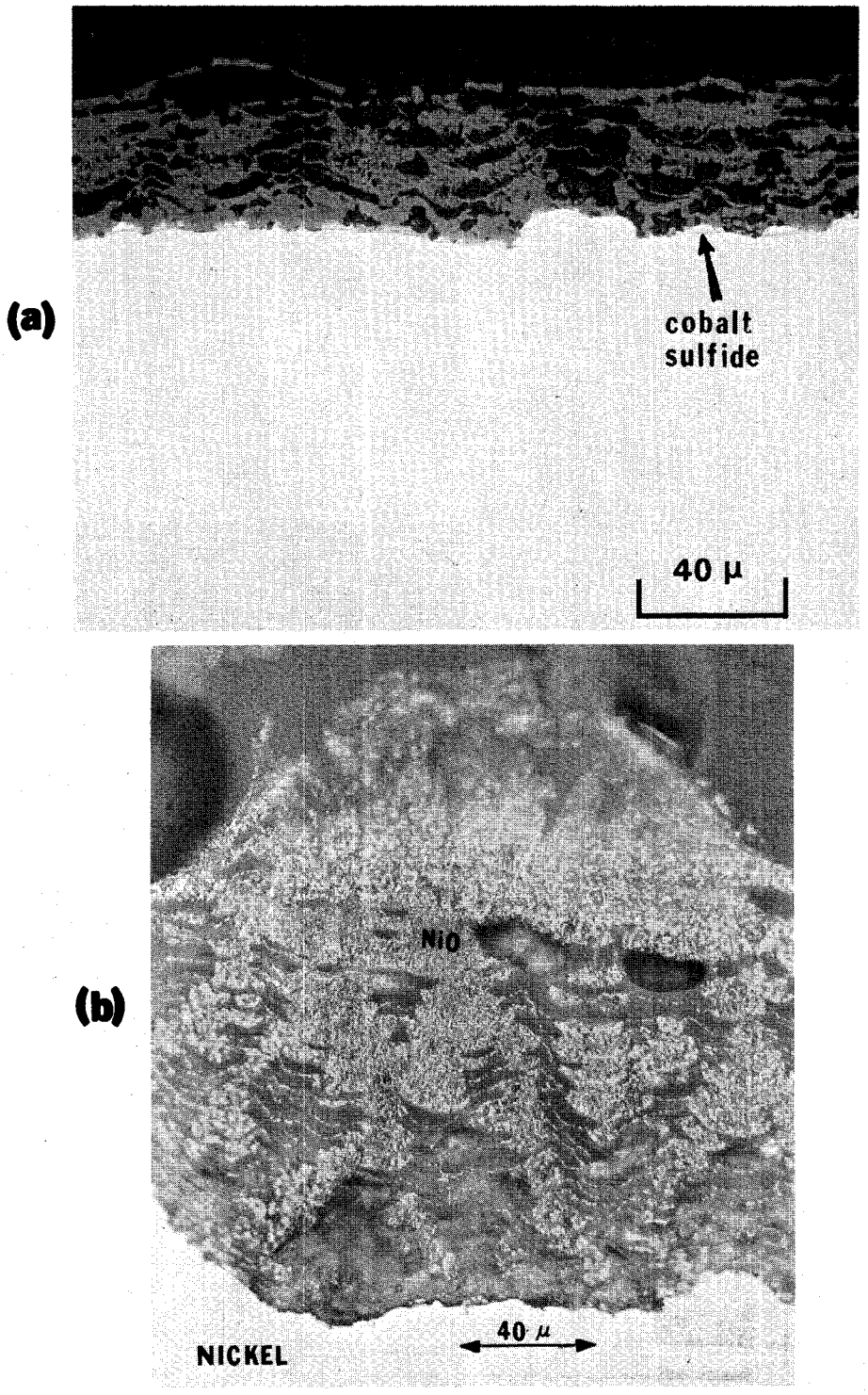

Figure 14 Photographs showing the layered texture of the oxide scales formed on Na_2SO_4-coated (0.5 mg/cm^2) cobalt (a), and nickel (b), after 3 min. oxidation at 1000°C in air.

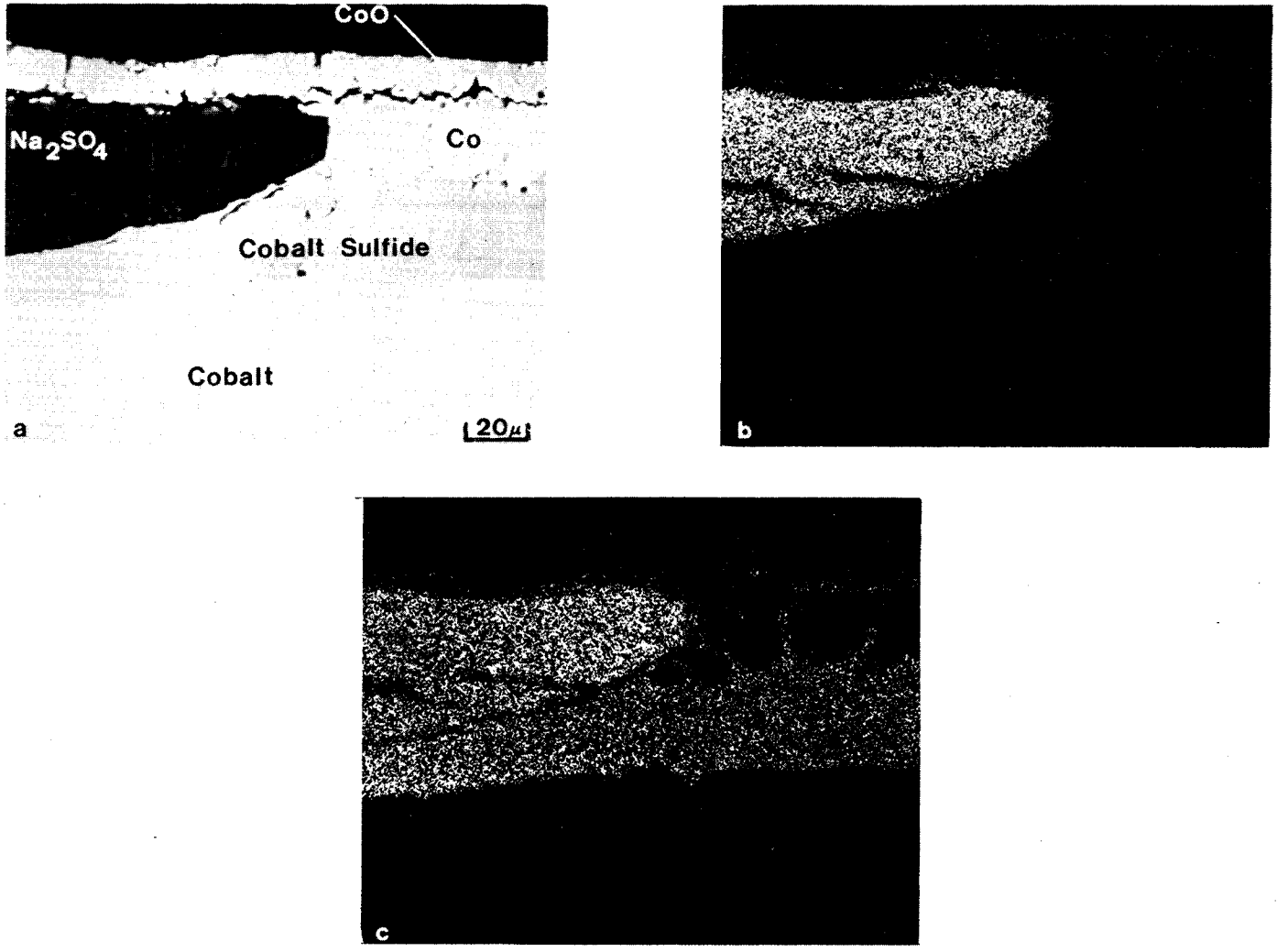

Figure 15 a) Electron back scatter photograph showing that Na_2SO_4 had spread laterally, beneath the oxide formed on presulfidized cobalt during oxidation at 1000°C in air. b) and c) X-ray images for sodium and sulfur, respectively.

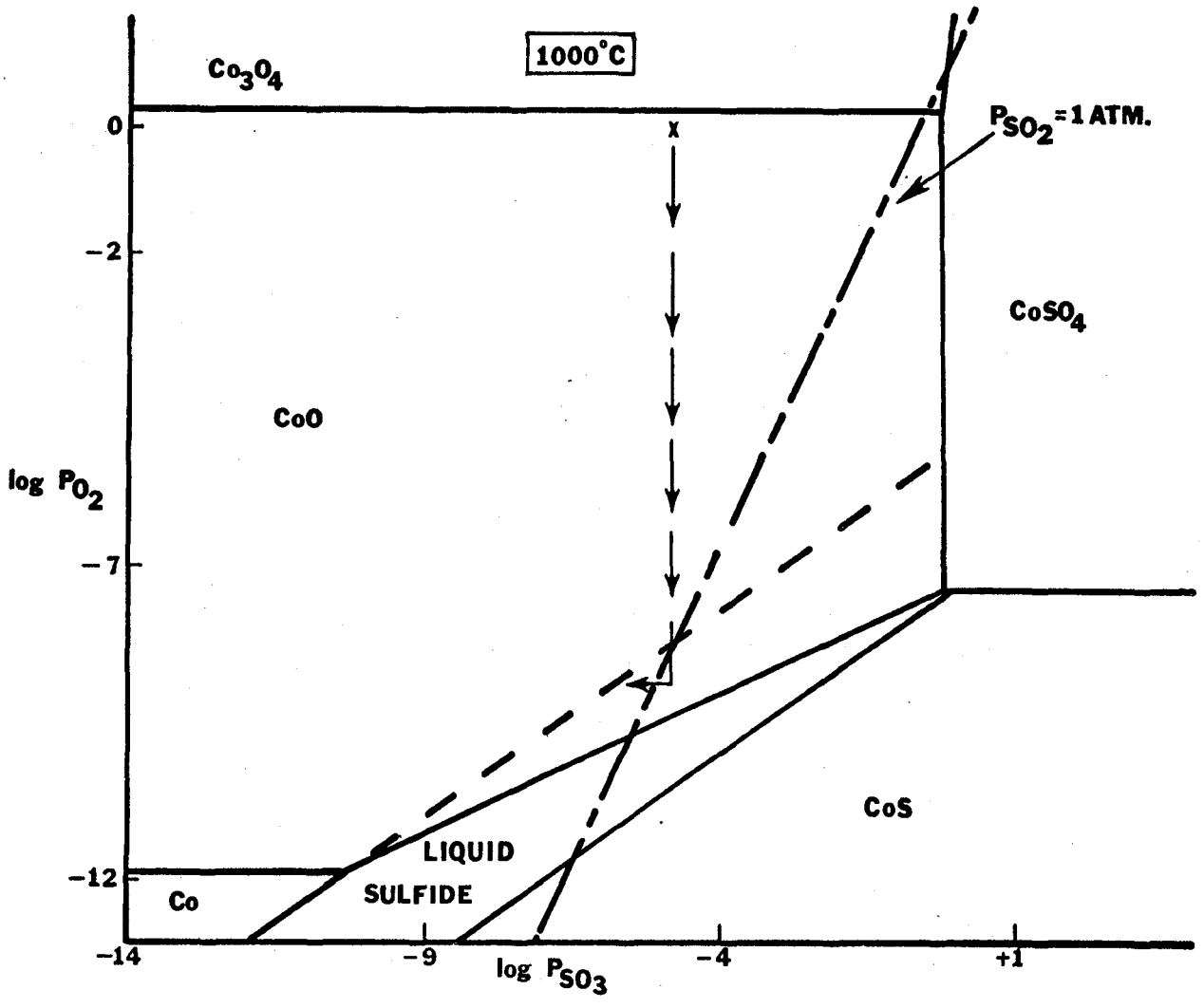

Figure 16 Stability diagram for the cobalt-oxygen-sulfur system showing the stable phases in Na_2SO_4 at 1000°C. The arrows indicate proposed changes in the composition of the Na_2SO_4 at the oxide/Na_2SO_4 interface as a result of removal of oxygen and sulfur from the Na_2SO_4 by the alloy. The dashed line indicates the sulfur pressure required to form cobalt sulfide at oxygen pressures equal to or less than that for the Co-CoO equilibrium. The dash-dot lines indicates the oxygen and SO_3 pressures for which the SO_2 pressure is 1 atm.

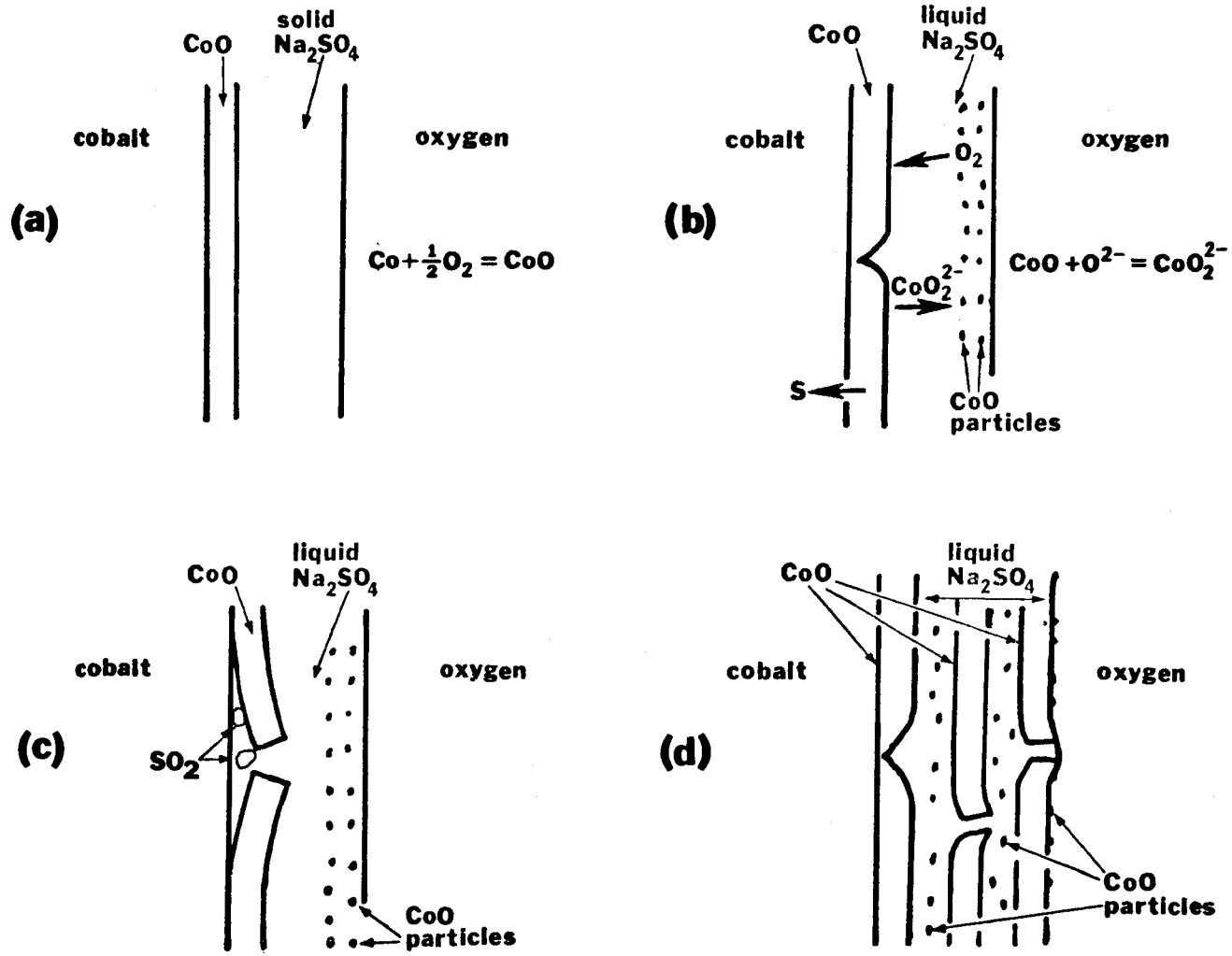

Figure 17 – Model for the Na_2SO_4-induced oxidation of cobalt. a) Upon heating a Na_2SO_4-coated specimen to temperature a layer of CoO is formed beneath the unmelted Na_2SO_4. b) After the Na_2SO_4 melts an oxygen gradient is developed across the liquid which in turn causes the sulfur activity of the Na_2SO_4 over the CoO to be increased and sulfur enters the metal. Oxide ions are therefore produced in the Na_2SO_4 and these ions react with oxide scale to form CoO_2^{2-} which diffuses to the Na_2SO_4/gas interface and decomposes. c) The oxide is penetrated by the Na_2SO_4 in localized areas which causes the oxide to become detached from the metal and SO_2 is evolved from the Na_2SO_4 in the crevices between the scale and the metal where the oxygen activity is very low. d) Successive layers of oxide are detached from the metal by the same mechanism. (The heavy arrows indicate diffusion directions.)

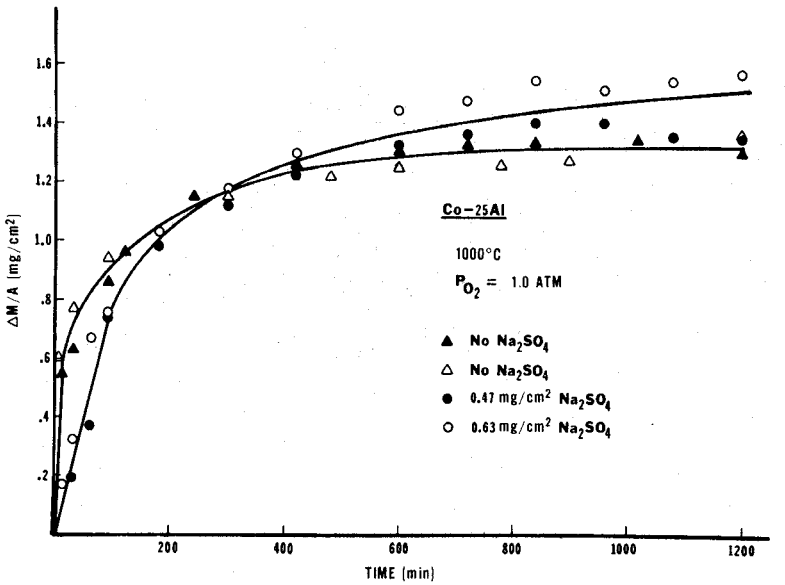

(a)

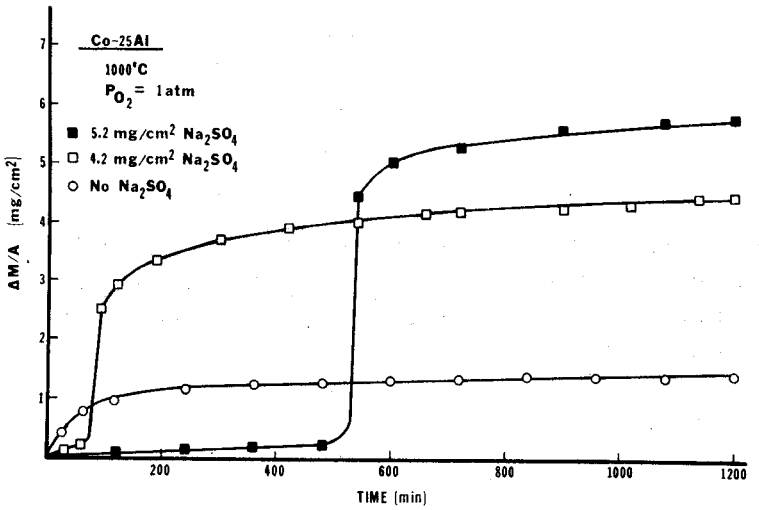

(b)

Figure 18 Comparison of the oxidation kinetics of Na_2SO_4-coated Co-25Al and Na_2SO_4-free Co-25Al, (a) 0.5 mg/cm^2 deposits, (b) 5 mg/cm^2 deposits.

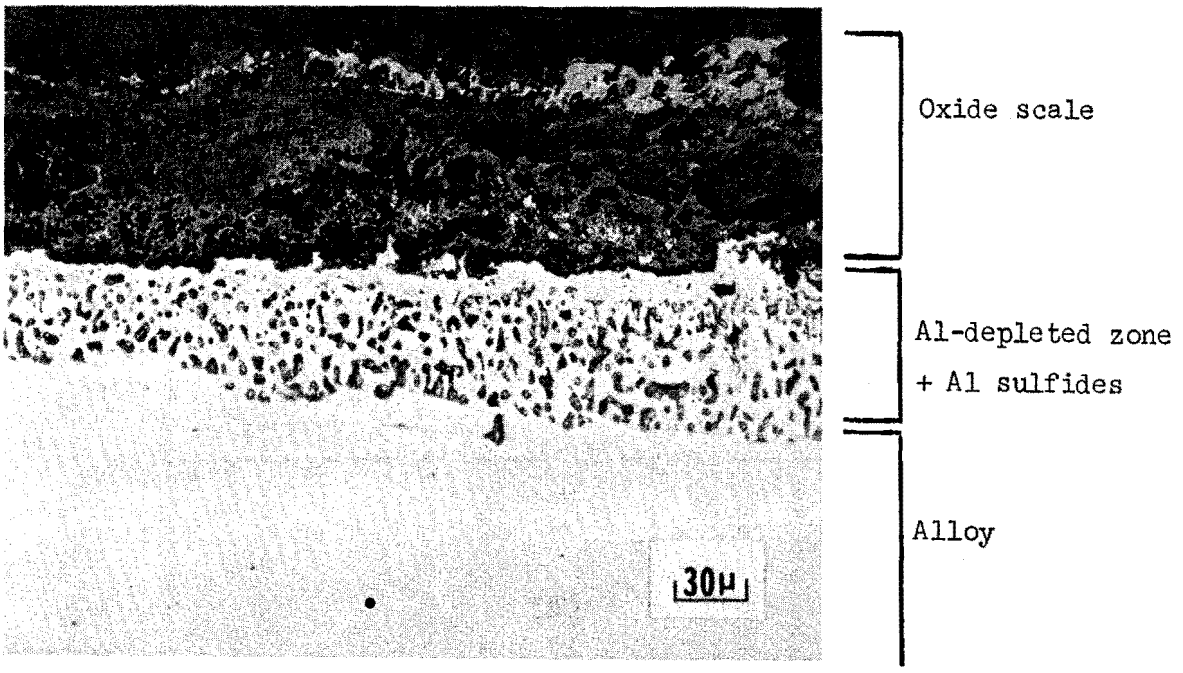

Figure 19 Transverse section of Co-25Al pre-coated with 5.2 mg/cm^2 Na_2SO_4 after 20 hours of oxidation at 1000°C in 1 atm oxygen. A thick non-protective oxide scale has formed externally, while particles of aluminum sulfide have formed within the alloy.

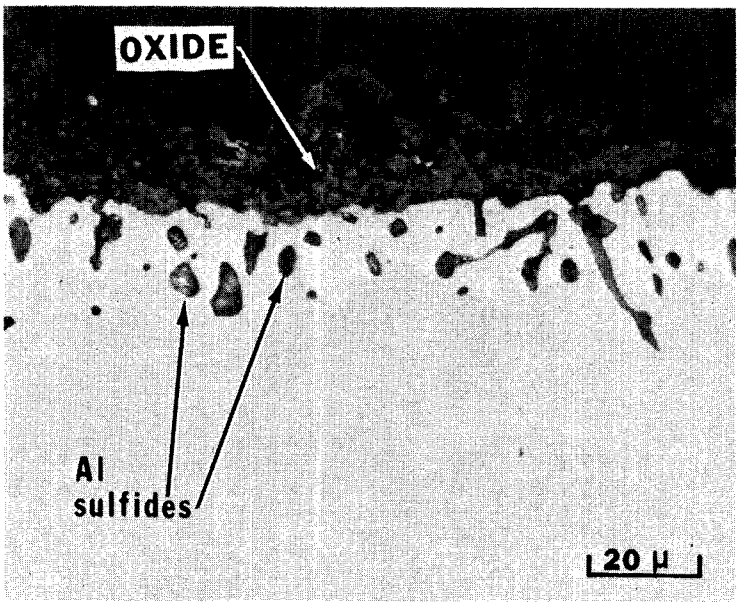

(a)

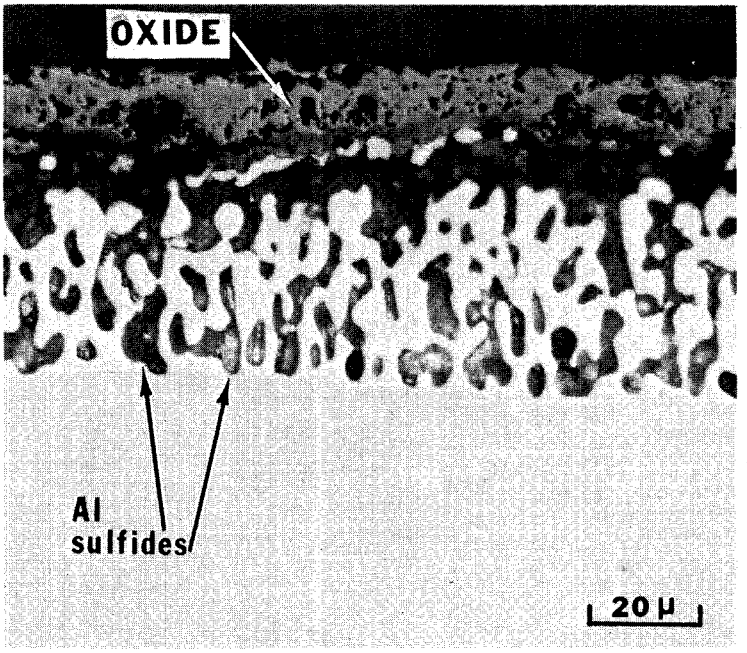

(b)

Figure 20 Photomicrographs of Co-25Al specimens that were oxidized in 1 atm of oxygen at 1000°C after presulfidation treatments of, (a) 170 minutes in an H_2S-H_2 mixture with $H_2S/H_2 = 2 \times 10^{-3}$ and, (b) 2 minutes in an H_2S-H_2 mixture with $H_2S/H_2 = 0.2$. Thick oxide scales containing other oxides in addition to Al_2O_3 have been formed on these specimens.

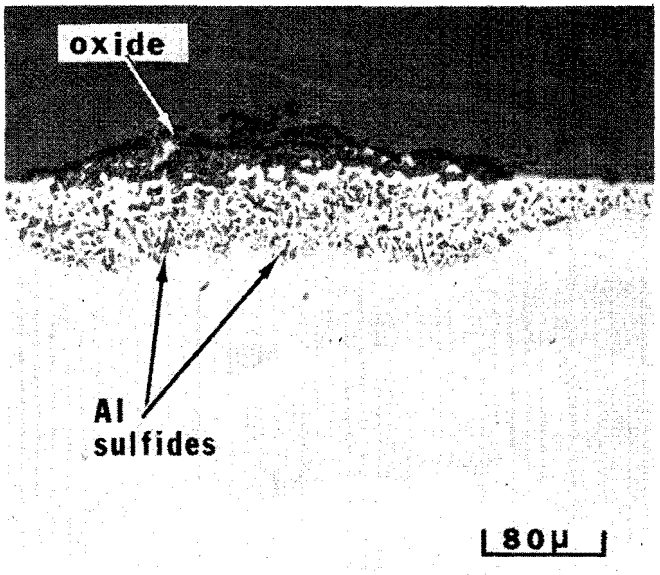

Figure 21 Photomicrograph of Co-25Al after 16 hrs. of oxidation in flowing SO_2 at 1000°C. Numerous sulfide particles are visible in the alloy and the oxide scale contains other oxides in addition to Al_2O_3.

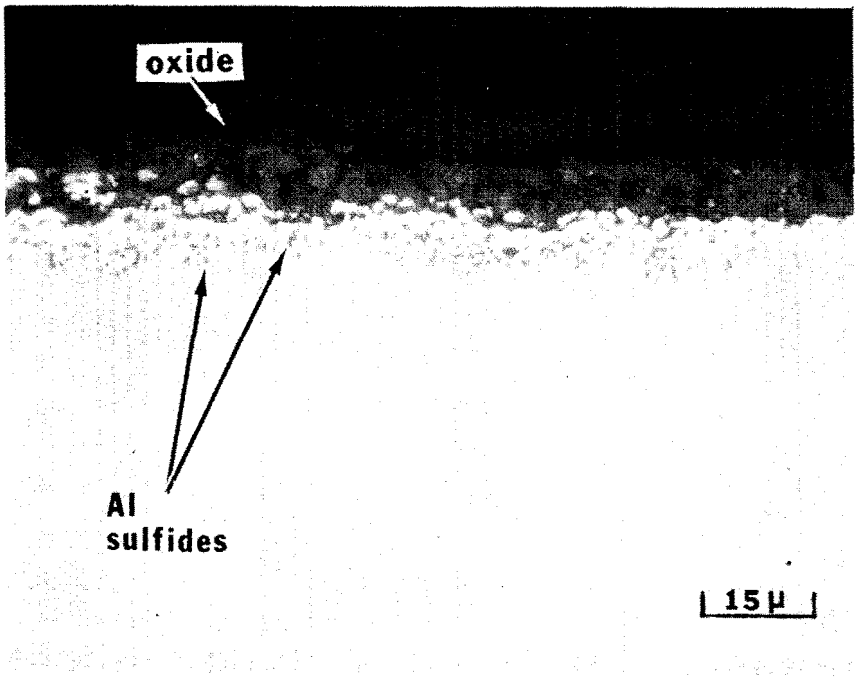

Figure 22 Photomicrograph of Na_2SO_4-coated (1 mg/cm^2) Co-25Al after 4 minutes of oxidation. The scale is at least 10 times thicker than that formed on Na_2SO_4 – free specimens. Accelerated oxidation was observed visually on this specimen by using the hot stage microscope.

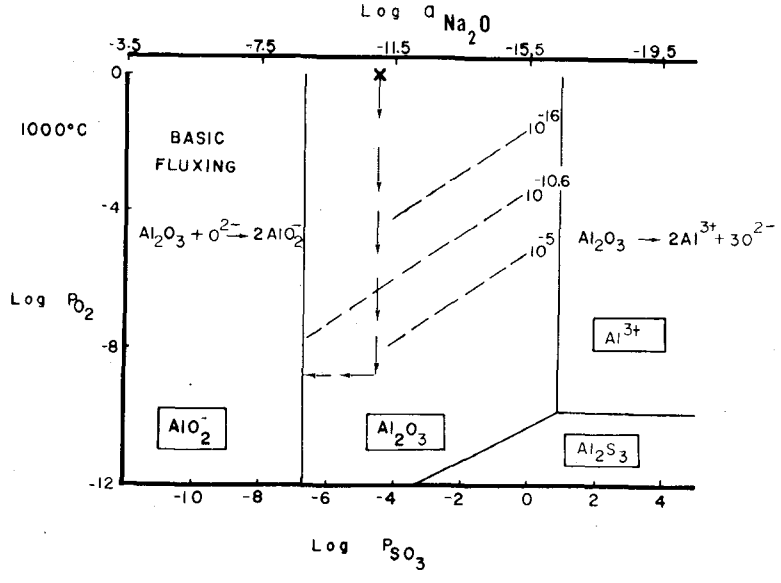

Figure 23 Stability diagram showing the phases of aluminum that are stable in Na_2SO_4 at 1000°C. The arrows show how the composition of Na_2SO_4 can change because of removal of oxygen and sulfur. The dashed lines are sulfur isobars and the isobar of $10^{-10.6}$ is the sulfur pressure required to form aluminum sulfide beneath an Al_2O_3 scale on Co-25Al alloy. This diagram shows that Al_2O_3 is stable in Na_2SO_4 with certain compositions, and Al_2O_3 reacts with Na_2SO_4 having either high or low activities of Na_2O (i.e. oxide ion activity).

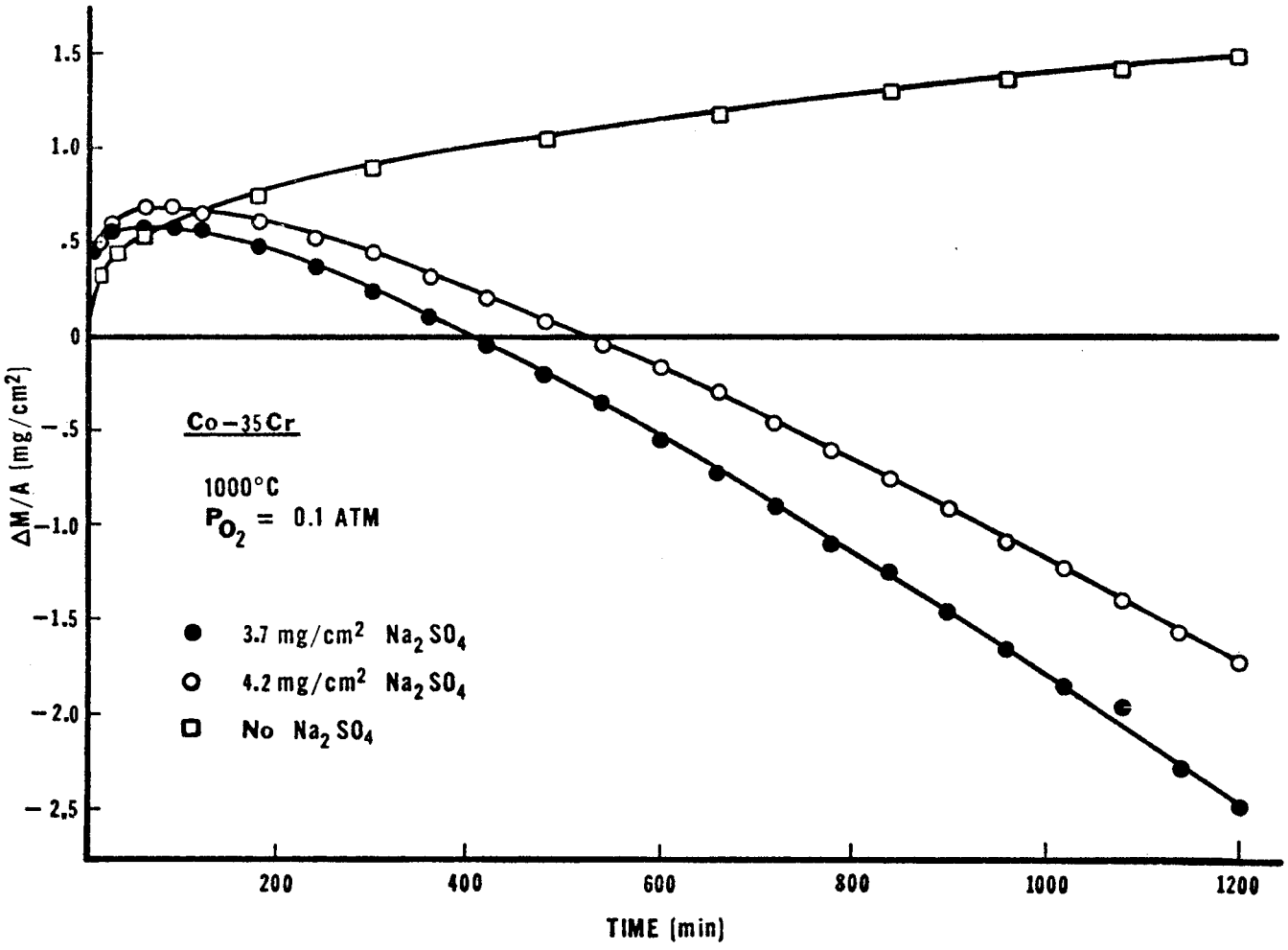

Figure 24 Comparison of results obtained from the oxidation of Co-35Cr with and without coatings of Na_2SO_4.

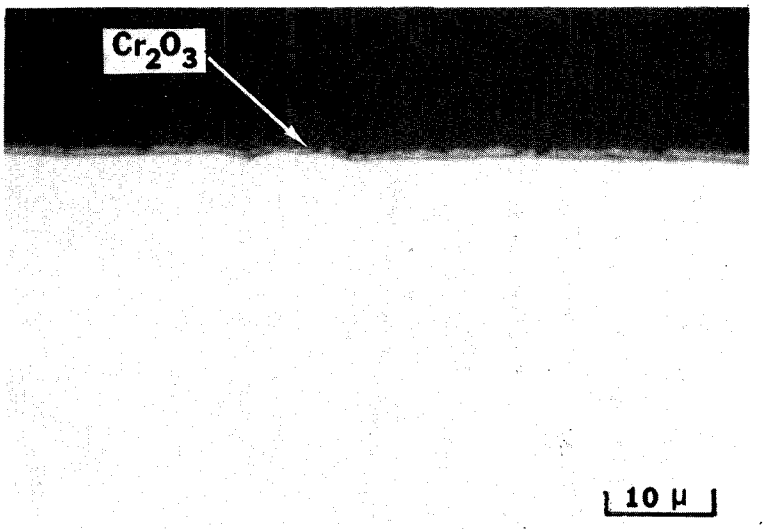

(a)

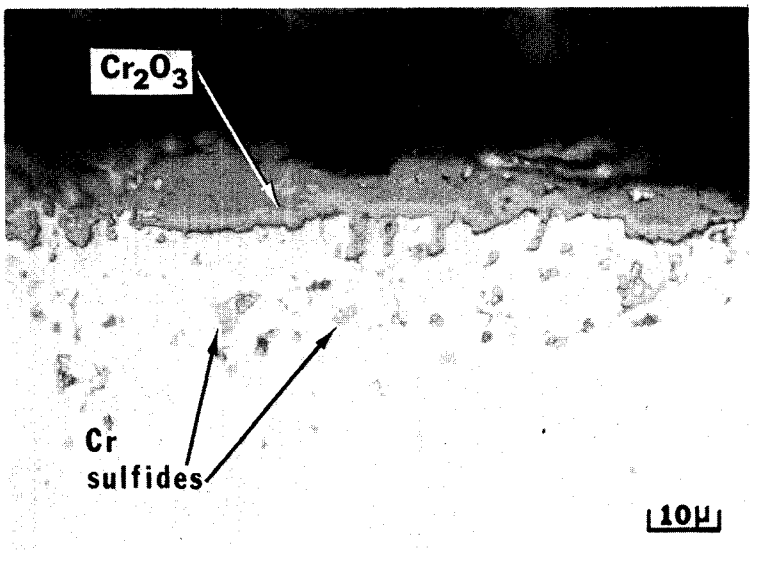

(b)

Figure 25 Comparison of the microstructures of Co-35Cr (a) and Na_2SO_4-coated (5 mg/cm^2) Co-35Cr (b) after 20 hrs of oxidation at 1000°C in 0.1 atm of oxygen. The oxide scale is thicker on the specimen with the Na_2SO_4 since it appears the transient oxidation period, during which a continuous layer of Cr_2O_3 is developed, has been extended.

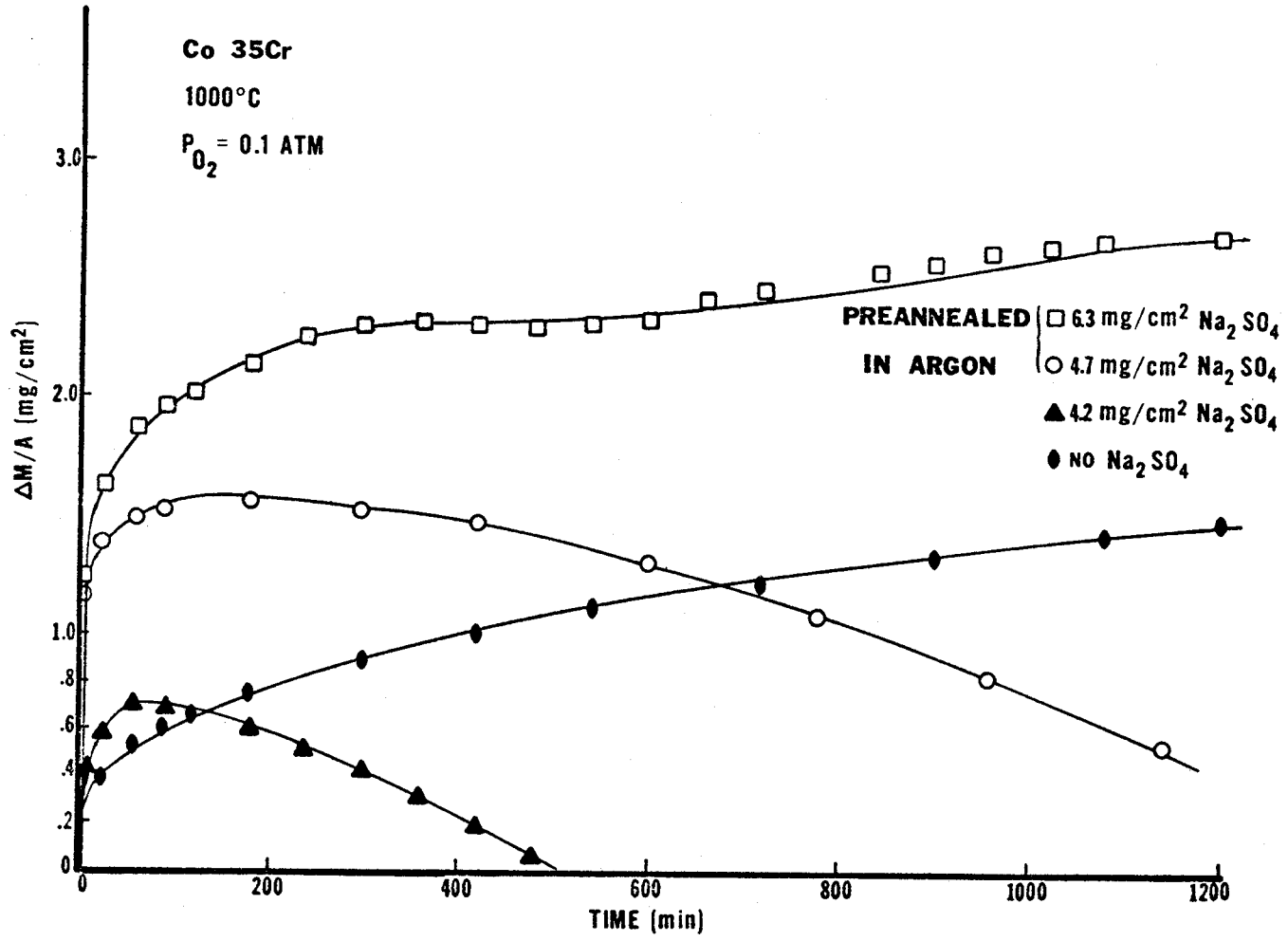

Figure 26 Weight change versus time curves for the oxidation of Co-35Cr and specimens of this alloy coated with Na_2SO_4. Some of the Na_2SO_4-coated specimens were annealed for 1 hr at 1000°C in argon prior to oxidation. The initial weight changes of all the Na_2SO_4-coated specimens indicate that Na_2SO_4 has induced accelerated oxidation of the Co-35Cr alloy.

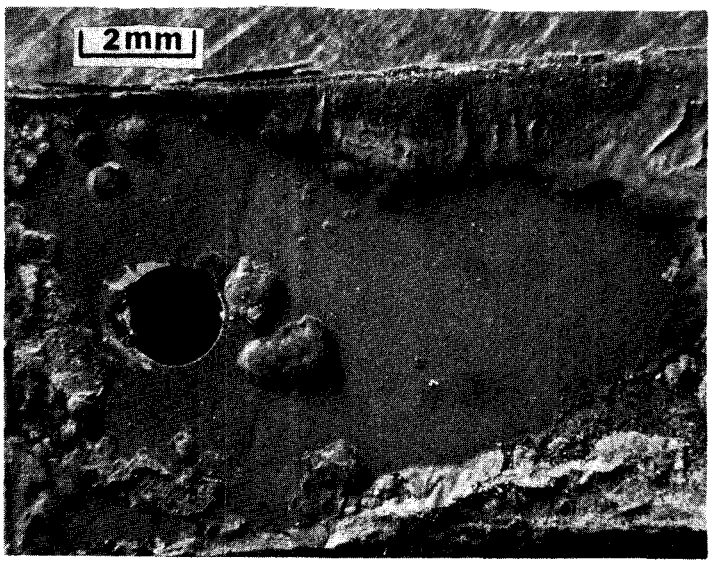

(a)

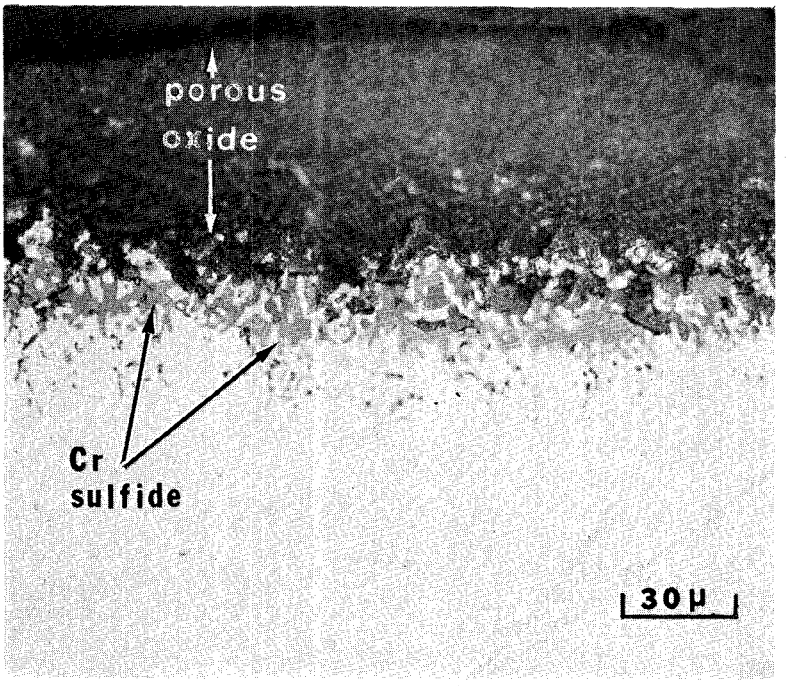

(b)

Figure 27 a) Surface photograph showing nonuniform attack of Na_2SO_4-coated (5 mg/cm^2) Co-35Cr alloy after 1 hr in argon at 1000°C. b) Photomicrograph showing the thick porous oxide developed on the specimen shown in (a) in those areas having the more severe attack.

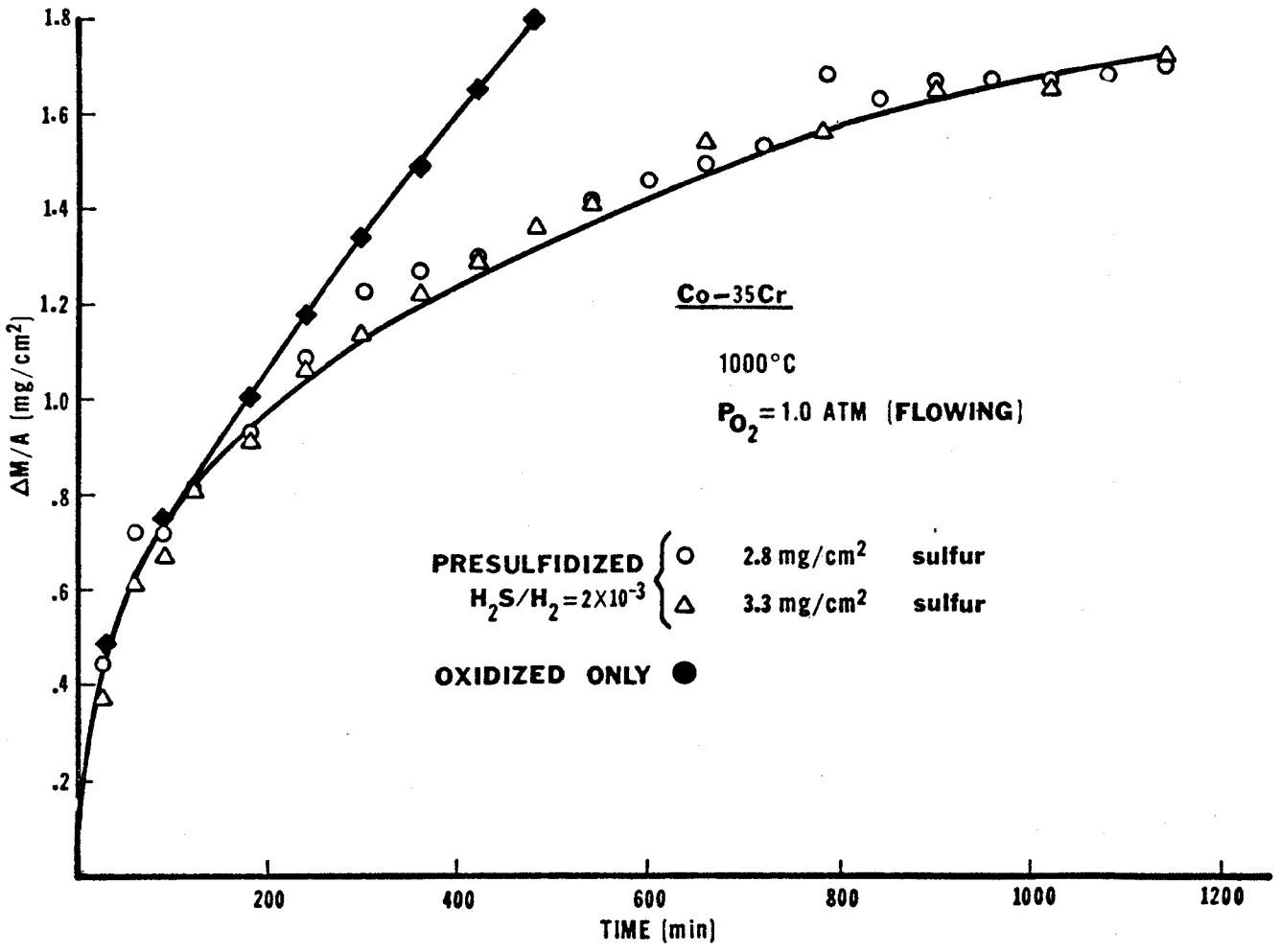

Figure 28 Comparison of weight change versus time curves for the oxidation of Co-35Cr and presulfidized Co-35Cr. The presulfidized specimens gained less weight than specimens of Co-35Cr that were not given this pretreatment.

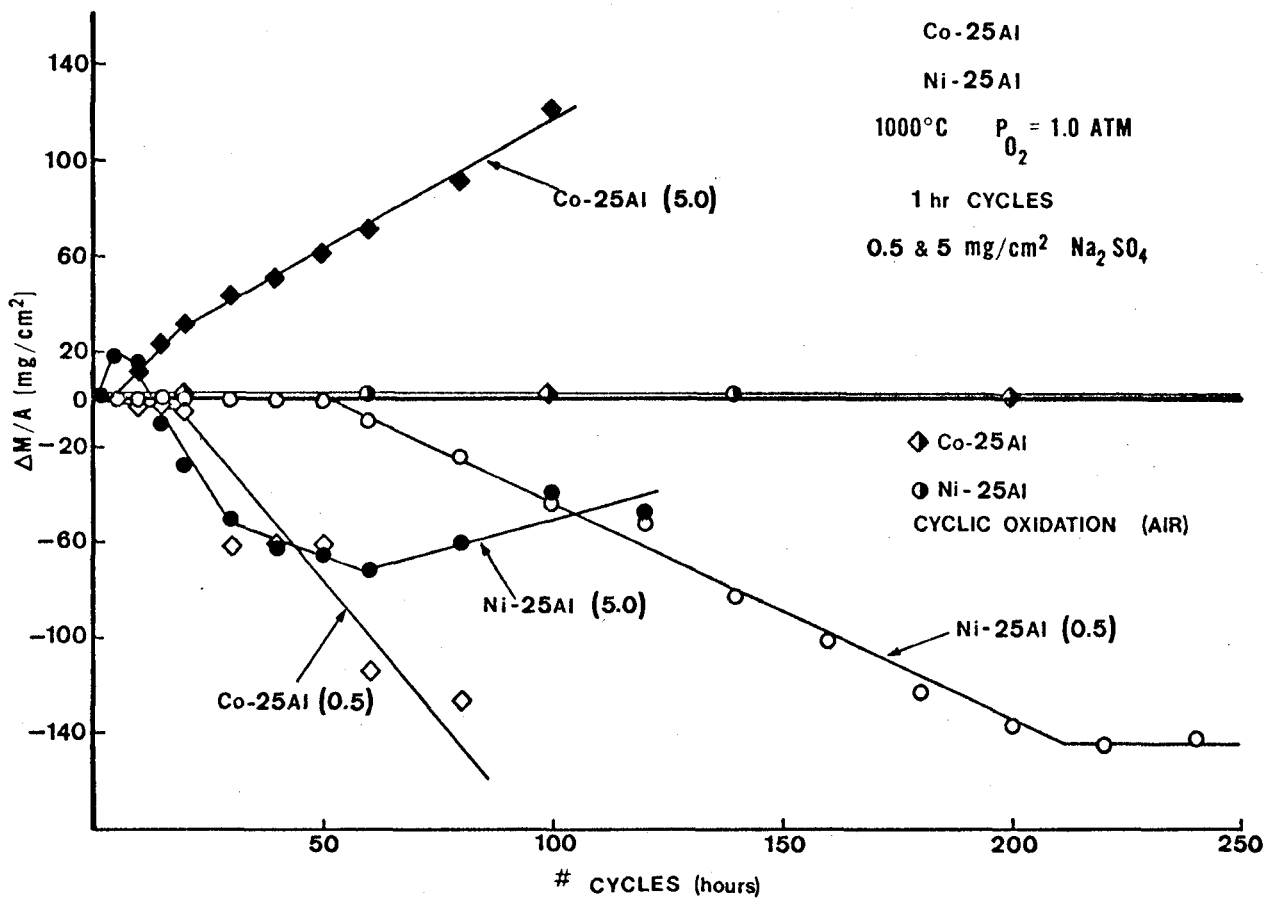

Figure 29 Weight change versus time curves obtained for the cyclic hot corrosion of Co-25Al and Ni-25Al alloy specimens which were coated with either 0.5 or 5 mg/cm^2 Na_2SO_4 at approximately 20-hour intervals. Cyclic oxidation data for specimens without Na_2SO_4 are also plotted for comparison.

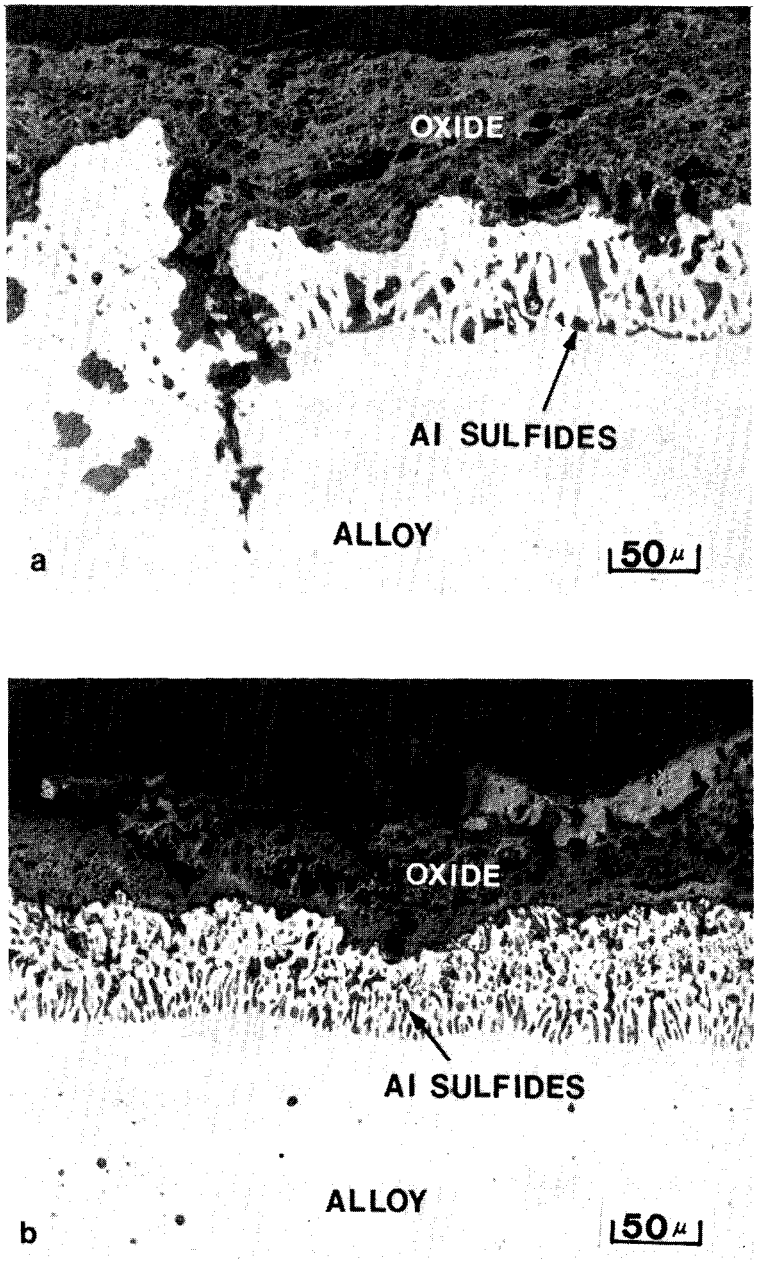

Figure 30 Comparison of transverse microstructures of Ni-25Al (a) and Co-25Al (b) coated with 0.5 mg/cm^2 Na_2SO_4 and cyclically oxidized at 1000°C. Ni-25Al specimen (a) was exposed for 260 one hr cycles, compared to only 80 cycles for Co-25Al (b).

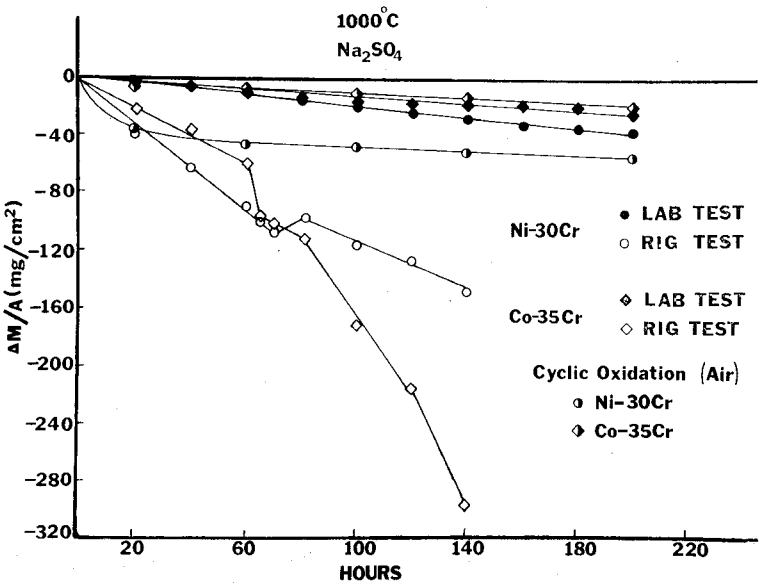

Figure 31 Comparison of weight change versus time data obtained for Ni-30Cr and Co-35Cr specimens in the laboratory hot corrosion test (5 mg/cm^2 Na_2SO_4 every 20 hrs) and in the ducted burner rig. Laboratory furnace cyclic oxidation data are included for comparison.

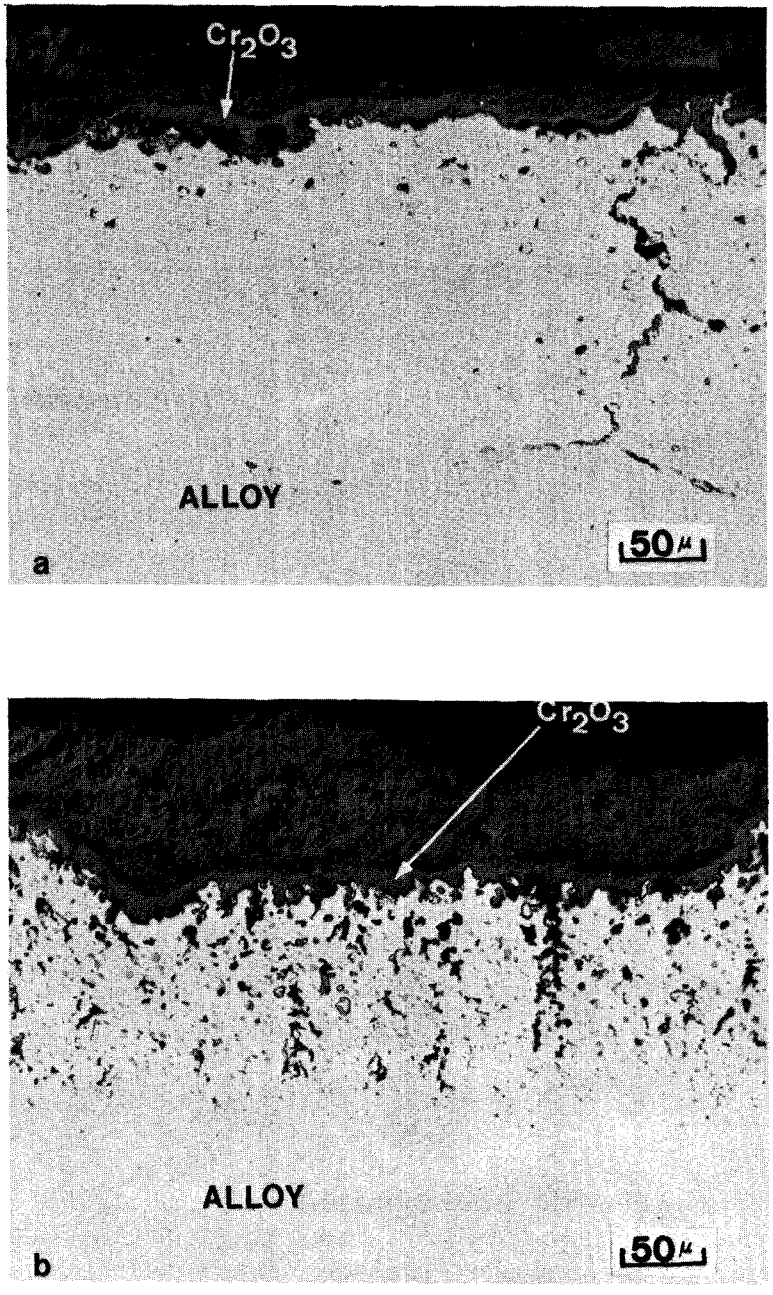

Figure 32 Comparison of microstructures of Ni-30Cr (a) and Co-35Cr (b) alloy specimens after 240 hours of cyclic hot corrosion at 1000°C. Specimens were coated with 0.5 mg/cm^2 Na_2SO_4 at approximately 20-hr intervals. Continuous layers of protective Cr_2O_3 are present at oxide/alloy interface for both specimens.

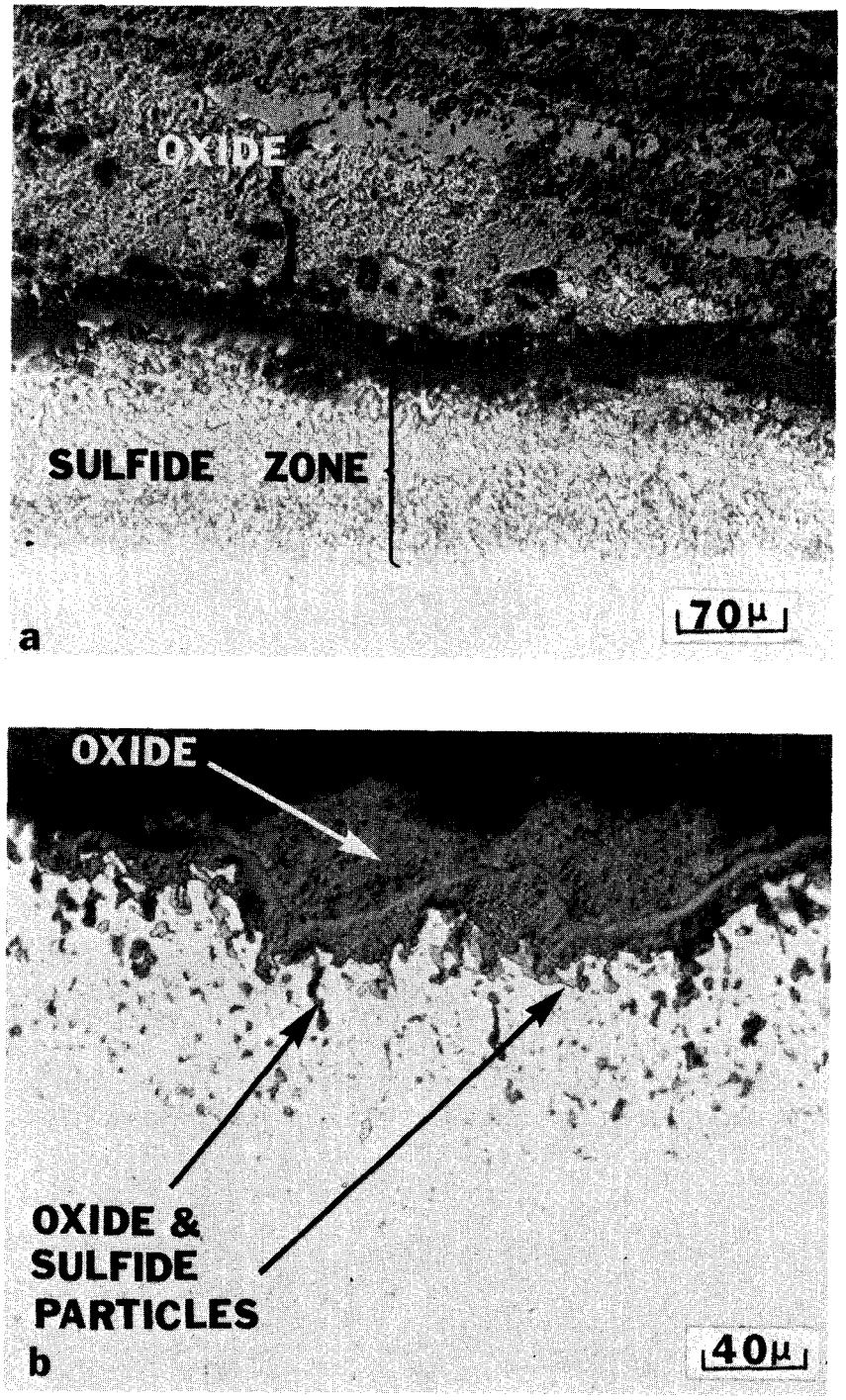

Figure 33 Photographs showing the microstructures of Co-35Cr specimens at the leading (a) and trailing (b) edges after 140 hrs in the ducted burner rig at 1000°C with a Na_2SO_4 deposition rate of 0.1 mg/cm^2-hr. After testing in the laboratory cyclic hot corrosion test (0.5 or 5 mg/cm^2 Na_2SO_4 applied every 20 hrs) the structure of this alloy was virtually identical to that of the trailing edge of the specimen from the ducted rig test.

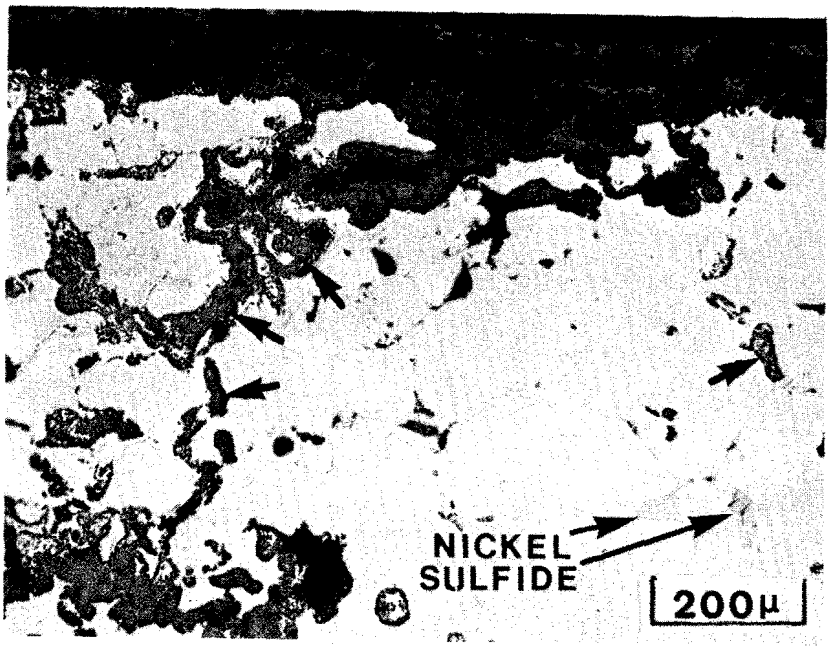

Figure 34 Transverse section of Ni-10Cr after 110 hrs of cyclic hot corrosion at 1000°C, 5 mg/cm^2 Na_2SO_4 applied approximately every 20 hrs. Arrows indicate stringers of liquid nickel sulfide which have been preferentially oxidized.

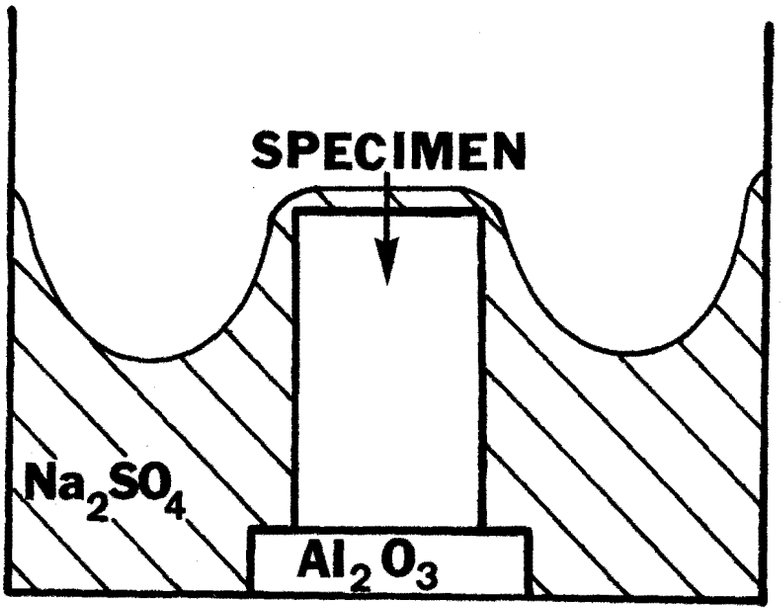

Figure 35 Schematic diagram showing features of crucible test.

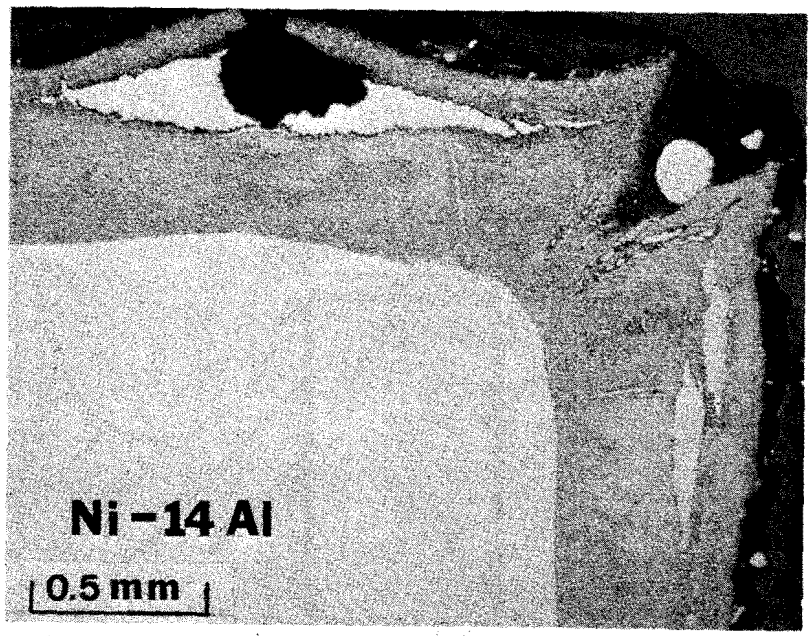

Figure 36 Microstructure of Ni-14Al after 7 min in Na_2SO_4 crucible test at 900°C in air.

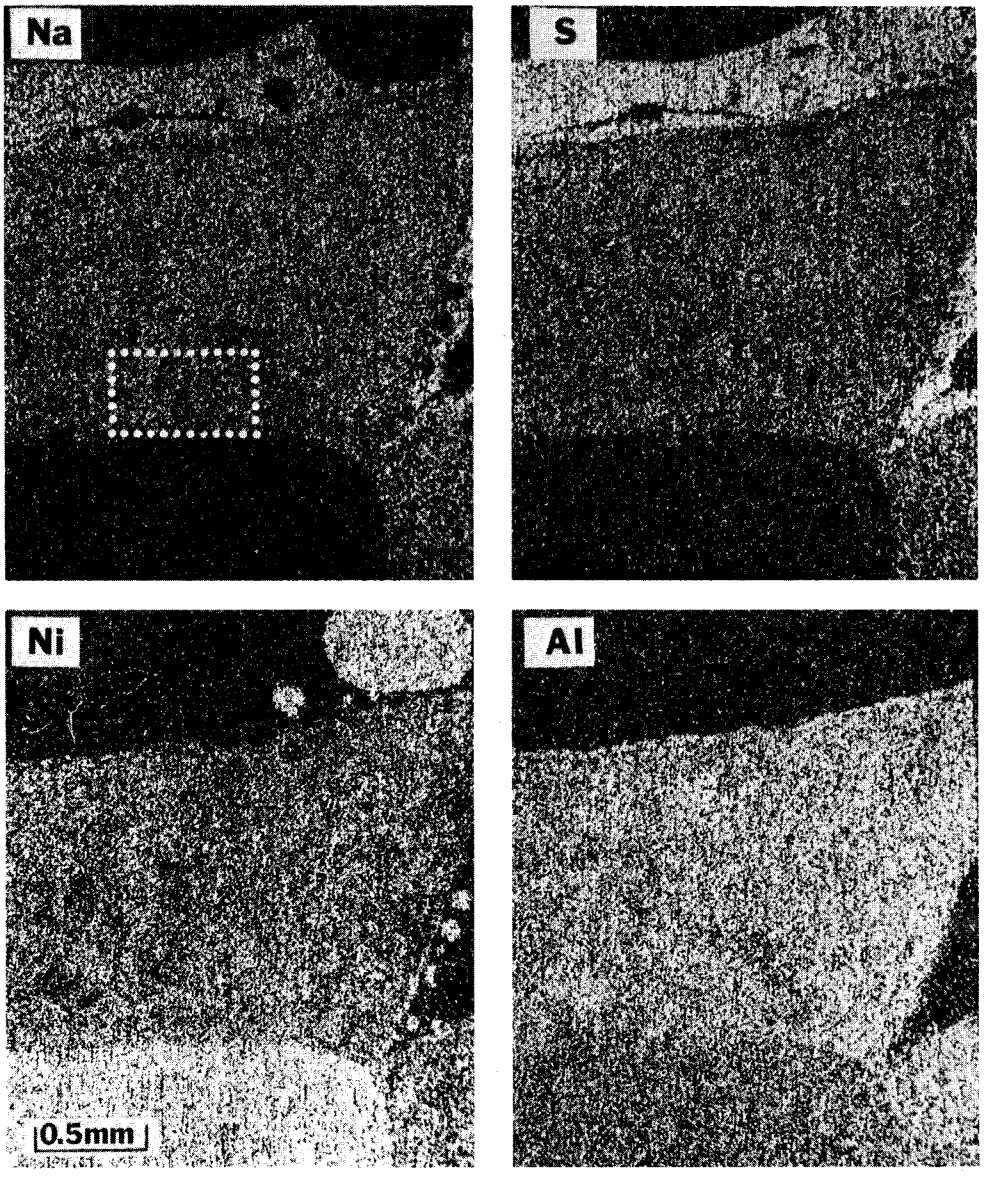

Figure 37 Electron microprobe x-ray images of specimen shown in Figure 36. Dotted lines in sodium x-ray image indicate area of detailed examination, shown in Figure 38.

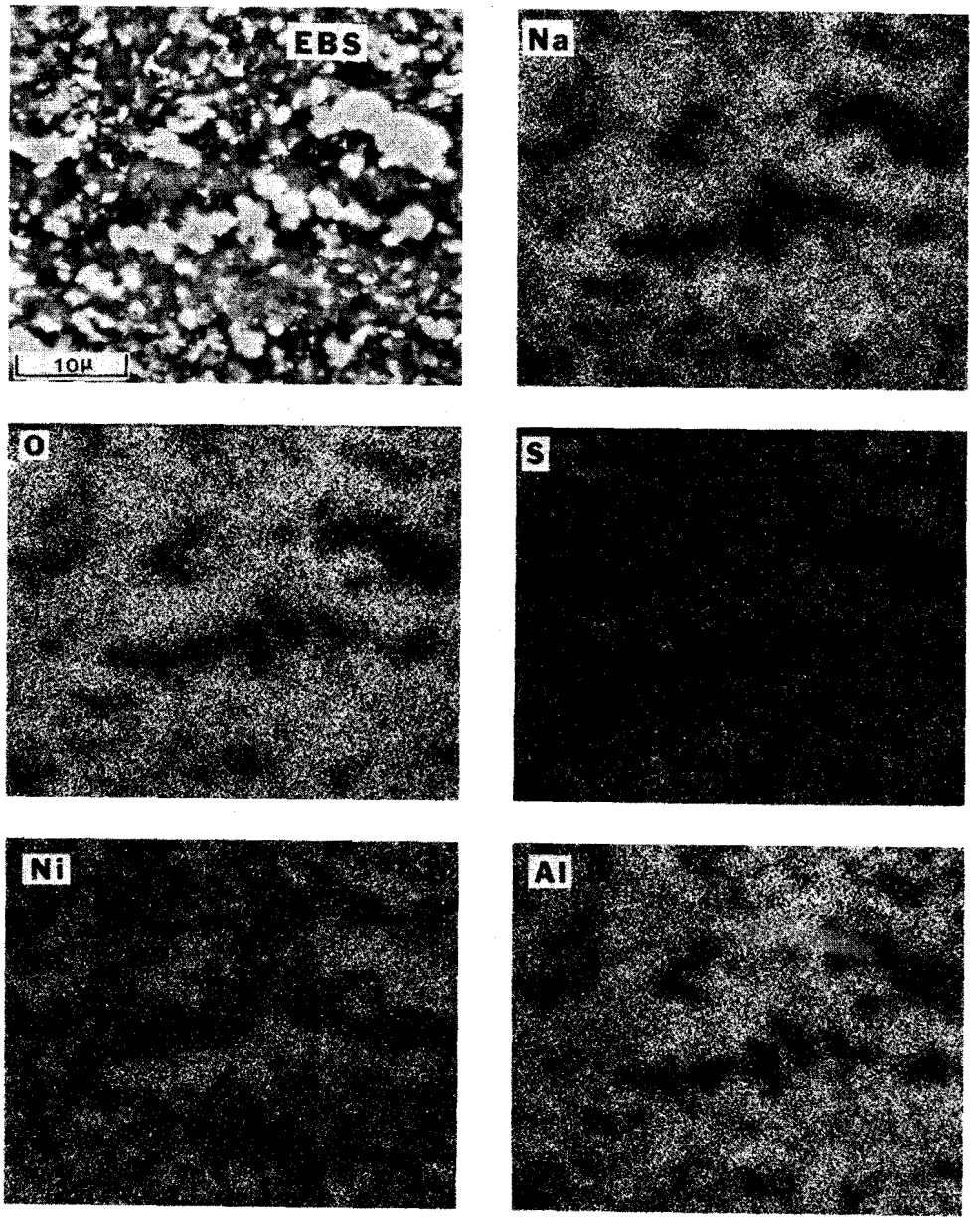

Figure 38 Electron microprobe x-ray images at area indicated in Figure 37. The metallic particles are nickel which are surrounded by a phase containing Na, O, S and Al, namely, a solution of Na_2SO_4 containing AlO_2^- ions. The images presented in Figure 37 show that at the Na_2SO_4-reaction product interface the metallic particles are nickel sulfide rather than nickel.

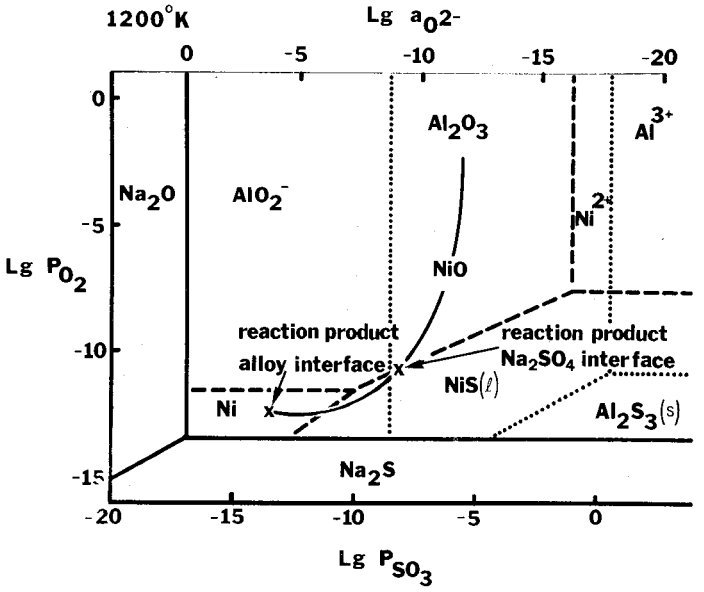

Figure 39 Stability diagram to illustrate the phases of nickel and aluminum which can exist in a Na_2SO_4 layer on a nickel-aluminum alloy. The Na_2SO_4 region is bounded by Na_2O and Na_2S and indicated by solid straight lines. The boundaries between the different nickel and aluminum phases are indicated by dashed and by dotted lines, respectively. The solid curve indicates the Na_2SO_4 compositional gradient that may be established when Na_2SO_4 is deposited on a nickel-aluminum alloy.

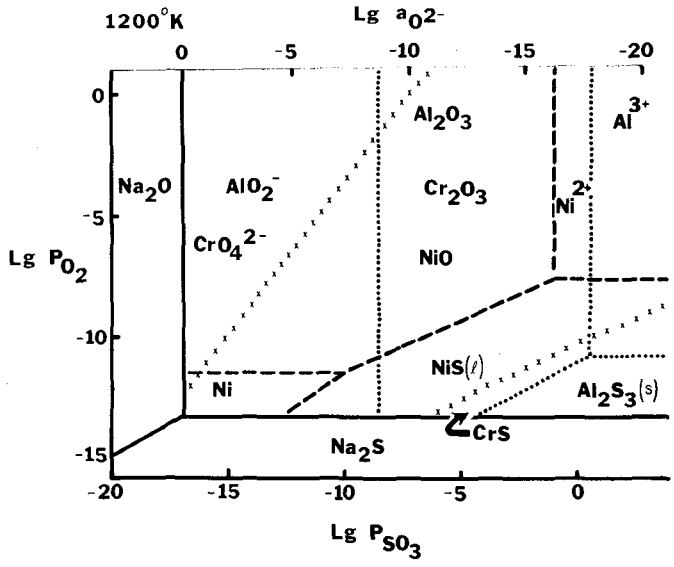

Figure 40 Stability diagram presented in Figure 39 but which also contains boundaries (X's) to show the phases of chromium that are stable in Na_2SO_4. It is to be noted that, since the reaction between Cr_2O_3 and oxide ions in the Na_2SO_4 is dependent on oxygen pressure, and the reaction between Al_2O_3 and oxide ions is not, at low oxygen pressures much larger oxide ion concentrations are required to dissolve Cr_2O_3 in Na_2SO_4 than Al_2O_3.

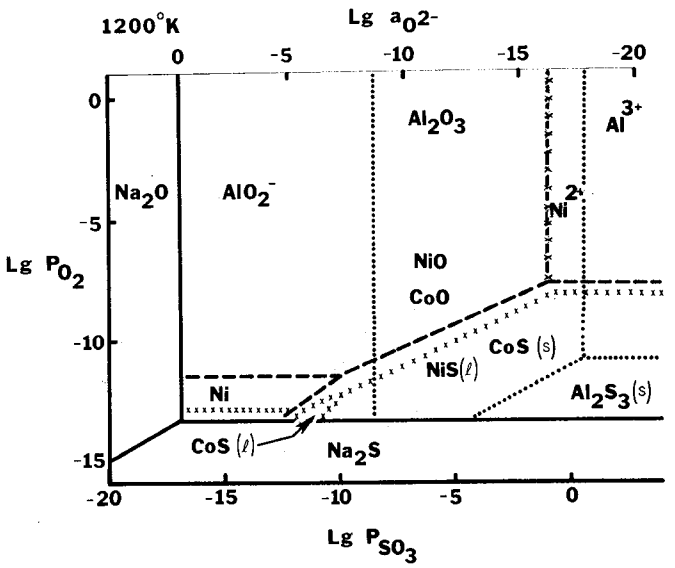

Figure 41 Stability diagram presented in Figure 39 but which also contains boundaries (X's) to show the phases of cobalt that are stable in Na_2SO_4. The oxygen activity of the Na_2SO_4 at which CoO and cobalt sulfide coexist is less than that for the coexistence of NiO and nickel sulfide. In addition the stability range for liquid nickel sulfide is greater than that for liquid cobalt sulfide.

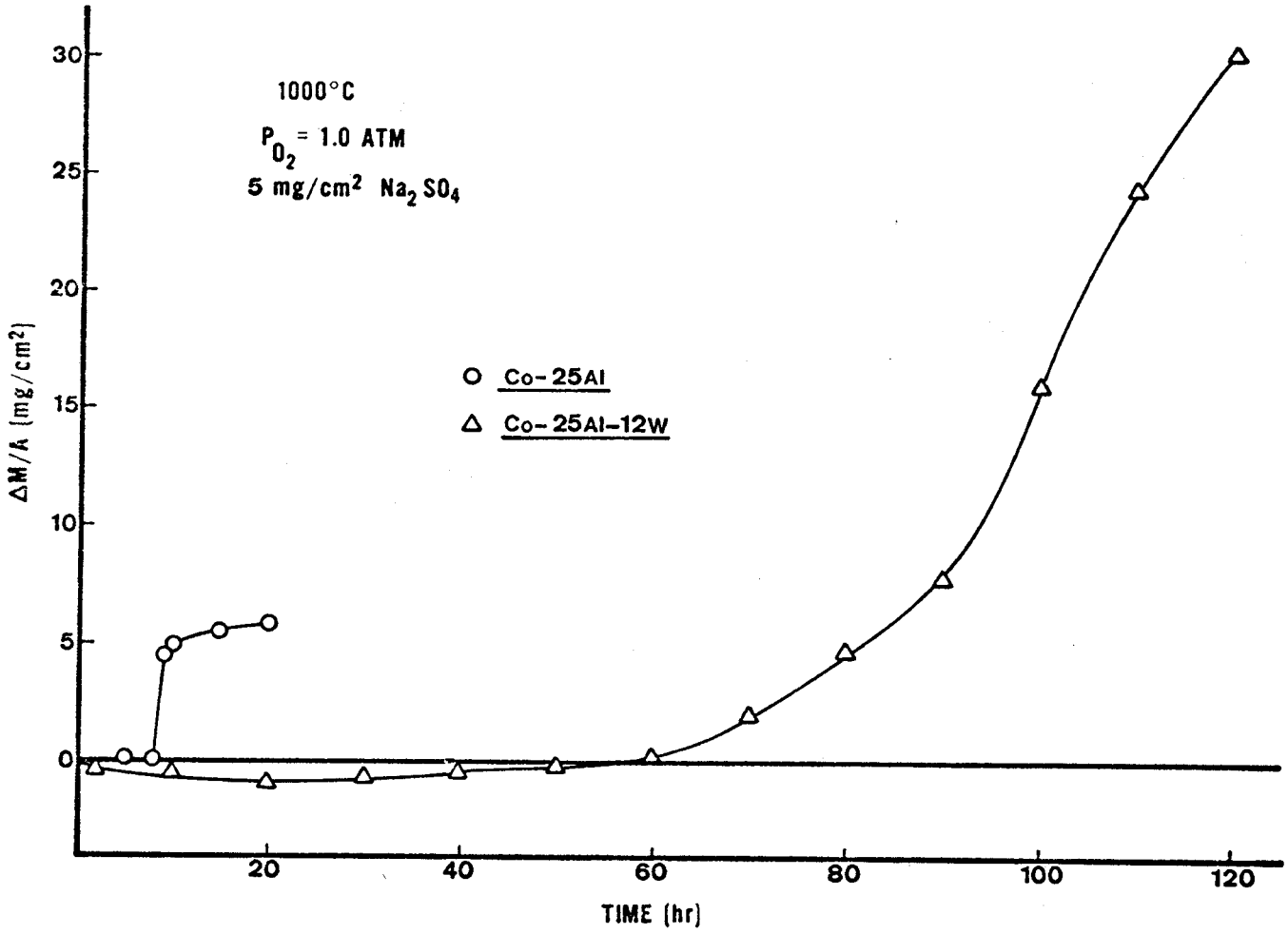

Figure 42 Comparison of the weight change versus time curves obtained for the isothermal oxidation of Na_2SO_4-coated specimens of Co-25Al and Co-25Al-12W.

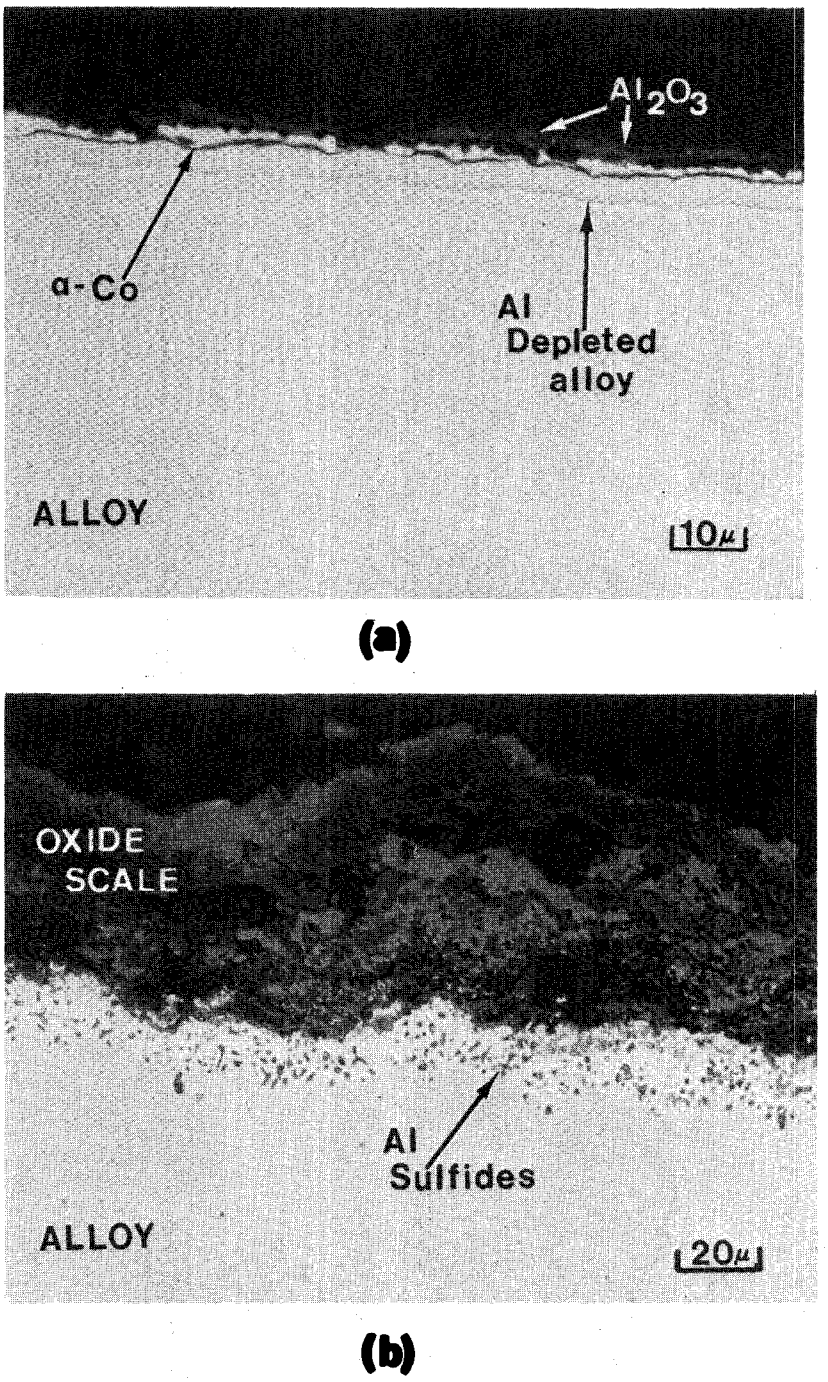

Figure 43 Photographs showing the microstructures of Co-25Al-12W alloy after 20 hours of oxidation at 1000°C in 1 atm of oxygen. (a) Alumina scale developed after oxidation without Na_2SO_4. (Etched in 50 lactic acid – 30 nitric acid – 2HF) (b) Oxide scales developed after oxidation with 0.8 mg/cm^2 of Na_2SO_4. The sulfide particles in the substrate are principally aluminum sulfide.

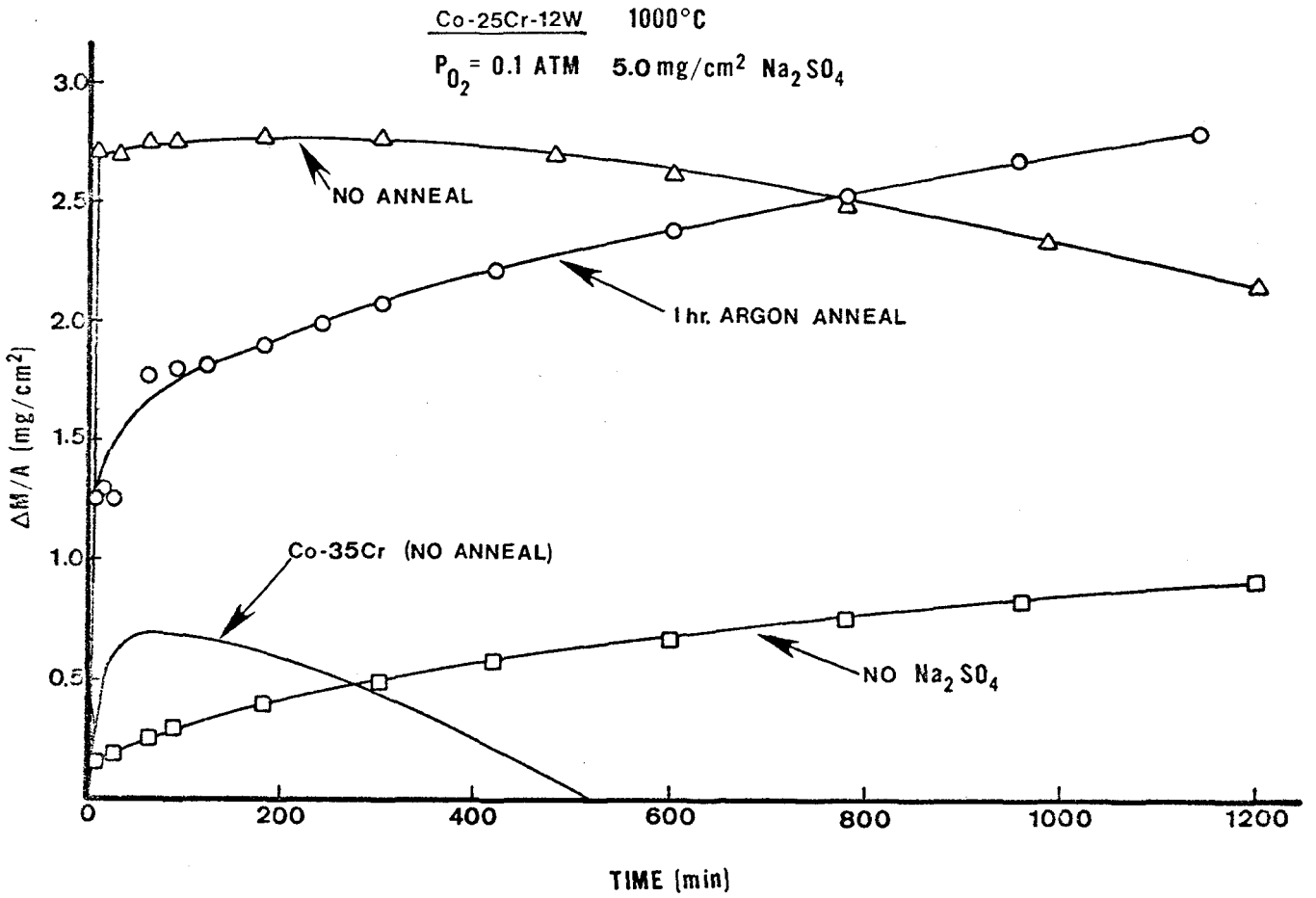

Figure 44 Comparison of the isothermal oxidation data for Co-25Cr-12W and Co-35Cr under different conditions. The data labeled "NO ANNEAL" are for specimens coated with 5 mg/cm^2 and oxidized. Data labeled "1 hr ARGON ANNEAL" are for a Na_2SO_4-coated specimen treated in argon prior to oxidation. Data for oxidation of both alloys in the absence of Na_2SO_4 is represented by the "No Na_2SO_4" curve.

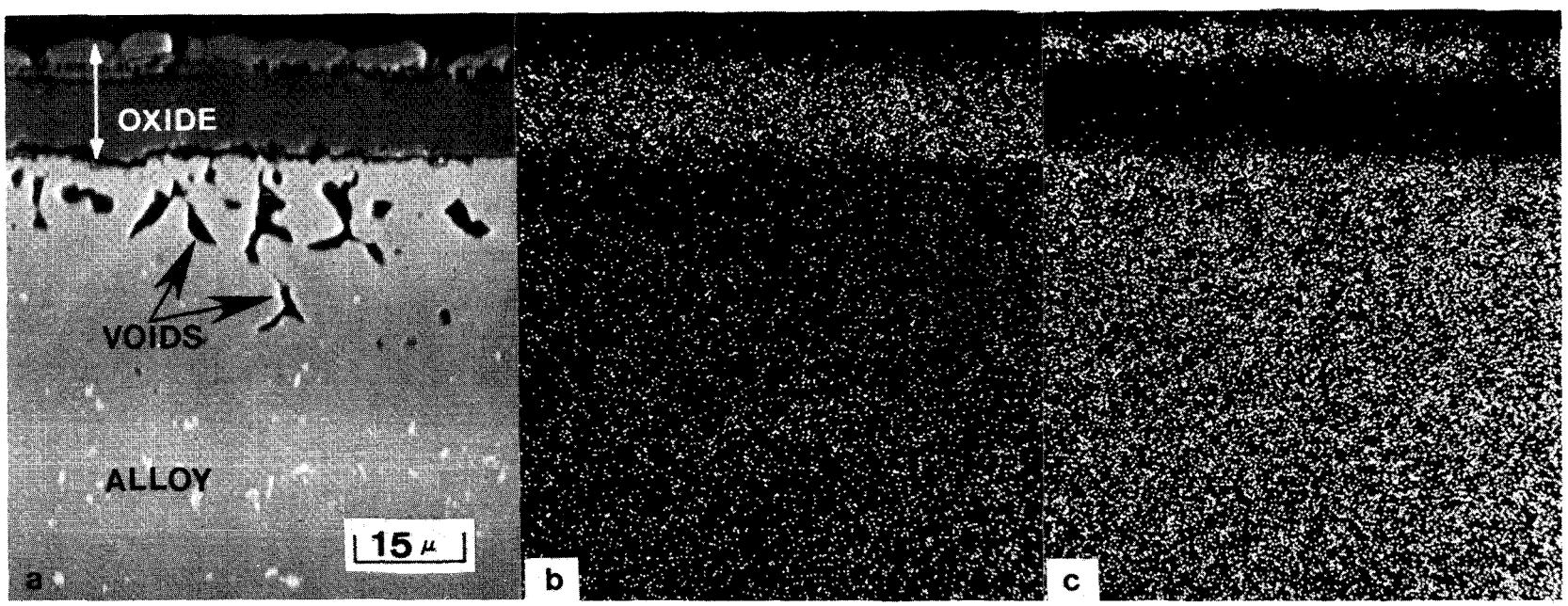

Figure 45 Photomicrographs obtained from the electron beam examination of a Co-25Cr-12W alloy that had been coated with 0.7 mg/cm^2 of Na_2SO_4 and oxidized 20 hrs in oxygen at 1000°C. (a) Electron back scatter photograph showing the oxide scale. (b) X-ray image showing the distribution of chromium. (c) X-ray image showing the distribution of cobalt.

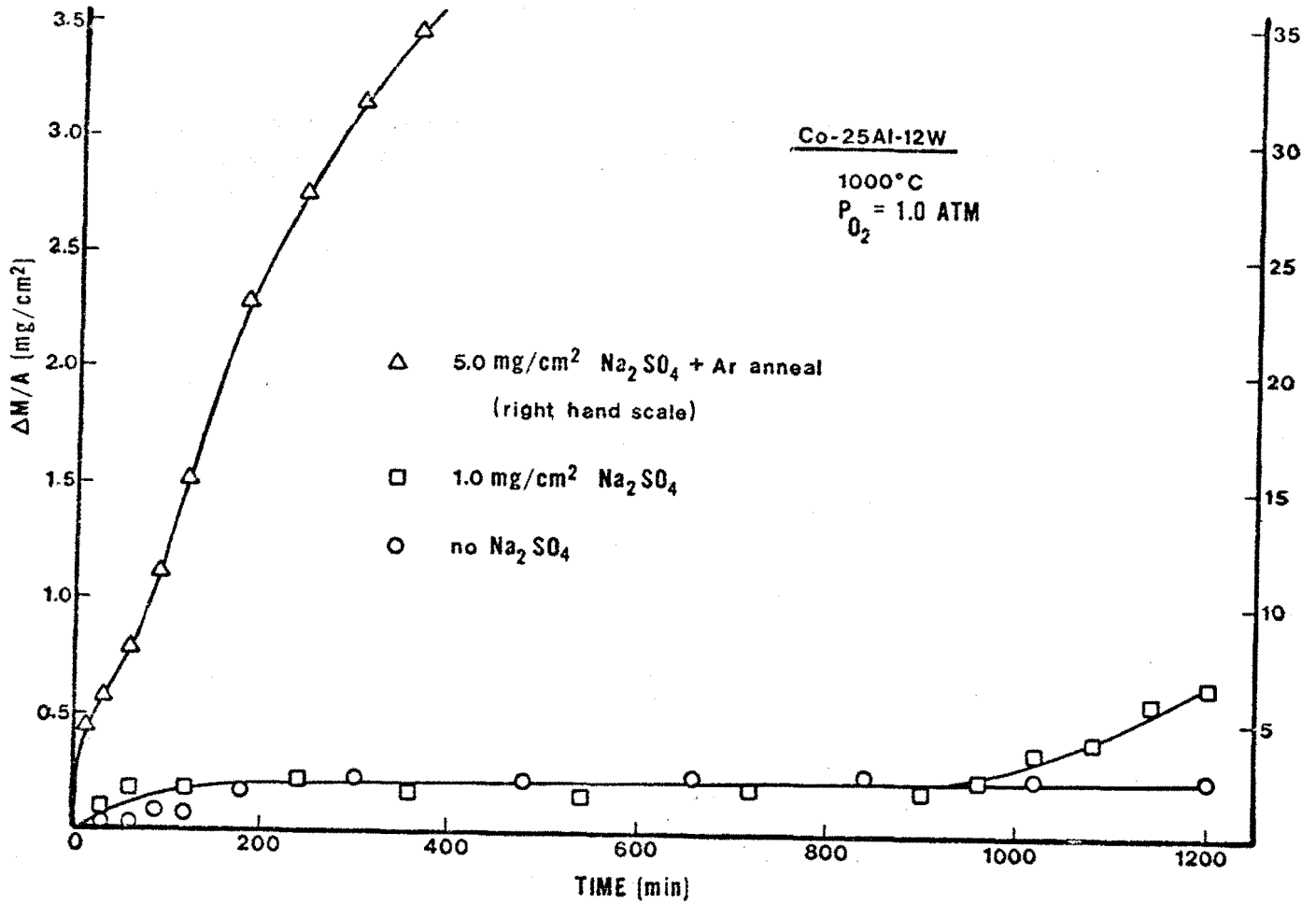

Figure 46 Comparison of the isothermal oxidation behavior of the Co-25Al-12W alloy under three different conditions. (The data points for the Na_2SO_4-coated and argon annealed specimens are plotted using the right-hand scale. All other data are plotted using left-hand scale).

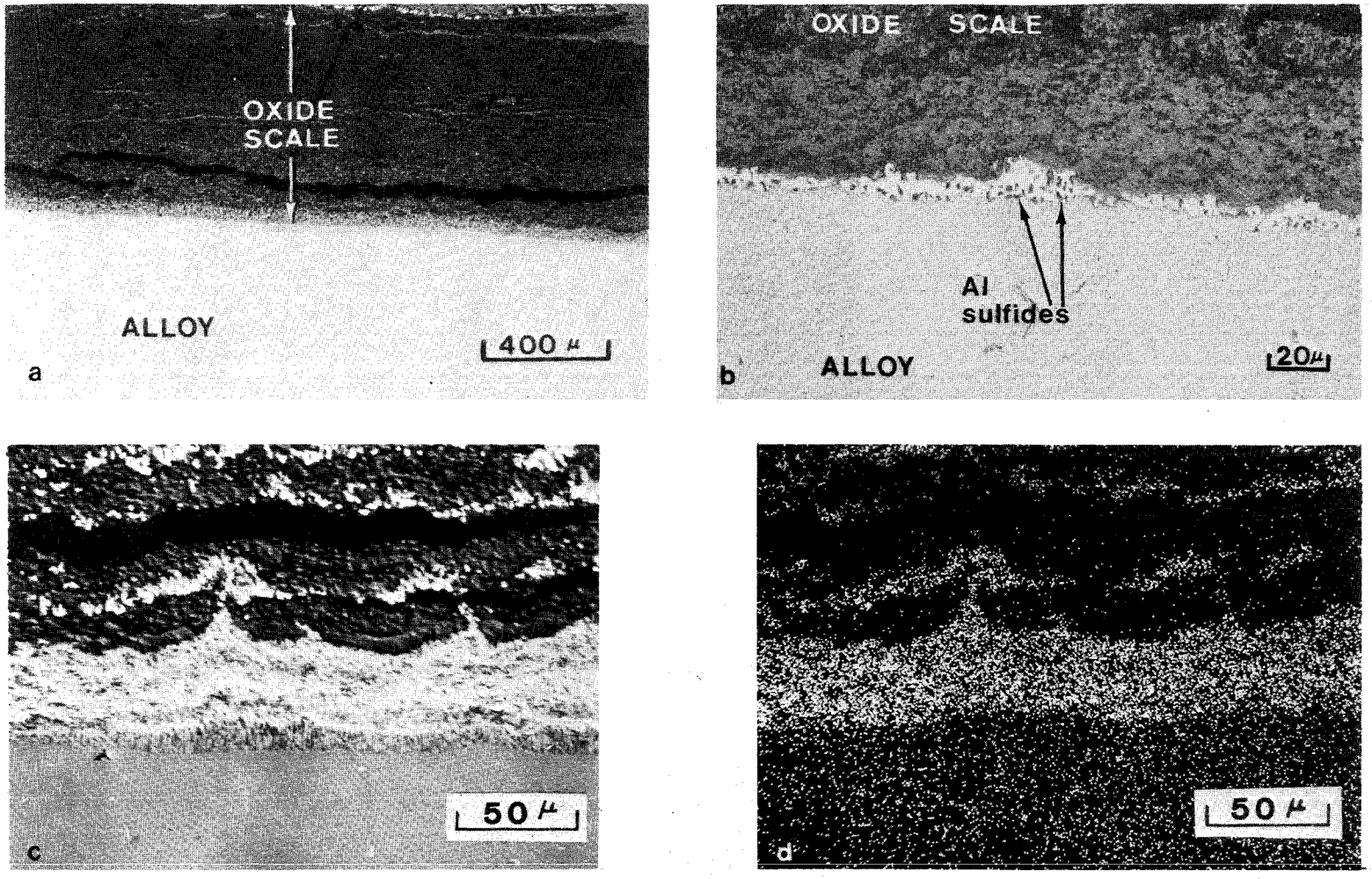

Figure 47 Photomicrographs and microprobe images of the microstructure of Co-25Al-12W after 20 hrs oxidation in 1 atm oxygen at 1000°C. Prior to oxidation this specimen was coated with 5 mg/cm^2 Na_2SO_4 and annealed for 1 hr in argon at 1000°C. (a) Optical micrograph showing overall scale thickness. (b) Optical micrograph showing details at the scale/alloy interface. (c) Electron backscatter image of scale/alloy interface. (d) Tungsten X-ray image showing that tungsten is enriched in the oxide scale at the alloy/scale interface.

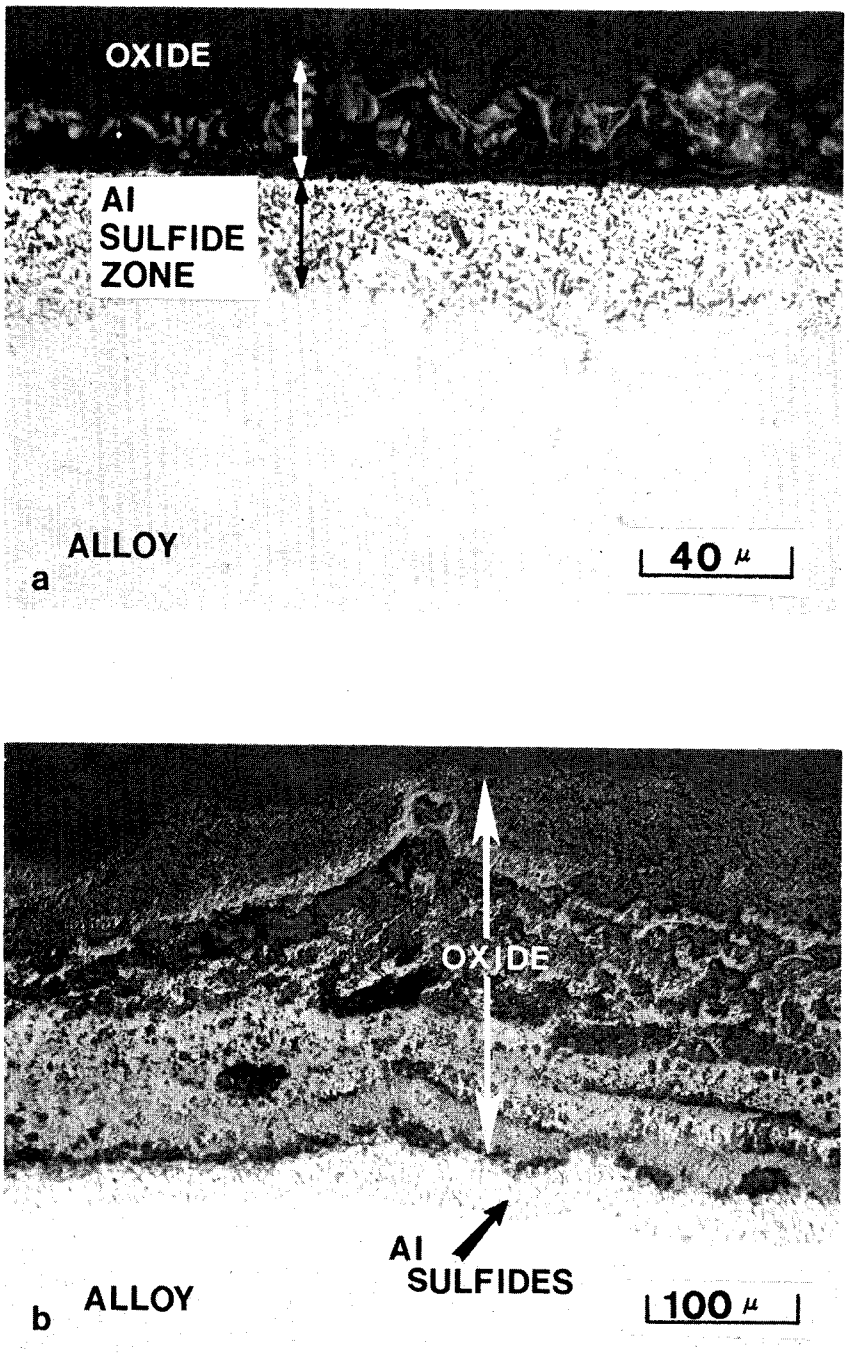

Figure 48 Microstructures of Co-25Al-12W alloy specimens. (a) Specimen coated with 5 mg/cm^2 Na_2SO_4 and annealed for 1 hr in argon at 1000°C. (b) Specimen treated as in (a) and subsequently oxidized 1 hr in oxygen (1000°C), water washed, and re-oxidized for 19 hrs in oxygen at 1100°C. The porous outer scale is believed to have formed during the first hour of oxidation, whereas the more dense inner scale probably formed after the water wash.

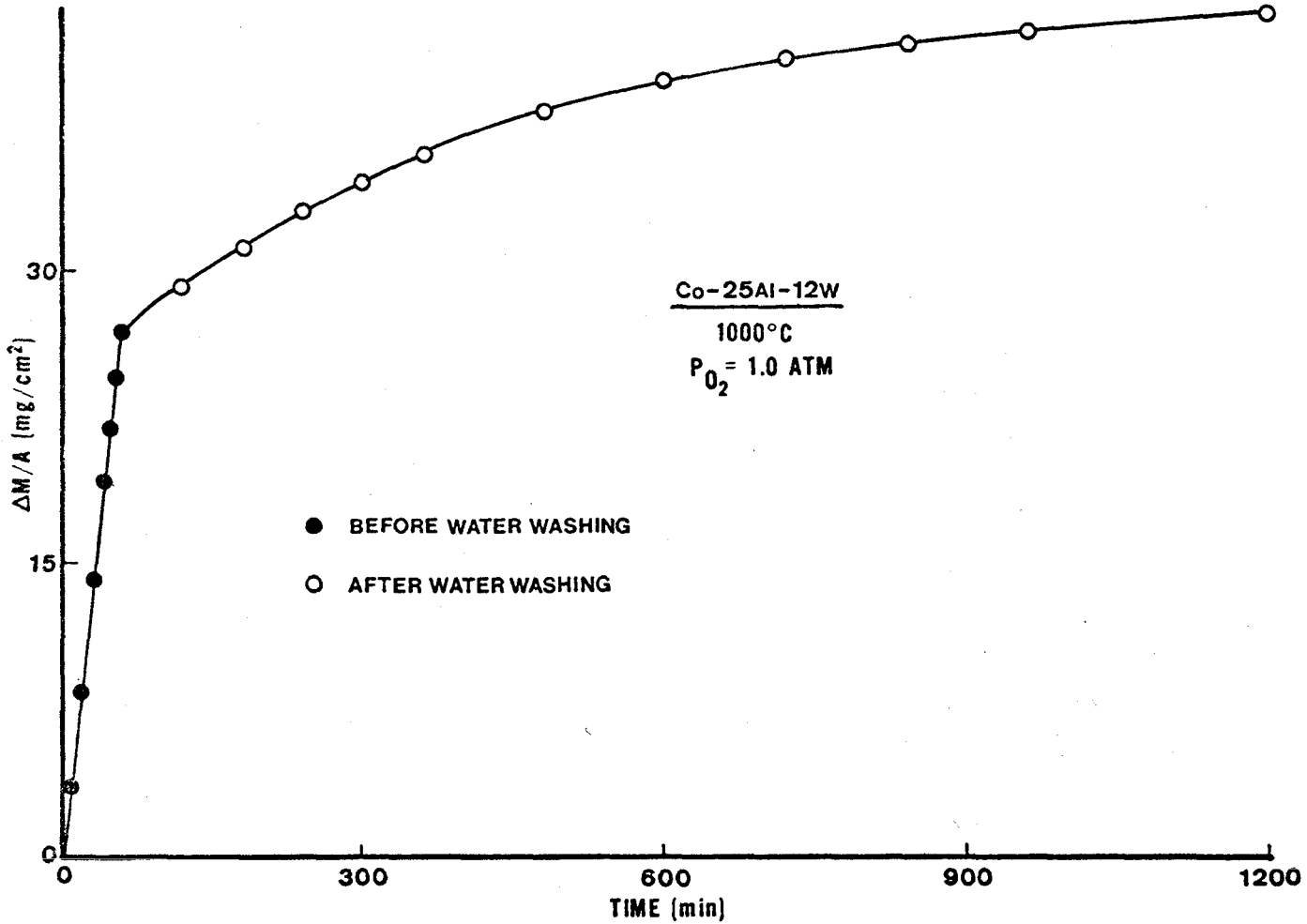

Figure 49 Weight change versus time curve obtained for the oxidation of a Na_2SO_4-coated (5 mg/cm^2) and argon annealed (1 hr at 1000°C) Co-25Al-12W specimen. After 1 hour of oxidation this specimen was washed in water and the oxidation experiment was continued.

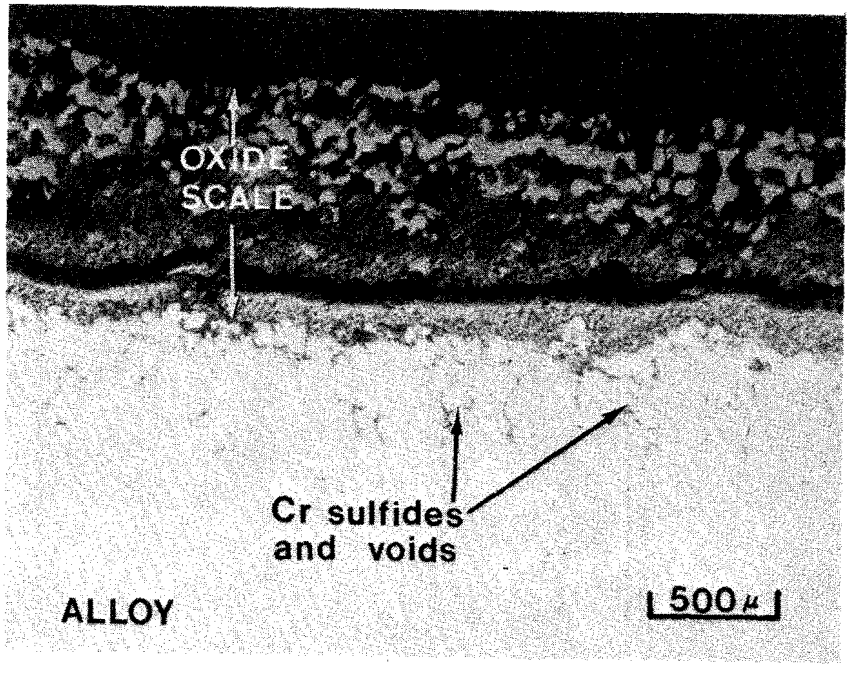

Figure 50 Photomicrograph of the oxide scale developed on the Co-25Cr-12W alloy after 20 hours of oxidation in 0.1 atm of oxygen at 1000°C. Prior to oxidation this alloy was coated with 5 mg/cm^2 of Na_2SO_4 and annealed for 1 hour in argon at 1000°C.

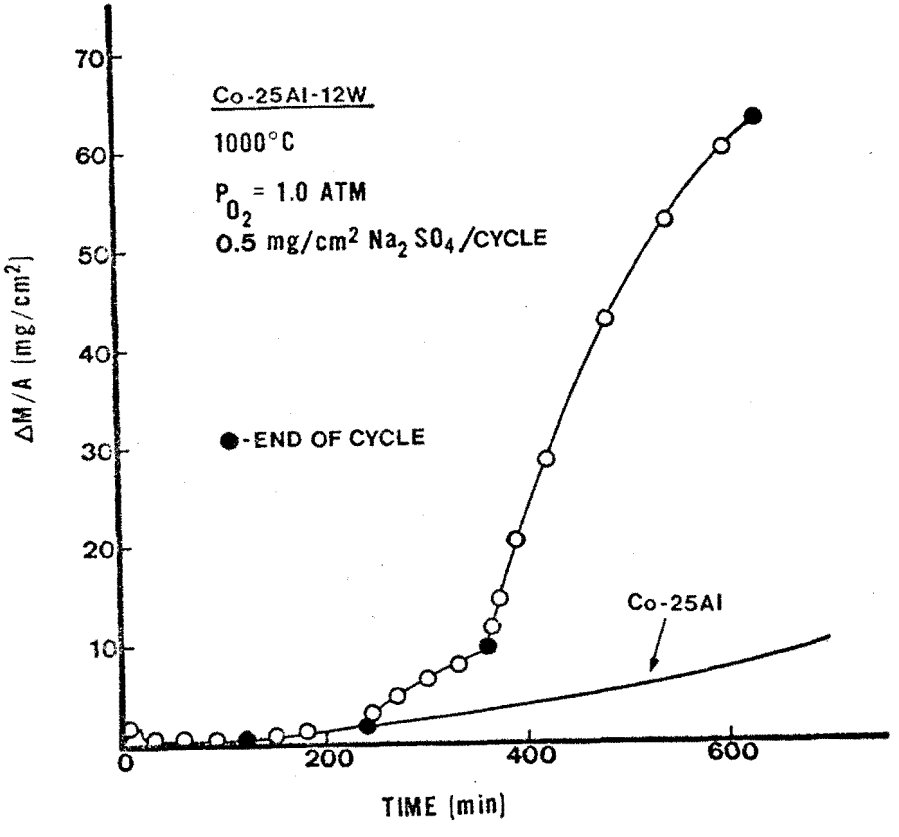

Figure 51 Cyclic oxidation kinetics of Co-25Al-12W and Co-25Al alloys. The specimens were recoated with 0.5 mg/cm^2 prior to each two hour oxidation cycle without removing previously deposited Na_2SO_4.

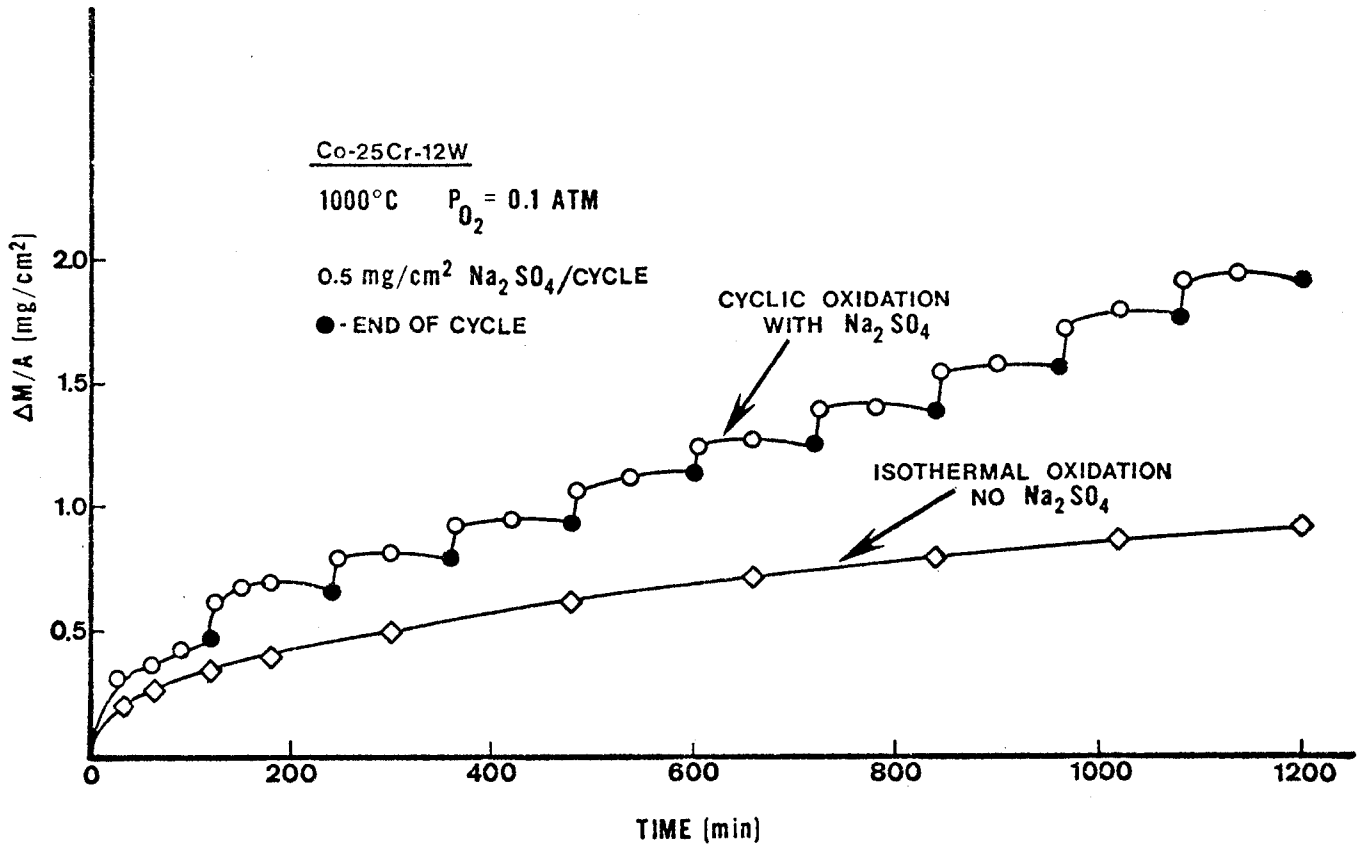

Figure 52 Comparison of the cyclic oxidation kinetics for the Na_2SO_4-coated Co-25Cr-12W alloy and the isothermal oxidation kinetics for this alloy with no Na_2SO_4. (In the cyclic test the specimen was recoated with 0.5 mg/cm^2 Na_2SO_4 prior to each two-hour oxidation cycle.)

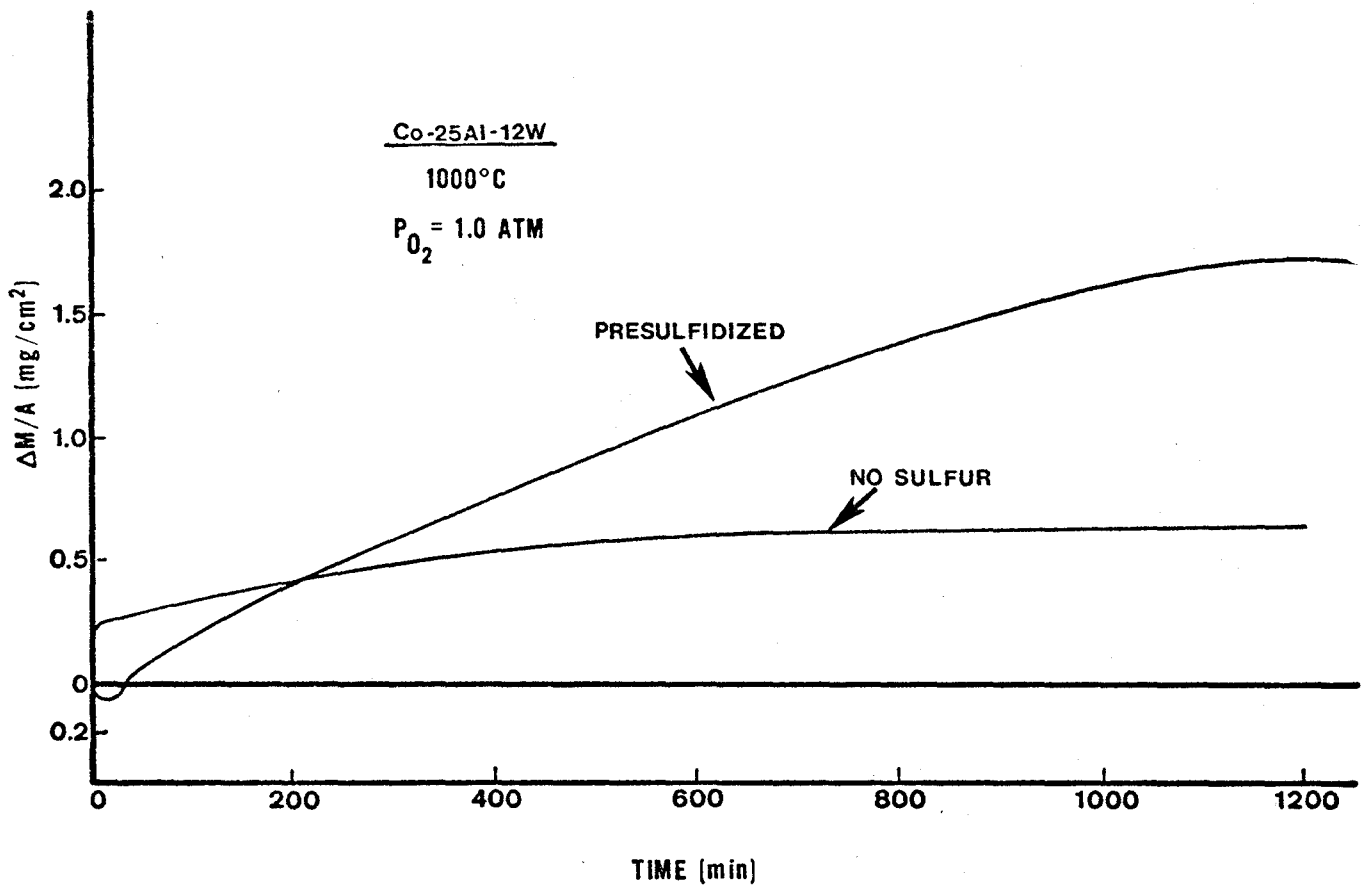

Figure 53 Comparison of the oxidation kinetics of the sulfidized Co-25Al-12W (two minutes at 1000°C in H_2S-H_2 mixture with H_2S/H_2 = 0.2) and the oxidation kinetics of this alloy without sulfur.

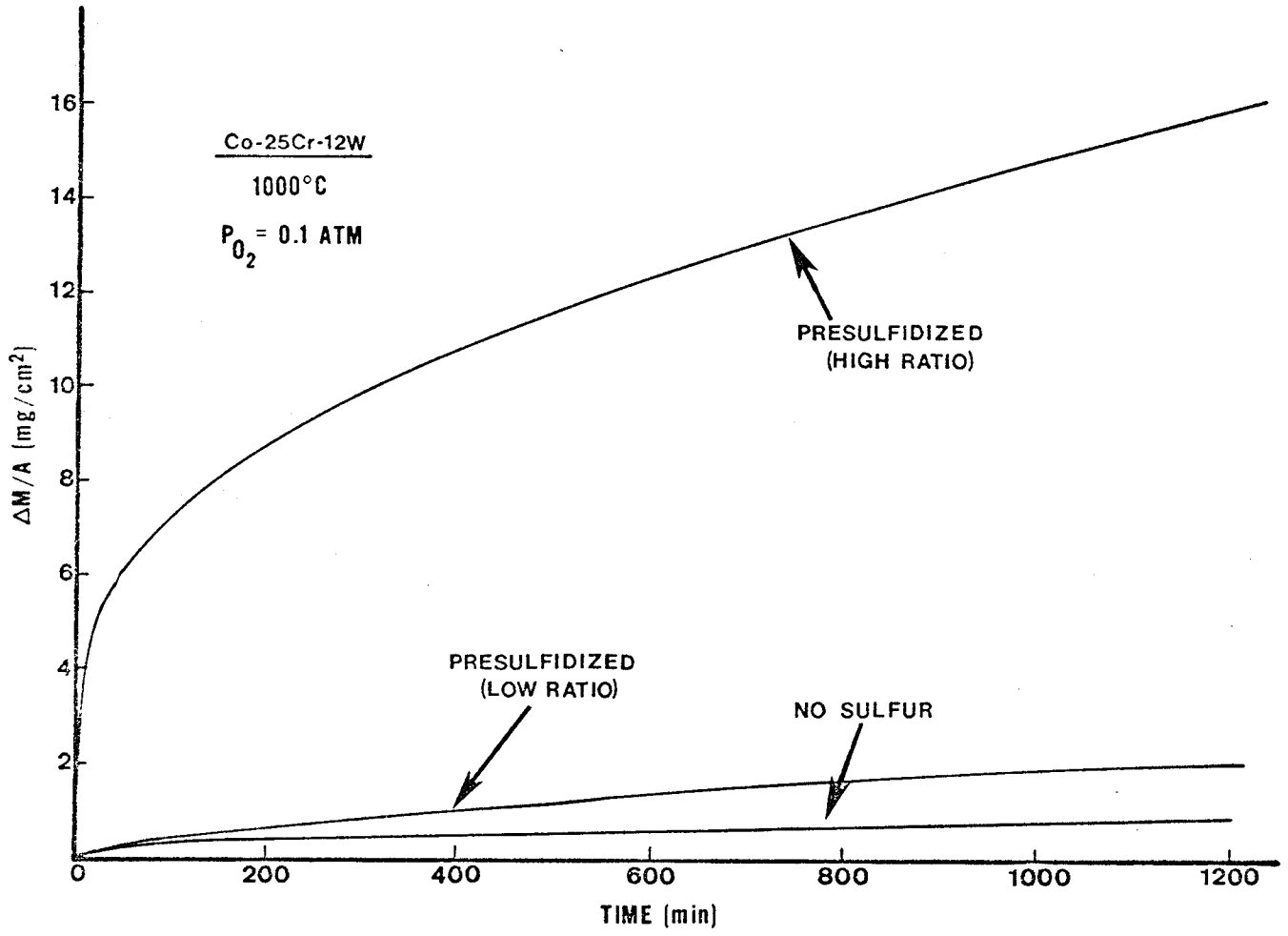

Figure 54 Comparison of the isothermal oxidation kinetics of presulfidized and non-presulfidized Co-25Cr-12W at 1000°C. Two H_2S/H_2 presulfidation ratios were used: (1) H_2S/H_2 = 0.2 (40 sec), and (2) H_2S/H_2 = 0.002 (180 min).

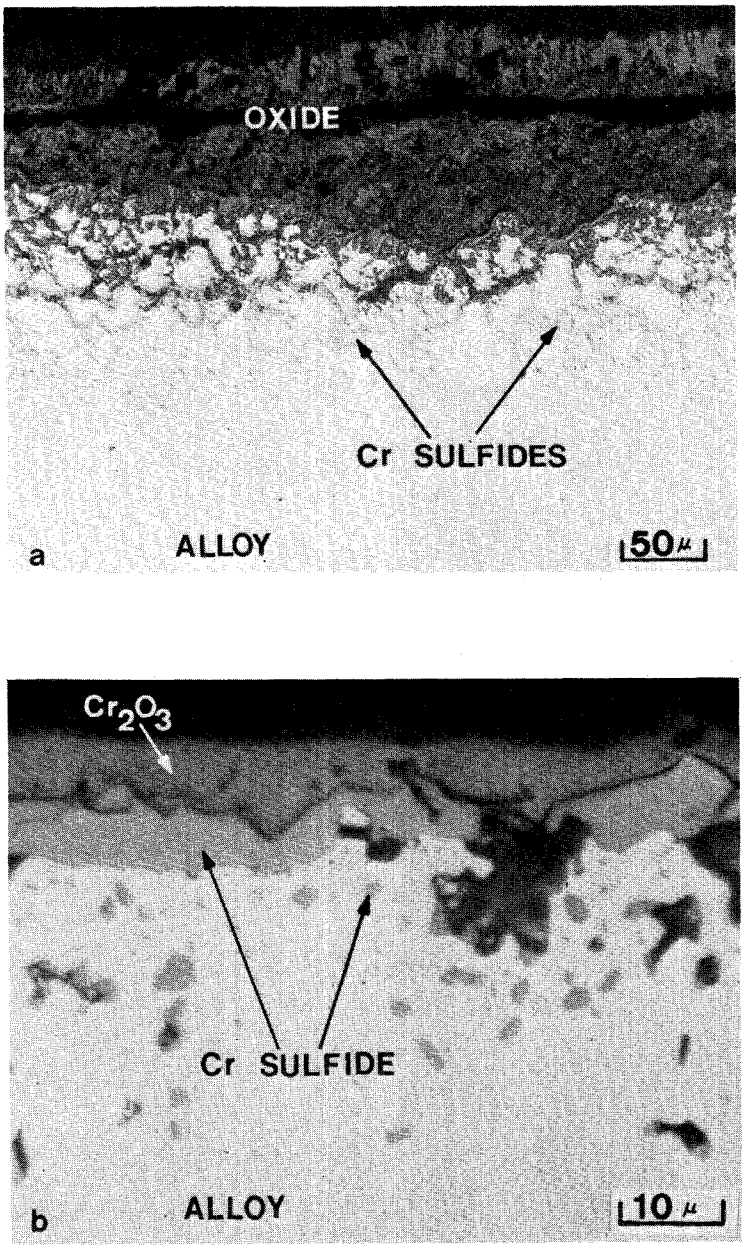

Figure 55 Microstructures of specimens of Co-25Cr-12W which were presulfidized and oxidized at 1000°C (a) Specimen presulfidized in H_2 S/H_2 = 0.2 for 40 sec followed by oxidation for 23 hrs in 0.1 atm oxygen. (b) Specimen presulfidized in H_2 S/H_2 = 0.002 for 180 minutes followed by oxidation for 20 hrs in 0.1 atm oxygen. A thick scale containing oxides of Co, Cr and W are formed on the specimen in (a) while only a thin layer of Cr_2O_3 has formed on the specimen pretreated in the gas mixture with the lower sulfur activity.

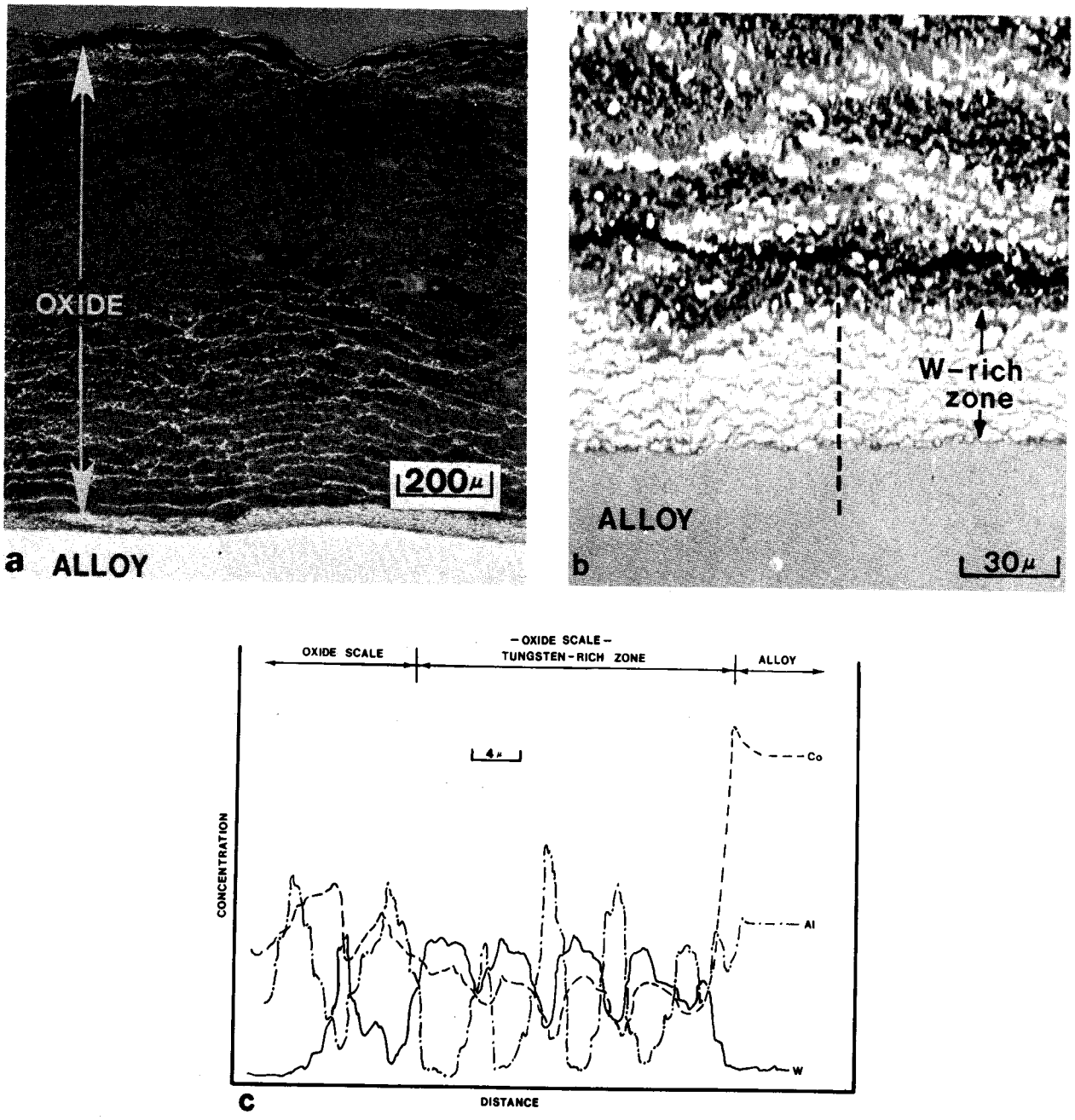

Figure 56 Photographs and microprobe intensity profiles obtained from a Na_2WO_4-coated, Co-25Al-12W specimen after 24 hrs of oxidation at 1000°C in flowing oxygen containing $(WO_3)_3$ vapor. (a) Photomicrograph showing general features of the oxide scale. (b) Electron backscatter photograph showing details of the oxide scale immediately adjacent to the alloy. (c) Intensity profiles showing the distribution of W, Co and Al across the zone of oxide shown in (b).

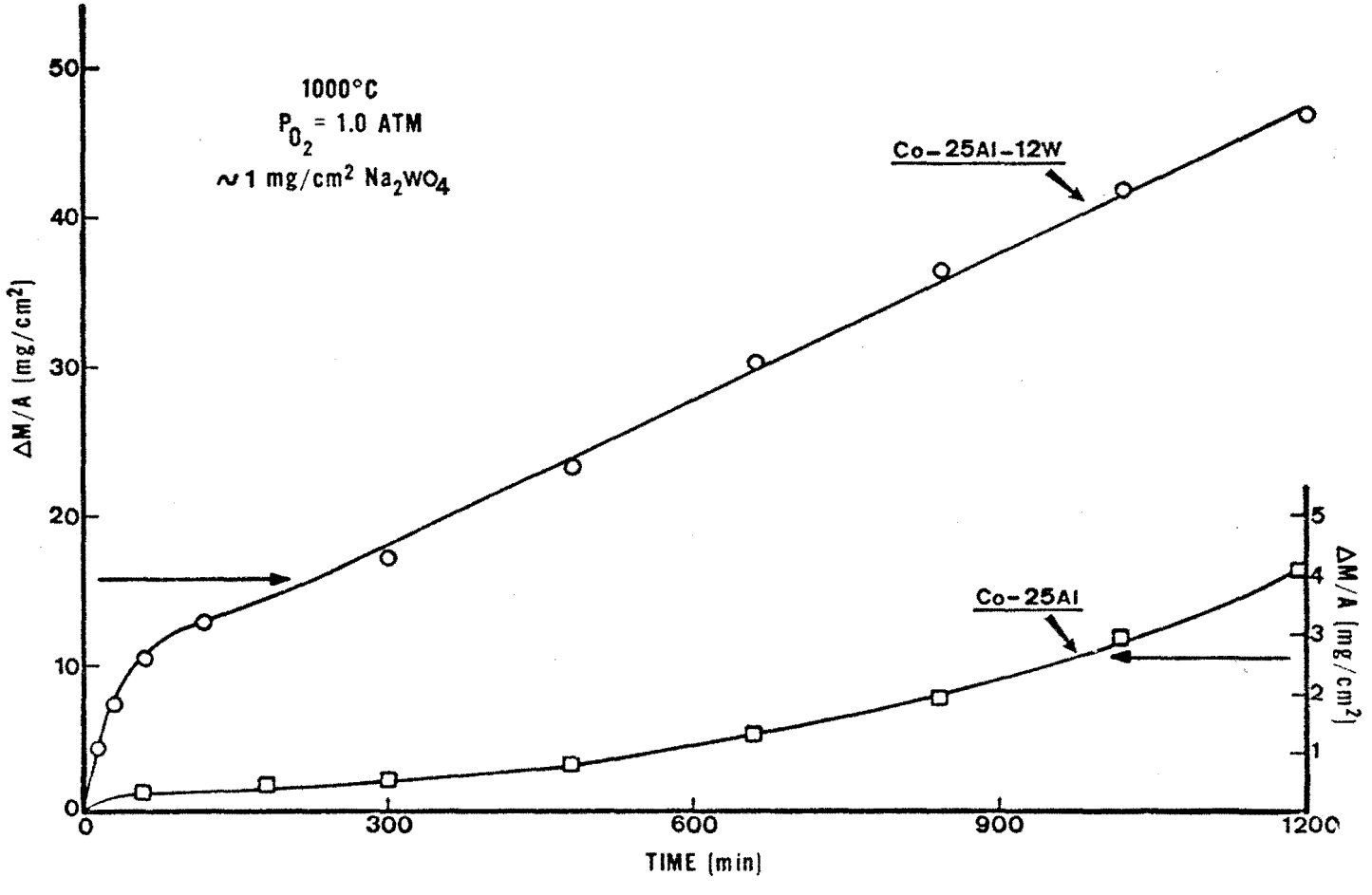

Figure 57 Weight change versus time curves obtained for the oxidation of Na_2WO_4-coated specimens of Co-25Al-12W and Co-25Al. Arrows indicate corresponding ordinate for each curve.

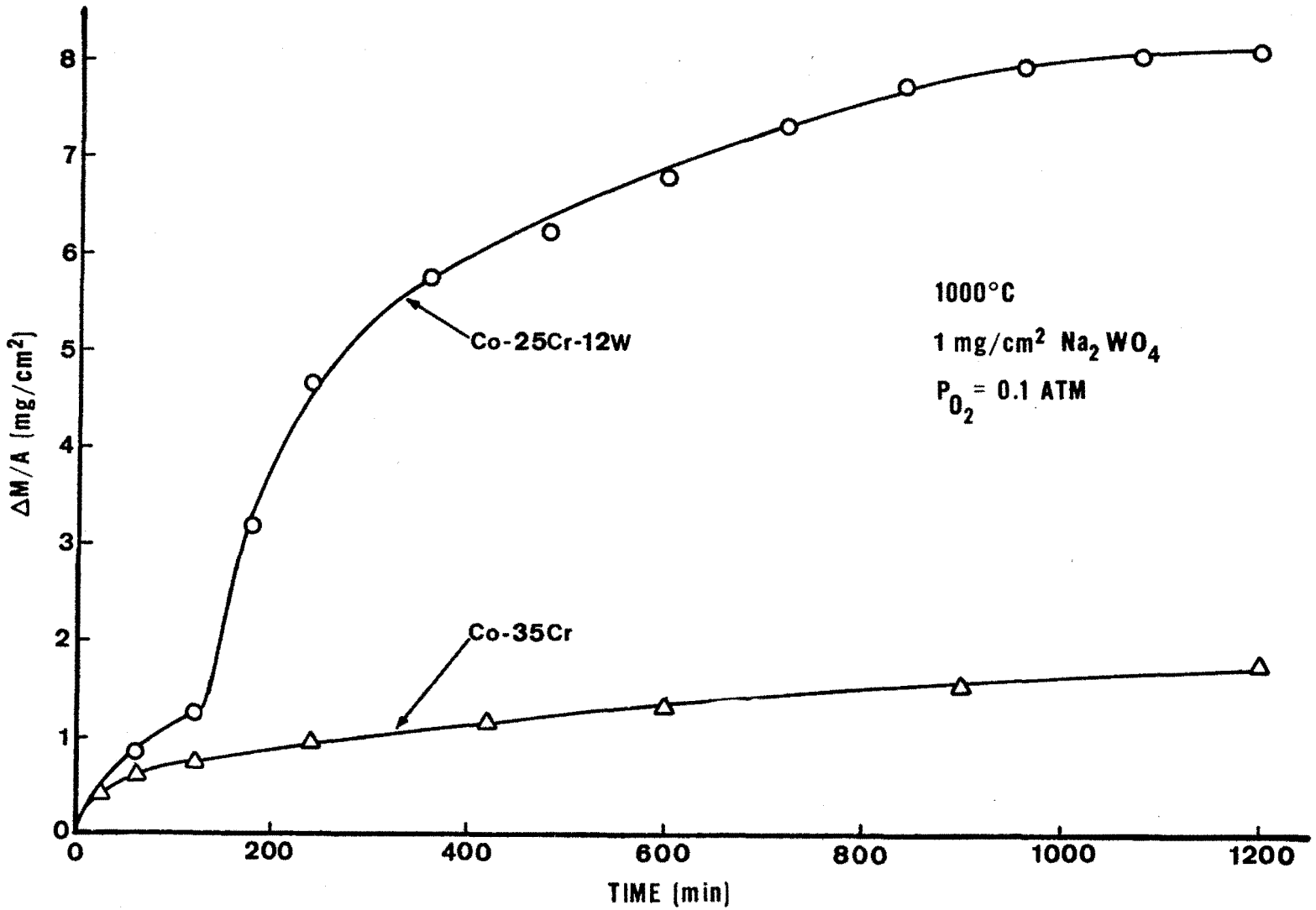

Figure 58 Weight change versus time curves obtained for the oxidation of Na_2WO_4-coated specimens of Co-25Cr-12W and Co-35Cr.

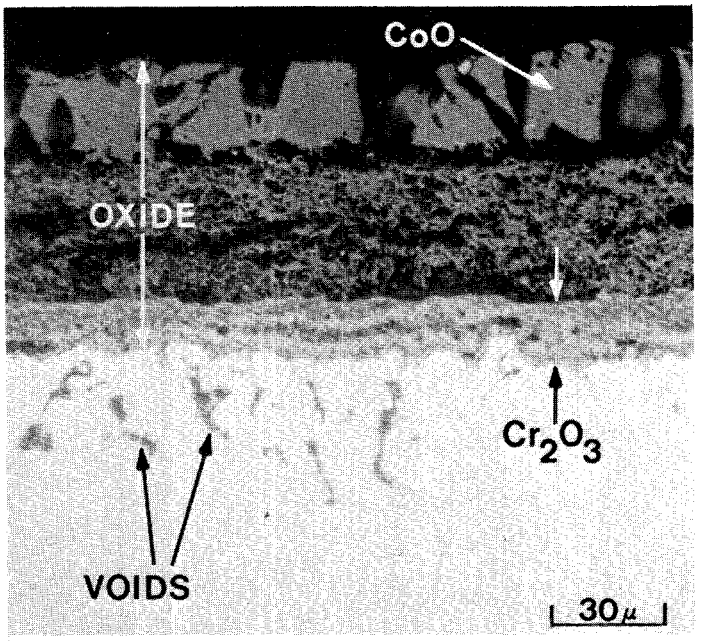

(a)

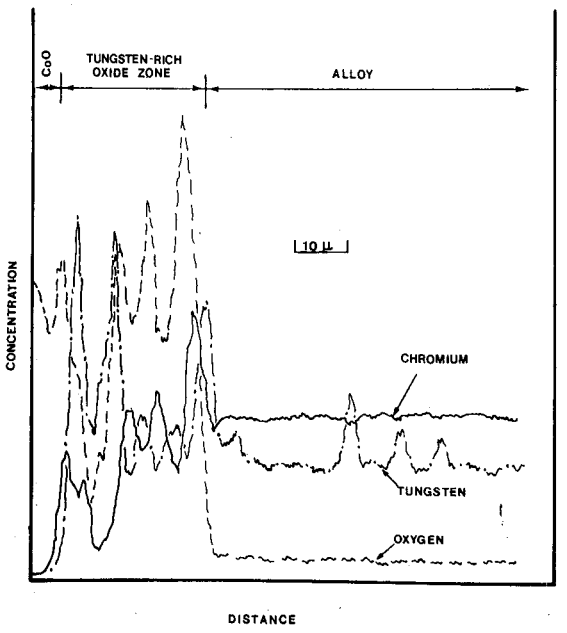

(b)

Figure 59 a) Photomicrograph showing microstructural features of Na_2WO_4-coated Co-25Cr-12 W after 20 hrs of oxidation at 1000°C in 1 atm of oxygen. b) Electron microprobe concentration profiles for Cr, W, O, across scale/alloy interface of Co-25Cr-12W specimen which was coated with Na_2WO_4 and oxidized 114 min. at 1000°C.

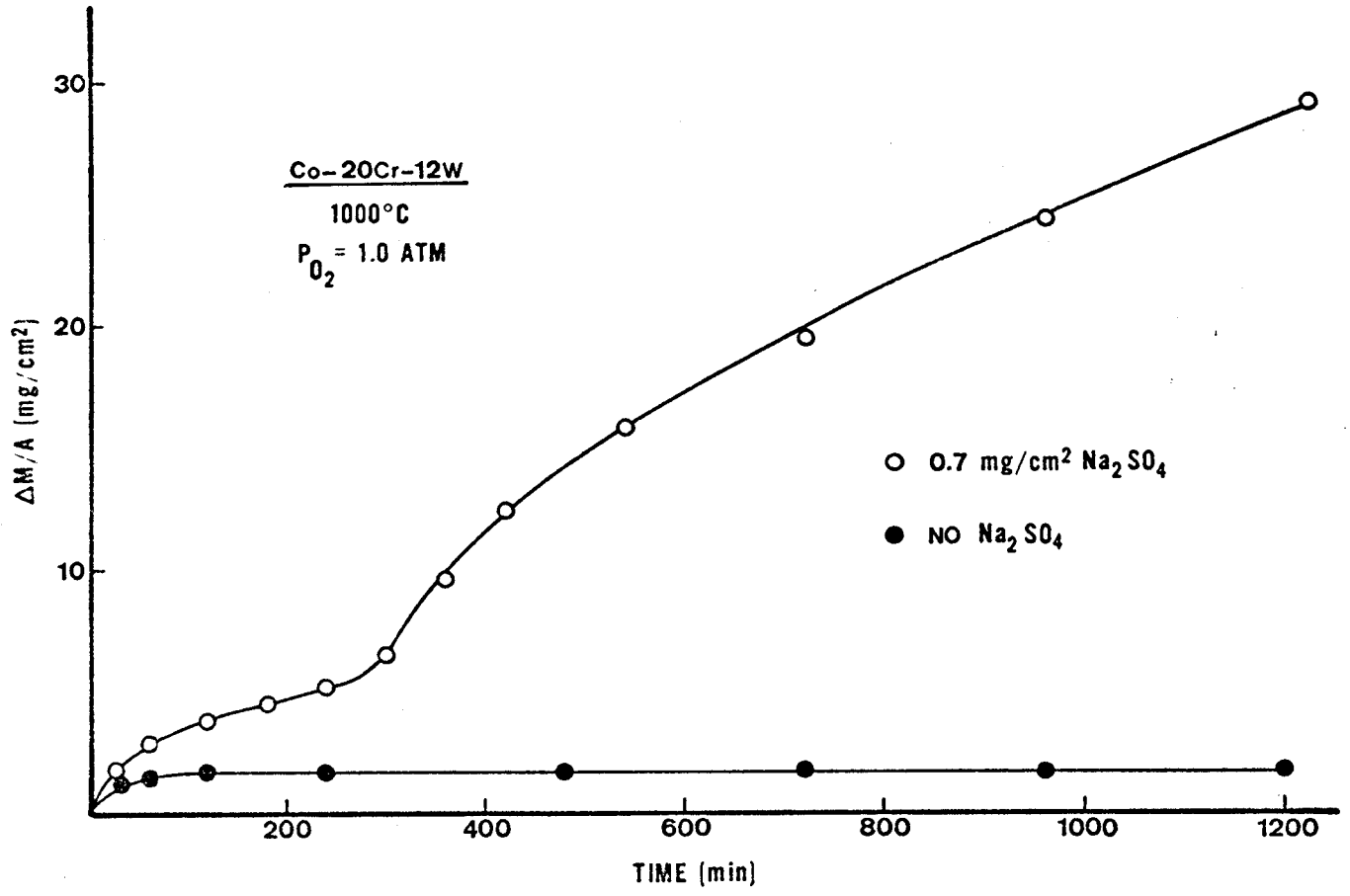

Figure 60 Comparison of the weight change versus time curves obtained for the oxidation of Co-20Cr-12W specimens with and without a coating of Na_2SO_4.

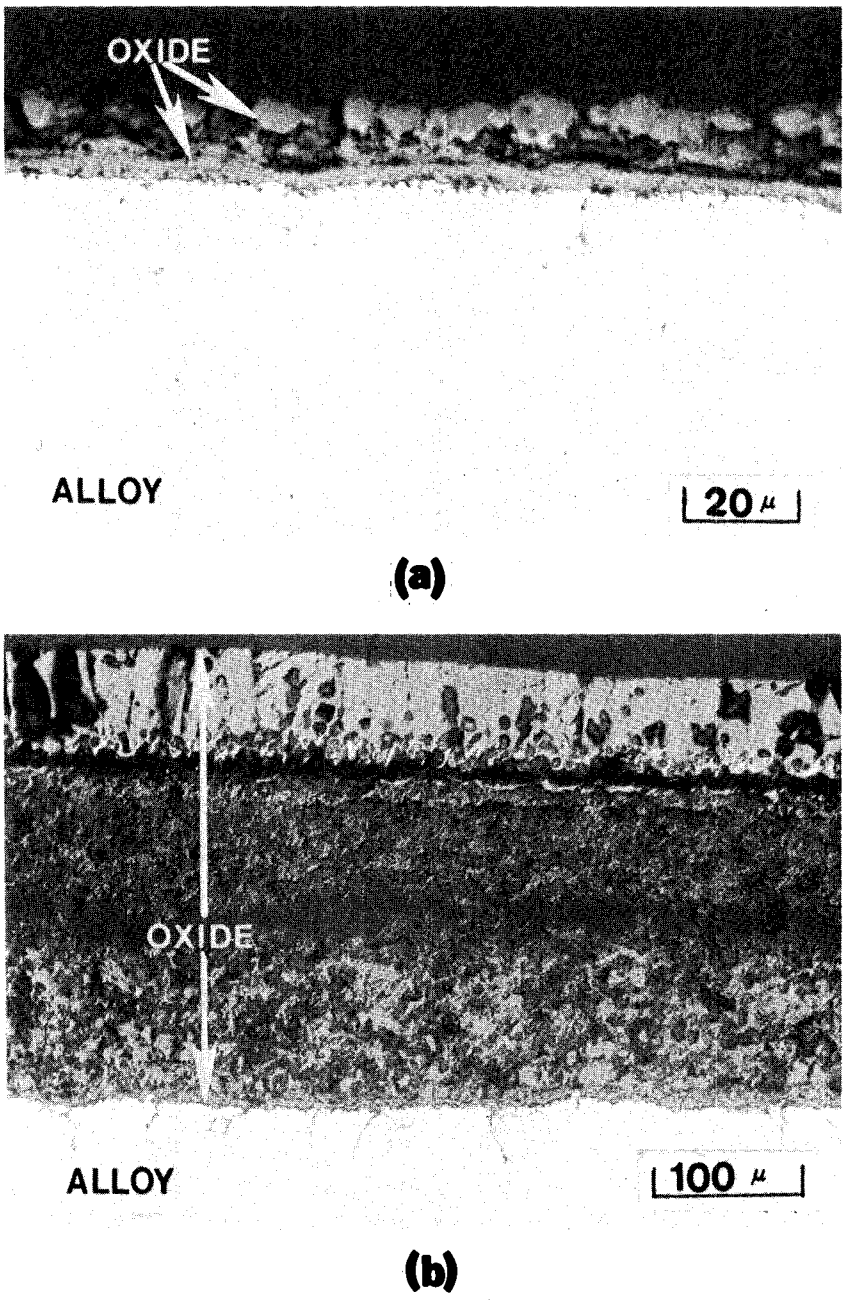

Figure 61 Photomicrographs showing microstructures of Co-20Cr-12W specimens without (a) and with Na_2SO_4 coating (b) after 20 hrs of oxidation in 1 atm of oxygen at 1000°C.

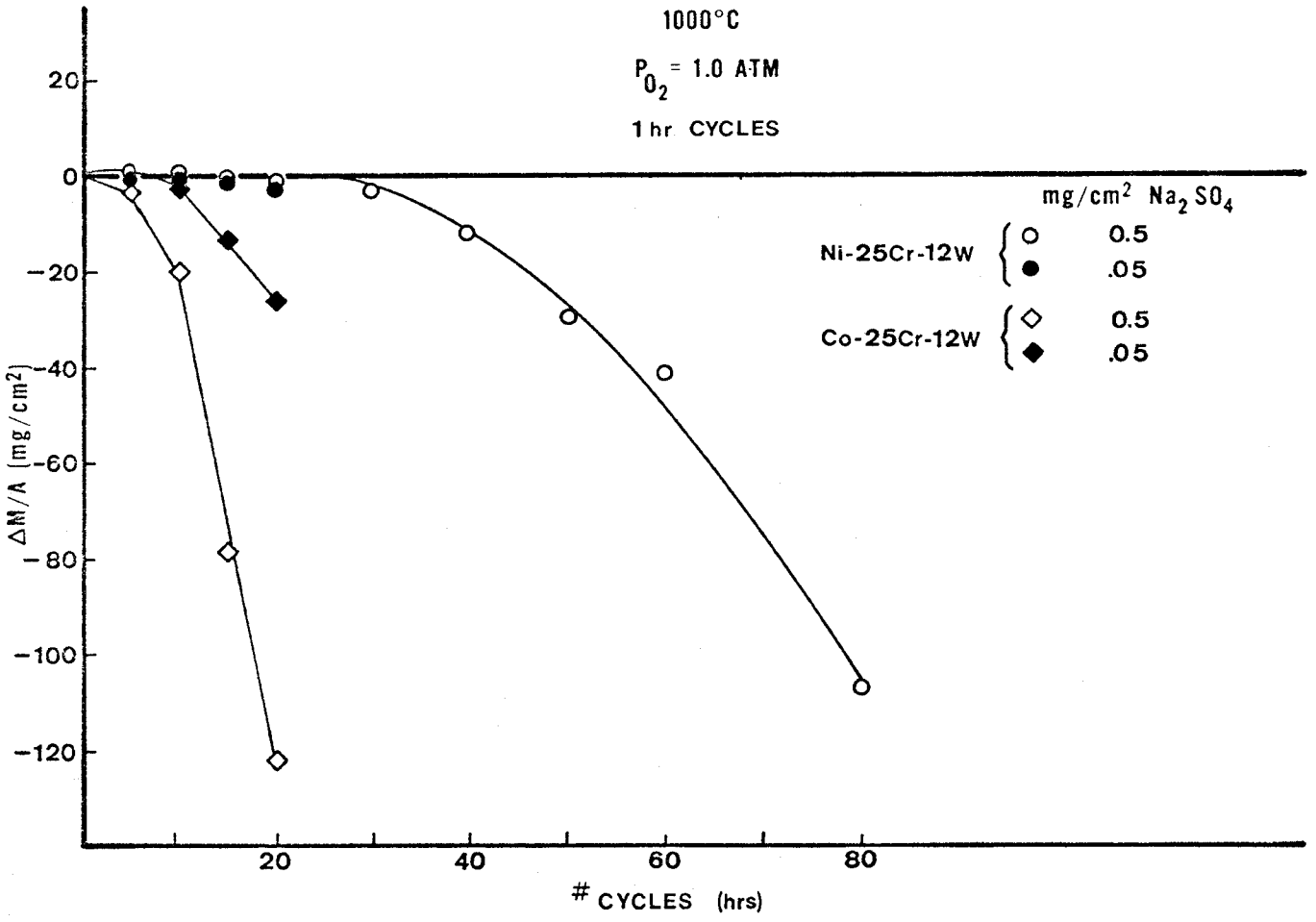

Figure 62 Cyclic oxidation weight change data for Na_2SO_4-coated specimens of Ni-25Cr-12W and Co-25Cr-12W alloys. Specimens coated with 0.5 mg/cm^2 Na_2SO_4 were more severely attacked.

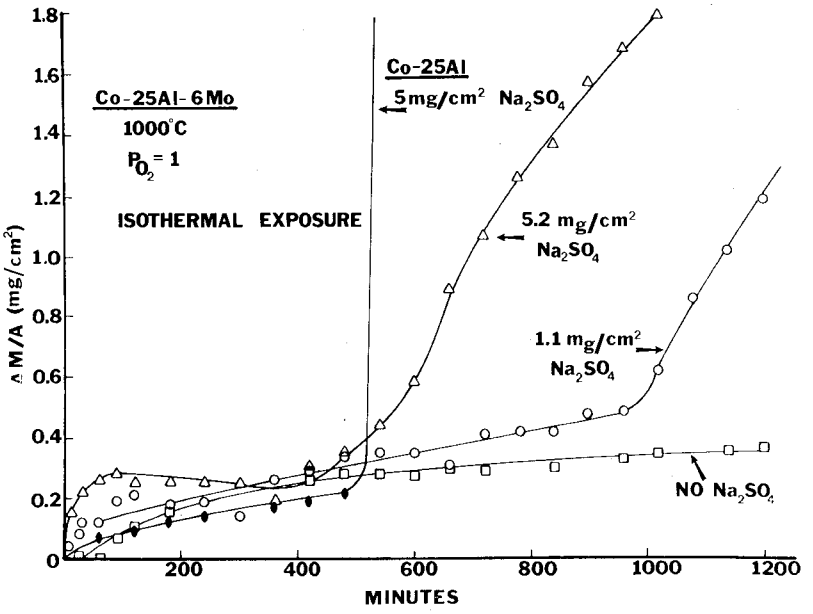

Figure 63 Isothermal weight change data for Co-25Al-6Mo with and without Na_2SO_4. Data for Co-25Al coated with 5 mg/cm^2 Na_2SO_4 are included for comparison.

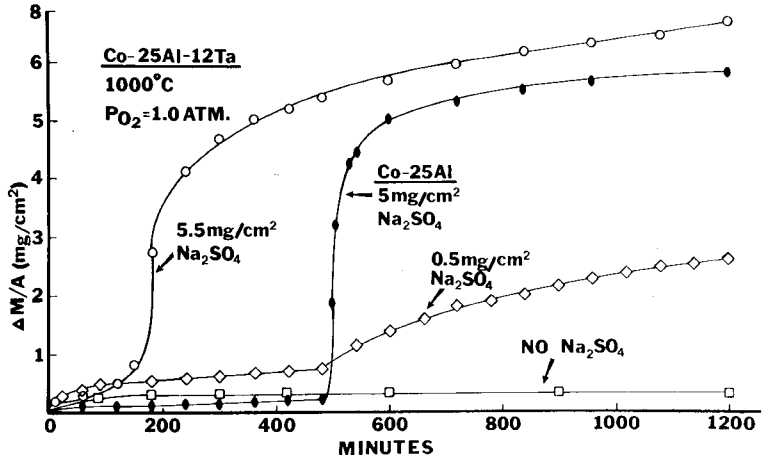

Figure 64 Isothermal weight change data for Co-25Al-12Ta with and without Na_2SO_4. Data for Co-25Al are plotted for comparison.

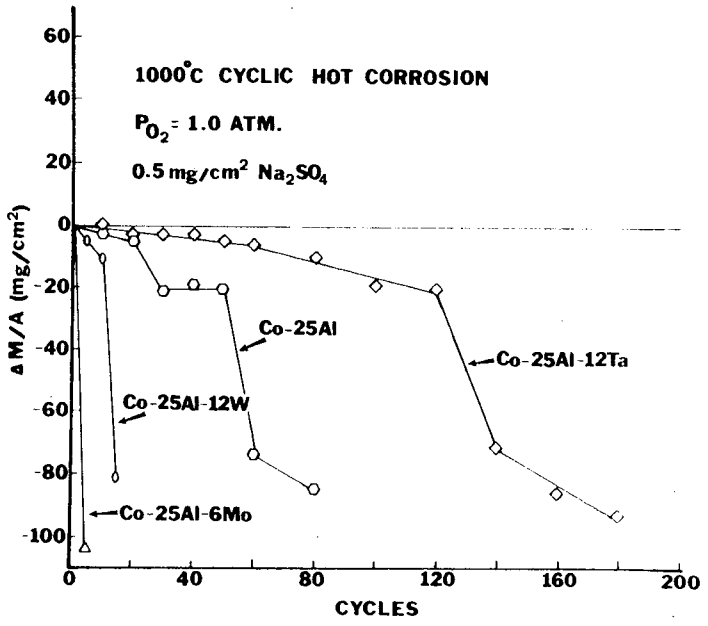

Figure 65 Comparison of weight-change data obtained in the cyclic hot corrosion test using Co-25Al alloys containing Mo, W or Ta.

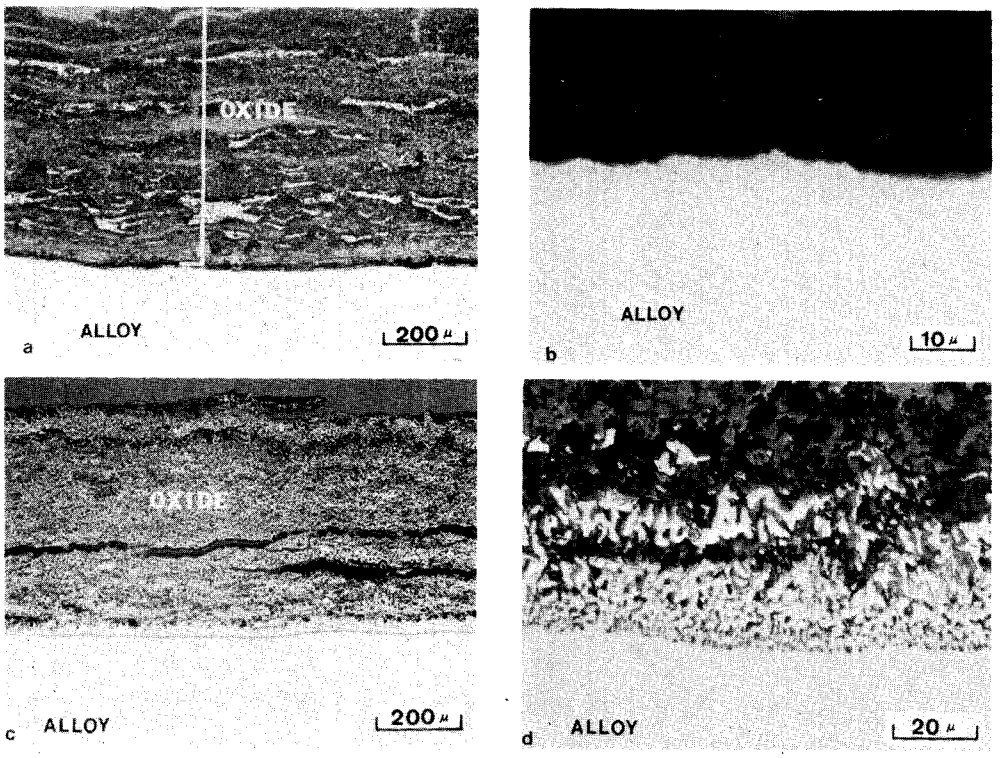

Figure 66 Photomicrographs showing structures of Co-25Al-6Mo and Co-25Al-12Ta alloys after cyclic hot corrosion testing at 1000°C in 1 atm of oxygen; a) and b) Co-25Al-6Mo after 10 cycles using 0.5 mg/cm^2 Na_2SO_4, c) and d) Co-25Al-12Ta after 30 cycles using 5 mg/cm^2 Na_2SO_4.

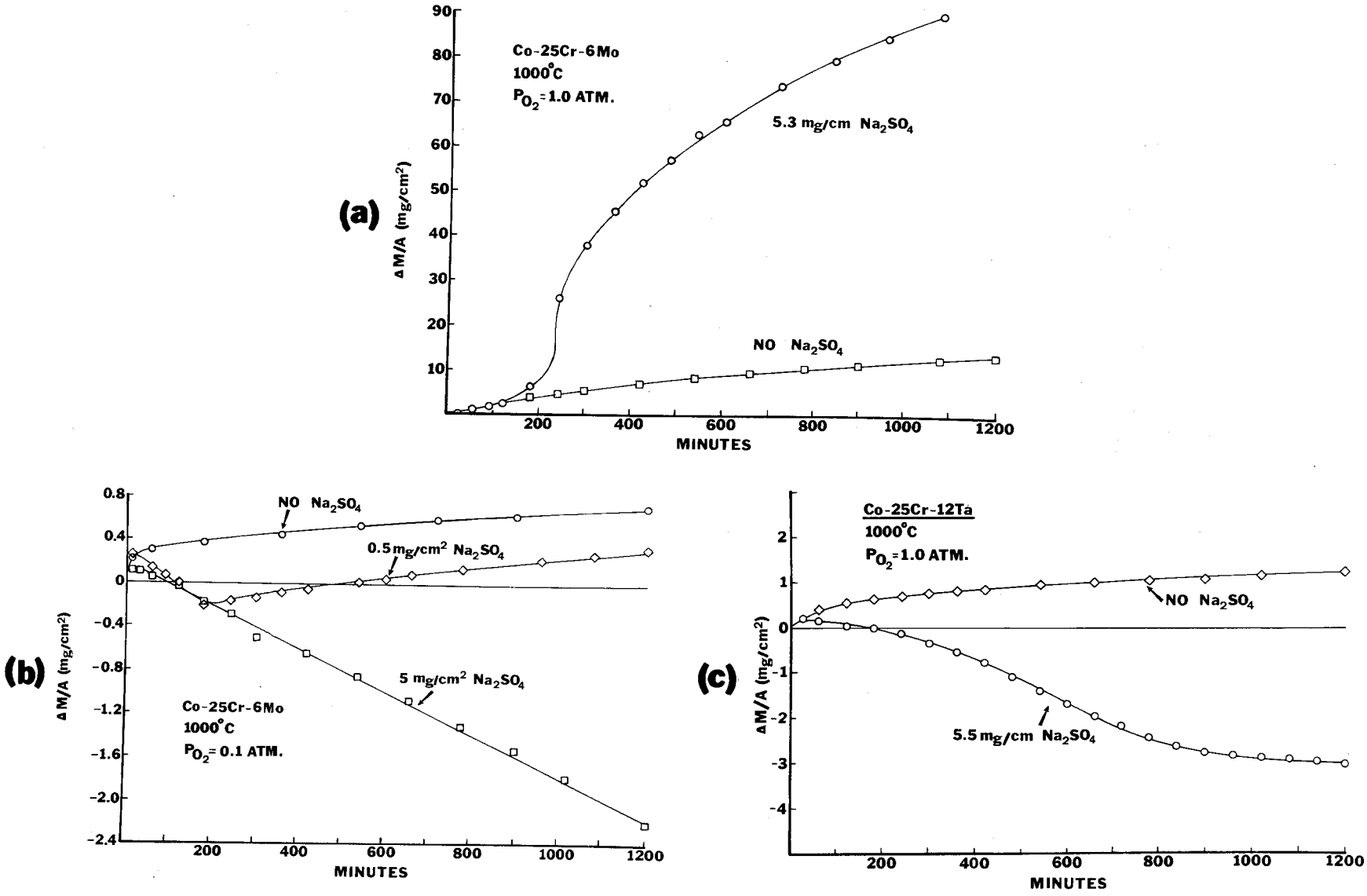

Figure 67 Weight change versus time curves obtained for the isothermal oxidation of Co-25Cr-6Mo in 1 atm (a) and 0.1 atm (b) of oxygen and Co-25Cr-12Ta (c) alloys with and without deposits of Na_2SO_4.

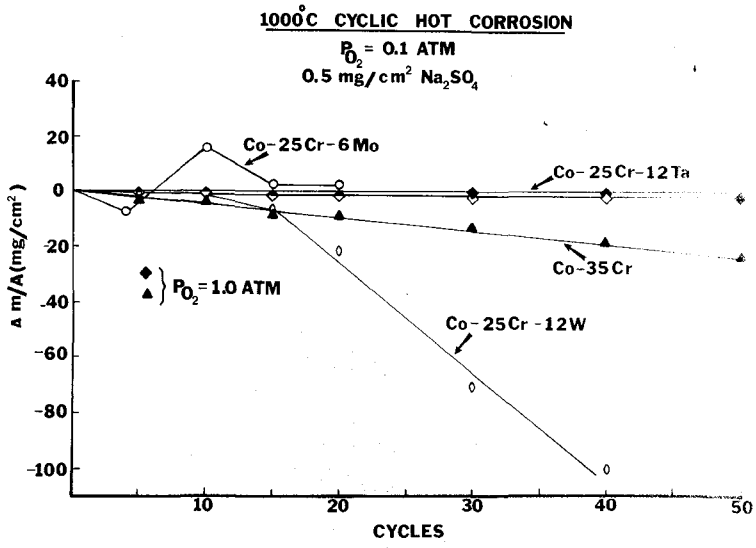

Figure 68 Comparison of weight change data obtained in the cyclic hot corrosion testing using cobalt-chroumium alloys containing Mo, W or Ta.

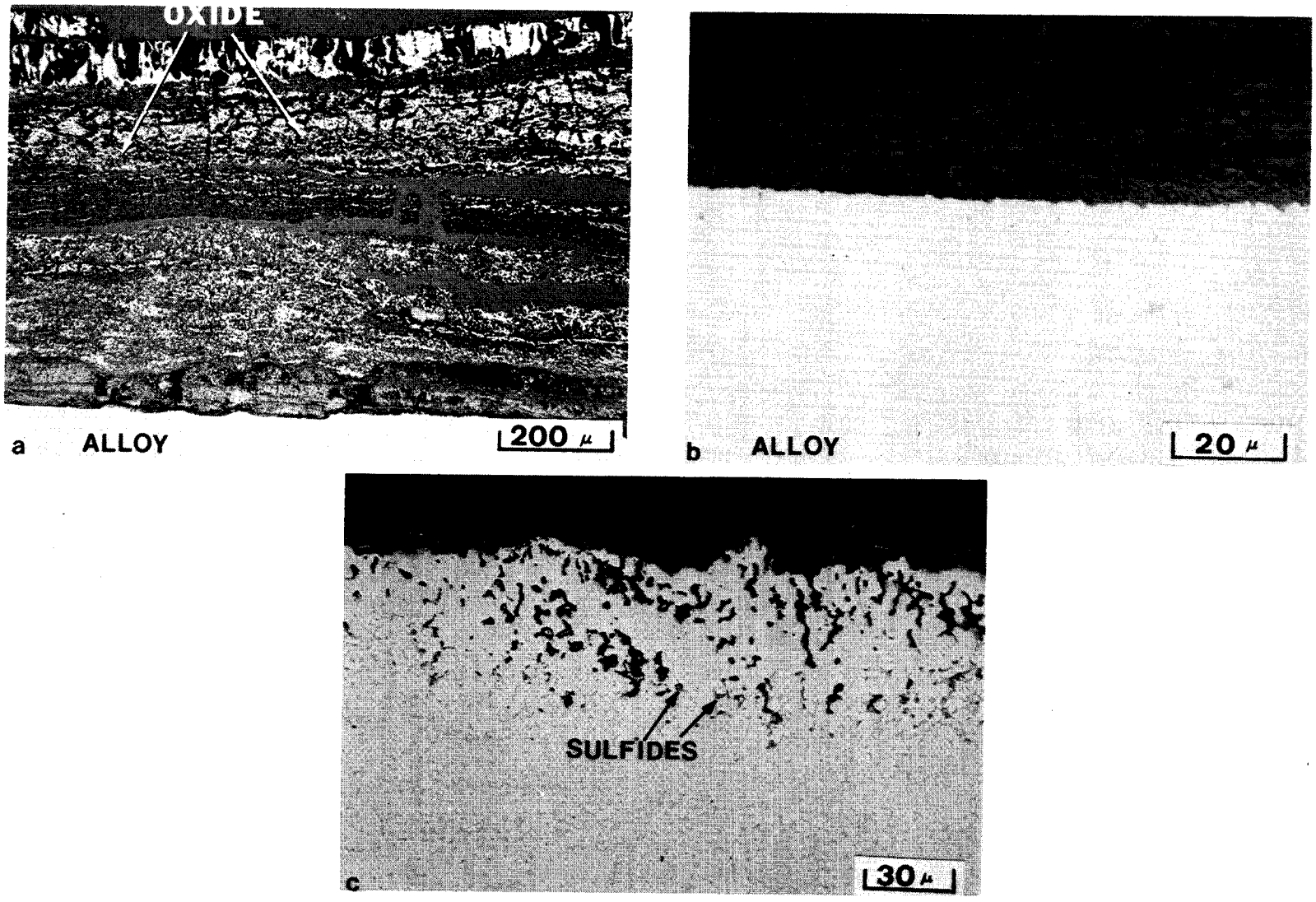

Figure 69 Photomicrographs showing structures of specimens after cyclic hot corrosion testing at 1000°C; a) and b) Co-25Cr-6Mo after 20 cycles in 0.1 atm of oxygen using 0.5 mg/cm^2 Na_2SO_4, c) Co-25Cr-12Ta after 40 cycles in 0.1 atm of oxygen using 0.5 mg/cm^2 Na_2SO_4.

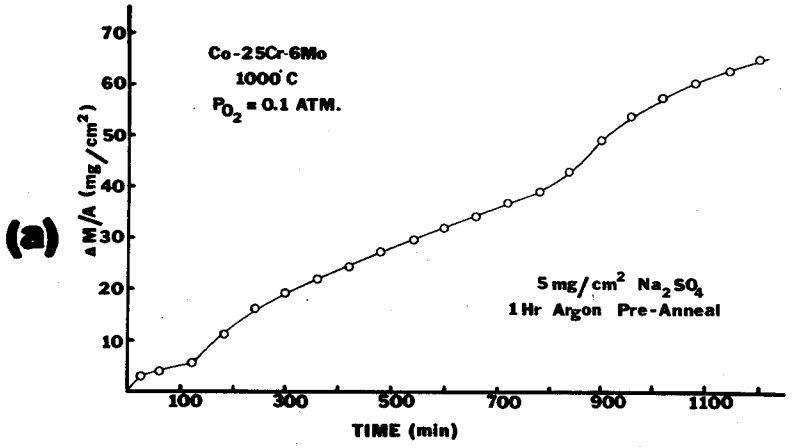

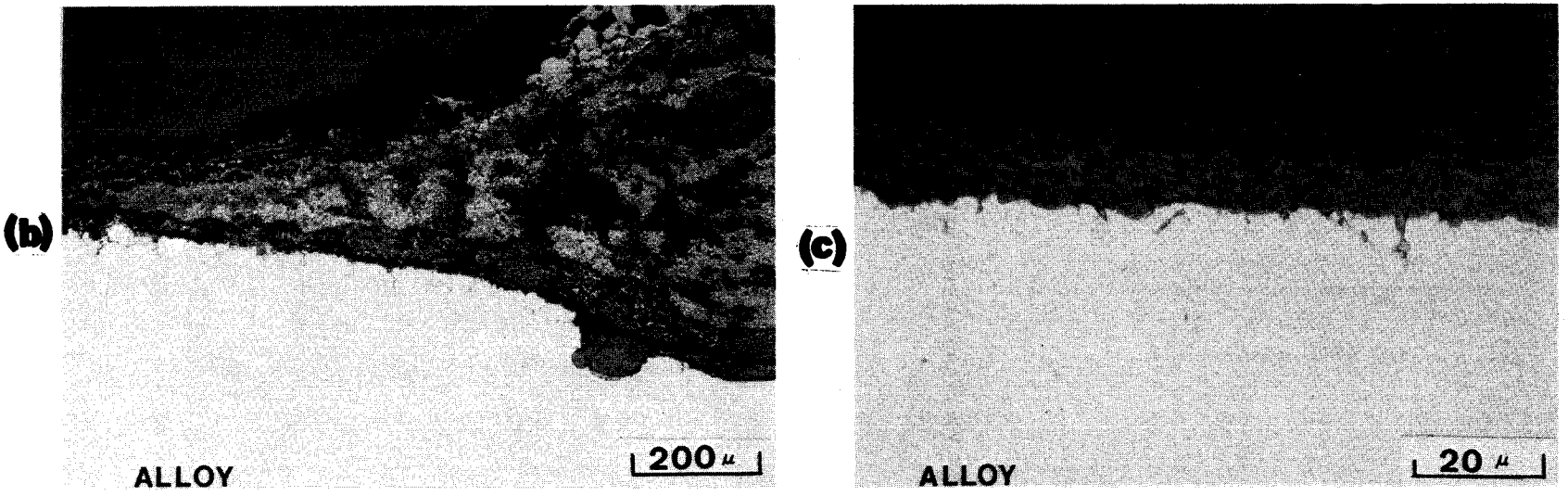

Figure 70 a) Weight change data for the isothermal oxidation of Co-25Cr-6Mo where the specimen was coated with 5 mg/cm^2 Na_2SO_4 and annealed for 1 hour in argon prior to oxidation. b) and c) Photomicrographs showing the structure of specimen described in (a).

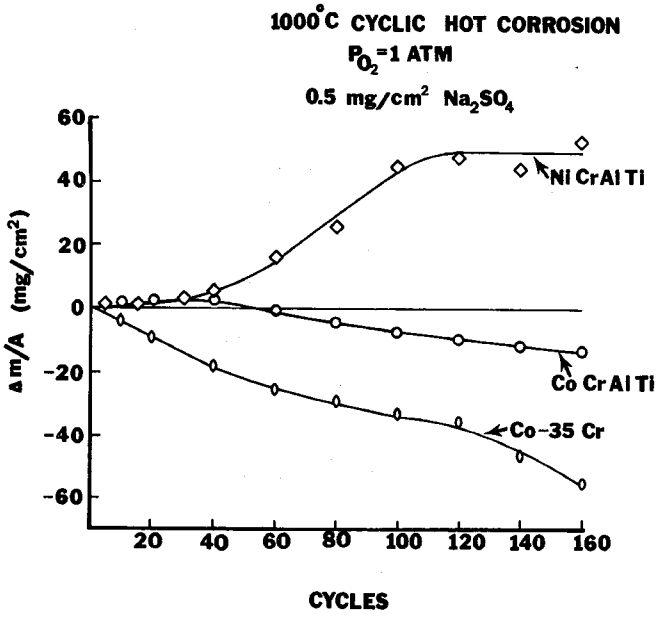

Figure 71 Weight change versus time data obtained in the cyclic hot corrosion test using Co-25Cr-3Al-3Ti, Co-35Cr and Ni-13Cr-3Al-5.3Ti.

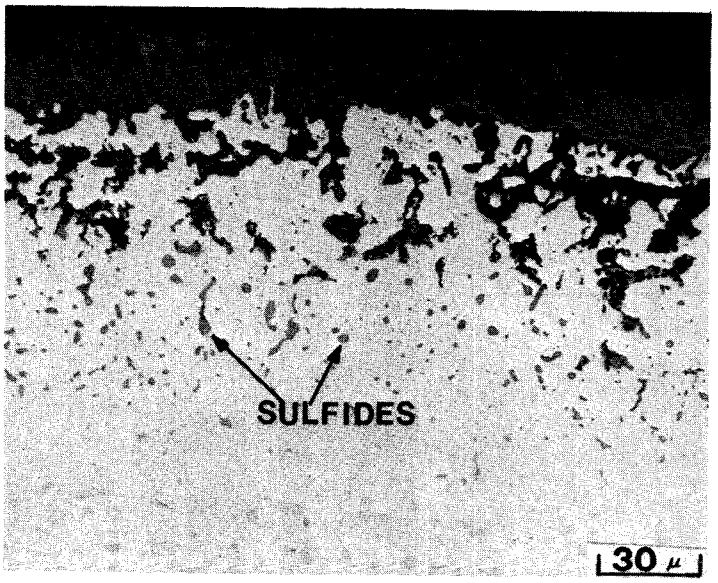

Figure 72 Photograph showing Co-25Cr-3Al-5Ti specimen after 300 cycles at 1000°C in 1 atm of oxygen using 0.5 mg/cm^2 Na_2-SO_4.

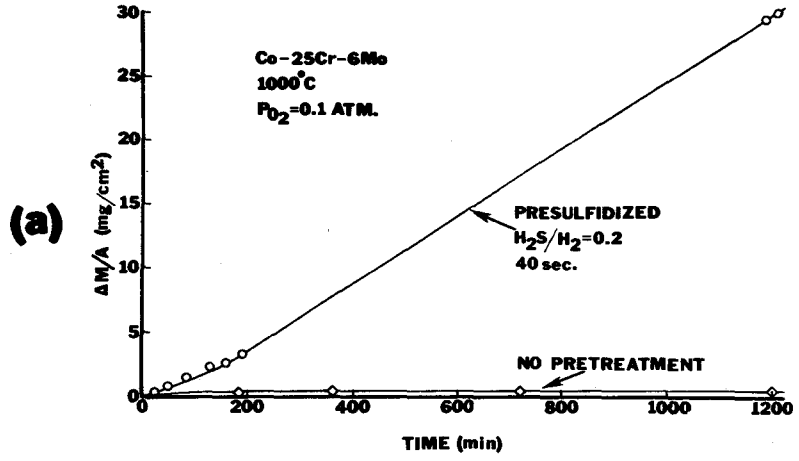

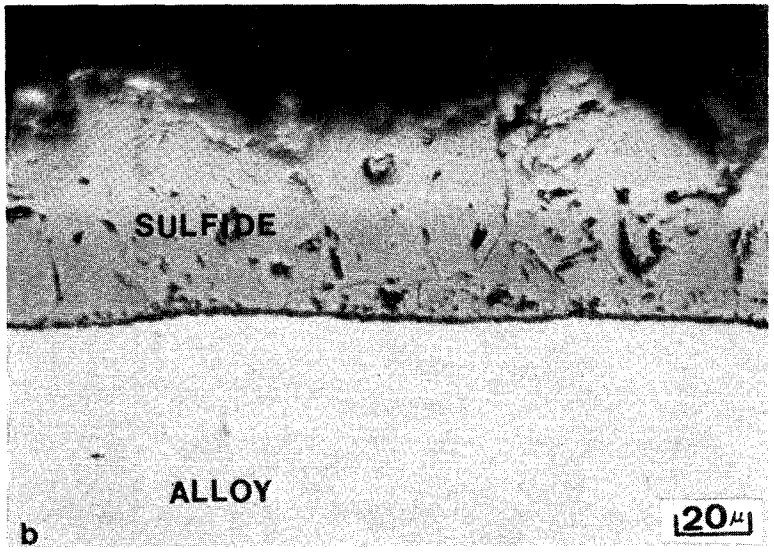

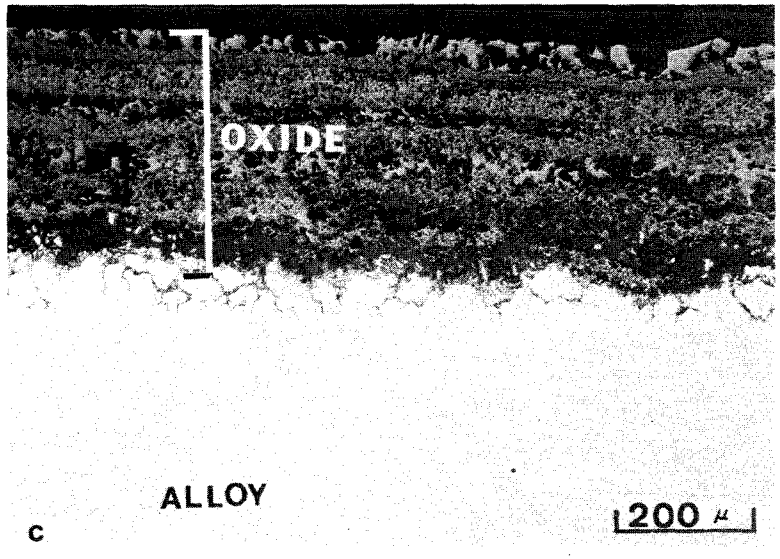

Figure 73 a) Weight change versus time data obtained for the oxidation of Co-25Cr-6Mo and presulfidized Co-25Cr-6Mo in 0.1 atm oxygen. b) Photomicrograph showing the microstructure of this alloy after the sulfidizing pretreatment. c) Photomicrograph showing the structure of the presulfidized specimen after oxidation.

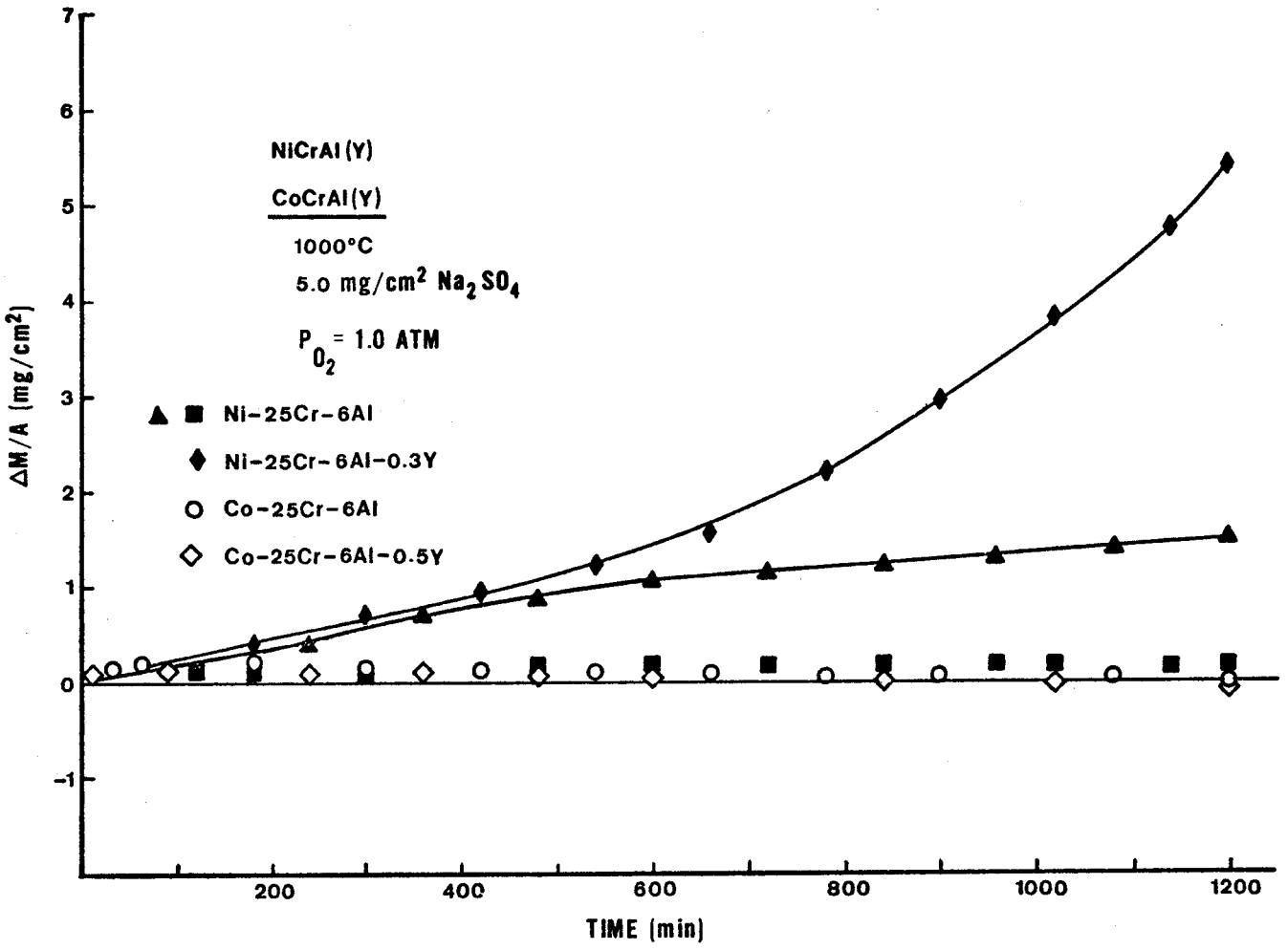

Figure 74 Weight change versus time curves obtained for the isothermal oxidation of Na_2SO_4-coated (5 mg/cm^2) NiCrAl(Y) and CoCrAl(Y) alloys.

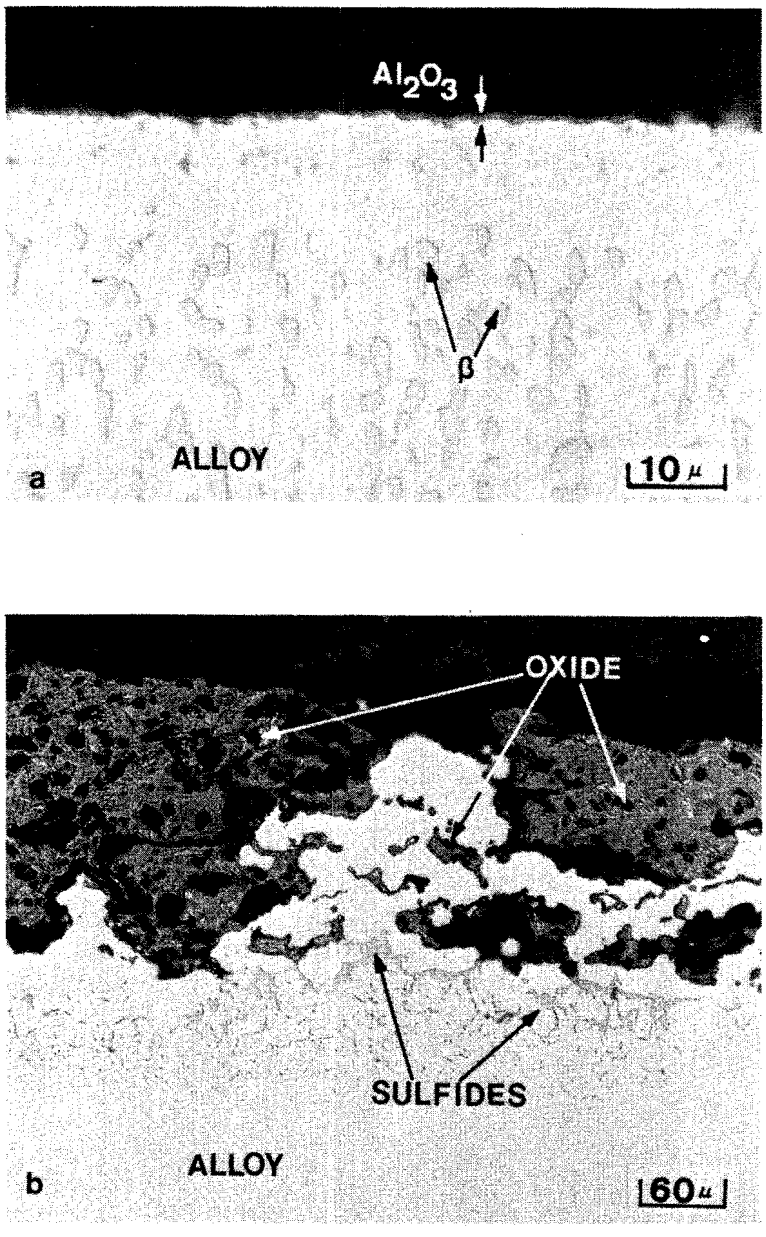

Figure 75 Microstructures of vapor-deposited alloy specimens which were coated with 5 mg/cm^2 Na_2SO_4 and oxidized isothermally in oxygen at 1000°C. (a) Co-25Cr-6Al-0.5Y oxidized for 20 hrs formed external Al_2O_3 scale. Alloy zone beneath oxide is devoid of β-CoAl phase, but does contain what are believed to be small yttrium-rich oxide or sulfide particles. (b) Ni-25Cr-6Al oxidized for 47 hrs suffered severe attack. Liquid-like morphology of sulfide stringers results from presence of liquid-nickel sulfide phase (not visible in this photo).

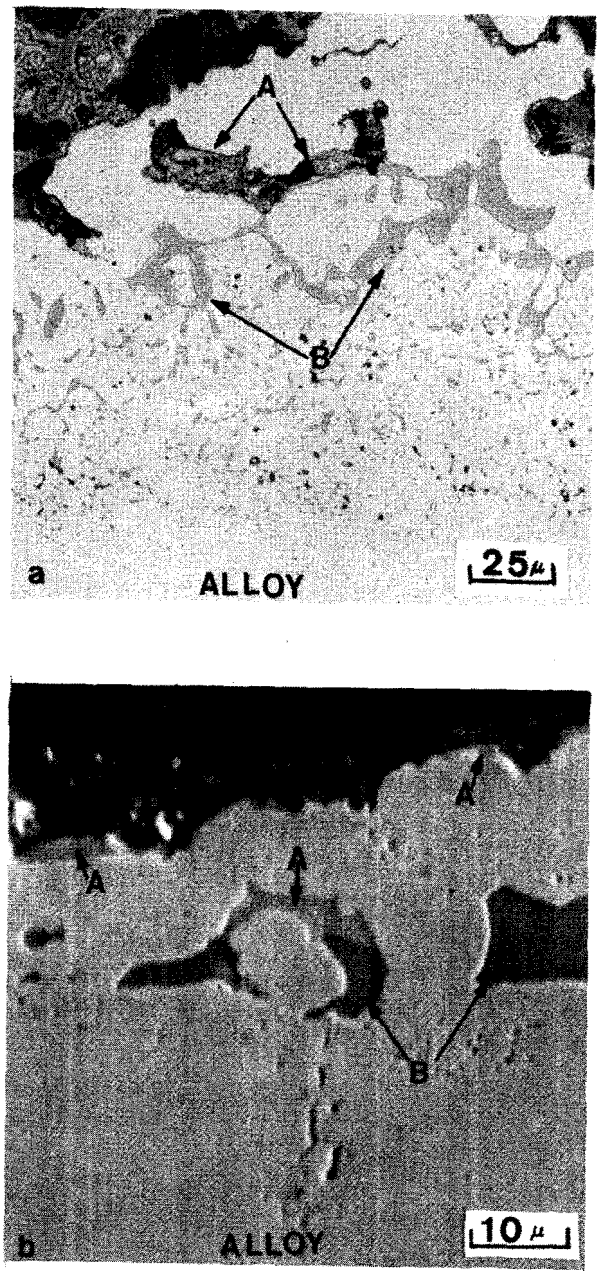

Figure 76 Details of isothermal hot corrosion microstructures of vapor-deposited Ni-25Cr-6Al-(.2Y) alloy specimens coated with 5 mg/cm^2 Na_2SO_4 and oxidized at 1000°C in oxygen. (a) Specimen of NiCrAl after 47 hrs. Preferential oxidation of sulfide stringers has occurred in area A; unoxidized stringers are indicated at B. (b) Electron beam backscatter image showing that sulfide stringers are composed of two sulfide phases: liquid nickel sulfide (A) and chromium sulfide (B).

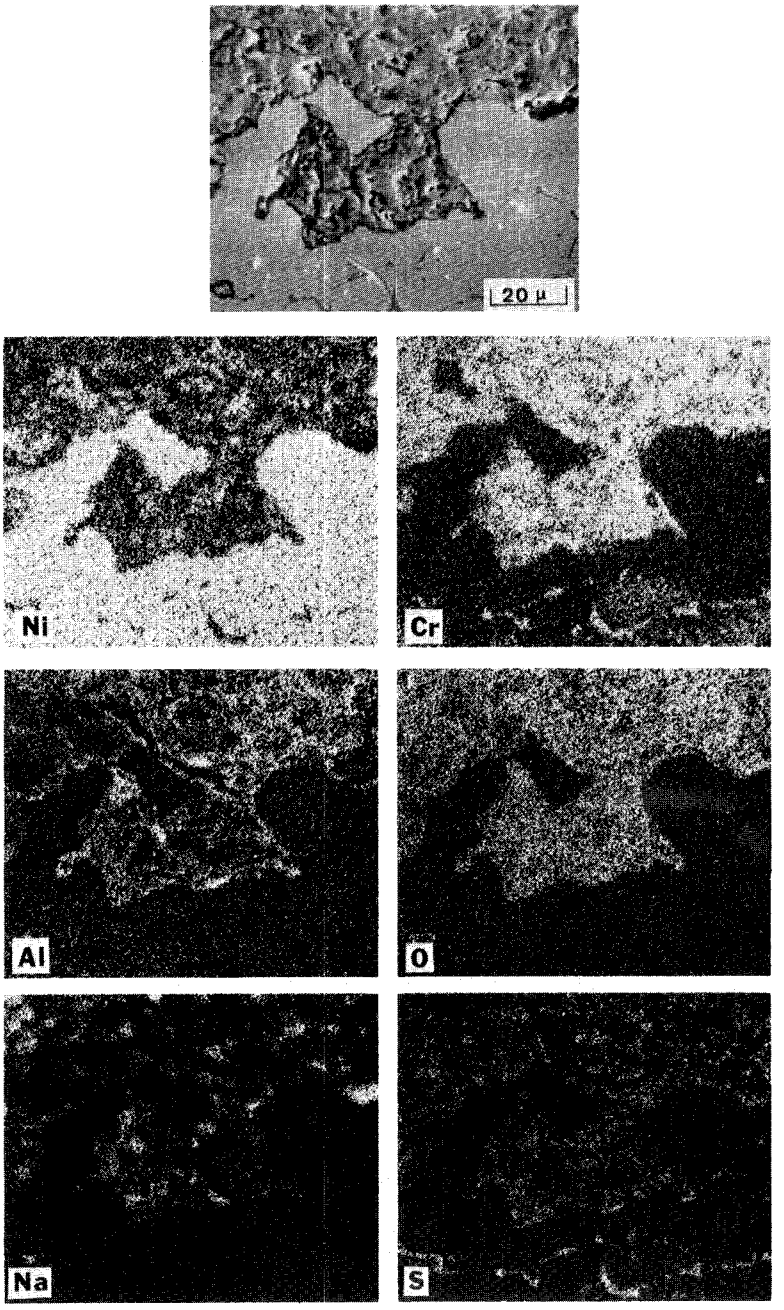

Figure 77 X-ray images for Na_2SO_4-coated NiCrAl after 8 hrs isothermal oxidation. Specimen was metallographically prepared without water to preserve residual sodium-containing compounds.

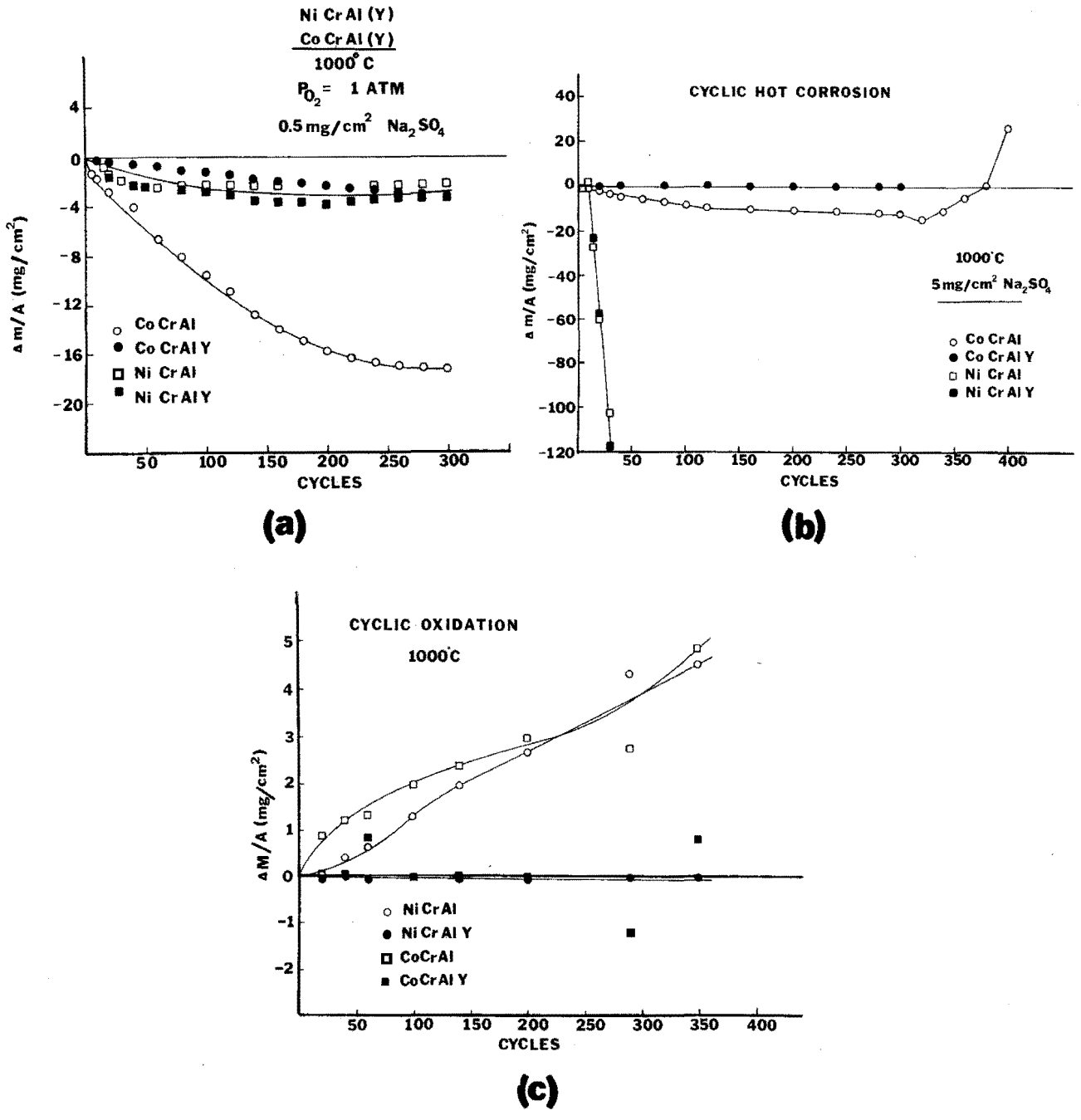

Figure 78 Comparison of the weight change versus time data obtained from cyclic hot corrosion and cyclic oxidation testing of NiCrAl(Y) and CoCrAl(Y) alloys; a) cyclic hot corrosion with 0.5 mg/cm^2 Na_2SO_4, b) cyclic hot corrosion using 5 mg/cm^2 Na_2SO_4, c) cyclic oxidation (nominal compositions are indicated in this Figure).

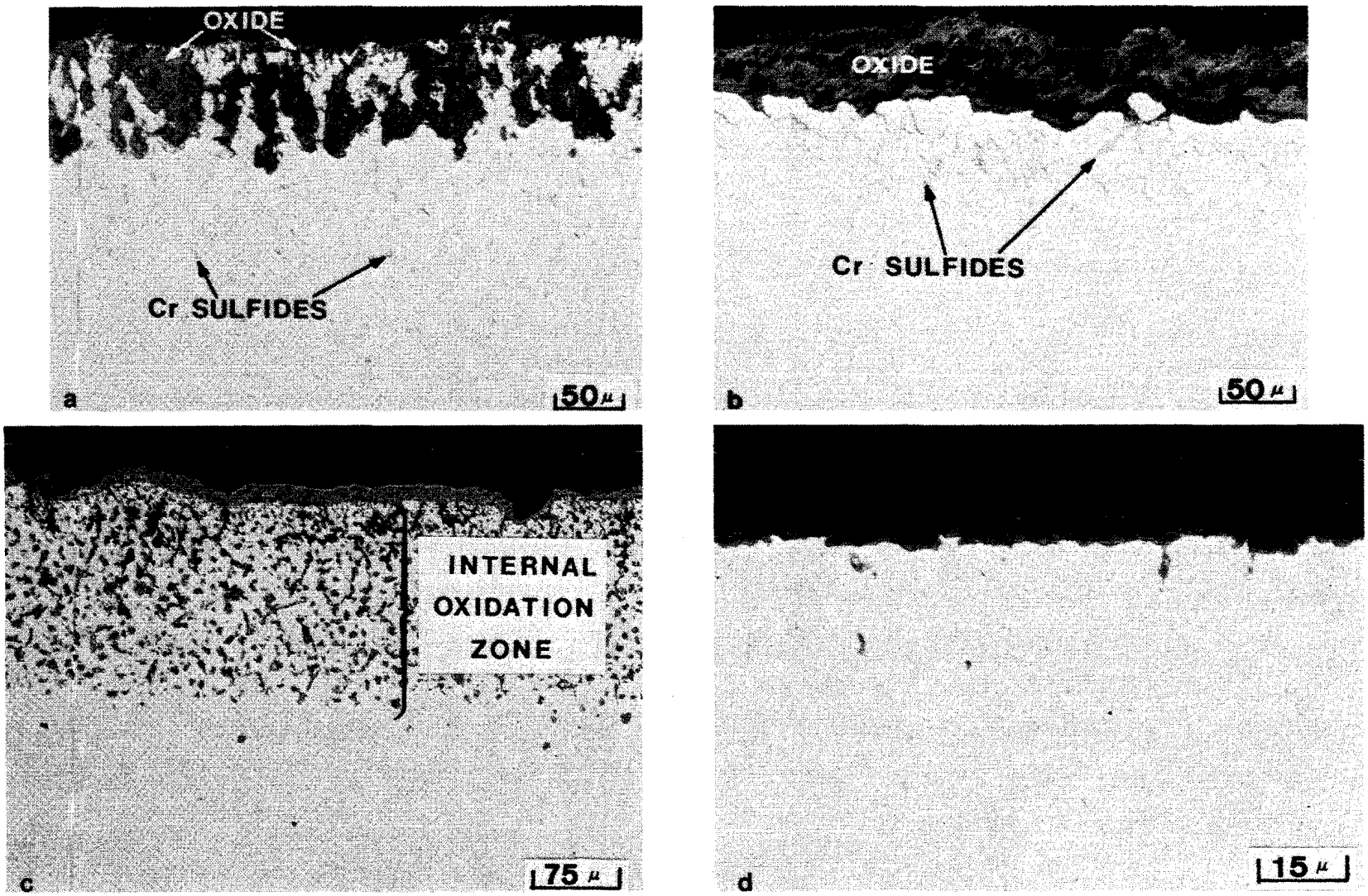

Figure 79 Photographs showing the microstructures of NiCrAl and NiCrAlY alloys after cyclic hot corrosion and oxidation testing at 1000°C; a) NiCrAl specimen after 300 cycles with 0.5 mg/cm^2 Na_2SO_4; b) NiCrAl specimen after 30 cycles with 5 mg/cm^2 Na_2SO_4 (an identical structure was observed with the NiCrAlY alloy), c) NiCrAl specimen after 350 cycles with no Na_2SO_4, d) NiCrAlY specimen after 350 cycles with no Na_2SO_4.

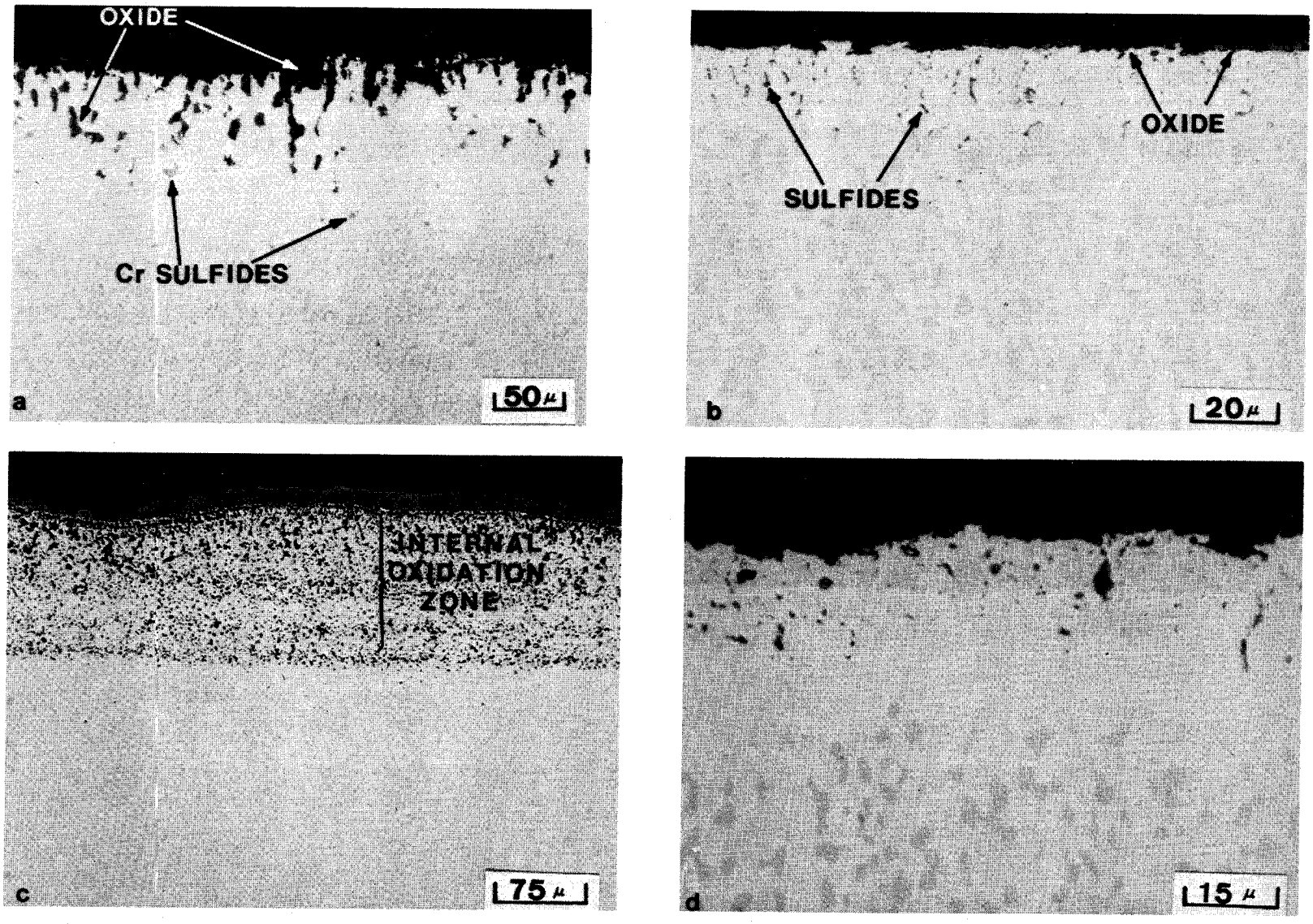

Figure 80 Photomicrographs of CoCrAl and CoCrAlY after cyclic hot corrosion and oxidation testing at 1000°C; a) CoCrAl specimen after 300 cycles with a 0.5 mg/cm^2 Na_2SO_4, b) CoCrAlY specimen after 300 cycles with 5 mg/cm^2 Na_2SO_4, c) CoCrAl and d) CoCrAlY specimens after 350 cycles of oxidation with no Na_2SO_4.

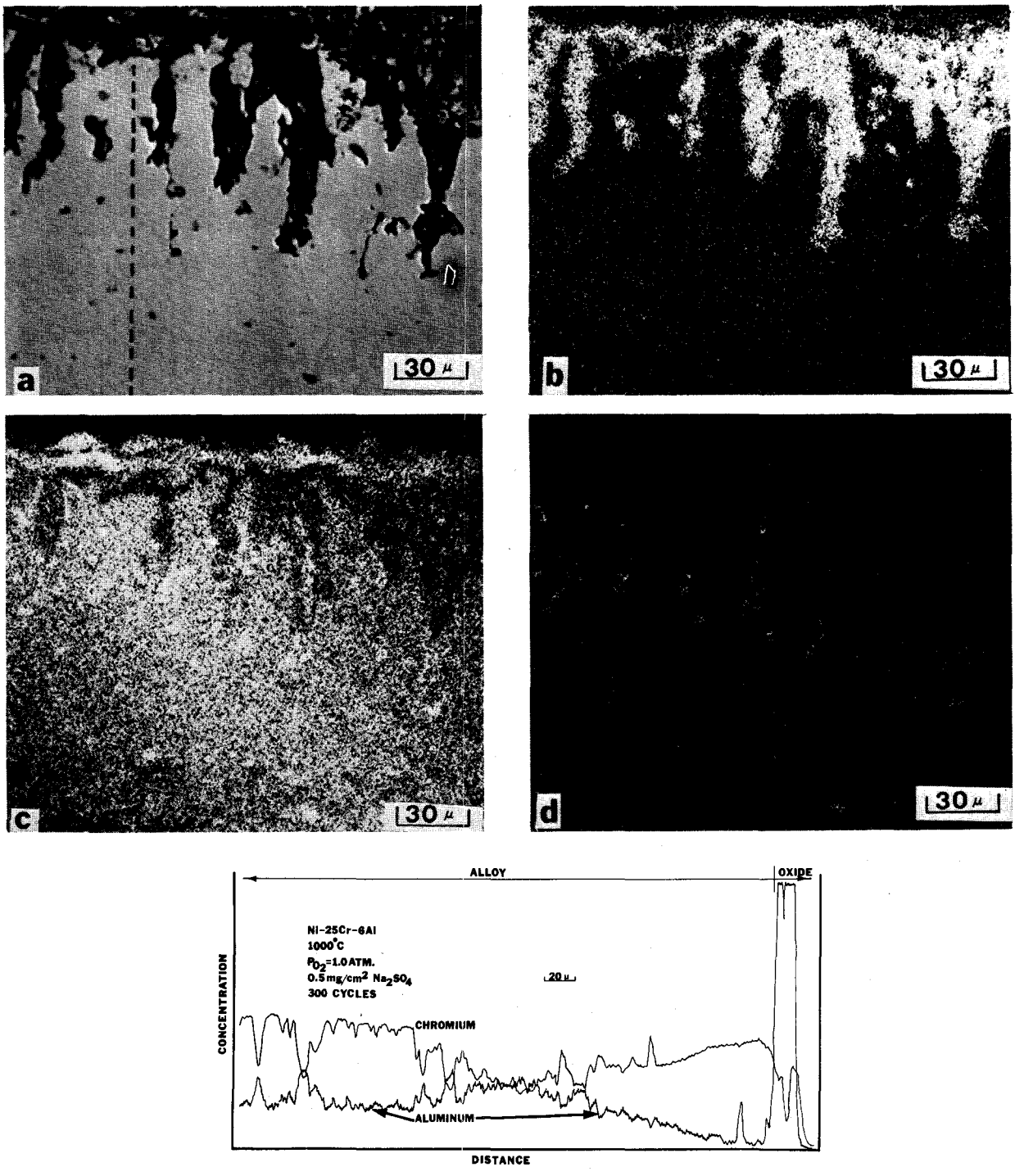

Figure 81 Electron back scatter (a) and x-ray images for aluminum (b), chromium (c), and sulfur (d) obtained with a NiCrAl specimen after 300 cycles in the hot corrosion test with 0.5 mg/cm^2 Na_2SO_4. The dashed line in a) indicates the traverse line for the composition profiles presented in (e).

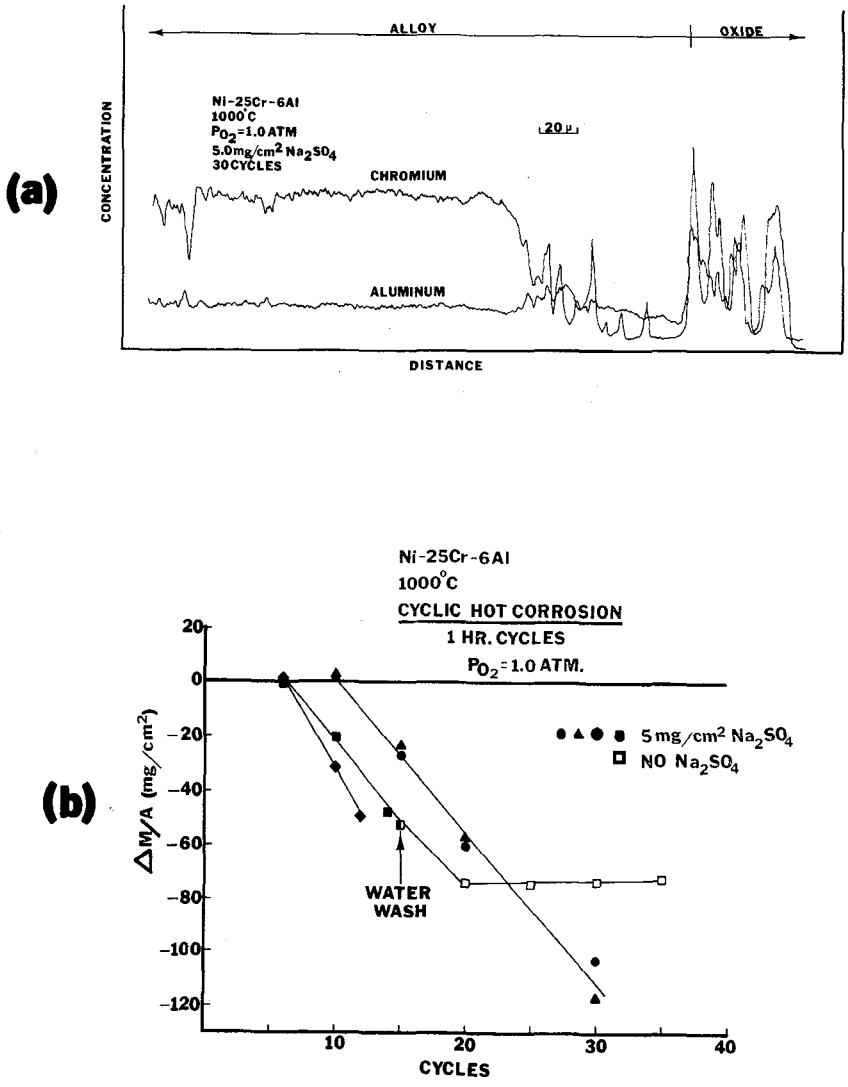

Figure 82 Compositional profiles and weight change data for NiCrAl. a) Chromium and aluminum profiles at the surfaces of NiCrAl specimen. The path of the traverse was normal to the scale-alloy interface of the specimen shown in Figure 79. b) Data obtained for the cyclic hot corrosion testing of Na_2SO_4-coated NiCrAl (b) which shows that continual deposition of Na_2SO_4 is necessary in order to have severe hot corrosion degradation.

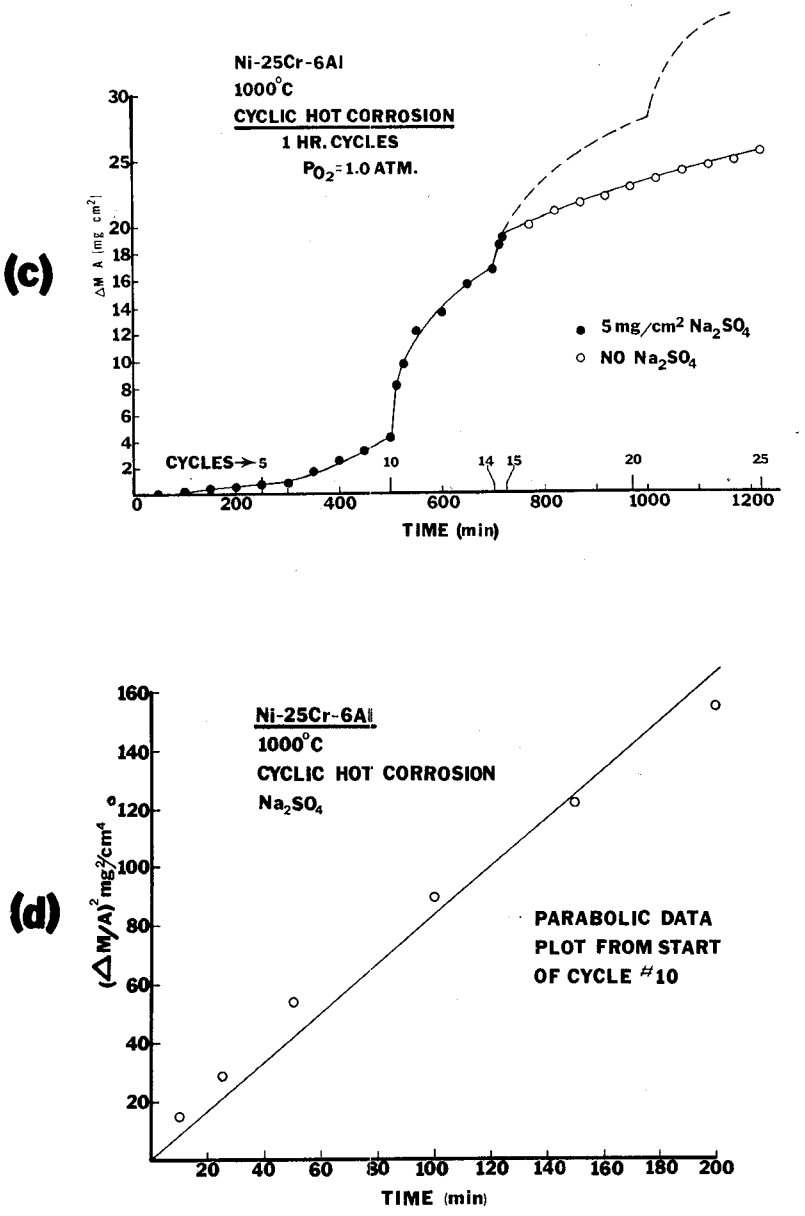

Figure 82 (Contd). c) Continuous weight change versus time data for the cyclic hot corrosion of NiCrAl. Specimen was recoated with Na_2SO_4 after cycles 5, 10 and 14. After the fifteenth cycle the specimen was washed in water and no Na_2SO_4 was applied. d) Weight change squared versus time for the data obtained between cycles 10 and 14 of (c) where the origin of this plot has been taken as the weight change and time at the conclusion of the tenth cycle.

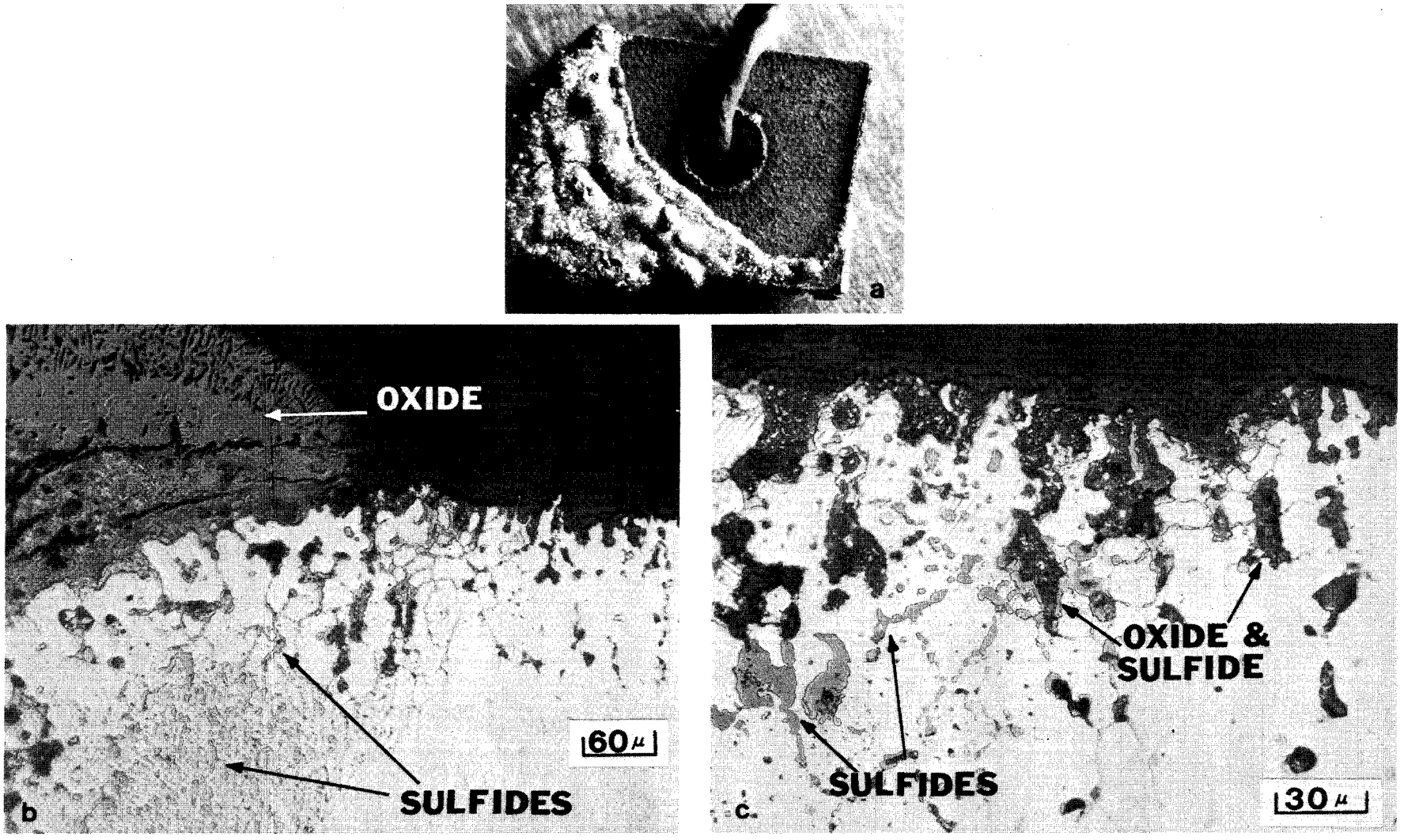

Figure 83 Photographs showing the surface and microstructure of CoCrAl after 400 cycles at 1000°C in 1 atm of oxygen with 5 mg/cm^2 Na_2So_4; a) Surface photographs showing severe hot corrosion, b) Transverse sections through specimens showing thick oxide scale, stringers of sulfide and particles of sulfide deeper within the alloy; c) Transverse section showing preferential oxidation of the stringers of sulfide.

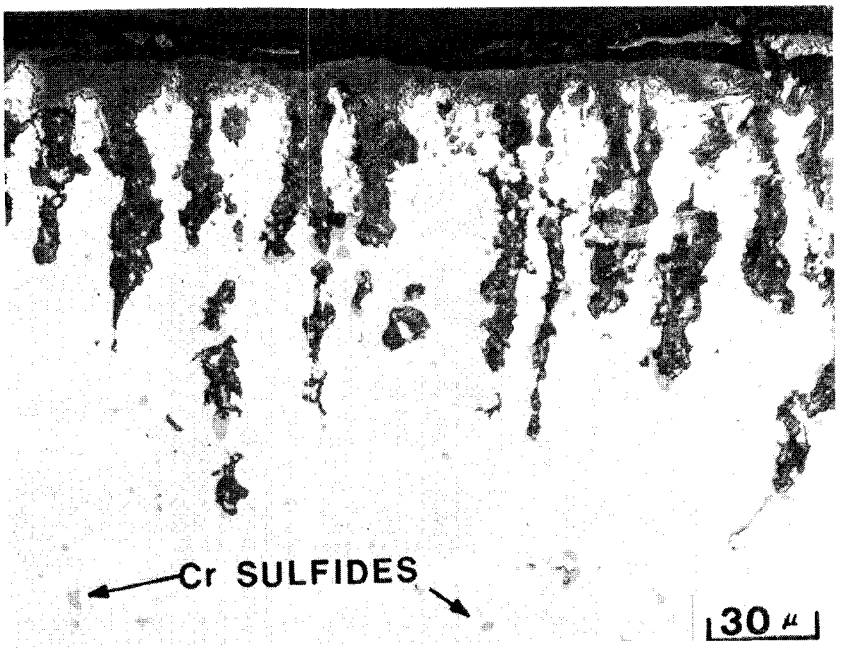

(a)

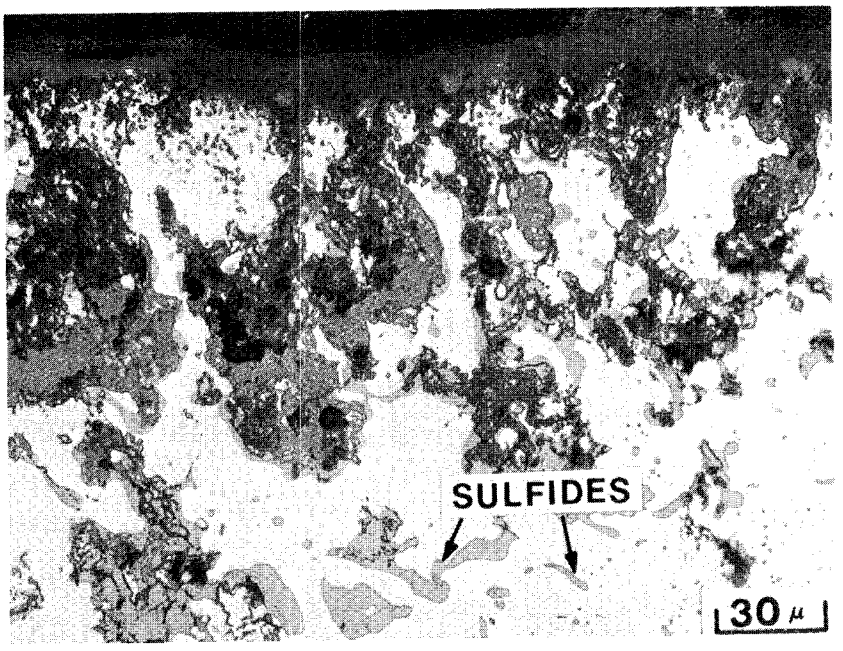

(b)

Figure 84 Photomicrographs showing the microstructures of Ni-15Cr-6Al specimens after 300, (a), and 520, (b) cycles in the cyclic hot corrosion test at 1000°C in 1 atm of oxygen using 0.5 mg/cm^2 Na_2SO_4.

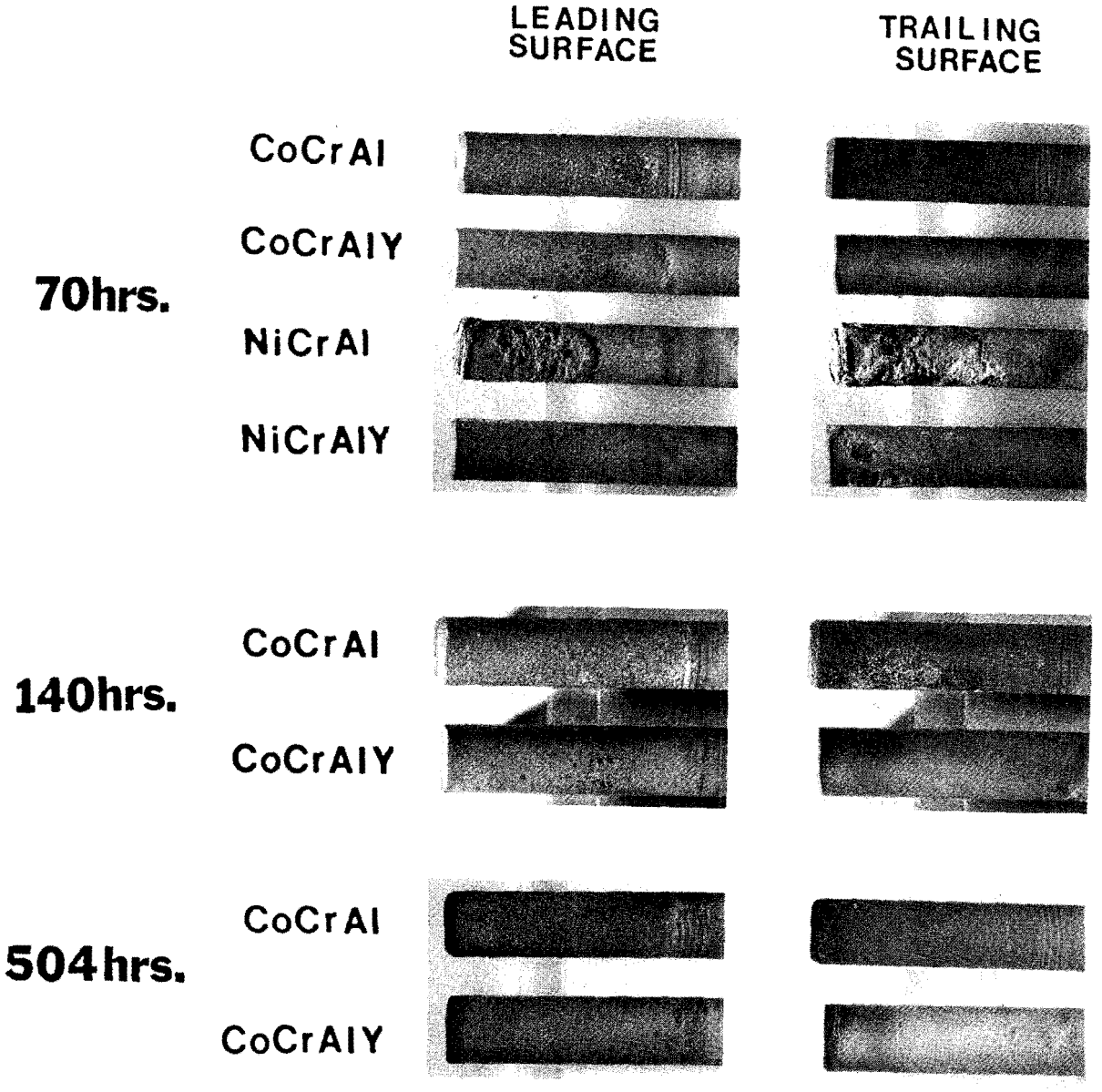

Figure 85 Photographs showing the surface condition of NiCrAl(Y) and CoCrAl(Y) specimens after different times in the ducted burner rig at 1000°C with a Na_2SO_4 deposition rate of 0.1 mg/cm^2-hr. The NiCrAl and NiCrAlY specimens were removed from the test because of excessive degradation after 70 and 100 hours, respectively.

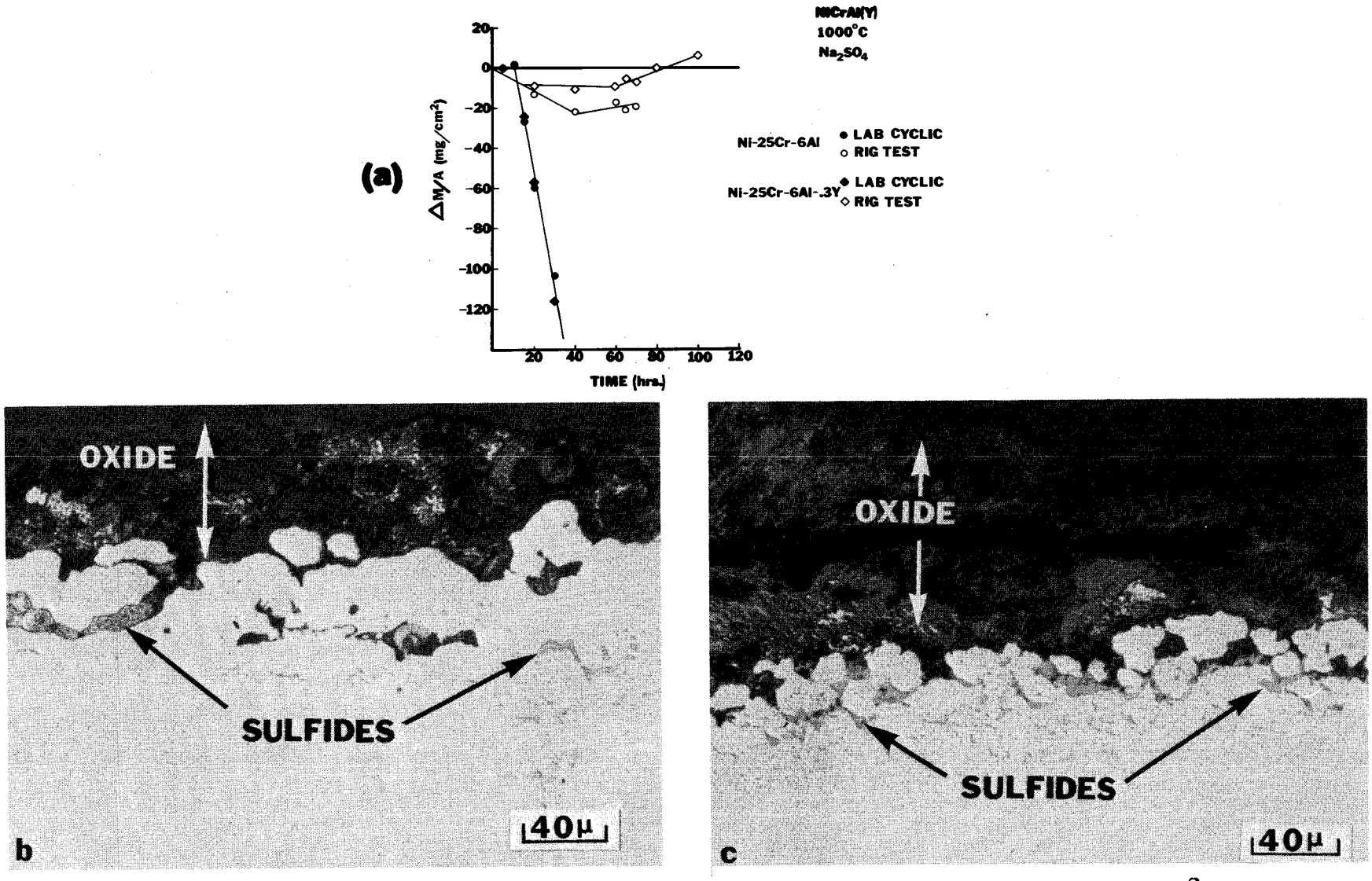

Figure 86 Comparison of data obtained for NiCrAl(Y) specimens in the laboratory hot corrosion test (5 mg/cm^2 Na_2SO_4 every 20 hrs) and in the ducted burner rig (0.1 mg/cm^2 Na_2SO_4 per hr); a) weight change versus time curves, b) photomicrograph of NiCrAl after 70 hrs in ducted burner rig; c) photomicrograph of NiCrAl after 12 hrs in laboratory cyclic hot corrosion test.

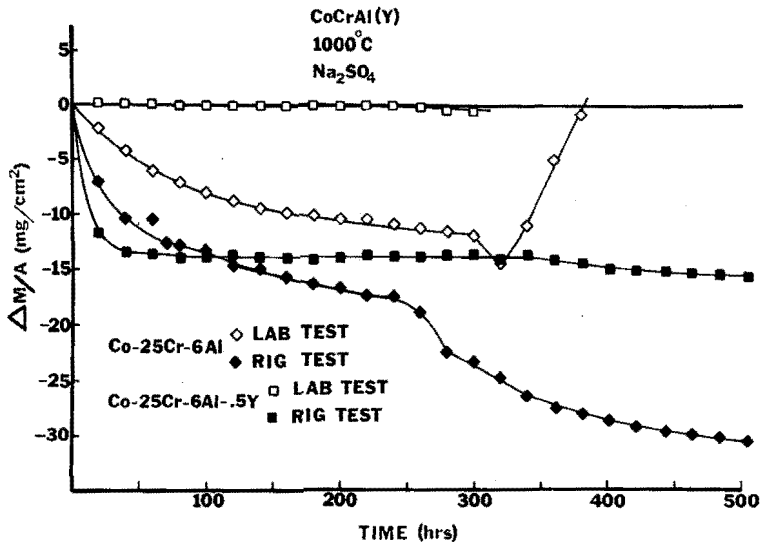

(a)

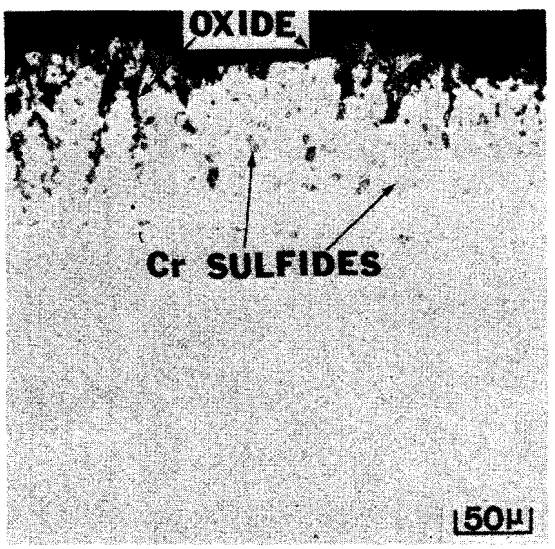

(b)

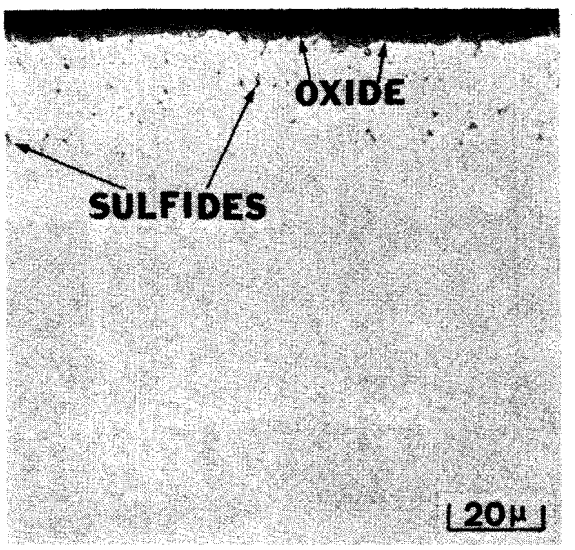

(c)

Figure 87 a) Comparison of weight change versus time data obtained for CoCrAl(Y) specimens in the laboratory hot corrosion test (5 mg/cm^2 per 20 hrs) and in the ducted burner rig (0.1 mg/cm^2 Na_2SO_4 per hr). b) and c) Photomicrographs of transverse sections of CoCrAl and CoCrAl Y respectively after 504 hrs exposure in the ducted rig at 1000°C. Microstructures are similar to those shown previously for laboratory cyclic hot corrosion specimens.

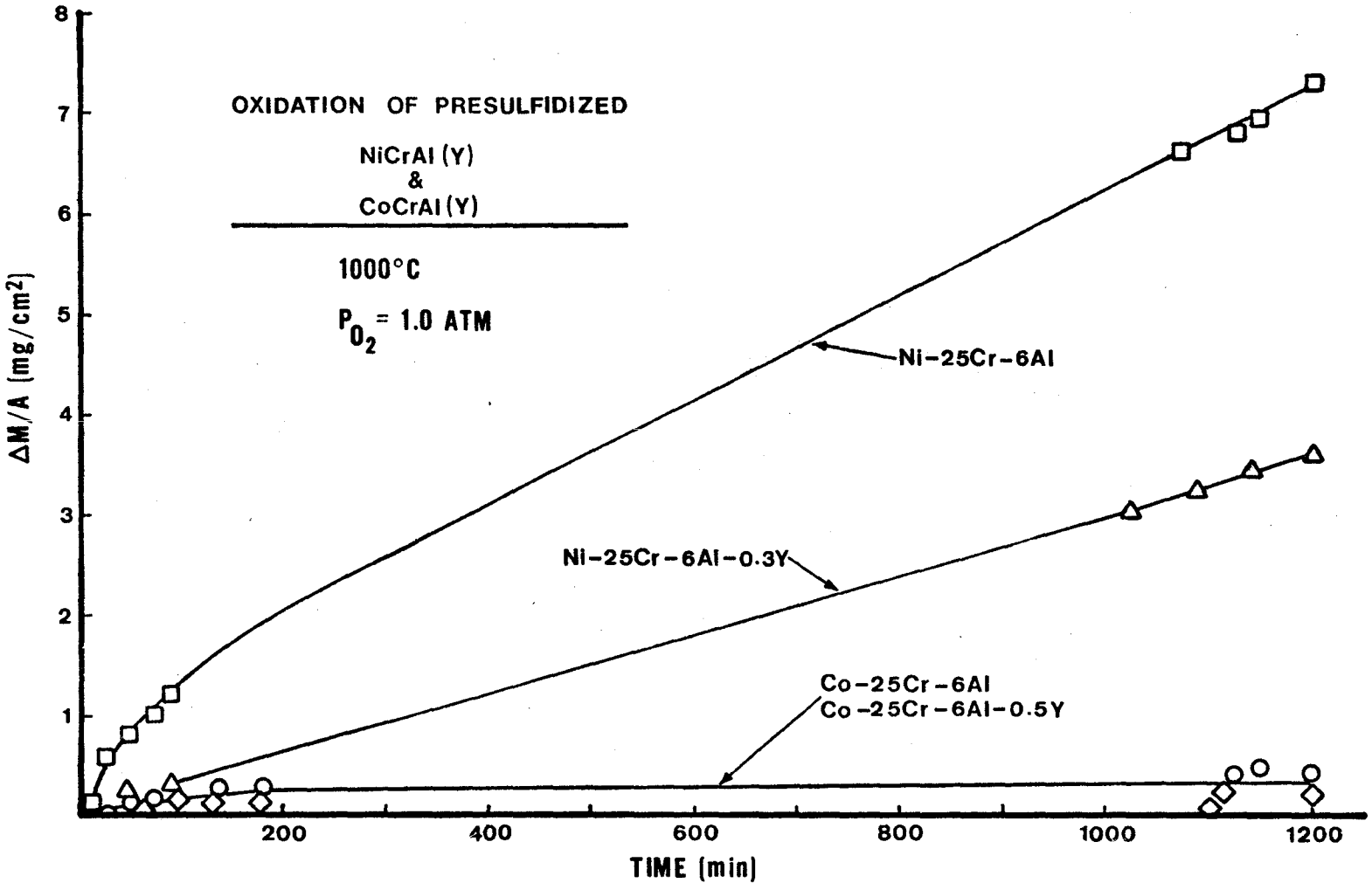

Figure 88 Comparison of weight change versus time curves obtained for the isothermal oxidation of presulfidized (20 seconds at 1000°C in H_2S-H_2 mixture with $H_2S/H_2 = 0.2$) NiCrAl(Y) and CoCrAl(Y) alloys.

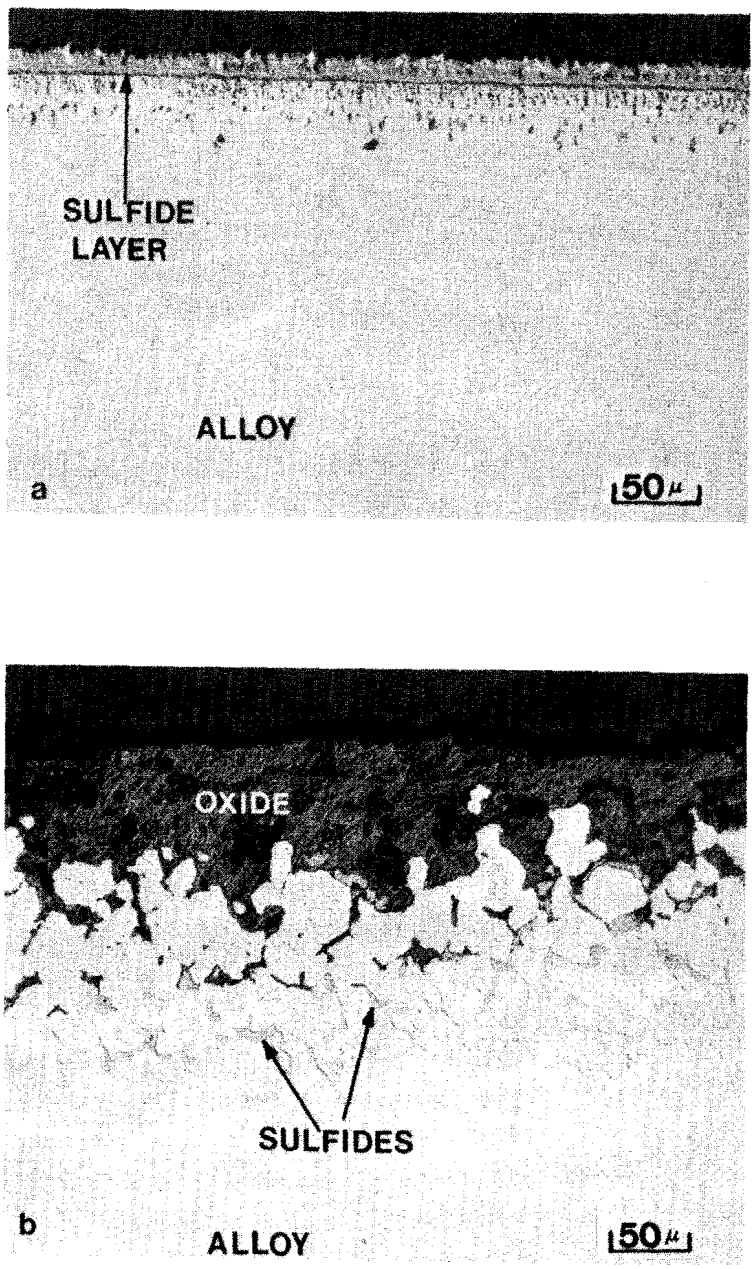

Figure 89 Photomicrographs of vapor-deposited Co-25Cr-6Al (a) and Ni-25Cr-6Al (b) alloy specimens which were first treated in H_2 S/H_2 = 0.2 for 20 sec, followed by oxidation for 20 hrs at 1000°C. The relatively thin Al_2O_3 scale, which formed on the cobalt-chromium sulfide layer during oxidation of the CoCrAl specimen, spalled on cooling. Severe attack of the NiCrAl specimen has occurred due to preferential oxidation of sulfide stringers consisting of nickel and chromium sulfides.

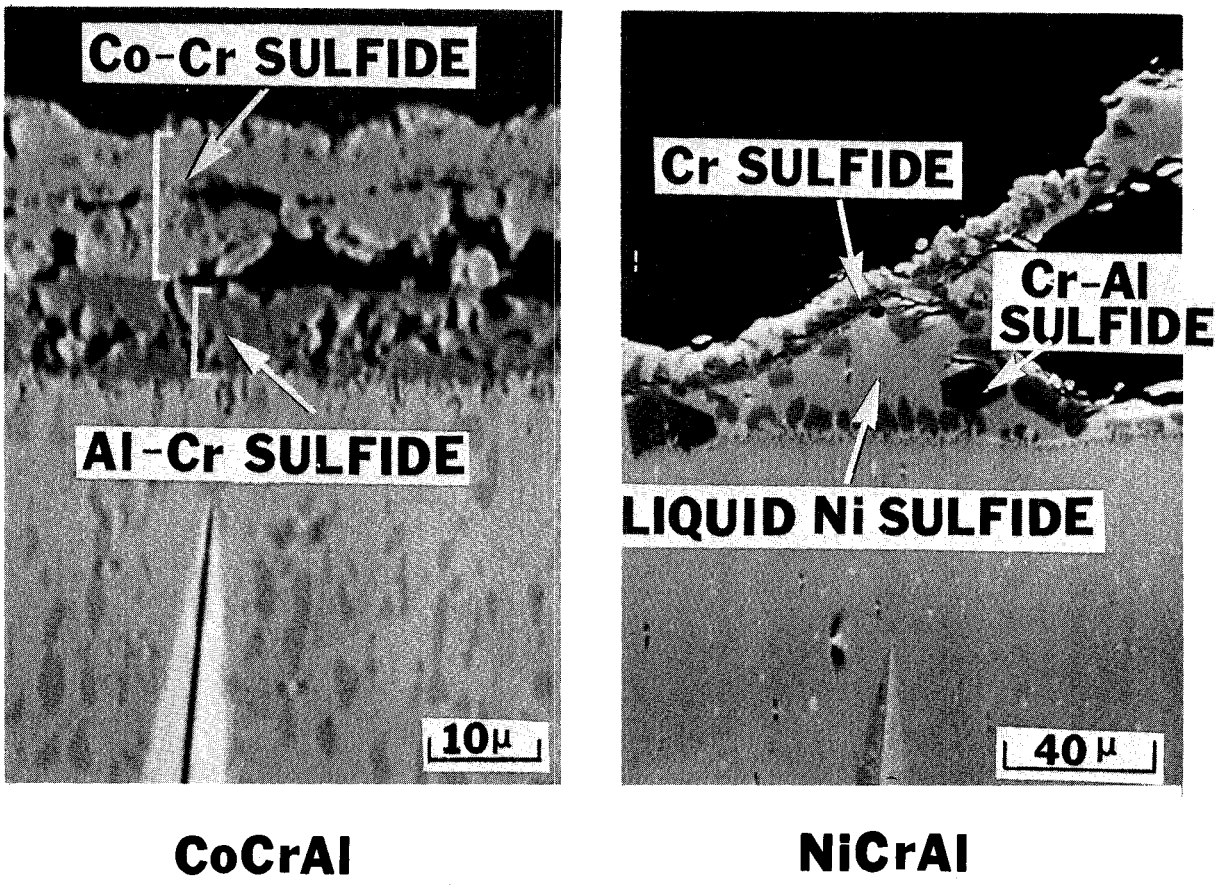

Figure 90 Electron back scatter images of sulfide layers formed on CoCrAl and NiCrAl specimens heated in H_2S/H_2 = 0.2 for 20 sec at 1000°C.

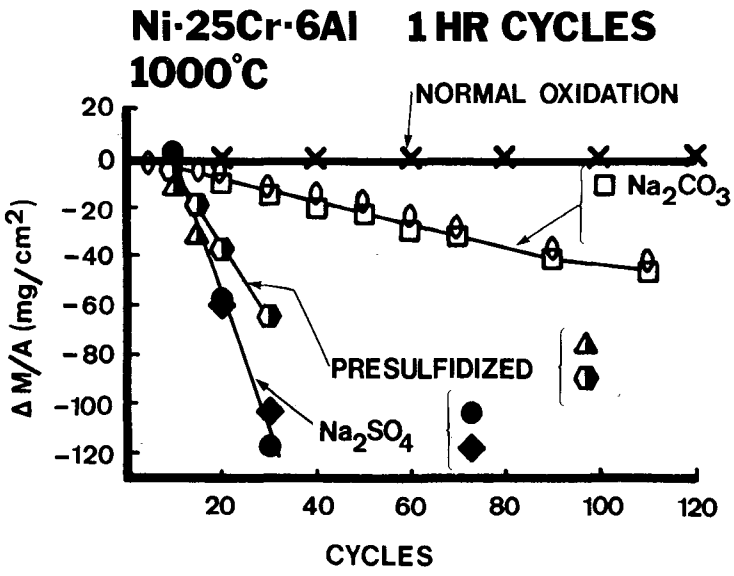

(a)

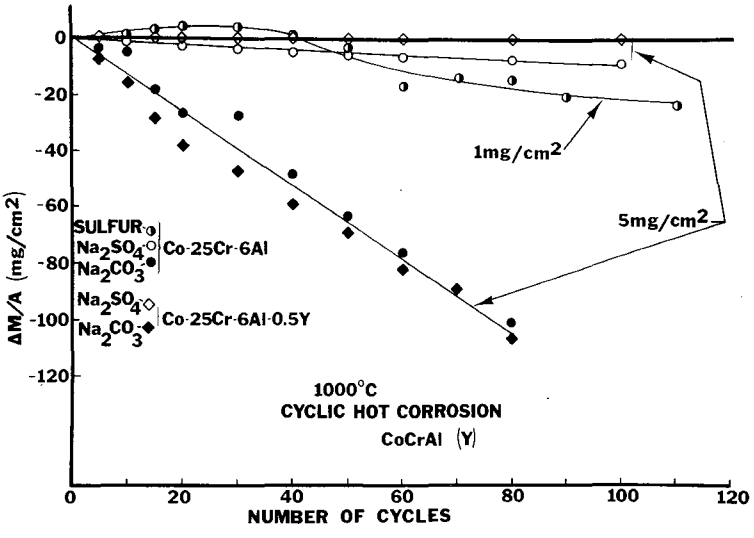

(b)

Figure 91 Comparison of the cyclic oxidation of NiCrAl, (a), and CoCrAl(Y), (b), alloys where the specimens were coated with Na_2SO_4, Na_2CO_3 or presulfidized by heating in an H_2S-H_2 gas mixture. Approximately 5 mg/cm^2 of Na_2SO_4 or Na_2CO_3 was added to specimens every 5 hrs. up to 20 hrs. and then every 10 hrs. beyond 20 hrs. The presulfidation was performed at the same time intervals as the salts were applied and the sulfur picked up was equal to the sulfur in a 5 mg/cm^2 Na_2SO_4 deposit.

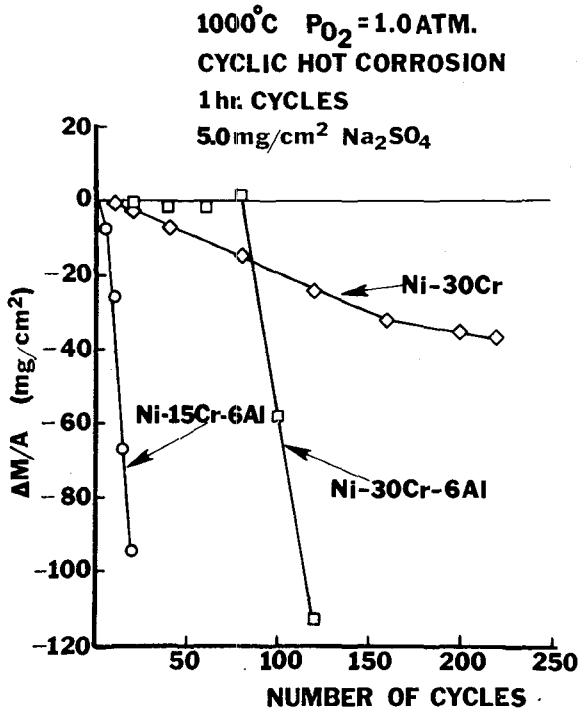

Figure 92 Weight change versus time curves obtained for the cyclic oxidation (5 mg/cm^2 Na_2SO_4 applied every 20 hrs.) of some nickel-base alloys having different chromium and aluminum concentrations.

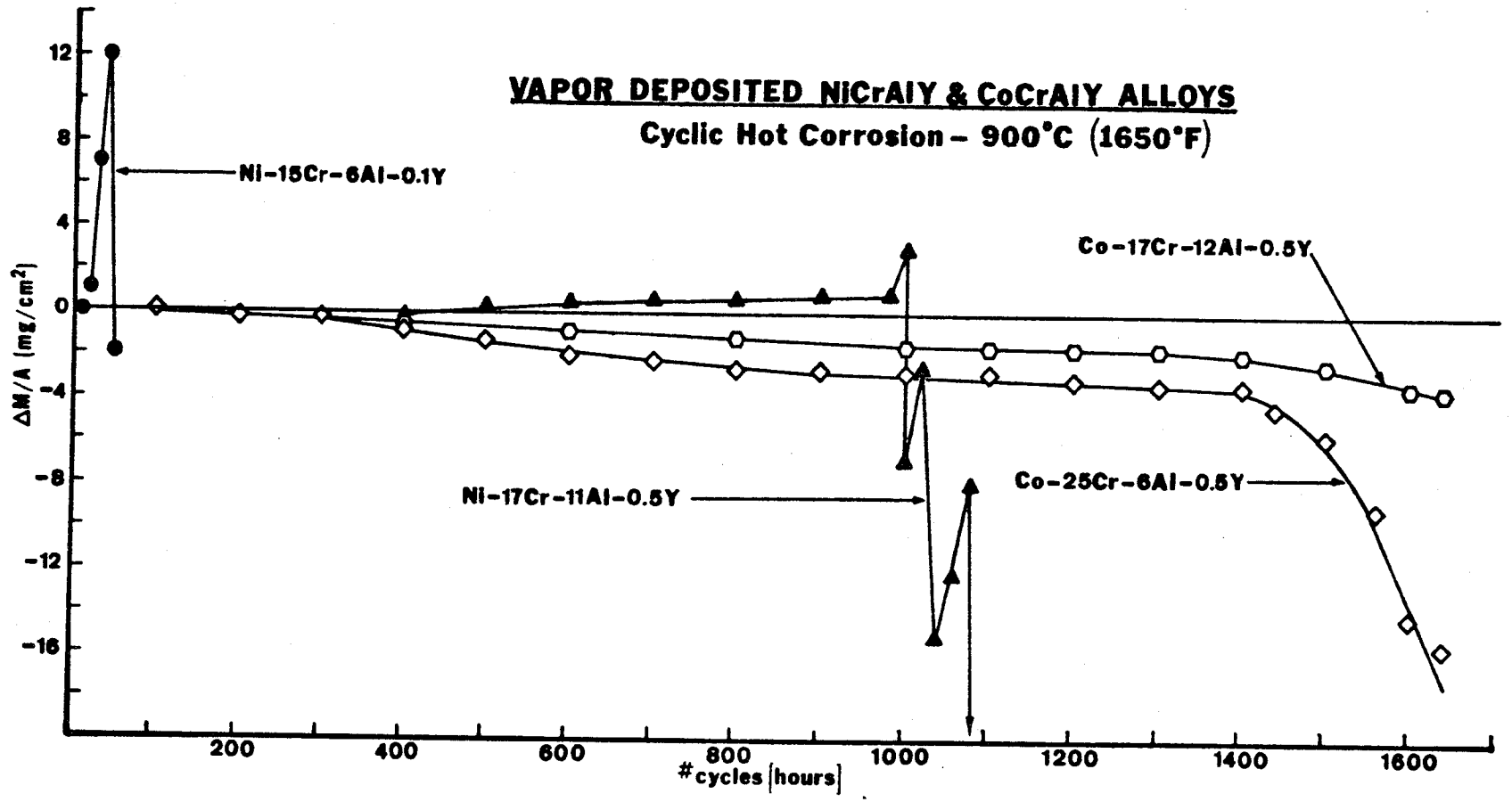

Figure 93 Weight change versus time curves obtained for the cyclic oxidation (1 hr cycles) of Na_2SO_4-coated (1 mg/cm^2 Na_2SO_4 applied every 20 hrs) NiCrAlY and CoCrAlY alloys.

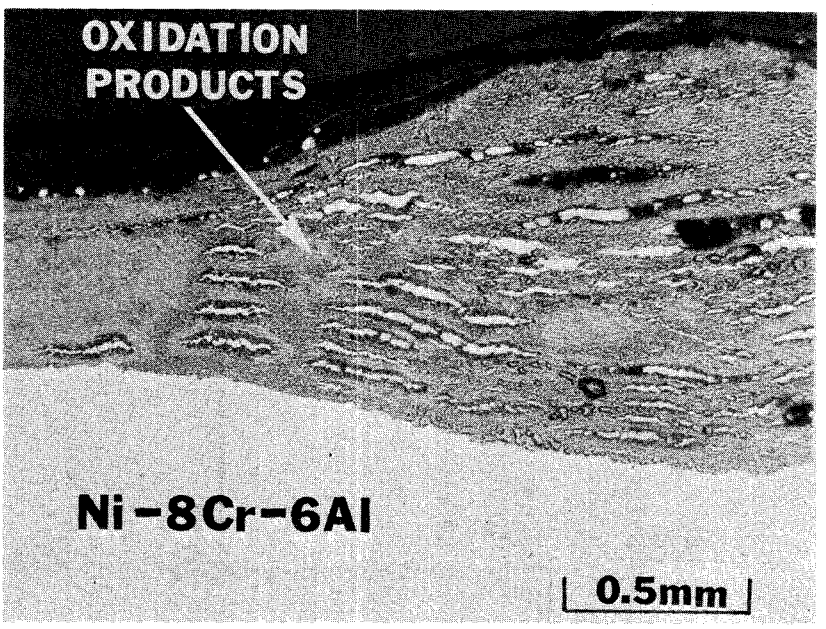

Figure 94 Photomicrograph of Ni-8Cr-6Al alloy after 7 minutes in air at 900°C in the modified crucible test. Results obtained with the electron beam microprobe showed the metallic particles in the scale were nickel and nickel sulfide but only nickel was present in the scale immediately adjacent to the alloy. The rest of the scale contained sodium, sulfur, oxygen, aluminum and chromium.

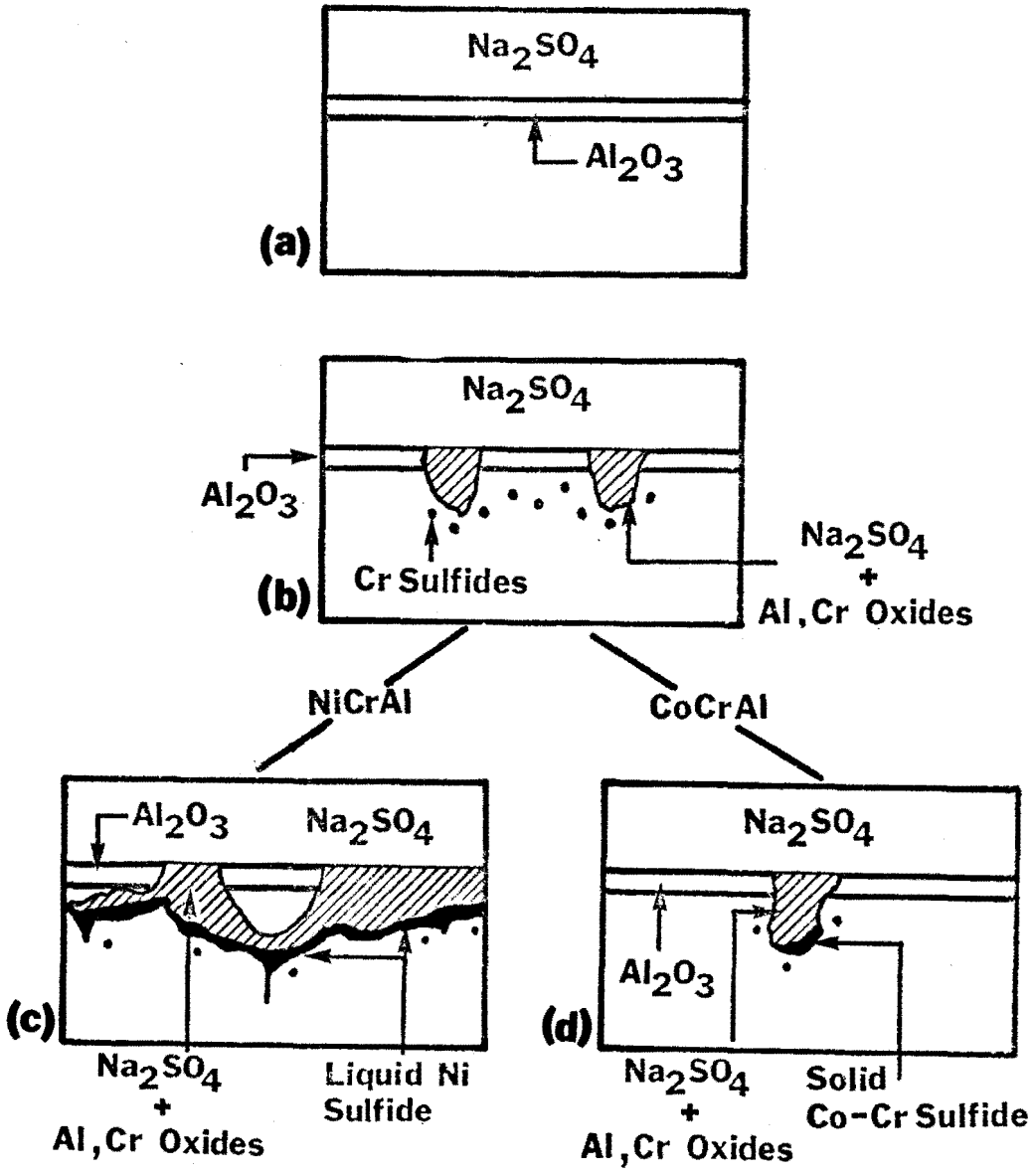

Figure 95 Schematic diagram illustrating the steps in the initial stages of hot corrosion of NiCrAl and CoCrAl alloys.

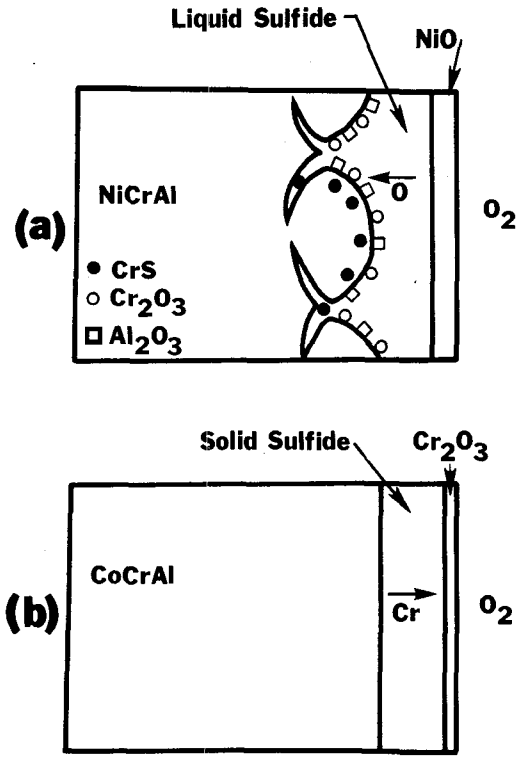

Figure 96 Schematic diagram illustrating how the liquid sulfide phase on NiCrAl results in nonprotective Al_2O_3 and Cr_2O_3 formation, whereas protective Cr_2O_3 can be developed when a solid sulfide is present on CoCrAl.

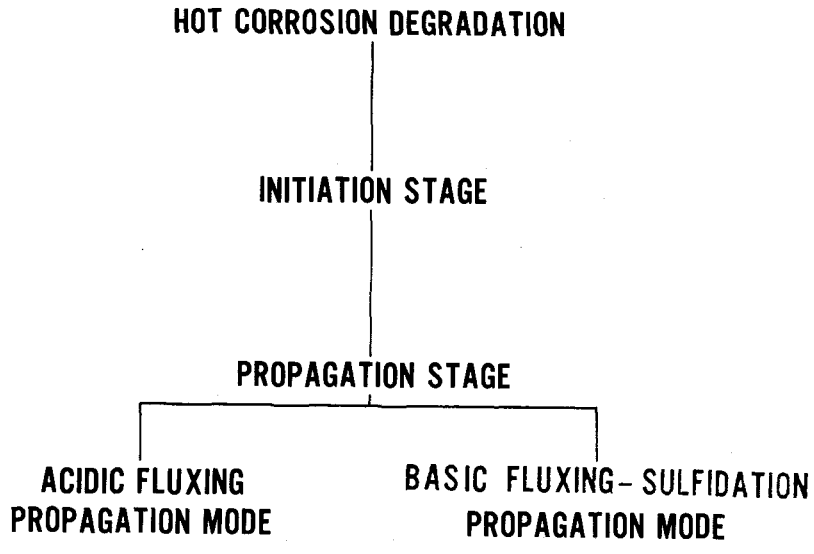

Figure 97 Schematic diagram illustrating the stages in the hot corrosion degradation of materials.

REFERENCES

1. Wagenheim, N. T., "Development of Hot Corrosion Resistant Cobalt-Base Alloys for Marine Engines", *Cobalt* Vol. 48, pp. 129-141 (1970).

2. Bergman, P. A., "Hot Corrosion of Gas Turbine Alloys", *Corrosion,* Vol. 23, pp. 72-81 (1967).

3. Kaufman, M. and Wasielewski, G. E., "Development of Hot-Corrosion Resistant Nickel-Base Alloys for Marine Gas Turbine Service". Prepared for U. S. Navy Ship Research and Development Laboratory, Annapolis, Maryland, Contract No. N00600-68-C-1036, July 1970.

4. Viswanathan, R., "High Temperature Corrosion of Some Gas Turbine Alloys", *Corrosion,* Vol. 24, pp. 359-368 (1968).

5. Donachie, M. J., Jr., Sprague, R. A., Russell, R. N., Boll, K. G. and Bradley, E. F., "Sulfidation of Hot Section Alloys in Gas Turbine Engines", ASTM Special Technical Publication No. 421, Hot Corrosion Problems Associated with Gas Turbines (1967).

6. Simons, E. L., Browning, G. V., and Liebhafsky, H. A., "Sodium Sulfate in Gas Turbines", *Corrosion,* Vol. 11, pp. 505-514 (1955).

7. Seybolt, A. U., "Contribution to the Study of Hot Corrosion", *Trans. AIME,* Vol. 242, pp. 1955-1961, (1968).

8. Seybolt, A. U., "Na_2SO_4-Superalloy Corrosion Mechanism Studies", General Electric Research and Development Center, Report No. 70-C-189, June 1970.

9. Bornstein, N. S. and DeCrescente, M. A., "The Role of Sodium in the Accelerated Oxidation Phenomenon Termed Sulfidation", *Met Trans.* Vol. 2, pp. 2875-2883 (1971).

10. Quets, J. M. and Dresher, W. H., "Thermochemistry of the Hot Corrosion of Superalloys", *J. Mater.,* Vol. 4, pp. 583-599 (1969).

11. Goebel, J. A. and Pettit, F. S., "Na_2SO_4-Induced Accelerated Oxidation (Hot Corrosion) of Nickel", *Met. Trans.* Vol. 1, pp. 1943-1954 (1970).

12. Goebel, J. A., Pettit, F. S. and Goward, G. W., "Mechanisms for the Hot Corrosion of Nickel-Base Alloys", *Met. Trans.,* Vol. 4, pp. 261-278 (1973).

13. Goebel, J. A., Pettit, F. S. and Goward, G. W., "Hot Corrosion Mechanisms in Stationary Gas Turbines", Deposition and Corrosion in Gas Turbines, A. B. Hart and A. J. B. Cutler, Editors, Essex, England (1973).

REFERENCES (Cont'd)

14. Conde, J.F.G., "What are the Separate and Interacting Roles of Sulphur, Sodium and Chloride in Hot Corrosion?" Specialist Meeting on High Temperature Corrosion of Aerospace Alloys, 34th Meeting of the Structures and Materials Panel, AGARD, Lynby, Denmark, 1972.

15. Hurst, R. C., Johnson, J. B. Davies, M. and Hancock, P., "Sulphate and Chloride Attack of Nickel-Based Alloys and Mild Steels", "Deposition and Corrosion in Gas Turbines", A. B. Hart and A. J. B. Cutler, Editors, Essex, England (1973).

16. Stringer, J., "Hot Corrosion in Gas Turbines", MCIC Report No. 72-08, NTIS, U.S. Department of Commerce, Springfield, Va., 1972.

17. Davin, A., Coutsouradis, D. and Habraken, L., "Influence of Alloying Elements on the Hot Corrosion Resistance of Co-Cr Alloys", *Werkstoffe and Korrosion,* Vol. 22, pp. 517-527, (1971).

18. Morral, F.R., "Corrosion of Cobalt and Cobalt Alloys", *Corrosion,* Vol. 25, pp. 307-322 (1969).

19. Sims, C.T., Bergman, P.A. and Beltran, A.M., "Progress in the Development of Hot Corrosion Resistant Alloys for Marine Applications", *Naval Engineers Journal,* p. 39, April 1970.

20. Davin, A., Coutsouradis, D. and Habraken, L., "Dry Corrosion of Cobalt-Chromium Alloys at High Temperature – Influence of Ternary Additions", *Cobalt,* Vol. 35, pp. 69-77, (1967).

21. Beltran, A. and Seybolt, A.U., The Behavior of Cobalt in High-Temperature Sulfur-Oxygen Environments, Appendix C, Hot Corrosion Mechanism Studies conducted for the U.S. Naval Marine Engineering Laboratory, Annapolis, Maryland, (1969), Contract No. N-(600) (61533)-63219.

22. Pettit, F.S., "Oxidation Mechanisms for Nickel-Aluminum Alloys at Temperatures Between 900° and 1300°C", *Trans. TMS-AIME,* Vol. 239, pp. 1296-1305, (1967).

23. Pettit, F.S., Yinger, R. and Wagner, J.B., Jr., "The Mechanism of Oxidation of Iron in Carbon Monoxide-Carbon Dioxide Mixtures", *Acta Met.,* Vol. 8, pp. 617-623, (1960).

24. Goebel, J.A. and Pettit, F.S., "The Influence of Sulfides on the Oxidation Behavior of Nickel-Base Alloys", *Met. Trans.* Vol. 1, pp. 3421-3429, (1970).

REFERENCES (Cont'd)

25. Kofstad, P., *High Temperature Oxidation of Metals,* John Wiley and Sons, Inc., New York, p. 122, (1966).

26. Carter, R.E. and Richardson, F.D., "Oxidation of Cobalt", *J. Metals,* Vol. 203, pp. 336-343, (1955).

27. Reising, R.F. and Krause, D.P., "Corrosion Product Characterization of a Nickel-Sodium Sulfate-Air System after Exposure to Temperatures Near 1000°C", *Corrosion,* Vol. 30, pp. 131-138, (1974).

28. Giggins, C.S. and Pettit, F.S., "Second Annual Report on Oxide Scale Adherence Mechanisms", for the Aerospace Research Laboratories, WPAFB, Ohio (Contract No. F33615-72-C-1702), July 1974.

29. Balajka, J. and Danek, V., "Corrosion of Ni in Molten Alkali Sulphates", *Werks. and Korr.,* Vol. 7, pp. 513-521, (1974).

30. Kear, B.H., Pratt & Whitney Aircraft; private communication.

31. Giggins, C.S. and Pettit, F.S., "Oxidation of Ni-Cr Alloys Between 800° and 1200°C", *Trans. TMS-AIME,* Vol. 245, pp. 2495-2507, (1969).

32. Dils, R.R., "Dynamic Gas Temperature Measurements in a Gas Turbine Transition Duct Exit", *Transactions of ASME,* Paper No. 73-GT-7, April 1973.

33. Hanby, V.I., "Sodium Sulfate Formation and Deposition in Marine Gas Turbines", *Transactions of ASME,* Paper No. 73-WALCD-2, November 1973.

34. Tschinkel, J.G., "Formation of Sodium Sulfate in Gas Turbine Combustors", *Corrosion,* Vol. 28, pp. 161-169, (1972).

35. Sander, W.A., "Dynamic Oxidation Behavior at 1000°C of Four Nickel-Base Cast Alloys: NASA VIA, B-1900, 713C and 738X", Report NASA TN D-7682, Lewis Research Center, Cleveland, Ohio, August 1974.

36. Giggins, C.S. and Pettit, F.S., "Oxidation of Ni-Cr-A1 Alloys Between 1000 and 1200°C", J. *Electrochem, Soc.,* Vol. 118, pp. 1781-1970, (1971).

37. Elliot, J.F. and Gleiser, M., *"Thermochemistry for Steelmaking",* Addison-Wesley Publishing Co., Inc., Reading, Mass. (1960).

38. Kirkaldy, J.S., Bolye, G.M., McCutcheon, D. and Young, D.J., "Phase Constitution of the Ni-Cr-S Alloy System Between 600° and 850°C", *Met. Trans.,* Vol. 4, pp. 1519-1526, (1973).

39. International Critical Tables, Vol. VII, p. 305, 1930.

☆ U. S. GOVERNMENT PRINTING OFFICE: 1976 — 657-630/571

AD A 044435

UNCLASSIFIED

SECURITY CLASSIFICATION OF THIS PAGE *(When Data Entered)*

REPORT DOCUMENTATION PAGE

READ INSTRUCTIONS BEFORE COMPLETING FORM

1. REPORT NUMBER: ARL 75-0235	2. GOVT ACCESSION NO.
3. RECIPIENT'S CATALOG NUMBER	
4. TITLE *(and Subtitle)*: HOT CORROSION OF COBALT-BASE ALLOYS	5. TYPE OF REPORT & PERIOD COVERED: Final Technical Report, 1 June 1972 - 31 May 1975
	6. PERFORMING ORG. REPORT NUMBER: PWA-5379
7. AUTHOR(s): J. A. Goebel and F. S. Pettit	8. CONTRACT OR GRANT NUMBER(s): F33615-72-C-1757
9. PERFORMING ORGANIZATION NAME AND ADDRESS: Pratt & Whitney Aircraft - Division of United Technologies Corporation, East Hartford, Connecticut 06108	10. PROGRAM ELEMENT, PROJECT, TASK AREA & WORK UNIT NUMBERS: 70210363
11. CONTROLLING OFFICE NAME AND ADDRESS: Aerospace Research Laboratories, Air Force Systems Command, United States Air Force, Wright-Patterson AFB, Ohio 45433	12. REPORT DATE: June 1975
	13. NUMBER OF PAGES: 186
14. MONITORING AGENCY NAME & ADDRESS *(if different from Controlling Office)*	15. SECURITY CLASS. *(of this report)*: Unclassified
	15a. DECLASSIFICATION/DOWNGRADING SCHEDULE

16. DISTRIBUTION STATEMENT *(of this Report)*

Approved for public release; distribution unlimited.

17. DISTRIBUTION STATEMENT *(of the abstract entered in Block 20, if different from Report)*

18. SUPPLEMENTARY NOTES

19. KEY WORDS *(Continue on reverse side if necessary and identify by block number)*

Hot Corrosion
Na_2SO_4-Induced Accelerated Oxidation
Cobalt-Base Alloys
Cobalt
Cobalt-Chromium Alloys
Cobalt-Aluminum Alloys

20. ABSTRACT *(Continue on reverse side if necessary and identify by block number)*

The sodium sulfate-induced hot corrosion of cobalt and a number of binary, ternary and quaternary cobalt-based alloys containing aluminum, chromium, tungsten, molybdenum, tantalum, titanium and yttrium has been studied at 1000-degrees Celcius in 1 atm of oxygen or air. The studies consisted of both laboratory experiments and testing with a dynamic burner rig. The results obtained from these studies were compared to those available for equivalent nickel-base systems. Those obtained from laboratory tests were in satisfactory agreement with those from dynamic burner rigs except that the loss of chromium from the alloys was more pronounced in the high velocity rig tests. It was determined that sodium sulfate deposits caused increased oxidation of all of the alloys studied. Mechanisms for the

DD FORM 1 JAN 73 1473 EDITION OF 1 NOV 65 IS OBSOLETE

UNCLASSIFIED

SECURITY CLASSIFICATION OF THIS PAGE *(When Data Entered)*

20. Abstract (Cont'd)

hot corrosion of these alloys have been developed. A substantial difference between the hot corrosion resistance of cobalt- and nickel-base alloys has been observed only for alloys containing chromium and aluminum with no refractory elements. Chromium and yttrium produced beneficial effects on the hot corrosion of alloys; aluminum also produced beneficial effects except at low concentrations of aluminum. Molybdenum and tungsten usually produced deleterious effects on the hot corrosion of alloys whereas tantalum and titanium were apparently innocuous.